

The Smart Retrofit Wing Technical Design

Final Report – July 4, 2017
Design Synthesis Exercise by Group 21

J. P. W. Arkesteijn	4371089
N. van den Bos	4274083
M. Eijkman	4365186
N. Faber	4350979
C. A. Meijerman	4208080
L. Ritzen	4272927
B. J. C. Vandereydt	4340434
R. M. Vervaat	4351487

Preface

Ten weeks ago we, a group of 8 aerospace engineers to be, started this project as an assignment to obtain our bachelor's degree. It turned out to be an engaging and versatile journey to a rewarding final result. In front of you, you will find the Design Synthesis Exercise final report 'The Smart Retrofit Wing' or, as we would like to call it, 'The BEAU-wing', which stands for the Bio-inspired Environmentally and Acoustically Upgraded wing. Words cannot express the long days spent on the process of the final design, the demanding and challenging hours as well as the satisfying profitable moments. This report aims to pave the way to a short-term, yet innovative and sustainable future for the aircraft industry. With this, we hope to cause a wider awareness of the importance of an environment-friendly transportation system and convince all readers that the prospect of such a system is within reach.

The final design of the retrofit wing could never have been obtained without the help of various people, who turned out to be of crucial importance for the project. First of all we would like to express our gratitude to Dr. Roeland de Breuker for providing the project framework, encouraging us with his enthusiasm and faith in the project and his especially valuable guidance concerning the structural aspects of the design. We want to thank Dr. Erwin Mooij for his all-encompassing engineering advice and for showing us that system engineering is essential in an extensive design project. Numerous moments we encountered Erwin Mooij's (fulfilled) prophecy: "Hours become days, days become weeks, weeks become months. Multiply this with 2, and you have a good approximation". We want to thank Nitish Anand and Morteza Abouhamzeh for helping us out whenever it was needed, and often coming by our table to offer guidance. Paul Lancelot, Jurij Sodja and Davide Nardi, for not only joining our meetings when some of our tutors could not be there, but also for providing us with new insights. We would like to thank Amber van Hauwermeiren from qlayers, for providing extra insight into the sharkskin concept. We would also like to express our sincere gratitude to Dr. Benjamin Woods for advising us on the FishBAC concept, Dr. Marios Kotsonis for sharing his valuable knowledge on, amongst others, pumps related to one of our retrofit concepts, Dr. Irene Fernandez-Villegas for her advice concerning material choices and Mr. James Mabe for giving information about chevron production and performance. Also we would like to thank Dr. Roelof Vos for sharing his knowledge about flap track fairings and Dr. Abhishek Sahai for his guidance with noise emission estimates. Similarly, our sincerest gratitude goes to Marco Oomen, Hans Poelgeest and Frank Stuijt from KLM for the priceless tour through KLM's hangars and for spending their precious time to answer our questions related to KLM and their attitude towards our retrofitting ideas.

Finally, we would like to thank you, reader. If you are reading this line you came so far as having read the first page of our final DSE report. We hope we achieved to capture your interest and that we will keep it all the way to our final retrofit design and further towards a greener future.

Executive overview

Aircraft account for a significant part of the global use of fossil fuels and emission of greenhouse gasses, such as CO₂ and NO_x. Considering the impending depletion of fossil fuels and the impact of greenhouse gasses on the environment, efforts are being made to make the aircraft industry more sustainable. The Advisory Council for Aeronautics Research in Europe (ACARE) has documented their visions in the Flightpath 2050 goals. These goals state that in 2050 the CO₂ and NO_x emissions from aircraft should be reduced by 75% and 90% respectively. Moreover, the effective perceived noise emission of aircraft should be reduced by 65%. While new, more environment-friendly aircraft are being developed at a rapid pace, it will take decades until all current generation aircraft are replaced, and a more short-term solution is found. New technologies can be applied to older aircraft, which is a process called retrofitting. In this project, the Airbus A330-200 was retrofitted in order to demonstrate a more short term and commercially attractive option to reduce the impact of the aircraft industry on the environment. The mission statement was defined as:

To provide a more sustainable wing solution which can be implemented on existing air frames, lowering the impact the aviation sector has on the environment.

Ideally, an airline fleet consists of the latest aircraft types containing state-of-the-art technologies. Unfortunately, this is usually not possible from an investment point of view. Therefore, an investigation into the feasibility of retrofitting state-of-the-art smart technologies was conducted. In addition to the mission need statement, the project objective statement is:

To provide a platform for the development of a sustainable A330-200 wing retrofit, guaranteeing the same or better performance whilst obtaining a lower or equal life-time cost.

Requirements

Once the main purpose of this report had been determined, requirements were established to ensure the objectives of the project were met. The driving requirements are stated below.

- The system shall be retrofitted to the reference aircraft, the Airbus A330-200.
- The concept used in the system shall use pre-existing concepts.
- The retrofitted aircraft shall generate a smaller impact on the environment when compared to the reference aircraft, as in line with the ACARE Flightpath 2050 goals:
 - The retrofitted aircraft shall achieve at least a 7.5% reduction in CO₂ emissions per passenger kilometre.
 - The retrofitted aircraft shall achieve at least a 9.0% reduction in NO_x emissions per passenger kilometre.
 - The retrofitted aircraft shall achieve at least a 6.5% reduction in the perceived noise emission of flying aircraft.
- The fuel consumption of the retrofitted aircraft on a reference mission shall be reduced by at least 7.5% per passenger kilometre compared to the reference aircraft.
- The retrofitted aircraft shall maintain an engineering budget equal to or better than the reference aircraft.
- The retrofitted aircraft shall maintain the same reliability standards as the reference aircraft.
- The retrofitted aircraft shall maintain the same safety standards as the reference aircraft.

Retrofit Concept Design

To fulfil the aforementioned requirements, a combination of five concepts was chosen. These concepts were all designed in more detail. The design effort covered aerodynamic design, structural design, material choices and integration into the A330. This section will cover the design process and results of each concept.

Chevrons

Chevrons are triangular plates at the end of the thrust-reverser sleeve. They reduce aircraft noise by aiding in controlled mixing of the exhaust air and the ambient air. Non-variable chevrons are already widely used on aircraft, but their advertised noise reduction is accompanied by a reduction in performance and as a result, variable geometry chevrons were chosen instead. They can alter their shape in different flight conditions, hence lowering the performance penalty. Azimuthally varying variable geometry chevrons were found to achieve a noise reduction of 2 dB when deployed. To design this morphing structure, shape memory alloys were used consisting of two flexing components: NiTiInol plates and a fibreglass composite cover, actuated autonomously. Both materials were shown to have excellent fatigue behaviour and are thus accepted for use on aircraft. The total added weight of this system was calculated to be 63 kg.

Winglets

To design a retrofit winglet for the A330, a vast amount of variables were analysed. The winglet could be either morphing or fixed, and other variables included aerofoil shape, toe angle, twist, sweep angle, and cant angle. Finally, if a morphing winglet was chosen, the morphing mechanism would either be electric or hydraulic. Aerodynamic simulations showed that the optimal design of the winglet would be optimal for all flight conditions, thus from an aerodynamic standpoint, no morphing was needed. Additionally, it turned out that a cant angle of 90° (a horizontal winglet) was the most optimum design, meaning the retrofit will effectively increase the span. To maximise the effect of the optimised winglet its span was increased to 3.5 m, such that the aircraft span would be exactly 65 m. A moderate sweep angle of 30° and a taper of 0.4 turned out to provide maximum performance benefits. Figure 1 shows the design of the retrofit winglet.

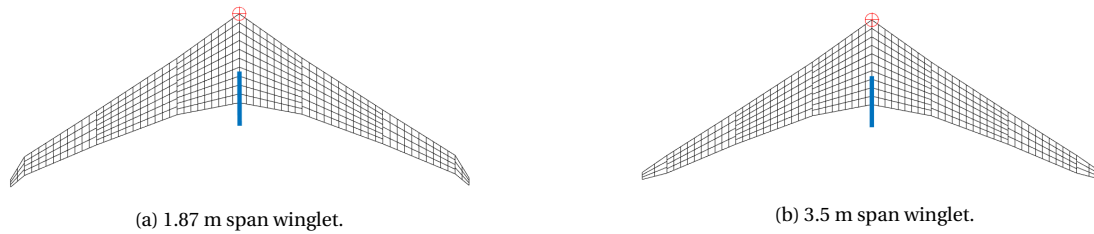


Figure 1: Top view of the wing with new winglet designs.

Once the aerodynamic design of the winglets was finalised, it was decided that a structural design needed to be conducted. A vertical winglet reduces the wing root bending moment, and introducing a winglet with a 90° cant angle meant a reassessment of the internal structures of the wing was needed in order to cope with the increased loading. From a structural point of view, morphing the winglet such that it can attain a 0° cant angle and thus decrease the bending moment exerted on the wing would benefit the overall performance of the wing. To ensure that the wingbox would not fail in the most critical conditions, a morphing winglet was once again introduced and chosen as a design option.

The next step in the design of the winglet was designing the morphing mechanism. One of the greatest constraints turned out to be the dimensions of the wing at tip to tip, another constraint was the vast amounts of loads the actuator would need to produce. This rendered the design of a morphing winglet via actuation not viable. As an alternative, a break-pin system was introduced, in which the winglet would only morph up to a cant angle of 0° under a specific aerodynamic load: the maximum allowable load of the wing. These loads would cause the pin to break and the winglet to morph up and relieve some of the wing root bending moment.

The final step in the winglet design concerned an aeroelastic analysis, during which wingtip divergence and flutter were assessed. It turned out the winglet design would not cause the wing to buckle, even under the ultimate loads. Both the wingbox design and the extended wingtip design were sized with the constraint tear-out of the skin near the root of the wingbox. The materials chosen in the design of the extended wingtip were:

- aluminium in the leading edge,
- aluminium in the trailing edge,
- carbon-fibre composite winglet skin,
- carbon-fibre composite spars and ribs and
- honeycomb structure for further strengthening of the winglet.

An overview of the winglet design parameters can be found in Table 1.

Table 1: Overview of the key wingtip extension parameters.

Parameter	Value	Unit	Parameter	Value	Unit
Span	65	m	Max. deflection	2.07	m
Winglet span	3.5	m	Deflection increase	4.83	%
Winglet sweep	30	$^\circ$	Max. twist	2.435	$^\circ$
New wing area	367.6	m^2	Twist increase	16.54	%
Wing area increase	1.83	%	Weight	14,016.7	kg
Aspect ratio wing	10.73	-	Weight increase	3.72	%
Taper ratio	0.4	-	Minimum cant angle	0	$^\circ$
			Maximum cant angle	90	$^\circ$

FishBAC

The FishBone Active Camber (FishBAC) is an alternative flap design that consists of a morphing flap mechanism with an internal actuation system. Prior to preliminary design, several design options were considered: an integrated morphing trailing edge with or without blowing, a hinged morphing flap or an extendable morphing flap. Ultimately, an integrated morphing trailing edge without blowing proved to attain the same lift characteristics as the single-slotted Fowler flap on the original A330, and was chosen for its simplicity when compared to other designs. An additional benefit of a flap with an internal actuation system was that the flap track fairings that contain an actuation mechanism to extend the Fowler flaps could be removed.

Aerodynamic design provided the required deflection and shape of the morphing flap, and also determined the aerodynamic benefits of reducing the flap fairings. This turned out to translate into a drag reduction of 1,222 N. Additionally, removing flap track fairings indicated a reduction in noise, since the gap between the Fowler flap and the aircraft is a notorious source of noise during take-off, approach and landing.

Once the aerodynamic design was determined, the structural design of the FishBAC could be conducted. A simplified model of the FishBAC was used to find a structure that could attain the required deflections without yielding or buckling in the process. Ultimately, the FishBAC structure would consist of a centre beam, stringers, a triangular tip, an actuator and tendons, all covered in a flexible morphing skin that is reinforced with aluminium strips. Figure 2 shows a cross-section of the non-actuated FishBAC flap.

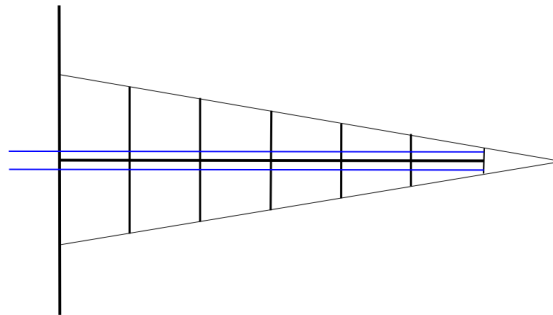


Figure 2: Cross-section of the non-actuated FishBAC flap.

The materials used in the FishBAC proved to be one of the biggest challenges of the design. The challenge of morphing structures is the delicate balance between flexibility and strength. The materials used in the FishBAC design are stated and elaborated below.

- Carbon Fibre reinforced polyphenylenesulphide (CF/PPS) was chosen as the material for the centre beams and the stringers. While CF/PPS in its regular form is very stiff, it was decided the design would be heated to 107 °C to soften the material and allow for deflection. Once the FishBAC would be deflected it would be cooled down and it would attain its original stiffness properties.
- Polyether-ester block copolymer with 10% glass fibre was chosen as the material for the flexible morphing skin that would cover the FishBAC. It was mainly chosen for its high quality and wide operating temperature range, specifically on the low temperature end.
- Dyneema was chosen for the tendon that actuates the FishBAC.
- Aluminium 6061 will be used for the tip of the FishBAC and reinforcement strips in the skin.

Once the internal structure and the required deflection loads had been determined, an actuator needed to be found that could provide the required deflection. In the end, the total design could be finalised. Table 2 displays the most relevant design parameters of the FishBAC.

Sharkskin

Sharkskin is a concept in which the riblet texture of a sharks skin is applied to an aircraft. This texture reduces skin friction drag in the turbulent regime. While the exact mechanism by which why a riblet texture reduces skin friction drag is not totally known, part of it can be attributed that a riblet structure reduces the wetted area in the sub-viscous boundary layer. The sub-viscous boundary layer is the layer of flow between the surface of an object and the complete turbulent layer further away from the object. While fully developed turbulence exhibits complete randomness in its velocity distribution, the sub-viscous boundary layer displays organisation. Stream-wise vortices dominate this sub-viscous boundary layer and are the cause of much of the chaos in the outer layers of the turbulent boundary layer. When a sharkskin riblet is used these vortices only interact with the tips of these riblets, instead of with the entire surface of a flat plate, reducing skin friction drag.

The coating would be made of a regular material for top-coats: epoxy. It could be applied to the aircraft in two ways: automated (3D printing) and via films. While automated printing would be a cheaper and more precise option, it

Table 2: Design parameters for the FishBAC flaps.

	nr	Inboard flap	Outboard flap	Unit		nr	Inboard flap	Outboard flap	Unit
w_{fb}		6.82	11.25	m	t_{str}	1	0.006	0.006	m
c_{fb}		1.8876	1.8876	m		2	0.003	0.003	m
r		0.35	0.35	m		3	0.005	0.006	m
n_{cb}		2	7	-		4	0.003	0.004	m
b_{cb}		0.061	0.06	m		5	0.003	0.003	m
h_{cb}		0.029	0.026	m	t_{sk}		0.005	0.005	m
sp_{cb}		2.773	1.4065	m	r_T		0.0055	0.004687	m
n_{str}		5	5	-	W_{tendon}		1.91	4.85	kg
sp_{str}		0.2563	0.2563	m	W_{skin}		106.47	210.55	kg
h_{str}	1	0.065	0.065	m	$W_{CF/PPS}$		242.33	386.78	kg
	2	0.055	0.055	m	W_{Al}		66.3	109.368	kg
	3	0.044	0.044	m	W_{tot}		417.01	711.55	kg
	4	0.032	0.032	m					
	5	0.024	0.024	m					

still requires a lot of development and at this point a manual application with films was chosen. The automated application is still considered as a future development.

A relatively new development in the functional coating field is birth feather herringbone riblets. These riblets are based on the texture of bird feathers and provide double the drag reduction of regular sharkskin. These riblets were chosen as a configuration for the sharkskin concept due to their superior drag reduction. It was calculated that a herringbone-riblet applied to as much of the aircraft as sensible would generate a 7.56% total drag reduction at a weight penalty of 346 kg.

Leading Edge Suction

Leading edge suction was one of the more promising concepts at the beginning of this final report. The concept of leading edge suction is based on the idea that a growing laminar boundary layer will be sucked away before it becomes turbulent, delaying the transition point on the wing and hence reducing drag. Four setups were considered in which different sections of the wing were covered. The drag reduction for the concepts ranged from 545N to 2,190N.

An additional implication of leading edge suction was the introduction of a Krueger flap to protect the suction holes from any potential insect residue. Since a Krueger flap would replace the current slat, its aerodynamic and structural impact were assessed. Performance-wise, the Krueger flap would slightly decrease the maximum lift coefficient of the aircraft and increase the stall speed, while the drag coefficient would stay the same. It was also concluded that a Krueger flap would not affect the stability of the aircraft. Noise was also found to be unaltered when the slat would be replaced by a Krueger flap.

The next obstacle in the design of suction was the suction mechanism, for which there were two design options: passive or active, both with many sub-options. An active, electrical compression pump was chosen. A setup was chosen in which each wing section will be covered separately. In the end, the total weight of the suction system ranged from 443.2 kg to 1,996.4 kg. While the initial expectations of leading edge suction were very high, further investigation proved that the benefits suction provided did not outweigh its cost and its weight penalties and the concept was dropped from the retrofit.

Full Aircraft Analysis

Figure 3 shows the final design of the Smart Retrofit Wing. The total retrofit, thus consisting of chevrons, an extended wingtip, FishBAC flaps and herringbone sharkskin would generate a decrease in fuel consumption of 10.51% in cruise, 13.05% in approach and 10.7% in a total reference flight of 7.5 hrs cruise time. Since both CO₂ emissions and NO_x emissions scale with engine setting or thrust and therefore with drag, both the 7.5% CO₂ and 9% NO_x requirements were met over the total reference flight.

The noise requirement was more complex. If the retrofit could achieve a 4 dB noise reduction, the aircraft would move down in the noise categories and get a 20% decrease in take-off charges. While noise quantification is outside of the scope of the Design Synthesis Exercise, it was concluded that the combination of chevrons removing of the flap track fairings and gaps between Fowler flaps and the wing, as well as a lower thrust setting due to the drag decrease would meet this 4 dB drag reduction.



(a) The Airbus A330 retrofitted wing with a 90 degrees cant extended wingtip.

(b) The Airbus A330 retrofitted wing with a 0 degrees cant extended wingtip.

Figure 3: Technical risk map before and after risk mitigation.

Communications

Introducing new and more complex additions to the wing changes the communication within the aircraft significantly. Therefore a new communication assessment of the retrofitted A330–200 was performed. Chevrons are actuated with heating elements that are turned on or off either manually or automatically. This required extra electricity and possibly interaction from the pilot. Chevrons also have heat and strain sensors that report back to the on-board computer and the pilot. The winglets are a passive system, the break-pin system will initiate automatically under a certain load. So while no input from either pilot or autopilot is required, a signal would be sent to the on-board computer when these pins break and the wingtip extensions are morphed. The FishBAC would be a replacement of the flaps, which implied it would require some communication with the (auto)pilot. The flaps could be actuated either manually or automatically, for which a signal must be sent to the central flap processing unit. Finally, the sharkskin was designed to be a fully passive concept and required no additional communication. All in all the aircraft was calculated to require an additional 9,000 W of electrical power to actuate all these concepts.

Return on Investment

Once the design of all the concepts and their integration into the A330 were completed, an analysis of the costs and profits could be conducted. The total development costs of all concepts on the Smart Retrofit Wing was calculated to be \$47M. One full retrofit would cost \$5.6M, including a profit margin for BEAU-wing. The break-even point was calculated to be at 52 retrofits, and the return on investment was found to be 4.83.

For the customer, the Smart Retrofit Wing would save \$1,810 per flight, plus the 20% (\$445) reduction in take-off and landing fees: a total of \$2,255 per flight. In addition to the price of the retrofit, the airline would also miss a profit of \$435,400 during the downtime of the retrofit. The break-even point of the aircraft was calculated to be 2,565 flights or 2 years and 11 months, and the return on investment on an aircraft with an expected lifetime of 15 years was 5.15.

Conclusion and Recommendations

The Smart Retrofit Wing comprised of four concepts: chevrons, an extended wingtip, FishBAC flaps and herringbone sharkskin. In total, these concepts were calculated to reduce the fuel consumption of the Airbus A330–200 by 10.7% in a reference flight of 7.5 hours. Another concept that was considered was leading edge suction. While this concept seemed to be promising initially, it was discarded due to underperformance and large weight penalties. While most driving requirements were fulfilled, the requirement concerning safety and reliability standards was yet to be validated in tests. Additionally, the engineering budget was changed, as the mass budget was violated.

In the final phase of the project, several recommendations for further development were established. Some concepts were discarded in the early design phase of the project, such as an active cant morphing winglet, acoustic liners and plasma actuators. These concepts were discarded for several reasons, however as new materials and concepts will most likely be invented in the nearby future, these discarded concepts might become viable for a future retrofit. Additionally, leading edge suction was discarded due to a combination of below-par aerodynamic improvement, required pump power and weight penalties. This concept might be revisited if a breakthrough improvement in this area happens in the future.

Contents

Preface	iii
Executive overview	v
1 Introduction	1
2 Pre-Design	3
2.1 Mission Statement	3
2.2 Functional Analysis	4
2.3 Market Analysis	7
2.4 Resource Allocation and Budget Breakdown	8
2.5 Concept Trade-Off Process	11
2.6 Sustainable Development Strategy	11
2.7 Risk Analysis	13
3 Design	17
3.1 Design Load Cases	17
3.2 Chevrons	18
3.3 Winglets	26
3.4 FishBAC.	42
3.5 Sharkskin	55
3.6 Leading Edge Suction	61
4 Full Aircraft Analysis	73
4.1 Configuration	73
4.2 Retrofit Characteristics	74
4.3 Communications	78
4.4 Verification and Validation	79
4.5 Reliability, Availability, Maintainability and Safety	91
4.6 Operations and Logistic Concept Description.	94
4.7 Sensitivity Analysis	95
4.8 Compliance Matrix	99
5 Project Implementation	101
5.1 Project Design and Development Logic	101
5.2 Project Gantt Chart	104
5.3 Production Plan.	104
5.4 Cost Breakdown Structure	111
5.5 Return on Investment.	111
6 Conclusion	115
7 Recommendations	119
References	123
A Functional Analysis Diagrams	127
B Design Options Trade-Off	131
C Task Division	133

Nomenclature

Abbreviations

ACARE	Advisory Council for Aviation Research and Innovation in Europe
ASTM	American Society for Testing and Materials
AVC	Azimuthally Varying Chevrons
CASMART	Consortium for the Advancement of Shape Memory Alloy Research and Technology
CBS	Cost Breakdown Structure
CF	Carbon Fibre
CFD	Computational Fluid Dynamics
EASA	European Aviation Safety Authority
EPNdB	Effective Perceived Noise Level in Decibels
FBD	Free Body Diagram
FEM	Final Elements Method
FH	Flight Hours
FishBAC	Fishbone Active Camber
HLFC	Hybrid Laminar Flow Control
ICAO	International Civil Aviation Organization
IDG	Integrated Drive Generator
ISA	International Standard Atmosphere
LE	Leading Edge
MAC	Mean Aerodynamic Chord
MAI	Manufacturing, Assembly and Integration
MFW	Maximum Fuel Weight
MH	Man Hours
MLW	Maximum Landing Weight
MTOW	Maximum Take-Off Weight
NASA	National Aeronautics and Space Administration
OEW	Operational Empty Weight
PEEK	Polyetheretherketone
PEI	Polyetherimide
PEKK	Polyetherketoneketone
PPS	Polyphenylenesulphide
RAMS	Reliability, Availability, Maintainability and Safety
RAT	Ram Air Turbine
SFC	Specific Fuel Consumption
SMA	Shape Memory Alloy
SME	Shape Memory Effect
TRL	Technology Readiness Level
UV	Ultra-Violet
VC	Variable Camber
VGC	Variable Geometry Chevrons
VLM	Vortex Lattice Method

Greek Symbols

α	Angle of attack	°
α	Ridge angle	°
β	Slenderness of plate	-
δ	Deflection	m
ϵ	Strain	-
θ	Deflection angle	°
μ	Dynamic viscosity	Pa·s
ν	Kinematic viscosity	m ² /s
ρ	Density	kg/m ³
σ	Deployment angle	°
σ	Stress	N/m ²
τ	Shear stress	Pa

Roman Symbols

a	Speed of sound	m/s
-----	----------------	-----

b	Base length	m
\bar{c}	Chord length	m
d	Distance	m
e	Oswald efficiency factor	-
f	Skin friction coefficient	-
h	Height	m
k	Correction factor	-
l	Length	m
m	Mass	kg
\dot{m}	Mass flow	kg/s
q	Shear flow	N/m
s	Distance	m
sf	Safety factor	-
t	Thickness	m
t/c	Thickness-over-chord ratio	-
w	Deflection angle	rad
w	Width	m
A	Area	m ²
A	Aspect ratio	-
B	Boom area	m ²
C	Coefficient	-
C	Constant of integration	-
D	Diameter	m
E	Young's modulus	Pa
F	Force	N
F_g	Flight profile alleviation factor	-
G	Shear modulus	Pa
H	Total gust width	m
I	Moment of inertia	m ⁴
L	Lift	N
L/D	Lift-to-drag ratio	-
M	Mach number	-
M	Moment	Nm
N	Normal force	N
P	Buckling load	N
Q	Volume flow	m ³ /s
R	Radius	m
R	Reaction force	M
R_1	Landing weight fraction	-
R_2	Zero-fuel weight fraction	-
Re	Reynolds number	-
S	Shear force	N
S	Surface area	m ²
S^+	Scaled Reynolds number	-
V	Velocity	m/s
W	Weight	kg
Z_{mo}	Maximum achievable altitude	ft

Subscripts

act	Actuator
cb	Centre beam
cr	Critical
cs	Carbon substrate
cs	Cross-section
d	Aerofoil drag
fl	Flat
fus	Fuselage
l	Aerofoil lift
l	Laminar
max	Maximum
p	Pressure

<i>pull</i>	Pulley
<i>sh</i>	Sharkskin
<i>sk</i>	Skin
<i>st</i>	Stringer
<i>surf</i>	Surface
<i>t</i>	Turbulent
<i>tc</i>	Top coating
<i>tot</i>	Total amount
<i>w</i>	Web
<i>wet</i>	Wetted
<i>y</i>	Yield
<i>Al</i>	Aluminium
<i>D</i>	Drag
<i>F</i>	Fuel
<i>H</i>	Horizontal tail
<i>L</i>	Lift
<i>P</i>	Power
<i>PU</i>	Power unit
<i>T</i>	Tendon
<i>V</i>	Vertical tail

Introduction

Aircraft account for a significant use of fossil fuels and emission of greenhouse gasses, such as CO₂ and NO_x. Considering the depletion of fossil fuels and the impact of greenhouse gasses on the environment, in the context of a growing demand, efforts are being made to make the aircraft industry more sustainable. The Advisory Council for Aviation Research and Innovation in Europe (ACARE) has documented their visions that show such efforts. Their Flightpath 2050 goals state that in 2050 the CO₂ and NO_x emissions should be reduced by 75% and 90% respectively, whereas the perceived noise emission should be reduced by 65%¹.

New concepts for more sustainable aircraft are being developed in a rapid pace. However, it takes decades to get an aircraft produced and as they are often also operated for decades, a more short-term solution is necessary. New technologies can be applied to older aircraft, in this case the Airbus A330–200, in order to boost this short-term solution. This process of adding new technologies to already existing aircraft is known as retrofitting. While some retrofitted technologies are already being used in general aviation, a system consisting of multiple different concepts that reduce fuel consumption significantly while maintaining its performance is yet to be released. The aim of this project was to design such a retrofit wing. Novice, smart technologies would be applied to the wing of an Airbus A330 in order to reduce its fuel consumption and greenhouse gas emissions. In addition to this, the technologies used to retrofit the wing would make the wing more sustainable. The foundation of the project was laid in the baseline and midterm report [1, 2].

This report describes the preliminary design for a retrofit on the Airbus A330–223. The retrofit aimed to reduce fuel consumption, the emission of CO₂ and NO_x as well as the perceived noise. This report covers the pre-design aspects of the final product, such as a market and risk analysis. The five concepts that were chosen to form the final product were investigated to a larger extent in order to obtain the final designs. A full aircraft analysis was conducted to determine whether or not the concepts negatively or positively impact each other, after which the return on investment was calculated. Finally, the recommendations were presented as more research has to be conducted in order to further develop certain concepts.

Regarding the pre-design phase, Chapter 2 elaborates on any activities that have to be performed in advance of the actual design phase. This includes operations such as conducting a risk and market analysis, as well as documenting the budget breakdown and sustainable development strategy. After these analyses had been established, the individual concepts were designed to a more detailed extent. This means the performance, cost and weight as well as the integration of the concepts will be discussed in Chapter 3. As the design of all concepts were known to a detailed extent, they can be implemented onto the aircraft to obtain the final configuration. The characteristics of this final configuration will be discussed in Chapter 4, along with the verification and validation of the individual concepts. Furthermore, the concepts will be assessed on reliability, availability, maintainability and safety and a sensitivity analysis will be presented.

In Chapter 5 the project Gantt chart as well as the production plan for the concepts will be presented. This chapter will be concluded with a return on investment calculation. Finally, in Chapter 6 the conclusion of the project will be presented, after which the recommendations will be discussed regarding future work and the development of the individual concepts.

¹URL <https://ec.europa.eu/transport/sites/transport/files/modes/air/doc/flightpath2050.pdf> [cited 27 June 2017].

Pre-Design

In advance of the design phase it is essential to analyse specific aspects of the product, such as its expected performance, the potential risks and the appropriate market. By evaluating these factors, a good estimation can be made on whether it is worthwhile to continue with the design phase.

First the mission statements will be discussed in Section 2.1, after which a functional and market analysis will be elaborated upon in Sections 2.2 and 2.3, respectively. A budget breakdown will be established in Section 2.4, after which the concept trade-off will be described in Section 2.5 and the sustainability approach will be explained in Section 2.6. Finally, the technical risks are documented in Section 2.7, showing the potential risks of the different concepts.

2.1. Mission Statement

Before any design process can be started, it is important to clearly identify the goal of the project. This goal is expressed in a mission need statement and a project objective statement. For this project, both statements were derived from the project description [3] and have been identified during the initial planning phase of the project. Next to this, a list of system and stakeholder requirements was established.

2.1.1. Mission Need and Project Objective Statements

The goal of any project can be subdivided into two statements, concerning the need and objective of the project. These statements express what the final product and the design team should do, respectively. The mission need statement was formulated as follows:

To provide a more sustainable wing solution which can be implemented on existing airframes, lowering the impact the aviation sector has on the environment.

Ideally, an airline fleet consists of the latest aircraft types containing state-of-the-art technologies. Unfortunately, this is usually not possible from an investment point of view. Therefore, the possibility of retrofitting state-of-the-art smart technologies to an existing commercial airliner in order to lower the impact on the environment must be investigated. In addition to the mission need statement, the following project objective statement was identified:

To provide a platform for the development of a sustainable A330-200 wing retrofit, guaranteeing the same or better performance whilst obtaining a lower or equal life time cost.

Together, the mission need statement and project objective statement form the basis for all subsequent design activities. In addition, requirements were identified with which the final product should comply.

2.1.2. Driving Requirements

During previous work a list of system requirements was identified. From this list, only the driving requirements are listed below. For a full list of system and stakeholder requirements the reader is referred to the midterm report [2]. The following driving system requirements were identified:

- SRW-01** The system shall be retrofitted to the reference aircraft, the Airbus A330-200.
- SRW-02** The concepts used in the system shall be pre-existing concepts.
- SRW-04** The retrofitted aircraft shall have a smaller impact on the environment when compared to the reference aircraft, in line with the ACARE Flightpath 2050 goals:
 - SRW-04-EMIS-01** The retrofitted aircraft shall achieve at least a 7.5% reduction in CO₂ emissions per passenger kilometre.
 - SRW-04-EMIS-02** The retrofitted aircraft shall achieve at least a 9.0% reduction in NO_x emissions per passenger kilometre.
 - SRW-04-EMIS-03** The retrofitted aircraft shall achieve at least a 6.5% reduction in the perceived noise emission of flying aircraft.
- SRW-05** The fuel consumption of the retrofitted aircraft on a reference mission shall be reduced by at least 7.5% per passenger kilometre compared to the reference aircraft.
- SRW-06** The retrofitted aircraft shall maintain an engineering budget equal to or better than the reference aircraft.
- SRW-07** The retrofitted aircraft shall maintain the same reliability standards as the reference aircraft.
- SRW-08** The retrofitted aircraft shall maintain the same safety standards as the reference aircraft.

2.2. Functional Analysis

To obtain a better overview of the process of the product from design to end of life, it is useful to create a functional flow diagram. Both a functional flow analysis and a functional breakdown have been conducted, resulting in the corresponding diagrams. The functional flow analysis describes all the different stages from design and pre-production to the disposal of the product in a time-wise fashion, whereas the functional breakdown discusses the breakdown of the complete system.

2.2.1. Functional Flow

This section discusses the functional flow. A functional flow diagram has been constructed and can be found in Appendix A. The top level blocks of this diagram are further elaborated upon below, together with the most significant lower level blocks.

Design and Pre-Production

The first phase in getting a new product on the market is always the design and pre-production phase. The most vital element of this phase is the design of the actual product. This phase started with the exploration and literature review of all different design options. Many of the concepts were found to be unfeasible during the literature study, which meant they did not progress to the next design phase. All of this has been reported in the baseline report [1]. The next step was to perform a trade-off which would yield a final design option. To this end, the previously performed literature study was used and all remaining concepts were further elaborated upon. A detailed description of this process was given in the midterm report. [2]. Once a final concept had been chosen, the preliminary design could finally start. Near the end of the preliminary design phase production methods were chosen, which is described in Section 5.3. As the production method heavily influences the structural strength and the economical impact of the product, this step should not be underestimated and verification and validation cannot start before the production plan has been completed. Sustainability was a heavy weighing factor in the determination of the production method.

After the production method has been chosen, the design can be validated and verified. All required parameters, such as cost, aerodynamic performance and weight, are determined and checked with the requirements. If they fall short, the product has to be altered or redesigned, or it has to be argued why a requirement was not met. Note that validation and verification are related, but not the same thing. When verifying the question to ask is *“Does the system developed meet the requirements?”* and for validation the question is *“Was the right system developed?”* [4].

In aviation, two main levels of certification exist for manufacturing. First of all, the manufacturing process has to be certified. This is a company related certification. Airbus sends people down to the factory in question and investigates the full process, from preparation to production and finishing. The next level of certification is the product certification, where the product made using a certified process is certified. Therefore, if a new product has to be certified, a prototype has to be made using a process which has already been certified. As it stands, no production facility is available. Due of this, to produce the prototype, a facility has to be found with processes which are already verified by Airbus. Here, the prototype components can be made and verified by Airbus. This means that later on, when a facility is available for production, only the production process has to be verified again and not the product. Another advantage of certifying the prototype before a production facility is set up is the decrease of risk, as with this certification, it is clear that the designed product works. This also helps in the marketing, as airlines or other investors will more easily invest in products that have already been certified.

With a certified product, a business plan can be made and marketing can be started. For the marketing, capital is raised, customers are found and contracts are made. In the business plan, certain long- and short-term goals are set and a risk plan is made. All of this reduces the economical risks immensely.

Once this has been done, pre-production can start. This is the most expensive phase of design and pre-production. Here, a facility is found where production will take place. The equipment is bought and the workforce employed and an extensive production plan is set up. This defines the ground plan of the factory, the production flow and storage methods. After this is done, prototype testing is performed once more. This allows for fine-tuning of equipment. Once a certain confidence level is acquired, the process can be certified by Airbus and production can start.

Production

Before production of components can start, materials have to be ordered. To keep the flow of material as efficient as possible, the inventory has to be tracked at all time. To make sure that the production hall never runs out of material, as this might lead to costly delays, remaining contracts have to be known and the market has to be predicted. This allows for predicting the amount of production at any time, and hence the required amount of material in inventory at any time. The warehouse manager has to make sure that there is enough room in the storage for the production materials and produced parts to be stored.

After this, the ordered parts can be produced using the certified process. All parts which have to be assembled are moved to the assembly hall and finally everything is stored. If parts require no assembly, they are stored immediately after

production, as a cluttered work space decreases the efficiency. When a certain amount of components is reached, they can be shipped to the hall where retrofitting takes place. This will either be in situ, or at the hall where the aircraft in question is stationed.

Retrofitting

Before retrofitting can start, the components and the aircraft have to be gathered. As mentioned before, this can either be done at the production facility, which decreases the shipment cost of the components tremendously, or it can be done on site at the hall where the aircraft is stationed, if the assembly process allows for this. If it is done at, or near, the production facility, an airstrip needs to be nearby on which the A330 can land and take off. After the aircraft and the components are gathered, the aircraft is prepared for the retrofit. The assembly jigs are aligned, a retrofit plan is made and the equipment is prepared.

When this is done, the retrofit can start. First, the components to be replaced are taken off. All the wiring and tubing are disconnected, and the component is taken off. These discarded components can be reused on other aircraft as spare parts, if their quality allows for it. For example, the thrust reverser sleeve can be used as a spare part, as there is a large market available for second-hand aircraft parts¹. If their state is not on par with the aviation regulations, the material of the components can still be recycled and sold. Once this is done, the retrofits can be mounted. The components are installed on the jig, and the wiring and tubing is done. After this, the component is mounted on the aircraft. When all components are installed, the assembled retrofit is tested. All the controls are tested, and the structural integrity is examined. If it passes the tests, the aircraft is delivered to the customer.

Operation

After the aircraft is delivered to the customer, it finally enters operation. The operation of the aircraft consists of three main parts. The first, and foremost, is of course the flight mission. Other than that, there is intra-flight parking and inspections and the planned and unplanned maintenance. Below, the flight mission is further elaborated upon.

Before the aircraft can take off, a pre-flight inspection is performed. Here, all the critical components of the aircraft are checked, such as tire pressure or possible damage to the wing. After the pre-flight inspection, the pilots go through to the start-up. Here the engine is started, and the electrical components are checked. After this is done, and the in-cabin electrical components work, the aircraft can be loaded. Sometimes, if the climate allows for this, the payload bay of the aircraft can be loaded before the engine starts.

After all tests have been performed and the baggage and passengers are loaded, the aircraft can taxi to the runway and prepare for take-off. During or before this taxiing, the chevrons should be heated up, such that they are morphed before take-off starts. The take-off itself starts with the pilots increasing the thrust levels to the specified level required for the take-off conditions at hand. This depends on many factors, such as tarmac conditions (wet or dry), or if the air conditioning is turned on or off [5]. After the power is increased, the velocity also increases. After the take-off decision speed is reached, the take-off can no longer be aborted, and has to be continued. When the rotation speed is reached, the aircraft rotates and takes off. After the screen height is reached, the power and high lift devices are adjusted. Finally, the landing gear is retracted and take-off has been accomplished.

Once the aircraft has successfully taken off, it can climb to its cruise altitude. For this, first the thrust is reduced to the optimal value for maximum efficiency. At the same time, the flight path is altered. After this has been concluded, the FishBAC (Fishbone Active Camber) and slats are retracted to the desired setting. If it has not already been done during take-off, anti-icing and air conditioning are turned on.

When cruise altitude is reached, the aircraft is taken out of climb mode and into cruise mode. Here, the aircraft flies as close as possible to its maximum lift-to-drag ratio. To this end, the FishBAC is further retracted and the angle of attack becomes a function of weight and cruise altitude. The winglets enter their cruise setting. Another factor to be maximised is the velocity-over-fuel-rate ratio. All of the settings required to optimise these two ratios should be specified in the flight plan.

After cruise, the aircraft enters its descent. For this, the ideal descent profile is calculated. This calculation gives the optimum glide ratio, such that the aircraft arrives in the airport controlled airspace with the desired top of descent altitude. Speed brakes can be used for this, but it should be considered that their effectiveness decreases with airspeed².

When the aircraft reaches the airport-controlled airspace, the approach is started. The landing gear is extracted and the FishBAC is set to the landing configuration. After this, the aircraft needs to go to its final approach speed. This can be done using the speed brakes and changing the engine settings. Finally, the cabin lights are dimmed for safety reasons. After the approach, the aircraft lands. This starts with it touching down, followed by braking. After the aircraft has landed, it taxis to the parking space and the engine is shut down.

¹Private communication, Hans Poelgeest [19 June 2017 14:00].

²URL https://www.skybrary.aero/index.php/Take-off_and_Climb_-_A_Guide_for_Controller [cited 1 May 2017].

End of Life

When the aircraft has reached the maximum amount of pressurisation cycles, it is moved to the disassembly hall and the aircraft is taken apart. All the components that can still be used are put aside and reused as spare parts. Components that are not in the desired condition are sold as scrap material. The empty shell is moved to a graveyard.

2.2.2. Functional Breakdown

To have a successful system, such as an aircraft or even a company, all the different functions need to be defined, together with their interrelationships. For this, a functional breakdown structure is a widely used tool. In this section, such a breakdown is constructed and elaborated upon. The final breakdown structure can be found in Appendix A. For ease of use, the system was split into two departments: the operations and the production department. Both departments will be further explained below.

Production Department

The first subtree of the functional breakdown structure is the production tree. This tree consists of three subfunctions of its own: the retail, manufacturing and retrofit department.

First of all, the retail department focuses on all logistics regarding the production of the components. This consists of production planning, sales and marketing and business planning. Production planning assures that the production happens as efficient as possible by optimising the work flow and the factory layout and by tracking the production capabilities. The sales and marketing department is responsible for sales planning and reporting, for finding new customers, for marketing strategy planning and for market research. All of this assures that the company is at all times profitable and growing. The final department of the retail section is the business planning department. They set the long- and short-term goals, as discussed before.

The second major department, the manufacturing department, deals with everything that happens on the factory floor. It consists of managing the production materials, producing components as ordered and the warehouse storage. The production material manager makes sure that, at all times, there is enough material in the warehouse and on the factory floor to continue production as normal. The component production department is in charge of actually producing the components. They receive the orders from the warehouse, prepare the equipment, manufacture the parts, check their quality and finally assemble them. This is optimally done in cells using an assembly line, such that every team is doing a certain task they were trained to do. The warehouse storage manager tracks the inventory and the orders, and makes sure the customer receives the components on time and as ordered.

The last major department of the production is the retrofit department. They actually install all the produced components on the aircraft. They have four main tasks: namely logistics, preparation and disassembly and retrofitting and assembly. The logistics department determines the site where the retrofit will be installed and gathers the aircraft and the required components and equipment. The preparation and disassembly department assembles the jig and takes off the to-be-replaced components. They then check their quality: if they are in a good state, they are reused during maintenance of a non-retrofitted aircraft of the same type. If their quality does not meet the strict standards, their material is recycled. The retrofitting and assembly department mounts the retrofit and tests it.

Operations Department

The second sub-tree of the functional breakdown structure is the operations tree. This encompasses everything related to the operation of the aircraft: it consists of support, the aircraft and end-of-life operations.

First of all, the support department. This department on its own consists of maintenance and retrofitting. The retrofit department also appears in the production subtree, as this is the connection between the production and the operations sections of the aircraft life. Since the retrofit department has been elaborated upon in the discussion of the production department, it will not be discussed in more detail here. The maintenance department, which is the other part of support, consists of planned and unplanned maintenance and the disposal of the parts replaced during maintenance. It is essential here that effect on the availability of the aircraft is minimal.

The second department of the operations is the aircraft department. This consists of the airframe and the mission profile. The airframe consists of all its different component groups, such as the fuselage, wing group and instrumentation. For the full list, see Figure A.5. The mission profile consists of all the different phases of the flight, and post-flight parking. It spans from engine start-up to parking. Again, the full list can be found in Figure A.5.

The final major department of the operations section is the end-of-life department. After the fuselage has reached a certain amount of pressurisation cycles, or when it has life-ending damage, the aircraft is disassembled and the materials are either recycled or reused.

2.3. Market Analysis

There is no use designing a commercial product if there are no customers to buy it. Therefore a market analysis, which specifies the costumers and the market, is vital for a concept to become reality. Moreover, an appropriate analysis of competitors should also be conducted.

2.3.1. Markets for the Smart Retrofit Wing

In the baseline report, a first version of the market analysis was presented [1]. It was decided that the smart retrofit wing would be sold directly to airlines and assembled in house, without the use of third parties. All the performance parameters of the retrofit would be defined and compared to the A330–223. If this was the only aircraft type the retrofit was designed for, the market for the product would be very limited. Therefore the entire Airbus A330–200 family was included, as the only relevant difference between the models are the engines. This is a market of 539 aircraft. Since the wing used on the A330–200 is essentially the same wing as that on the other aircraft in the A330 family, the complete family could be included in the market as well [6]. For most concepts, the decrease in fuel consumption or drag would be roughly the same. Only for the chevrons a notable difference might arise, as this is greatly dependent on the engine. This increases the potential market to 1,238 aircraft. These will be the primary market targets.

Other market options for the retrofit technologies are other aircraft types, outside of the A330 family. This is especially the case for the sharkskin and chevrons, as their integration is not extremely aircraft-specific. Any aircraft which does not already have these could easily be retrofitted by BEAU-wing. For the other concepts this could also be an option, but first it will need to be investigated if the retrofit will be worth it. For example, for a Boeing 747 with its three-part flaps a FishBAC might not be possible. For an A340 on the other hand, which has a near identical wing to the A330, all concepts should be viable.

Finally, markets outside of aerospace. The concepts discussed in this report were specifically designed for aircraft, but this does not mean they can exclusively be used for aircraft. Winglets might be limited to aircraft, but all other concepts are not. FishBAC might for example be applied in the automotive industry, for the use of spoilers in cars. Here, to be able to efficiently adapt the amount of down-force to a given situation can be revolutionary. Active aerodynamics, as it is called, is becoming a regular thing nowadays in high-end sports cars. For example the latest iteration of Ferrari's high-end V12 supercar, the 812 Superfast, has active aerodynamics for everything from its rear diffuser to channels for brake cooling³. The sharkskin could be applied to any industry where drag due to turbulent air is of importance, again the automotive industry would be suitable.

For markets outside of the A330, BEAU-wing could offer its services in multiple forms. It could, for example, produce and retrofit parts for other aircraft or other products, as discussed before. The technology patented by BEAU-wing could also be sold or lent to other companies. And finally, BEAU-wing could offer services in the form of consultancy, helping other companies tailor and integrate concepts into their design.

2.3.2. Distribution of Aircraft

There are currently 539 Airbus A330–200 aircraft in operation, according to Airbus delivery catalogues⁴.

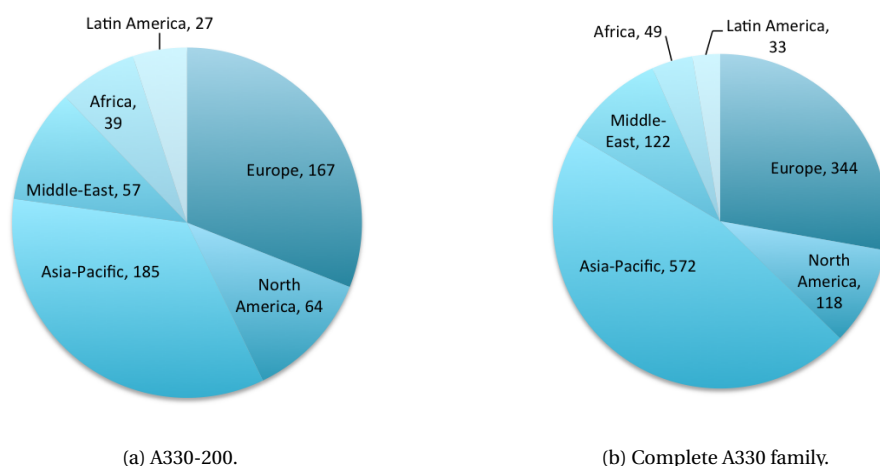


Figure 2.1: Distribution of A330 aircraft per continent.

Figure 2.1a shows an overview of the distribution of Airbus A330–200 aircraft worldwide; the market is especially large in Asia and Europe. Starting in Asia would be an obvious strategy, but there are some advantages to starting in Europe. Considering this is a Delft-based project, connections of TU Delft could be used to establish connections

³URL <http://812superfast.ferrari.com/en/aerodynamic> [cited 25 June 2017].

⁴URL <http://www.airbus.com/company/market/orders-deliveries/> [cited 3 May 2017].

within Europe more easily than in Asia. Also, setting up production and doing business is easier within Europe. The disadvantages are also minimal. The largest disadvantage, the distance, can easily be overcome as the A330 can bridge the gap between Asian and European markets. Other than the A330-200, also the other A330 types (A330-200F, A330-300) are clear markets. In Figure 2.1b the distribution of all A330s in operation can be found in the same manner as before. It became clear that for all A330 type aircraft, the Asian market dominates. Also it must be noted that only 43.5 percent of the A330s in operation are A330-200s. Therefore, by only including the other aircraft of the same family, the market is more than doubled, from 539 to 1,238 aircraft.

2.3.3. Marketing Strategy

Another option for increasing the market was by offering a custom-made retrofit package which includes a subset of the retrofits available. Here, instead of offering a single, large-scale retrofit package, the customers can choose from the available concepts for the ones which match its fleet. This is because each concept will have its own break-even interval, advantages and disadvantages. For one customer, for example, noise might be extremely important, but fuel consumption not so much. Therefore, the ability to build the retrofit package increases possibilities tremendously. This will be further elaborated upon in Section 5.5.

This also helps with the fact that different airlines have different market strategies, and different attitudes towards retrofitting. For example, KLM has the rule that a retrofit or an upgrade needs to be profitable within two years⁵. These two years would be possible for some of the concepts, such as sharkskin and chevrons, but not for others. Other airlines have other rules on return on investments, and might not be put off by larger break-even intervals.

2.3.4. Competitor analysis

A competitor analysis is very important for any new business, as they decide how large the market share is. For most minor changes, the airlines perform the retrofit themselves, for example for new bleed air valves⁵. As this retrofit goes far and beyond minor changes, it was concluded that the airlines will not be seen as competitors, but only as customers. Other than these minor changes, not many readily available retrofits for the A330 were out there. Fokker offers hybrid laminar flow control (HLFC), new (non-morphing) winglets and sharkskin as retrofits, but all of these have a very small scale, with the HLFC never having been applied before and the sharkskin having been applied only on very select locations⁶. Other than Fokker, no companies were found to offer retrofits even remotely related to the ones considered in this research. Most available retrofits are for in-cabin equipment, such as new toilets or galleys⁷.

2.4. Resource Allocation and Budget Breakdown

An essential tool for designing and producing a concept was the allocation of resources and the corresponding budget breakdowns. By stating a maximum value for specific technical resources such as mass and power and regularly updating their budget, one can assess whether or not the maximum allowance will be exceeded in the future, when also keeping in mind the contingencies established in the baseline report [1].

As five concepts were chosen to be further worked out to obtain a more accurate representation of the performance of the final product, the budget breakdown for several technical resources had to be updated. These technical resources were chosen to be weight, power, aerodynamic performance, noise and cost. As no maximum or target values have been set, they were stated for each budget before further research regarding the concepts will commence. These values were set according to the requirements or any empirical relations between the resources. When more information was gathered concerning the resources for each concept, another evaluation was conducted to check whether or not the final design is still within the set boundaries. The budget breakdown tables for each resource were created according to the information gathered during the elaborate literature review, which was presented in the midterm report [2]. This meant the values in these tables were a first indication and thus would most likely change after the design calculations for each concept were presented in this report. The budget breakdown of each resource was revisited after the certain resource parameters have been calculated more accurately. Only then another conclusion could be made on whether or not the final product would exceed the maximum allowable values for each specific budget, either at that moment or in the near future.

It was chosen to adhere to a slightly different approach with respect to the resource allocation and budget breakdown. Normally one would set a maximum value and state absolute values in the breakdown tables, however, it was decided to make use of relative values. It was decided that this would better suit the project, as the goal is to retrofit certain components instead of designing a completely new product. This means the values in the tables will represent the difference of the new component with respect to the 'old', currently installed, component for each specific resource, where a minus sign indicates a reduction of the resource and a plus sign indicates an increase of that resource.

⁵Private communication, KLM (19 June 2017 17:00).

⁶URL http://www.fokker.com/sites/default/files/media/Files/Services/Retrofit/RETROFIT_D5.4_FS_V2.0_29022012_web.pdf [cited 26 June 2017].

⁷URL <http://beaerospace.com/products/water-waste-systems/airline-retrofit-solutions> [cited 26 June 2017].

2.4.1. Mass

The first budget breakdown that was established concerns the mass of the concepts that form the final design. The most beneficial scenario would have included a decrease in an overall mass or no impact on the mass whatsoever. However, since most likely actuators and different materials were going to be used to implement these concepts, the total mass would probably increase. The masses that can be found in Table 2.1 represent the mass increment that was present after implementing the concept onto the wing. This meant the budget breakdown of all concepts would be assessed with respect to the components that are currently present on the Airbus A330. Therefore, one could also state that the budget breakdown can be expressed as the mass of the components that will be replaced by the retrofit concept (e.g. the mass of the flaps, in case of the FishBAC concept). The added mass due to the application and implementation of the concepts had to be at most 0 kg. This maximum allowable value strongly correlated with the performance increase, as an increase in performance resulted in a decrease of fuel consumption. This process started a snowball effect, where theoretically less and less mass will be necessary for flight. If this effect from the fuel reduction was larger than the additional mass due to the structural weight of the concepts, a positive performance increase was achieved. A slight mass increase is thus allowed, as long as the performance increase compensates for this.

Table 2.1: Top-level mass budget breakdown for final product.

Concept	Mass change [kg]	Concept	Mass change [kg]
Chevrans	100	Sharkskin	0
Winglets	200	LE suction	2,000
FishBAC	-100		
		Total	2,200

As can be seen from Table 2.1, the allowable value of 0 kg was exceeded by a decent amount. This meant that either compromises have to be made, or the performance increase would have to compensate for this structural mass increase. To check where mass could possibly be saved, individual budget breakdowns could be constructed for the different concepts. This should show the distribution of mass for that specific concept and thus give a better overview. These distributions were presented after more elaborate calculations had been conducted on the specific concepts.

2.4.2. Power

The second resource that was broken down is the power budget. As some concepts were most likely going to require electrical power to excite the actuators, as is the case for the chevrons, it was essential to document a power breakdown. From the literature study, presented in the midterm report [2], it was found that three concepts required electrical power for their actuation system to work as intended. For chevrons electrical power was necessary to heat the actuators, whereas for the suction system a pump was required to expel the air through the ducts, and finally the FishBAC concept used heating elements to control the deflection of the control surface. The power budget breakdown can be found in Table 2.2, showing the estimated extra power required for all concepts.

However, this extra power required does not have a concrete meaning, unless a maximum value is established. If it is assumed that the Airbus A330 is already optimised with respect to the power available, the maximum value would be 0 W. This means that if any of the concepts require a significant amount of power, either a shift in power distribution will be necessary or an external power source must be consulted. As this power source will also have a mass, this mass was documented in the total mass distribution of the specific concepts after the more elaborate calculations.

Table 2.2: Top-level power budget breakdown for final product.

Concept	Power change [W]	Concept	Power change [W]
Chevrans	3,000	Sharkskin	0
Winglets	2,000	LE suction	3,000
FishBAC	1,000		
		Total	9,000

As can be seen from Table 2.2, a significant amount of extra power was required to supply all the actuators of electricity. Therefore, an external power source was necessary. This was investigated for each of the concepts, if the final design for those specific concepts still requires an actuator.

2.4.3. Aerodynamic Performance

As aerodynamic performance is a favourable resource, so long as it does not hinder other important parameters, it is hard to state a maximum allowable value. The aerodynamic performance will be expressed in a percentage of fuel reduction, as the requirements state that a 7.5% fuel reduction will have to be achieved after applying the retrofit

concepts to the wing. The decision was made to set a minimum value instead of a maximum value, to make sure the requirements were met. This way budget updates will give an indication whether or not the requirement will still be met, whereas any extra fuel reduction will always be beneficial, as long as it does not hinder other parameters (e.g. fuel reduction by adding a particularly heavy system that increases maximum take-off weight (MTOW) significantly). It made sense to put the minimum value at 7.5%, as this was a requirement of the final product. The change in fuel consumption for each individual concept can be found in Table 2.3.

Table 2.3: Top-level performance budget breakdown for final product.

Concept	Performance change [%]	Concept	Performance change [%]
Chevrons	0	Sharkskin	4
Winglets	8	LE suction	10
FishBAC	8		
		Total	30

As can be seen in Table 2.3, the combined total fuel reduction of the individual concepts exceeded the 7.5% by a significant amount. However, as it was yet unknown how the concepts interact with each other when they are all implemented onto the wing, this fuel reduction percentage will most likely decrease after a full aircraft analysis has been conducted. Another important note is that these percentages were obtained from literature and often the studies conducted in these papers differ significantly from the case that is being investigated in this report. The last thing that must be mentioned is that these percentages show improvement with respect to no concept. As there was already a winglet present on the Airbus A330, the increase in performance due to the new morphing winglet might not be as high as estimated from the research papers. It was important to reassess the performance breakdown after the full aircraft analysis has been conducted, to check whether or not the final product still met the requirements and was within the set boundary.

2.4.4. Noise

Another technical resource that is essential for the final product was the noise emission. During the literature review it was found that the only concepts that cause a noise reduction or increase are the chevrons and the FishBAC flaps. It was found that the other concepts have a negligible contribution to the noise emission. As noise behaves the same as the aerodynamic performance regarding the maximum allowable value, it was hard to state a boundary value. As the requirements state that a 6.5% reduction in noise emission should be achieved, it made sense to set the minimum allowable value on 6.5%. This meant that any further decrease in noise was an additional benefit, as long as no other resources were penalised. The estimated change in noise due to the different concepts can be found in Table 2.4.

Table 2.4: Top-level noise budget breakdown for final product.

Concept	Noise reduction [dB]	Concept	Noise reduction [dB]
Chevrons	3	Sharkskin	~0
Winglets	~0	LE suction	~0
FishBAC	~1		
		Total	4

As the noise requirement was stated as a percentage and literature quantifies the noise levels in decibels (dB), a calculation had to be done in order to convert the percentage requirement to a decibel requirement. In this way it can easily be assessed whether or not the final product will meet the requirement. Therefore it is not known yet if the total amount of dB in Table 2.4 will meet the noise requirement. A more accurate noise estimation for all concepts must be conducted, after which the full aircraft will be analysed to obtain a conclusion regarding the noise requirement.

2.4.5. Cost

The last non-technical resource that was evaluated and discussed is the cost. A cost budget has already been established in the midterm report [2], together with approximations for the cost of the different concepts. However, these cost estimations also included development costs and other costs not related to the direct implementation of the specific concept. Therefore, slight adjustments were made regarding the values obtained from the midterm report. The values shown in Table 2.5 represent the cost required to implement the concept onto the wing, from the machined materials to the man hours necessary for the integration process. The maximum allowable value depends on the aircraft age, however, for simplification a brand-new aircraft will be used a guideline (i.e. age is zero years). In this case, the maximum allowable value for cost comes down to \$45.3M [2].

As can be seen in Table 2.5, the total cost was significantly below the maximum allowable cost. This meant that, in the case of a new aircraft, money is available for further development and research of other potential concepts. If an

Table 2.5: Top-level cost budget breakdown for final product.

Concept	Cost [\$M]	Concept	Cost [\$M]
Chevrons	1	Sharkskin	0.5
Winglets	5	LE suction	5
FishBAC	3		
		Total	2,200

aircraft is older, less money will be available for a retrofit, which could be to the extent where certain concepts cannot be purchased. In this case only several of the five concepts were applied to the aircraft to still satisfy the customer, of which the marketing strategy has been discussed in Section 2.3.

2.5. Concept Trade-Off Process

In order to obtain the concepts that will form the final design, a trade-off was conducted and documented in the mid-term report [2]. A preliminary concept elimination discarded non-feasible concepts; the elaborate trade-off resulted in five concepts that were investigated in this report to gain more accurate specifications of the final design.

Before this trade-off was conducted, several trade-off criteria and weights were set up. The justification of the chosen trade-off criteria and weights can be found in the mid-term report [2]. With all necessary tools available to assess the remaining concepts, trade-off tables could be constructed that contained the results for each concept. These trade-off tables can be found in Appendix B. The five chosen concepts that form the final design are the following:

- LE suction,
- winglet retrofit,
- FishBAC flaps,
- chevrons and
- sharkskin.

The justification behind these concept choices can be found in the mid-term report, together with a sensitivity analysis that assesses the validity of the trade-off tables [2].

2.6. Sustainable Development Strategy

The dictionary definition for sustainability is given as “*the quality of not being harmful to the environment or depleting natural resources, and thereby supporting long-term ecological balance*”⁸. Following this definition, complete sustainability is achieved when the product is not in any way harmful to the environment and does not consume any natural resources. Due to the fact that prototypes will have to be manufactured and tested, ‘pure’ sustainability will most likely not be possible within the near future. However, in the specific case of the smart retrofit wing, it is said that sustainability is achieved when, after retrofitting the product, it leads to a reduction in emission and depletion of natural resources over the total lifetime of the aircraft when compared to the technology that is currently being used. The sustainability approach and indicators of positive sustainability traits will be explored in this chapter.

2.6.1. Sustainability Approach

As it is essential to take sustainability into account during the different phases of the product lifetime, a division was made to clearly obtain an overview. These phases are visualised in Figure 2.2, where the areas of focus are also established and summarised for each phase.

Design and Certification

During the design process, sustainability was taken into account if non-toxic materials were chosen or if a marketing strategy is chosen that focuses on sustainability. As the product of a design process is often heavier than estimated during the early design phase, it was essential to design for low mass. The reason for this lied in the fact that a heavier aircraft requires more lift, which means more drag will be present. This drag had to be countered by an increase in thrust and thus the fuel consumption will also increase, again resulting in a heavier aircraft. This snowball effect had a negative impact on the sustainability, as more fuel will be burnt and thus NO_x and CO₂ emissions will significantly increase. As the design goal of this project was to achieve a significant decrease in fuel consumption, noise and greenhouse gas emissions, concepts were chosen that primarily focus on these parameters. Another aspect related to sustainability was the certification of specific components. As certification often requires excessive testing, it would not be a sustainable approach if this testing might be unnecessary. This could be the case when other options are present that achieve similar results, but have already been certified.

⁸URL <http://www.dictionary.com/browse/sustainability?s=t> [cited 26 April 2017].

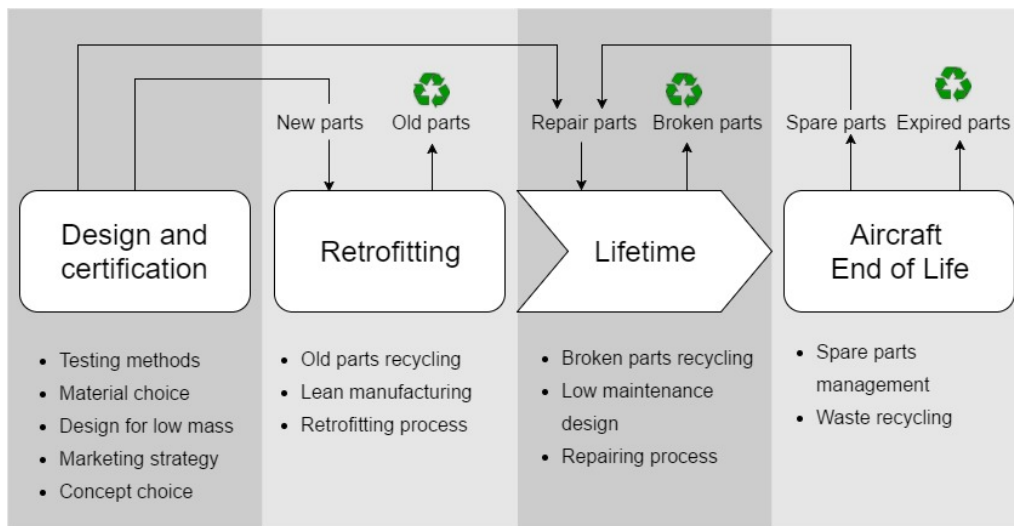


Figure 2.2: Sustainability diagram highlighting focus areas for every lifetime phase of a retrofitted part.

Retrofitting Process

With regard to the retrofitting process, sustainability was taken into account when parts were designed that can easily be recycled. Parts and components that can be recycled mean minimal or zero waste will be present, which is beneficial for the environment. However, as during the retrofitting process one can only account for sustainability to a limited extent, another approach has to be consulted. During the manufacturing process, every task which does not add to the value of the part must be minimised as much as possible. This approach is known as lean manufacturing.

Lifetime and Operations

During the lifetime phase, the major focus is set on operations, maintenance and reliability. By designing a more efficient aircraft, and thus reducing the fuel consumption, the noise as well as the NO_x and CO₂ emissions will be reduced significantly. An aspect closely related to the operational phase was that of maintenance and reliability. By designing and implementing the concepts in such a way that they require a minimum amount of maintenance over a prolonged period of time, maintenance man hours could be kept relatively low. When aircraft are brought in for maintenance due to damage of certain components, it would be beneficial if these component could be recycled. As composite structures are often not recyclable, the use of them was limited to a certain extent, however, they are also lightweight and might reduce the fuel consumption to a greater extent to counteract the negative aspect.

Aircraft End of Life

It was possible that the retrofit components have a longer lifetime than the aircraft itself, which means they could be utilised as spare parts for repairs on other aircraft, or even as a cheaper alternative retrofit option [7]. This can be the case with composite structures because, as already mentioned, they are often not recyclable.

2.6.2. Indicators

During the assessment of sustainability, several indicators can be determined. Each indicator provides, to a certain extent, a measure of sustainable development. Following the definition of sustainability that was presented earlier this chapter, sustainability was achieved by reducing two factors: fuel usage and emission. However, there are empirical relations that relate these two parameters to each other, which means they can effectively be seen as one parameter. The indicators that have the largest impact on sustainability are presented below.

Lift-To-Drag Ratio

Since it was assumed that the the retrofit does not significantly increase the aircraft weight (and thus the required lift), drag is the biggest contributing factor. When developing a sustainable retrofit for the wing, outperforming the reference aircraft was aimed for. This is because drag directly translates into required thrust. If the retrofitted aircraft would not outperform the baseline aircraft, there would be no incentive for the customer to buy the product. Finally, the increased emissions during the design and certification phase should be compensated for in later life cycle phases in order to make the product sustainable. Thus, at a certain aircraft weight (and thus lift), the lift-to-drag ratio was designed to be higher for the newly developed product.

Mass

There is a direct correlation between aircraft mass and required thrust. Therefore it was desirable to keep the aircraft weight to a minimum. This meant that the mass of the newly developed product should at most be equal to the mass of the current Airbus A330. There is a strong relation with the lift-to-drag ratio: when a significant increase is achieved in one aspect, it might not be necessary to achieve an improvement in the other.

Waste

The waste aspect can be divided into two categories. First, excess materials can be present that have to be discarded, whereas on the other hand waste can be identified in the context of lean manufacturing. Here, anything that does not add value to the product was considered waste and decreases sustainability. For example, when transport is not optimised during the design phase, unnecessary emissions will be present.

2.7. Risk Analysis

At the start of the design process for the individual retrofit concepts a preliminary technical risk identification was performed. The approach to how risks are handled during the design process and the technical risks that might occur during the development of the product will be presented in this section.

Risk Approach

Technical risks may have the consequence that technical performance requirements, schedule requirements or cost requirements are not met. Keeping this in mind, it was crucial that risks were properly identified at the start of the design process and updated regularly. Before starting the preliminary design phase, all main risks were identified and incorporated in a risk map, which can be found in Figure 2.3a. The risks that appear in the red zones were paid special attention to during the preliminary design. The identification of high risks affected the approach of the preliminary design: special attention was paid to the high risk aspects, so that it was clear as soon as possible if the risk could be mitigated or if it turned out to be a killer for the concept. The approach for risk management was to cross out all risks that are not of importance anymore during the preliminary design process and add new risks once they become apparent. This resulted in two risk maps: one for the start of the preliminary design process, which can be found in Figure 2.3a, and one for the end, which can be found in Figure 2.3b. It can be seen that the second risk map has almost no high risks anymore, as desired.

All technical risks that were identified are elaborated upon below. Each risk was assigned a specific code, in which the categories affected are indicated with a letter. A risk map is presented in Figure 2.3a. Behind each risk, letter codes indicate to which concept (or concepts) the risk applies. The retrofit concepts are indicated with letters: sharkskin (S), chevrons (C), winglets (W), suction (Su) and FishBAC (F). The following categories are considered:

- Cost risks (C)
- Schedule risks (S)
- Technical performance risks (T)

Cost and Schedule Risks

- CS1** The aircraft has to be recertified. Making large changes to the current wing might impose the need for recertification, which is expensive and time-consuming. The probability of recertification is moderate for winglets, suction and FishBAC, as these come with considerable modifications to the current wing design. For sharkskin and chevrons occurrence is unlikely, as neither requires significant alterations to the wing. Should recertification be required, its impact on both cost and schedule is high.
- CS2** The aircraft regulations related to the product are changed. This may result in the need for design alterations, which affects both cost and schedule. It is however very unlikely that this will occur, as changes to the regulations will apply to all aircraft currently in operation. Therefore, any changes in regulations will not be such that they require extensive design modifications. The impact of this risk is thus medium at most for all concepts.
- CS3** The retrofitting process takes longer than expected. This risk has an effect on both schedule and cost, as the aircraft will be out of service longer and more man hours will have to be paid. For the winglets, suction and FishBAC it is likely that this will happen, because significant alterations will have to be made to the wing. It is expected that the probability of occurrence for this risk will reduce over time, corresponding to the learning curve of the assembly team. It is unlikely that retrofitting will take too long for the sharkskin and the chevrons, as the required alterations are less complex than for the other three concepts. For all concepts, occurrence will have medium impact.
- CS4** Due to a low technology readiness level (TRL) of the concept a lot of additional research and testing is needed after the duration of the project. Since a lot of development is required for concepts with a low TRL, this risk affects both cost and schedule. The TRL of the different concepts was identified during the concept trade-off in the midterm report [2]. Corresponding, occurrence is likely for the FishBAC, moderately likely for suction and winglets and unlikely for sharkskin and chevrons. For winglets, suction and FishBAC the impact of a low TRL is high, as these are all complex systems which will require a lot of testing. In case of a low TRL for sharkskin and chevrons the impact is medium, as the systems are less complex (especially sharkskin, which is just a coating) and will thus not require as much testing as the other concepts.

Cost Risks

- C5** The retrofit results in changes in stability and control of the aircraft and thus extra pilot training. This is obviously a cost risk, as these trainings must be paid for by the airline. It is highly likely that this will happen for

the winglets, suction and FishBAC, where significant weights are both introduced and removed from the wing, whereas for sharkskin and chevrons it is unlikely. Regardless of the potential change in stability and control, some amount of training will be unavoidable as the pilot will have to get acquainted with the new actuator controls. Impact of this risk is low, as training costs will be insignificant compared to the price of the total retrofit.

- C6** The interaction between system and pilot is complex. When designing complex systems, it is highly likely that this will include complex controls. The pilot will have to get acquainted with these controls, which will mean higher training costs for more difficult control systems. This risk is applicable to the winglet, suction and FishBAC; neither sharkskin nor chevrons requires active actuation from the pilot. Impact of these costs is low: as stated before, they will be negligible compared to the total retrofit cost.

Technical Performance Risks

- T7** No materials are available which achieve the desired performance. This might be the case when, for example, a material is required to accommodate bending but should also be very stiff to resist loads, or when excessive deformations are required for which no material is flexible enough. Occurrence of this risk is unlikely for sharkskin, chevrons and suction. All of these concepts have been tested, or are being used, on operational aircraft. Moreover, none of these concepts encompass large bending deformation. Since the latter is not the case for the winglets and FishBAC, occurrence is moderately likely for these concepts. Should no suitable materials be available, impact will be high for sharkskin, chevrons and suction and catastrophic for winglets and FishBAC. The latter two are expected to yield the largest aerodynamic performance improvement. Therefore, if either of these concepts cannot be developed the project requirements will probably not be met.
- T8** No suitable actuator is available for the retrofit component. Obviously, this risk does not exist for the sharkskin. All other concepts use actuators, for which a sufficient output force is required. In case of the winglets, a two-dimensional actuator is required. If no suitable actuator is available, a result is that the concept cannot be developed. For chevrons it is unlikely that this will happen, for winglets and FishBAC it is moderately likely and for suction it is likely. Impact is catastrophic for winglets and FishBAC, whereas it is high for chevrons and suction. This is in line with **T7**, as both risks result in the fact that the concept cannot be developed.
- T9** A potential weight increase is not compensated for in aerodynamic performance. This includes any modifications to the wingbox that might be necessary. A weight increase is not detrimental, as long as it is compensated by the aerodynamic performance increase and thus yields a reduction in fuel used (or, in case of the chevrons, a reduction in noise emitted). Occurrence of this risk has a catastrophic impact for the winglets, suction and FishBAC, as these concepts are expected to be the largest contributors to aerodynamic performance improvement. If this risk occurs for any of these three concepts, the probability is high that the retrofit package will not meet the project requirements. Impact is medium for sharkskin and chevrons. Since the sharkskin coating will have a thickness of about 1 mm, the weight penalty will never be high. Moreover, it is not the largest contributor to aerodynamic performance improvement. For chevrons, only a small amount of weight will be added as well. Occurrence is unlikely for sharkskin, chevrons and the FishBAC (the actuation mechanism is expected to be much lighter than the currently used system) and likely for winglets and suction.
- T10** A retrofit component fails. This risk is not applicable to the sharkskin: apart from wear out over time, no sudden failure will occur to the coating. For the other concepts failure is moderately likely, as each concept comprises actuators, but none of these actuation mechanisms is too complex. Impact is low for chevrons, winglets and suction: the aerodynamic gain will be lost, but the aircraft will still be able to fly and land safely. For the FishBAC however, the impact of failure is catastrophic. Complete failure of the system would mean that the trailing edge high lift devices are no longer controllable.

Updating Risk Map

During the preliminary design process, new risks were identified and risks which were already identified were mitigated or simply not relevant anymore. The new risks that arose are described below. The updated risk map is presented in Figure 2.3b.

- T8 Suction.** This risk has, amongst other risks, caused the LE suction concept to be discarded. The actuator needed for suction is too heavy.
- T9 Suction.** This risk has, amongst others, caused the leading suction concept to be discarded. The performance increase does not compensate for the major weight increase as has been found by calculations.
- CS3 Suction.** This risk has, together with the aforementioned two risks, caused the LE suction concept to be discarded. The retrofit process includes the creation of countless tiny holes, which have to be made by a laser. After analysis it turned out that this takes more than 200 days, which is catastrophic for this concept.
- T11 Winglets.** The drag performance of the current wing with a retrofit winglet is not accurately assessed, which leads to a non-optimal design choice. The program used for aerodynamic analysis of the wing with retrofit winglet only incorporates induced drag in its calculations, other forms of drag (reductions) have to be theoretically assessed. There is no well-known method for these calculations: in reality, most performance assessment is done through windtunnel or flight tests.

Impact	Catastrophic	T9 (F)	T7 (W,F) T8 (W,F) T10 (F)	T9 (W,Su)	
	High	CS1 (S,C) T7 (C,S,Su) T8 (C)	CS1 (W,Su,F) CS4 (W,Su)	CS4 (F) T8 (Su)	
	Medium	CS2 (All) CS3 (S,C) CS4 (S,C) T9 (S,C)		CS3 (W,Su,F)	
	Low	C5 (S,C)	T10 (C,W,Su)		C5 (W,Su,F) C6(C,W,Su,F)
		Unlikely	Moderately likely	Likely	Highly likely
		Probability			

Impact	Catastrophic	T8 (F) T9 (W)	T7 (W,F) T8 (W) T10 (F)		T8 (Su) T9 (Su) CS3 (Su)
	High	CS1 (S,C) T7 (C,S,Su) T8 (C)	CS1 (W,Su,F) CS4 (W,Su) T13 (S) CS4 (F)		
	Medium	CS2 (All) CS3 (S,C) CS4 (S,C) T9 (S,C)	T12 (S) T15 (C) T16 (F) T17 (W) CS3 (W,F)	T11 (W, Su)	
	Low	C5 (S,C)	T10 (C,W,Su)		C5 (W,Su,F) C6(C,W,Su,F)
		Unlikely	Moderately likely	Likely	Highly likely
		Probability			

(a) Preliminary risk map.

(b) Risk map after mitigation, including new risks.

Figure 2.3: Technical risk map before (a) and after (b) risk mitigation.

- T11 Suction.** The drag performance of the current wing with a retrofitted suction system is not accurately assessed, which leads to a non-optimal design choice. The resources available during the project did not allow to use accurate calculation methods for the aerodynamic analysis.
- T12 Suction.** The component life of LE skin is less than expected, due to the lack of resources to extensively analyse fatigue of the perforated titanium skin.
- T13 Suction.** Performance of the Krueger flap is insufficient. It might be too heavy, not reach the same aerodynamic performance as slats or it might be too big such that it is not possible to integrate into the wing. Further research is needed in this area.
- T15 Chevrons.** The performance characteristics are worse than expected. The chevrons might weigh more, negatively affect the performance of the aircraft more, decrease noise less or use more electricity than expected.
- TC16 FishBAC.** In case of failure of a component of the FishBAC it will be required to replace to entire FishBAC. This is due to the difficulty of reaching components within the FishBAC: most likely, components are connected with chemical bonding or welding.
- T17 Winglets.** The bending moment will not be most critical at the root, but at another location along the span of the wing. The leading design constraint on which the design choice is based is the maximum root bending moment: the maximum bending moment is not analysed at other span-wise locations on the wing. This could be a risk, since the area of the stringers is varying along the span of the wing. In addition to this, other factors play a role, such as the location of the fuel, engine and landing gear.

The following risks were mitigated or are not relevant anymore:

- CS3 Winglets, Suction and FishBAC.** This risk is mitigated by detailed research on the retrofit process. Details about the A330 maintenance processes are researched, which this ultimately leads to a good approximation of the retrofitting process.
- CS4 FishBAC.** This risk is partially mitigated by careful assessment of the feasibility of this concept. Aspects such as the performance of a FishBAC compared to the performance of the current flaps were extensively researched. This risk cannot be entirely mitigated, since extensive testing is still needed for the FishBAC.
- T7 FishBAC.** This risk is entirely mitigated for the FishBAC. Suitable materials have found for the FishBAC design for all the components.
- T8 FishBAC.** This risk is mitigated for the FishBAC. After researching, it was found to be quite unlikely that there will be no suitable actuator available for the FishBAC. However, the risk is not entirely discarded since a more detailed design of the actuator still needs to be established. During this process, new findings might arise.
- T9 FishBAC.** This risk can be entirely discarded for the FishBAC. Through calculations, the weight of the FishBAC has been compared to the weight of the current flaps. The FishBAC is significantly lighter, mostly due to the use of composite material for the beam.
- T9 Winglets.** This risk is mitigated for the winglet concept. To mitigate this risk, certain constraints regarding the required reinforcements were stated before making design decisions. An excessive increase in (bending) loads, which would require excessive wingbox reinforcements, was avoided.

As the five concepts that form the final design have been selected in the midterm report [2], they will have to be designed and analysed to a more detailed extent in order to obtain valuable results to check whether or not the final product meets the requirements. First, the design load cases which are going to be used during the design will be established. Then the design of the chevrons, winglets, FishBAC, sharkskin and leading edge suction system will be elaborated upon in Sections 3.2 to 3.6. For each concept, the respective section will describe the design choices that were made, the performance results that were calculated and the conclusions that were drawn regarding whether or not applying the design is beneficial to the current Airbus A330.

3.1. Design Load Cases

The first step in the structural analysis of every section of the aircraft was the identification of critical load cases for which the sizing process could be run. The critical load cases are often found in the outer edges of the flight envelope, as well as some extraordinary aircraft operations. All cases have been plotted in the so-called 'load potato'. The load potato can be seen in Figure 3.1: on the x-axis the root bending moment is plotted and on the y-axis the root shear force. To analyse the most critical situations, the critical load cases in occurrence of a gust are also implemented into the load diagram. The load cases which were considered can be found below, all cases assume a flat-lying winglet, since this is the most critical loading situation.

- MTOW at 2.5G lift.
- MTOW at 1G lift during a gust.
- No lift, hard landing (2G landing).
- Zero fuel, 2.5G lift.
- Zero fuel, 1G lift during a gust.
- Dive speed at low altitude.
- High altitude take-off.
- High altitude take-off during a gust.
- Low altitude take-off.
- Low altitude take-off during a gust.
- Cold temperature take-off or landing.
- Hot-temperature take-off or landing.
- Maximum flight velocity at cruise altitude with a gust.
- Maximum flight velocity at moderate altitude with a gust.

As can be seen in the load case overview, many of the cases included the evaluation of a gust. Gusts can take stable and otherwise uneventful flight phases and transform them into critical, structurally threatening cases. Gusts, however, have the added disadvantage of being hard to predict, both in strength and moment of occurrence. In order to aid designers and ensure uniform aircraft strength minima, regulatory bodies have introduced reference gust levels. Below an introduction into the European Aviation Safety Agency (EASA) method, as published in CS-25, is given[8].

CS-25 states that an aircraft's maximum anticipated gust level is a function of aircraft design masses, as well as the altitude at which an aircraft flies. The reference gust speeds are set at fixed altitudes by EASA and should be linearly interpolated between. Equation (3.1) from CS-25[8], shows the method in its mathematical form, from here one can observe the relationship between aircraft parameters and the gust speed.

$$\left\{ \begin{array}{l} \text{gust speed} = \frac{\text{design gust speed}}{2} \left[1 - \cos\left(\frac{\pi S}{H}\right) \right], \quad \text{where } S \text{ ranges from } 0-2H \quad (3.1a) \\ \text{design gust speed} = \text{reference gust speed} \cdot F_g \left(\frac{H}{350}\right)^{\frac{1}{6}}, \quad \text{where } F_g = \frac{F_{gz} + F_{gm}}{2} \quad (3.1b) \\ F_{gz} = 1 - \frac{Z_{mo}}{250000}, \quad F_{gm} = \sqrt{R_2 \tan\left(\frac{\pi R_1}{4}\right)}, \quad \text{where } Z_{mo} \text{ is the maximum achievable altitude in feet} \quad (3.1c) \\ R_1 = \frac{\text{Maximum landing weight}}{\text{Maximum take-off weight}}, \quad R_2 = \frac{\text{Maximum zero fuel weight}}{\text{Maximum take-off weight}} \quad (3.1d) \end{array} \right.$$

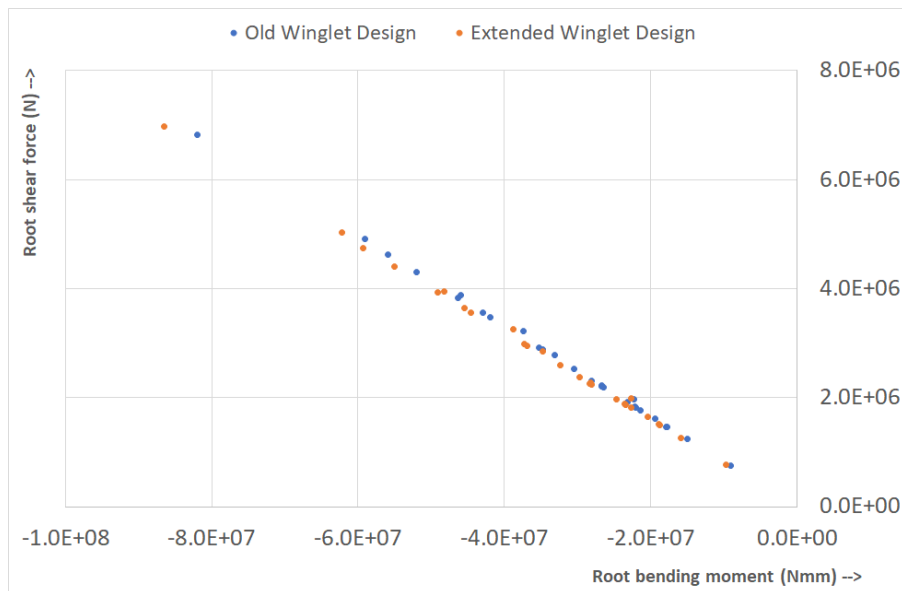


Figure 3.1: Load 'potato' for the design cases.

Once the worst case gust speed was known, the influence this has on the aircraft in the form of an additional perceived angle of attack was calculated. The additional worst case angle of attack stemmed from the assumption that the gust speed will be perpendicular to the direction of flight and a simple geometrical evaluation. Two cases stood out as the clear ultimate load case for the original winglet. This load cases, the maximum flight velocity at moderate altitude and high altitude with a gust, posed the highest bending moments, as well as the highest shear forces. In order to ensure complete safety in the design, a safety factor was placed on top of the loads in order to ensure that no failure would occur due to assumptions and uncertainties inherent to any modelling process.

3.2. Chevrons

In this section, the variable geometry chevrons (VGC) will be discussed. These chevrons are triangular plates at the end of the thrust-reverser sleeve. They help with the controlled mixing of the exhaust air and the ambient air [9]. In Figure 3.2a the thrust-reverser sleeve can be seen with the chevrons, while in Figure 3.2b they can be seen installed on a Boeing 777-300ER.



(a) Thrust-reversers sleeve¹.



(b) VGC installed on engine.

Figure 3.2: Variable geometry chevrons installed on Boeing 777-300ER.

Their main purpose is to decrease the noise emission during take-off and approach. Non-variable chevrons have already been successfully applied to the Boeing 787 Dreamliner. These come with a performance penalty though, because they are a compromise for cruise, approach and take-off conditions. Therefore, variable geometry chevrons are more ideal, as they can alter their shape during approach, take-off and cruise, lowering or eliminating the performance penalty. This concept was already successfully tested in-flight, on the Boeing 777-300ER depicted in Figure 3.2b.

3.2.1. Aerodynamics

In this section the aerodynamic performance of the chevrons will be discussed. This includes not only implications on performance, but also on noise. For this, data gathered from scientific articles was used. This was chosen over a possible simulation or test. A simulation was not deemed viable, as noise simulations are complicated and not

¹URL http://www.boeing.com/news/frontiers/archive/2006/march/photos/march_i_tt_2.jpg [cited 11 May 2017].

yet robust enough. For example, one of the noise codes available, FLIGHT, does not have a high enough resolution for the code to see the differences between setups. Most codes use very strict models for the engine, which cannot be altered^{2,3}. To get representative results, both a computational fluid dynamics (CFD) and computational aeroacoustics simulation would be required, which goes too far for the purpose of this project. A test was not viable, because there were no facilities available in which a model could be tested accurately enough. For the final phase of the design, a flight test was advised to get accurate results. Within this report, data from literature were sufficient to obtain a first order estimate on noise reduction.

It was found that as the chevron immersion increased, the low-frequency noise decreased. This, however, did come with an increase in high-frequency noise. This high-frequency noise was due to increased turbulence levels near the nozzle [9]. Therefore, to optimise for aircraft noise, the best balance between a decrease in low-frequency noise and an increase in high-frequency noise would need to be found. High-frequency noise will have the highest impact on the environment during take-off, as during cruise most of the high frequency-noise gets absorbed by the atmosphere⁴.

For this, a different chevron design was advised [10–12]: the azimuthally varying chevron (AVC). AVCs are larger close to the the engine pylon, as can be seen in Figure 3.3. This was done because the engine pylon leads to an asymmetric flow. This asymmetric flow then leads to an asymmetric interaction of the jet exhaust with the wing. All of this has a negative effect on the acoustic properties of the aircraft [13].



Figure 3.3: AVC installed on the Quiet Technology Demonstrator 2 airplane by Boeing [9].

As can be seen in Figure 3.3, the shape of the chevrons changes azimuthally. With this, a reduction in noise of up to 2 dB in the low-frequency range was found, at a set take-off power setting [9]. This test was performed using actual flight tests with engines with- and without the AVC, using far-field microphones. Here, corrections were used for atmospheric conditions and for velocity differences, due to possible gusts or other wind conditions. These results correspond with the results found by other researchers, who found a reduction in overall sound pressure level of 2 to 3 dB [14]. Therefore, for this stage in the design process, a 2 dB reduction in far-field noise was assumed.

Using the same test piece, the researches later found that there was a reduction in low-frequency noise of up to 5 dB on the outer fuselage skin and up to 2 dB in the cabin [13]. They also found that there was a loss in thrust coefficient of less than 0.05% in cruise, using their fixed AVCs. Therefore, as most mixing is done by the chevrons near the engine pylon, it was possible to only have a certain amount of chevrons to be variable geometry chevrons, namely the larger ones near the pylon, as they will be responsible for most of the loss in thrust coefficient. With this, the weight and complexity of the complete system were minimised.

The previously mentioned test flights were all performed using a General Electric GE90-115B jet engine. The A330 has a Pratt and Whitney PW4168A. Therefore, to get a more accurate first-order estimate, the results found for the General Electric needed to be scaled to the PW4168A [15, 16]. This was also outside of the scope of this report, as it requires parameters currently not known.

3.2.2. Structures

Regarding the structural aspect, a simple fatigue analysis will be conducted, after which the additional mass due to the chevrons will be computed. As the thrust-reverser sleeve will be replaced by one that contains only minor changes, no additional structural analysis is performed. Fatigue of the chevrons was considered important, as they need to flex and unflex at least twice every flight. The chevrons have two flexing components, the NiTiNol plates and the fibreglass composite cover. NiTiNol has excellent fatigue properties, partly due to its shape memory characteristics [17, 18].

²Private communication, Antonio Filippone [19 May 2017 10:00].

³Private communication, Abhishek K. Sahai [13 June 2017 12:00].

⁴Private communication, Abhishek K. Sahai [22 May 2017 10:00].

For the fibreglass composite covers, also acceptable fatigue properties were found. The failure sequence in bending of fibreglass composite is also known [19]. First there will be nucleation, with grain growth of the superficial damage. Then the longitudinal matrix will start cracking, the fibres will break, and finally there will be delamination. Hence, any fatigue failures of the chevrons will be able to be prevented by simple inspection. If the chevrons do fail, it will not be a catastrophic failure. This will lead to an increase in noise, and possibly fuel consumption. It is not expected, though, that any other damage will occur, as the chevrons are located near the exhaust of the engine. This means they will not be sucked into the engine and possibly damage the engine beyond repair.

Weight

As the thrust-reverser sleeve would be taken off the aircraft and the retrofitted sleeve would not necessarily have a different area, it was assumed that the weight of the raw new sleeve does neither increase nor decrease. This indicates that the only addition of weight was due to the attached parts and components that are necessary to activate and control the VGCs. These components are summarised below:

- carbon composite substrate,
- Shape memory alloy (SMA) actuators and
- electrical wiring, control system, sensors and power supply.

Carbon Composite Substrate

The weight of the carbon composite substrate could be approximated if one knows the dimensions of each chevron, the amount of chevrons present at the trailing edge of the thrust-reverser sleeve and the density of the used material. As it was extremely complicated to design chevrons specific to the Airbus A330, the chevrons of the Boeing 777 test aircraft were used as a reference [20]. These chevrons contain a carbon composite substrate that is 59.7 cm wide (23.5") and has a chord length of 35.5 cm (14"). This carbon composite substrate is visualised in Figure 3.4.

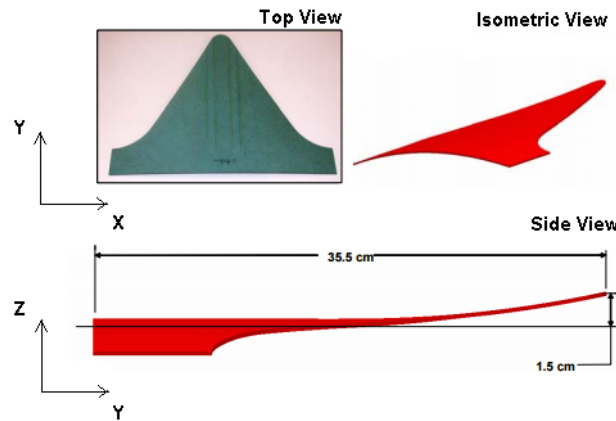


Figure 3.4: Chevron carbon composite substrate dimensions [20]

If the radius of the trailing edge of the thrust-reverser sleeve was assumed to be roughly 1.5 m [20, 21], it was possible to calculate the amount of chevrons present on each sleeve. According to the calculation, this radius corresponded to 16 chevrons on each thrust-reverser sleeve.

Since the amount of chevrons and the surface area of the chevrons were known, only two parameters remained to calculate the weight addition of the carbon substrates: the thickness and the density of the material. With the thickness assumed to be 0.2 cm [20] and the density obtained through literature⁵, one could easily obtain the mass increment due to the substrate. The result can be found in Equation (3.2).

$$\begin{cases} m_{CS} & \approx \frac{1}{2} \cdot l \cdot w \cdot t \cdot \rho & (3.2a) \\ m_{CS} & \approx \frac{1}{2} \cdot 35.5 \cdot 59.7 \cdot 0.2 \cdot 1.55 & (3.2b) \\ m_{CS} & \approx 328.5 \text{ g} = 0.329 \text{ kg} & (3.2c) \\ m_{CS_{tot}} & = 0.329 \cdot 32 = 10.5 \text{ kg} & (3.2d) \end{cases}$$

However, as the final design used azimuthally varying chevrons, the total mass addition would be lower than the value that was found. Therefore, in the case of the mass approximation, each subsequent chevron would have a surface area of 10% smaller than the first, starting at the top chevrons. This assumption resulted in a different mass addition, of which a calculation can be found in Equation (3.3).

⁵URL <http://www.clearwatercomposites.com/resources/Properties-of-carbon-fiber> [cited 12 June 2017].

$$m_{CS_{tot}} \approx \sum_{n=0}^7 0.329 \cdot (1 - 0.1 \cdot n) \cdot 2 = 3416.4 \text{ g} = 3.42 \text{ kg} \quad (3.3)$$

SMA Actuators

As for the additional mass due to the SMA actuators, the same actuators will be used as were used on the Boeing 777 test aircraft [20]. However, as these actuators were quite large and the chevrons get smaller as one progresses from the top to the bottom of the trailing edge cross-section, the actuators would only be placed on the six chevrons present at the top. As the small and wide chevrons near the bottom would be hard to move, no actuation mechanism and SMAs will be present on these specific chevrons.

With a density of 6.7 kg/m^3 for 60-NiTiInol [22] and the dimensions of the actuator known [20], it was possible to calculate the weight addition due to the SMAs. The result can be found in Equation (3.4).

$$\left\{ \begin{array}{l} m_{act} = 3 \cdot (25.4 \cdot 3.8 \cdot 0.295) \cdot 6.7 \\ m_{act} = 572.3 \text{ g} = 0.57 \text{ kg} \\ m_{act_{tot}} = 6 \cdot 0.57 \cdot 2 = 6867.8 \text{ g} = 6.9 \text{ kg} \end{array} \right. \quad (3.4a)$$

$$\left\{ \begin{array}{l} m_{act} = 572.3 \text{ g} = 0.57 \text{ kg} \\ m_{act_{tot}} = 6 \cdot 0.57 \cdot 2 = 6867.8 \text{ g} = 6.9 \text{ kg} \end{array} \right. \quad (3.4b)$$

$$\left\{ \begin{array}{l} m_{act_{tot}} = 6 \cdot 0.57 \cdot 2 = 6867.8 \text{ g} = 6.9 \text{ kg} \end{array} \right. \quad (3.4c)$$

Auxiliary Power Unit

The only component of the VGC remaining was the electrical actuation system. This included the electrical wiring, the power supply and the necessary control systems and sensors. The power required to heat up the three NiTiInol strips and thus to actuate the chevrons can be found in Figure 3.5.

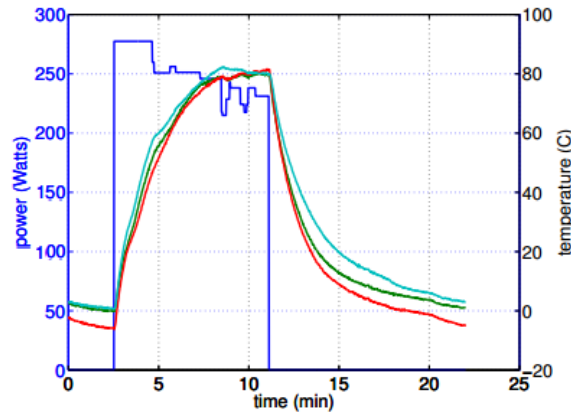


Figure 3.5: Behaviour of SMA actuators after power input [21].

The power to actuate one chevron was calculated to be roughly 275 W, as can be seen in Figure 3.5. As 12 chevrons would be present on the thrust-reverser sleeves, a total of 3,300 W will be required to change the chevron geometry. During boarding, this power is available to heat the NiTiInol for take-off and thus this high power requirement poses no problem. However, in order to transfer this power, adequate cables will have to be present that can deal with the temperature of the engine. Since the spanwise distance from the nacelle to the fuselage is about 9.5 m [23], the amount of cables and wiring required was estimated. An extra wire was necessary to transfer the control input from the cockpit to the power supply, which was calculated to be roughly 23 m long⁶. As each chevron contains 3 actuators and there are 6 variable chevrons present on each thrust-reverser sleeve, 36 cables will go from the power supply to the chevrons themselves. A last wire will go from the cockpit to the power supply to give an input signal to actuate the chevrons, which is roughly 23 m long. As very little information is available regarding the size of the cables and wiring, a diameter of 4.3 mm was assumed, which has a corresponding cable density of 64.5 g/m [24]. The result of the rough estimate regarding the weight addition of the electrical actuation system can be found in Equation (3.5).

$$\left\{ \begin{array}{l} m_{PU} = (9.5 + 9.5) \cdot 64.5 \\ m_{PU} = 1,225 \text{ g} = 1.225 \text{ kg} \\ m_{PU_{total}} = 1.225 \cdot 3 \cdot 6 \cdot 2 + 23 \cdot 0.0645 \\ m_{PU_{total}} = 45.6 \text{ kg} \end{array} \right. \quad (3.5a)$$

$$\left\{ \begin{array}{l} m_{PU} = 1,225 \text{ g} = 1.225 \text{ kg} \\ m_{PU_{total}} = 1.225 \cdot 3 \cdot 6 \cdot 2 + 23 \cdot 0.0645 \\ m_{PU_{total}} = 45.6 \text{ kg} \end{array} \right. \quad (3.5b)$$

$$\left\{ \begin{array}{l} m_{PU_{total}} = 1.225 \cdot 3 \cdot 6 \cdot 2 + 23 \cdot 0.0645 \\ m_{PU_{total}} = 45.6 \text{ kg} \end{array} \right. \quad (3.5c)$$

$$\left\{ \begin{array}{l} m_{PU_{total}} = 45.6 \text{ kg} \end{array} \right. \quad (3.5d)$$

In this calculation it was assumed that the new thrust-reverser sleeve is of similar weight as the old thrust-reverser sleeve. This assumption was valid if the new thrust-reverser sleeve with chevrons was slightly longer than the original

⁶URL <http://www.airbus.com/aircraftfamilies/passengeraircraft/a330family/a330-200> [cited 13 June 2017].

thrust-reverser sleeve. In this case the extension caused an increase in area, whereas the chevrons cause a reduction in sleeve area. Thus, with this rough estimate, a weight addition of ~63 kg was obtained.

3.2.3. Materials

In order to implement the concept of variable geometry chevrons to the A330, it was necessary to know how the actuation will be achieved, as well as what materials would be suitable for this concept. First, the actuation mechanism will be discussed, after which the material choice will be elaborated.

Actuation Mechanism

The core components of the variable geometry chevrons are the SMAs, which cause the change in configuration of the chevrons themselves. Previous studies had demonstrated that shape memory alloys are an ideal choice regarding actuation mechanisms in the case of VGCs, as they have a high energy density and a considerable dynamic strain capability [20]. Four key properties that are related to the SMA actuators are [25]:

- material strength and fatigue,
- transition temperatures,
- transformation strain and any 2-way shape memory effect (SME) and
- dimensional stability.

As can be observed from the key properties, the appropriate material had to be chosen in order for the VGC to fulfil its purpose. As the maximum strain capability of current SMAs is about 4%, they would be underutilised when embedded in a structural material with a lower maximum strain. Therefore the best approach was to attach the actuator to a morphed structure [25].

The actuation mechanism by using SMAs is based on converting thermal energy to mechanical energy. This change in thermal energy can be achieved in two ways, either autonomous or powered. In the case of autonomous actuation, the fan flow heats the SMA above its transition temperature during take-off to the so-called austenitic form, whereas in cruise conditions the SMA transforms into the martensitic form, after which the composite substrate behaves as a return spring and pushes the VGC back into its retracted position [25]. The SMA strips that cause the change in configuration of the chevrons can be seen in Figure 3.6.

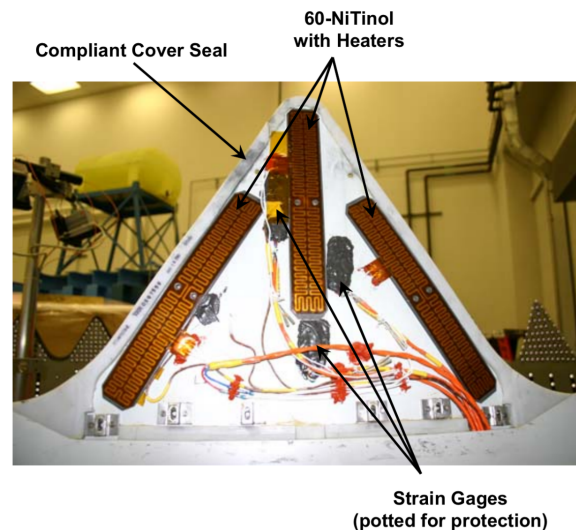


Figure 3.6: Variable Geometry Chevron mechanism [20].

Between the two options of autonomous or powered VGC, the autonomous chevrons would be optimal for production and operation, as no heating elements are present. These heating elements require power, electrical wiring and a control system. All of this added costs, weight and complexity. The downside of the autonomous chevrons was the limited tip deflection, due to a lower temperature range. The powered chevrons were also capable of optimising their shape for each flight condition to a much larger extent than the autonomous chevrons [20]. A combination of the two was also possible, with a powered chevron which becomes autonomous when the heating elements fail or a combination of autonomous and powered chevrons installed on the same engine.

Material Choice

Earlier it was shown that SMAs are an ideal choice for the actuation mechanism of the VGC. In order to morph the chevrons to achieve the acoustic and performance objectives, a compact, light-weight, robust and thermally-activated

SMA was preferred. 60-NiTiInol, a nickel-titanium alloy, is particularly well-suited for this application. As 60-NiTiInol has excellent thermo-mechanical stability, its transition temperature can be set by a heat-treating process and as it does not require cold work, its properties were superior over the commonly used 55-NiTiInol alloy [20]. One of the most important consequences of these properties is that, since 60-NiTiInol does not require cold work, the hot forming of complex shapes becomes a possibility, whereas this is not the case for 55-NiTiInol. Tests have been conducted where 60-NiTiInol and 55-NiTiInol have been compared, and these tests have yielded that the properties of 60-NiTiInol are repeatable and predictable, which means the actuators can be designed with this material if a proper design is developed [20, 25, 26].

As the VGC system does not only consist of the SMA strips but other components are also present, it is necessary to select the correct materials to avoid premature failure (e.g. due to non-compatible thermal strains). The cross-section showing the different components of the VGC system can be found in Figure 3.7.

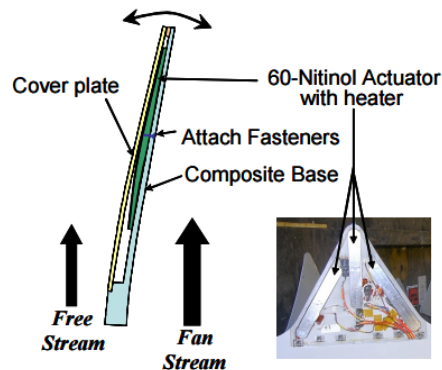


Figure 3.7: Cross-section of VGC mechanism (modified from [25]).

The material used for the composite substrate is different from the material used for the thrust-reverser sleeve. This indicates that the composite substrate consists of a standard-modulus carbon fibre with a non-toughened epoxy resin, pre-impregnated into the carbon fibre. Both bi-directional fabric and uni-directional tape forms of the prepreg are used and a basic, quasi-isotropic 15-ply lay up of fabric can be used for areas that require local reinforcement [20]. The carbon composite would provide the necessary stiffness and as the substrate is relatively thin, the flexibility of the chevron will not be compromised⁷.

In order to cover up the wiring, NiTiInol actuators and the composite structure, a cover plate was applied onto the chevrons. This cover plate should consist of a material that is flexible and strain- and fatigue-resistant. An ideal lightweight material that possesses these characteristics is a fibreglass composite [21]. Fibreglass is less resistant to fatigue when compared to carbon fibre [27, 28], however, as the cover plate can be easily replaced this will not be a significant problem. The cover was free to move in-plane relative to the substrate via sliding connectors and a conformable rubber seal, to further reduce any possible fatigue problems [20]. As the thrust-reverser sleeve is also made out of fibreglass, this cover will be the best option to avoid any strain or thermal incompatibilities.

The reason these materials in particular were considered, is because research papers present these materials as the most optimal choice [14, 20, 25]. As these research papers are presented in well-respected journals and are published by reliable sources such as Boeing and NASA, the same materials will be chosen for the chevron design presented in this report. However, as most likely new combinations of materials (alloys) will be found in the future, it is essential to investigate new lightweight options that can still perform as desired. Although for now the material selection process will not be necessary, it will be elaborated in Chapter 7.

3.2.4. Integration and Configuration

Certification and Design Allowables

As stated before, one of the larger issues of NiTiInol is the certification. Since the use of NiTiInol as an actuating system is relatively new, and has not yet been applied in the aerospace industry (the F-14 had NiTiInol components, but its special actuating mechanism was not used), there are currently no internationally accepted standardised test methods for NiTiInol as an SMA [29]. A lot of progress in standardising the test methods has been made in the last few years, though. For example Boeing, Texas A&M University, NASA Glenn and NASA Langley founded in 2006 the Consortium for the Advancement of Shape Memory Alloy Research and Technology (CASMART). Their purpose is to *‘Coordinate resources to enable the design of revolutionary applications based on SMA technology’*⁸.

⁷Private communication, Freek Sluis [8 June 2017].

⁸URL <http://casmart.tamu.edu> [cited 9 June 2017].

Other than CASMART, many other independent organisations have pushed towards standard testing for SMAs. In 2015, for example, a research team with members from Texas A&M Engineering, Boeing, NASA Glenn Research Center, SAES Getters S.p.A, Rolls-Royce, Rafael Advanced Defense System and ATI Specialty Alloys and Components wrote an article on standardisation of SMA testing for certification of aerospace applications [29]. Mr. Mabe also informed the team that there are two new articles on new standard test methods in the making, and that they are expected to be published through the American Society for Testing and Materials (ASTM), an internationally acknowledged standards organisation, later this year.

Since the current development regarding certification, it was expected that by the time the retrofit will go into production standardised tests will be available. This belief was further strengthened by the fact that ASTM has already published standard testing methods for the use of SMAs for medical experimentation [30–33].

Integration

Integration of the chevrons was very straightforward, as the new thrust-reverser sleeve will have the same attachment points as the old one. This thrust-reverser sleeve can be seen in Figure 3.8.

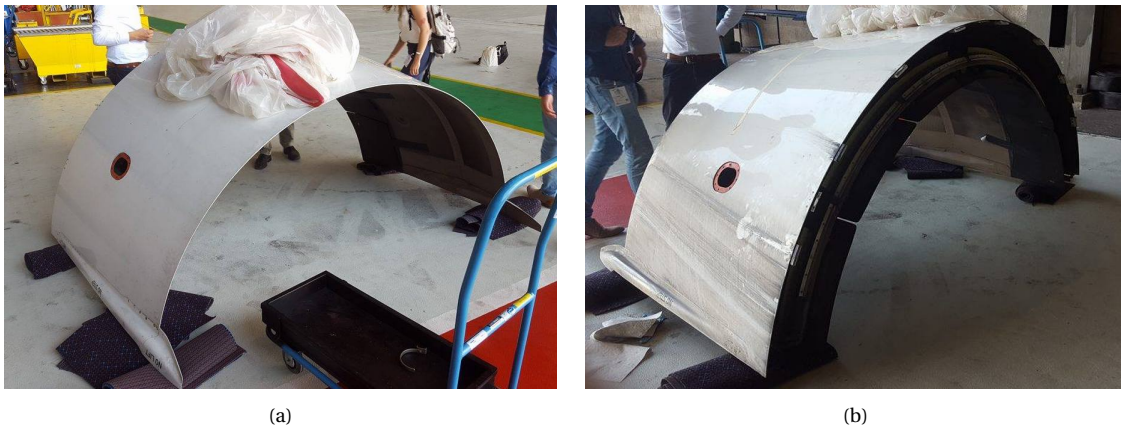


Figure 3.8: Thrust-reverser sleeve A330.

As can be seen in Figure 3.8, each thrust-reverser sleeve consists of two pieces. The new ones would also consist of two pieces. All of this should lead to the simplest integration possible.

3.2.5. Cost

With the general design of the chevrons known, it is possible to conduct a rough cost estimation. As the cost is a major parameter that influences the design choices by a significant amount, it is essential to perform a cost-benefit analysis. In other words, if the cost exceeds the amount after which the concept is not beneficial anymore (either financial or environmentally), the concept is very unlikely to be adopted by potential customers.

In the case of the environmental benefits, the chevrons reduce jet noise and thus airport noise, which can be a critical factor for airlines when noise becomes an issue. This meant that there will be no true case of money saving for the airlines, unless airlines will be charged extra for aircraft noise in the future⁹. An airline will thus have to invest in the initial retrofit and will not achieve a break-even point or make profit over time; the main benefit of chevrons is a noise reduction and for a profit the chevrons have to be combined with other concepts. However, if in combination with other noise reduction techniques the aircraft can get into a lower noise category, a substantial amount of money can be saved. This will be further discussed in Section 5.5.

Product costs

As the initial purchase cost mainly consists of the required man hours (MH), the necessary outsourcing and the essential materials, the cost estimation was based on these parameters. The NiTiNol actuators can be purchased from a third party, as the production process is relatively hard and thus it would be inefficient to purchase the appropriate tools. Off-the-shelf NiTiNol sheets are roughly \$15 per pound¹⁰, which means the total cost of the NiTiNol plates will come down to \$228. However, as the actuators are bought from a third party and new production techniques are still being investigated, these NiTiNol plates will most likely be purchased for significantly more than only the raw material cost. Furthermore, the quality of the 60-NiTiNol will most likely be better than the off-the-shelf NiTiNol, which means the cost will increase by a significant amount as well. Therefore, an amount of \$1,000 will be assumed for the machined NiTiNol that is ready for assembly. This assembly process will consume approximately 36 man hours, which

⁹URL http://www.fokker.com/sites/default/files/media/Files/Services/Retrofit/RETROFIT_D4.1_Report_Proposed_Future_Retrofit_Programs.pdf [cited 14 June 2017].

¹⁰URL <http://www.memry.com> [cited 21 June 2017].

means another \$900 will be added to the total cost, if an hourly wage of \$25 is assumed. Therefore, the total cost of the NiTiInol and its assembly will be approximately \$1,900.

In the case of the carbon composite substrates, the same approach was taken as was done for the NiTiInol actuators. As the total weight of the substrates will be roughly 3.4 kg and the price of aerospace grade carbon-fibre composite lies at approximately \$30 per kg¹¹, the total cost of the raw materials will be \$102. If the appropriate machining tools are present, the carbon composite can be cut and finished relatively easily and only labour will increase the total cost of the substrates. If 32 substrates have to be machined and every substrate will take approximately 3 hours to cut and finish, 96 man hours are required to obtain all the finished substrates. The man hours are most likely overestimated, however, this estimation also takes into account the cost for worn-out tools, the integration process and spare composite when the structural integrity of the substrate is compromised. If an hourly wage of \$25 is assumed, the total cost of the man hours and raw materials will be approximately \$2,500.

The prices for the wiring differed significantly, as each wire performs better on a different aspect (e.g. heat-resistant or flexible). Therefore, an average was taken of the cost of the wires that were deemed feasible. As 36 cables will travel a distance of roughly 9.5 m, and a last cable of 23 m is necessary to send the input signals, the total wire distance will be 365 m. If a value of \$5 per foot is assumed for the wiring [24], the total cost of the wires would be approximately \$3,650. However, the necessary man hours must still be included to obtain the total integration cost, and thus if an hourly wage of \$25 is assumed, together with the approximation of 20 man hours, the total cost of the wiring will come down to \$4,150.

The last component that was essential for the chevrons is the thrust-reverser sleeve. According to the KLM Royal Dutch Airlines, one rear of a thrust-reverser sleeve costs roughly \$400,000¹², however, this is the acquisition cost and not the production cost, which means the 'true' value of the thrust-reverser sleeve is lower. A new ready-to-use rear thrust-reverser sleeve will have to be produced in order to allow for a quick retrofit process to reduce downtime cost. This means that, for a quick cost estimation, the assumption will be made that the new sleeves will have the same cost as when one would purchase them from a third party. This is a very rough approximation, however, the prices of the sleeves will give an estimate of the production cost. As the production cost is most likely lower than \$400,000, but man hours and machining is required, one could assume these factors cancel out to a certain extent. As one rear sleeve costs roughly \$400,000, it is assumed that two rear sleeves will cost a total of \$800,000. If the appropriate tools and machines are present, the serrated shape can be autonomously machined and no further purchase cost will be present. The only cost remaining is that of the assembly and integration of the sleeve and its components. According to KLM, replacement of the rear of one thrust-reverser sleeve can be accomplished within roughly 4 hours by 4 employees. This meant that when the rear sleeves have to be detached and the new sleeves have to be re-attached, an additional \$1,600 in labour costs were added to the total cost, if again an hourly wage of \$25 was assumed.

Development costs

Not only components to be manufactured were included into the price, but also development costs. Since chevrons were at a very late stage in the design process already, this will be dominated by flight test costs. For this report, a team of two engineers worked on chevrons part-time for 5 weeks. They estimated that, if they worked full-time on it, it would take about a year for the complete design. This includes simulations of different chevron shapes, integration, production methods, flight test, etc. Taking the median salary of an aerospace engineer, which is \$83,398 per year¹³, and the average mark-up an employer pays for an employee in the Netherlands, due to for example taxes and insurance, a total price of \$100,414 a year was found per engineer¹⁴. For two engineers, this would be \$200,828 for a year. For the flight test, it was assumed that the aircraft will be out of operation for a week. From Section 3.3.5 the downtime costs of an A330 are taken. For seven days, this adds up to \$50,865.5. Assuming that the aircraft goes through half a tank of fuel for each day (69,545 kg, or 86,499 litres) due to constant take-offs and landings, the amount of fuel for one week was estimated to be 605,493 litres. With a kerosene price of 0.358 dollar per litre, this led to \$216,766.5. To be able to test the chevrons, test models will be made as well. It was assumed that three different chevron types will be tested, leading to a cost of \$3,240,000. Hence, for development cost, with a safety factor of 1.3, a total of \$4.8M was found.

This meant that the total cost of retrofitting chevrons to the Airbus A330 would come down to approximately \$810,000 for the retrofit, and \$4.8M for the development. This estimation was purely based on the purchase cost, the cost of the materials, the machining cost, development cost and the labour cost. A significant amount of other elements were not taken into account, such as film heaters and temperature and strain sensors. However, as the estimation in this stage of the design process was not expected to be accurate to the preferred extent, more research has to be done in order to obtain a better estimate. This research consists of obtaining better cost estimates for the individual materials as well as the cost for the essential machining tools.

¹¹URL <http://netcomposites.com/guide-tools/guide/reinforcements/carbon-fibrefiber> [cited 21 June 2017].

¹²Private communication, Hans Poelgeest [19 June 2017 14:00].

¹³http://www.payscale.com/research/US/Job=Aerospace_Engineer/Salary [cited 27 June 2017].

¹⁴<https://www.berekenhet.nl/ondernemen/loonkosten-werkgever.html> [cited 27 June 2017].

3.3. Winglets

In this section all steps relevant for the final retrofit winglet design are presented. This includes the design process, analysis programs used, results and conclusions. Two programs were used for the design, a program for calculating the aerodynamic performance of winglets with different configurations and a program for the structural aspects of the entire retrofit wing. To provide some overview in the extensive design process of the retrofit winglets the main steps taken are indicated below. Less relevant sidesteps in the design process are left out.

1. Requirements and constraints related to the winglet were analysed. A major constraint is related to the maximum allowable total span of the wing, which puts a constraint on the span of the winglet. The span of the aircraft cannot be larger than 65 m, if it is to remain within the same aerodrome sizing category. The winglet was designed for the maximum performance increase, while simultaneously benefitting the overall aircraft performance after possible required reinforcements of the wingbox.
2. A design option tree was created to have an overview of all possible retrofit winglet concepts.
3. Through the aerodynamic Vortex Lattice Method (VLM) program Tornado, the effect of changing various winglet parameters was found. The optimal winglet design was generated for three different situations: during approach, in cruise, and during take-off and climb. Through this it was concluded which parameters were beneficial to morph for aerodynamic performance.
4. The design load cases were found, such that it is known what load cases the wingbox should be sized for (sizing means the potentially needed reinforcements).
5. The entire wing with various relevant winglet configurations was structurally analysed for the design load cases. The various wing configurations included the wing with the current winglet, the wing retrofitted with the various most optimal winglets and some more extreme cases. It was taken into account that in case of a morphing winglet a heavy actuator will be needed, this weight was added to the winglet weight during the analysis.
6. It was analysed which failure modes were critical and what reinforcements of the wingbox would be necessary. Based on this, it was decided if another iteration was needed.
7. Finally the morphing parameters: the morphing mechanism and related actuators were chosen.

Winglet Design Option Tree

In order to obtain a design for the retrofit winglet, a starting point needed to be specified. For the winglet design at hand, it was chosen to start from the legislative constraint the International Civil Aviation Organization (ICAO) poses on the operation of the aircraft. The aircraft span cannot be larger than 65 m, if it is to remain within the aerodrome sizing category[34].

The trade-off in the midterm report concluded that a morphing winglet is the best design option for a retrofit, however, it did not specify the exact design of the winglet itself [2]. When designing a winglet, there are a lot of parameters which can be changed. This is especially valid for a morphing winglet, where a certain parameter might be beneficial during take-off, but must be changed in-flight to also provide benefits during cruise. To map all different design options, a design option tree has been made specifically for the winglet. This can be seen in Figure 3.9.

There are three main categories under which different choices could be made. First of all, the wingtip could be made of a single surface, like on the current A330. It could also be made of multiple surfaces, as on the new Boeing 737 MAX¹⁵. Secondly, for all parameters of the surface it was defined whether they shall be fixed, or whether they will be able to morph during flight, in order to maximise performance. Each actuation system would, however, add weight, so it must be assessed whether this added weight was compensated by the increased performance. Finally, the morphing mechanism had to be chosen. This could be either an electrical or an hydraulic system.

3.3.1. Aerodynamics

In order to analyse the aerodynamic performance of different winglet designs, Tornado VLM was used. In Section 4.4 the software specification is presented and verification of Tornado is done. The results from the program are presented in this subsection, the design choices are argued with and the aerodynamic performance of the final design is calculated and shown.

Conditions and Variables

During the winglet design process the following questions needed to be answered:

- Will the morphing winglet perform better than an optimised fixed winglet?
- What will be the winglet variables that are beneficial to morph?
- What will be the set values for the winglet variables that are not beneficial to morph?

During the design the following winglet variables were considered: taper, sweep, cant and twist. Taper would most likely not be morphed, since this would require a complicated actuator system, however, it was still interesting to

¹⁵URL <http://www.b737.org.uk/images/winglet-at.jpg> [cited 2 June 2017].

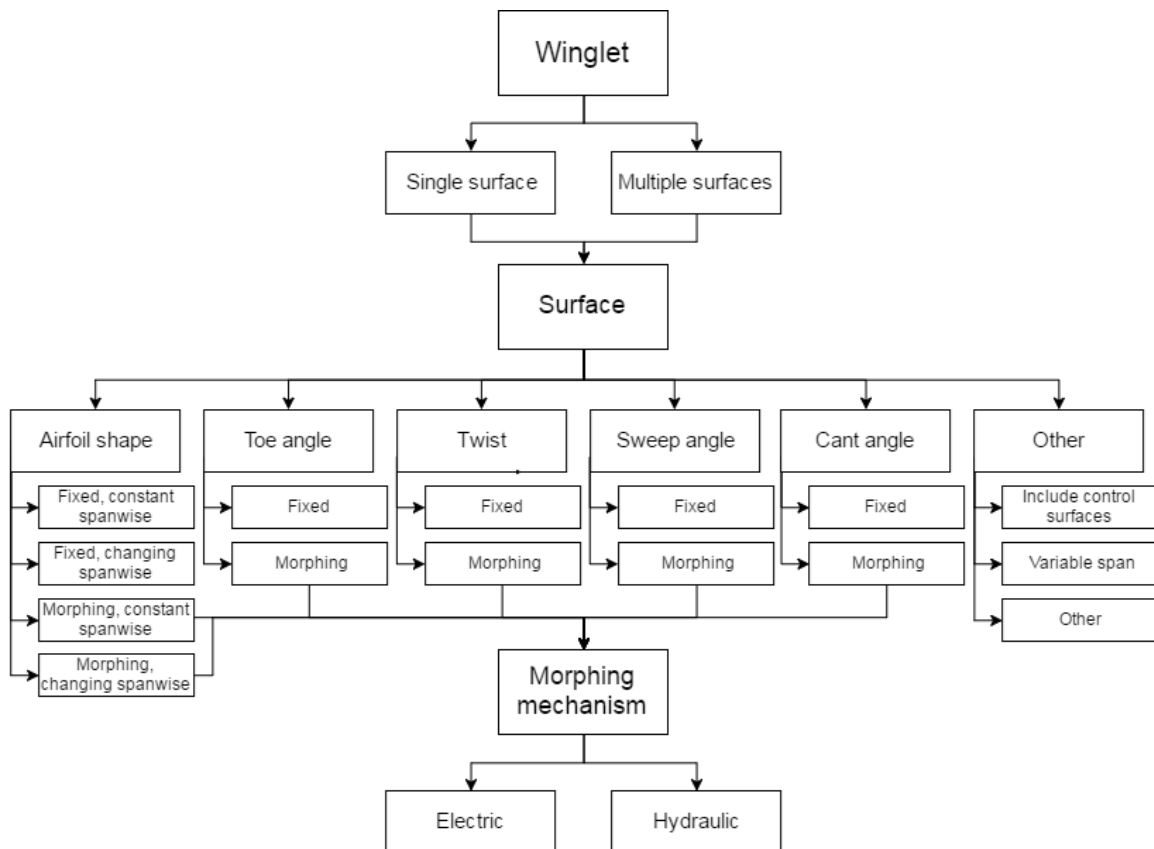


Figure 3.9: Winglet design option tree.

see how taper affects performance. For all variables plots were generated in Tornado in three different situations, specified below. In each situation the optimal variables were identified. From the identified values it could be seen which variables are beneficial to morph. If the optimal values were majorly different for different situations, morphing could improve performance. The following situations were analysed, per situation the Tornado settings are specified below:

- **Situation 1: Cruise.** During cruise the aircraft flies at $M = 0.82$. The performance was analysed for the range of angle of attack $0^\circ \leq \alpha \leq 2^\circ$. During cruise, the required C_L will be 0.585 [1]. The winglet will be optimised for the highest lift-to-drag ratio (L/D), and therefore the highest product of aspect ratio A and Oswald efficiency factor e , since this is the only factor in the drag equation which Tornado can model. This is further elaborated upon in Section 4.4.2.
- **Situation 2: Approach.** During approach the aircraft flies at $M = 0.21$. The performance was analysed for the range of angle of attack $5^\circ \leq \alpha \leq 15^\circ$. During approach, the winglet would have to be optimised for the highest $C_{L_{max}}$.
- **Situation 3: Take-off.** During take-off, the aircraft has a speed of $M = 0.21$. The performance was analysed for the range of angle of attack $0^\circ \leq \alpha \leq 15^\circ$. A high C_L is needed. During take-off, the winglet would have to be optimised for the highest L/D and the highest $C_{L_{max}}$.

The last two options could not be simulated in Tornado due to the inability of Tornado to simulate stall, as explained in Section 4.4.2. Optimisation is therefore, just as in cruise, done for the highest Ae . Due to the same flight conditions, these two situations will be simulated as one situation. This situation has a speed of $M = 0.21$, for angles of attack $0^\circ \leq \alpha \leq 15^\circ$.

Results

First, an analysis was done for a morphing winglet which has the same span as the current A330 winglet, in order to avoid excessive loads. After this, another analysis was done for a winglet with a larger span, to see if the performance improvement would increase. A total of four parameters were varied: twist, cant angle, sweep angle and taper ratio.

What could immediately be seen in the results was that Ae is independent of the Mach number. It varied very little (less than 1%) with angle of attack. The trend for this variance was constant for all design options. Therefore, it was decided to run all simulations for aerodynamic design on $\alpha = 0^\circ$ and $M = 0.82$. This resembles the cruise situation.

Together with the fact that Tornado cannot simulate the zero-lift drag, which is explained in Section 4.4.2, it was concluded that an optimal design of the winglet will be optimal for all flight conditions. Therefore, morphing for aerodynamic reasons was not needed.

Current A330 Winglet Optimisation

The current A330 winglet was varied over the parameters taper, twist-, sweep- and cant angle. Due to the fact that these are four parameters, which cannot all be plotted in one graph, it was first decided to look at the variance of A_e due to taper, sweep- and cant angle. The results of this can be seen in Figure 3.10. Immediately, it was concluded that a cant angle of 90° (a 'flat' winglet) was most favourable for all cases of taper and sweep. The optimal case would be a taper of around 0.4 and a sweep of 55° . This is a local optimum. Next, the effect of twist was assessed. It could be concluded that a non-zero twist was not beneficial to the efficiency of the wing: both negative and positive twist angles resulted in lower A_e values.

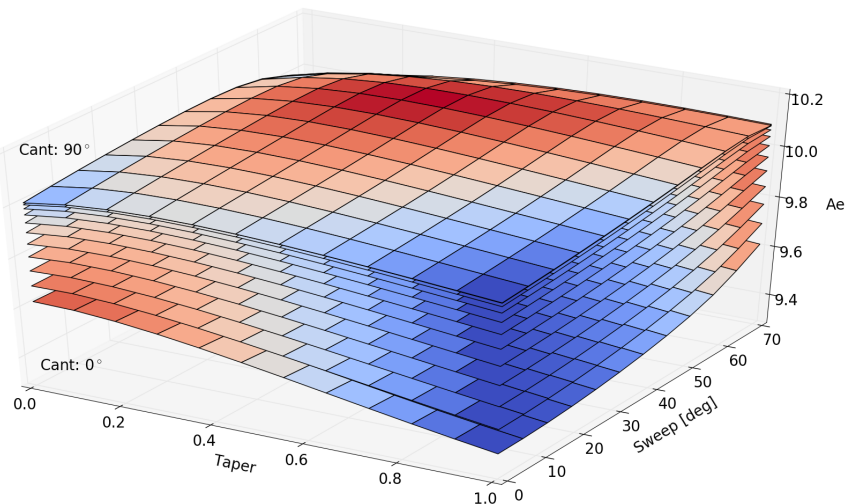


Figure 3.10: Taper, sweep- and cant angle plotted against A_e . The surfaces are different cant angles, varying from 0° – 90° .

The design of the improved winglet is shown in Figure 3.12a. Due to the high sweep angle and the taper ratio, it looks like a raked wingtip, a concept used by Boeing. This improved winglet provided a 1.8% improvement in A_e , resulting in a 1.8% decrease in induced drag.

Increased Winglet Span

With the optimised design of the A330 winglet known, it was decided to go one step further and increase the winglet span. The span was increased from 1.87 m to 3.5 m. This number was taken so that when the winglet would be extended, the total span of the aircraft would be exactly 65 m as set by ICAO. Again, the taper, twist-, sweep-, and cant angle were varied. This time, in order to reduce computing time, the range of taper and sweep was set to be 0.4–0.8 and 30° – 70° , respectively. The minimum for the sweep angle was set due to the fact that the wing itself is designed to fly at $M = 0.82$, and sweep angle plays a big role in this, since it increases the critical Mach number of the wing. A very swept-back winglet with this span would look unnatural to customers, while also providing structural implications, therefore, the maximum has been set at 70° . Taper was at these values due to aesthetic reasons, and the fact that in previous simulations an optimum was present between these values. This resulted again in a cant angle of 90° and zero twist. However, sweep and taper show different behaviour. This can be seen in Figure 3.11. A low sweep angle of 30° , as well as a low taper of 0.4, was now favourable. Higher taper and sweep would both cause a decrease in performance.

The new design is shown in Figure 3.12b. What can be seen is that this design leans towards a wingtip extension, instead of being an actual winglet or sharklet. Due to the low taper and relatively low sweep, it seemed as if this design maximises the aspect ratio and the Oswald efficiency factor by making the wingtip shape more elliptical. This design improved A_e by 9.2% and therefore reduced the induced drag with 8.4%. Due to this great improvement, the wing and extended wingtip design were structurally analysed in Section 3.3.2.

3.3.2. Structures

The penalty to pay for any improvement in production of lift was the increase of bending moment generated by this lift, which in turn caused the need for reinforcements of the wingbox, making the structure heavier. Any design should be the optimum between the performance gain and the structural penalty. Below, the structural aspect of the design

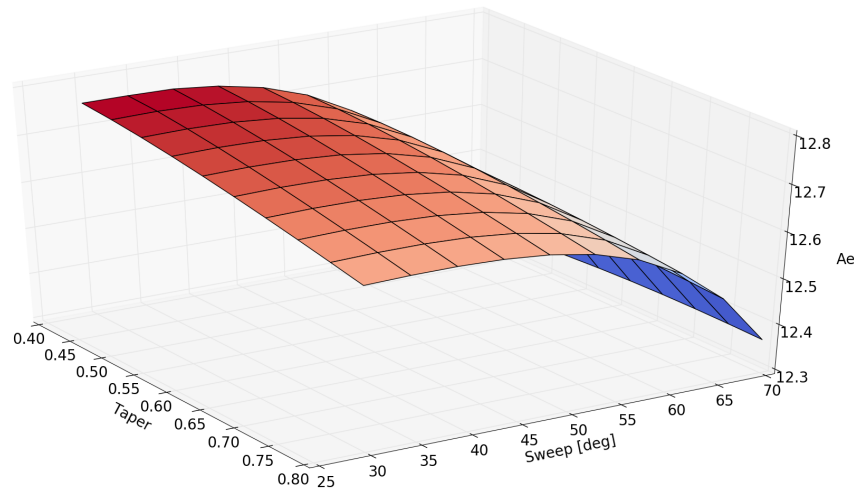
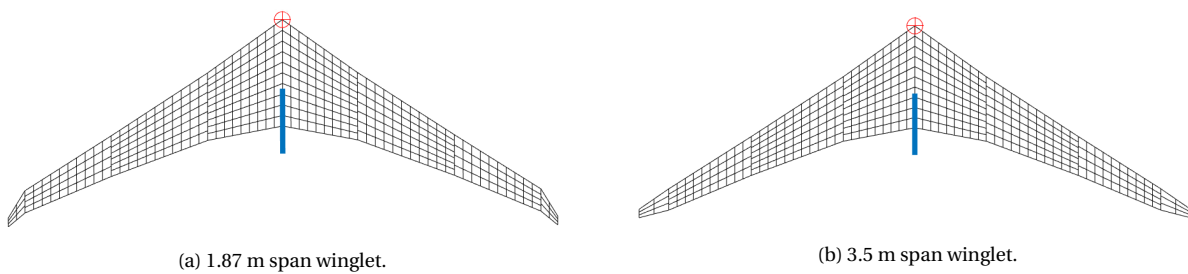


Figure 3.11: Taper, and sweep angle plotted against A_e .



(a) 1.87 m span winglet.

(b) 3.5 m span winglet.

Figure 3.12: Top view of the wing with new winglet designs.

process is presented. The program used for the analysis is elaborated upon, the leading design constraint (ICAO aerodrome category limitations) will be explained, the results from the program are presented and finally the structural performance and the needed wingbox reinforcements of the final design are calculated.

Assumptions Structural Analysis

Once the first iteration of the aerodynamic shape had taken shape, a structural model was constructed in order to perform a first order structural sizing of the wingbox. From this, the adaptations needed on the current wingbox of the aircraft when retrofitting the winglet could be analysed. The wingbox model took into account four main modes of failure: buckling of the wingbox stringers, skin yielding due to tension, intra-stringer buckling of the skin due to torsion and finally the shearing-out of the entire wing structure. Next to the considerations on the actual failure of the structure, additional constraints were placed on the amount of deflection, both in the translational and rotational sense. However, integral to the success of any model is the correct application of assumptions, in order to arrive at a both accurate and time-efficient method to solve the design problem at hand. Below, an overview of the main assumptions in the development of the structural wing model can be found.

- WL-S-1** The wingbox is modelled as a symmetrical box with two (differently sized) spars enclosing the box on each side. Therefore, this assumption does not take into account the distribution of stringers on the top and bottom surface of the wingbox and the shift in centre of gravity and force distribution as a result of this.
- WL-S-2** Structural idealisation is performed on the wingbox. As a result of this assumption, the shear flows between stringers will be constant. The shear flow will therefore be an overestimate of the actual stress levels.
- WL-S-3** The wing is divided into a finite number of spanwise sections. As a result, calculations are performed on individual sections, after which they are superimposed with the correct boundary conditions in order to obtain the complete wing behaviour. In reality, the wing will have a smaller deflection than the predictions based on a finite span division. However, with the decrease of span station pitch a closer estimate is obtained.
- WL-S-4** The size of the wingbox is assumed to linearly decrease with the span of the aircraft. This means that, unlike in reality, the structure will be overdesigned at sections where the forces drop with a higher than linear factor.

- WL-S-5** The amount of stringers is assumed to decrease in three discrete steps along the span of the aircraft. The discrete steps model the internal structure of the wingbox. However, discrete steps may cause some spikes or other non-smooth transitions in the stresses/strains of the wing.
- WL-S-6** The wing is assumed to experience no drag or thrust forces. This assumption means that the structure will not deform in the flight direction.
- WL-S-7** Stringers are assumed to be simple blocks of area and therefore lead to a conservative estimate of the moment of inertia.
- WL-S-8** The concentrated lift vector is always assumed to act at the quarter-chord point. In reality, and especially with alteration of angle of attack, the lift distribution will shift around along the chord direction.
- WL-S-9** Wing weight and other attachments such as the landing gear and engine are modelled as if they act through the centre of gravity of the wingbox and do not cause any additional torsion.
- WL-S-10** The skin is only loaded in shear and tension. This means that the buckling load will be carried only by the stringers and spars, leading to a conservative estimate of the wingbox strength.
- WL-S-11** A finite number of buckling modes is considered in the approximation of both the intra-stringer skin buckling and buckling of the stringers themselves.
- WL-S-12** The wingbox is assumed to be constructed entirely of the Aluminium 7075 alloy. This assumptions means that the structure will not be optimised with specific materials, which boast beneficial properties in specific use and therefore lead to yet again a conservative estimate of the actual structure, which does make use of optimised materials.
- WL-S-13** The wing is modelled as a straight structure with no bending when the load is initially applied. This means that all loads generated on the wing will have the maximum moment arm and lead to an overestimate of the actual force the wing is subjected to.
- WL-S-14** Constant rib spacing is assumed. The maximum value is taken, leading to a higher strength at locations where there is a smaller rib spacing.
- WL-S-15** The beam is assumed to deform elastically.
- WL-S-16** The material is assumed to have no deformations. This causes the overall strength of the plate to be slightly lower than assumed in the calculations: for this reason, safety factors were introduced.

Structural Model

The four failure modes, as well as the two deflections, all come with their own set of expressions for analysis. First, a set of geometrical properties of the cross-section were established, which were derived from the cross-sectional shape of the wing(box). The first of these parameters is the actual cross-sectional shape of the wingbox, which scaled linearly with the actual chord of the wing, such that the wingbox size follows the function as presented in Equation (3.6). However, this left the stringer area constant along the span of the wingbox and only decreasing at three discrete locations, which can be seen in Figure 3.13¹⁶.

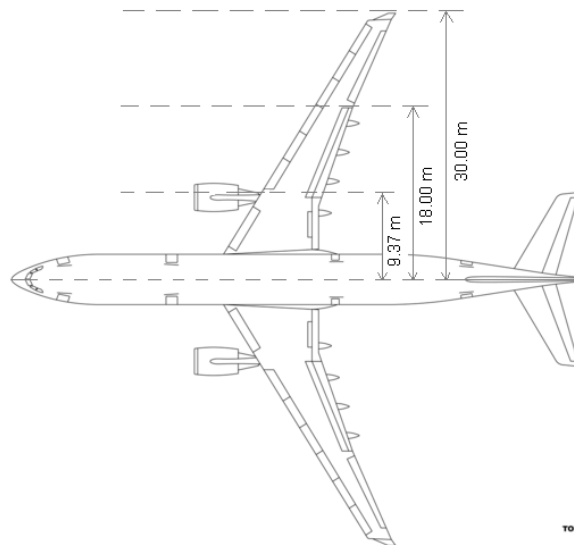


Figure 3.13: Respective ending locations of the different stringers.

$$\text{wingbox dimension} = \left(1 - \frac{\text{current span station y-location}}{\text{half span length of aircraft}} \right) \cdot \text{wingbox root dimension} \quad (3.6)$$

¹⁶URL <https://commons.wikimedia.org/wiki/File:A330-300v1.0.png> [cited 3 July 2017].

Taking as inputs the lift loading of each individual section, the shear force and the bending moment were calculated by summing up the forces from the discrete wing sections further to the tip of the section in question. Each spanwise section, however, did not only have a lifting force acting on it. Counteracting the lifting force is the structural weight of the wingbox, the carried fuel and other wing-mounted devices such as the engine, flaps and slats. The net force acting on each section will therefore be the summation of the lifting force and the relief forces. For the winglet, the additional consideration was the cant angle under which it was morphed, which has an influence on the arm this force has on the wing. The definition of the cant angle can be seen in Figure 3.14¹⁷.

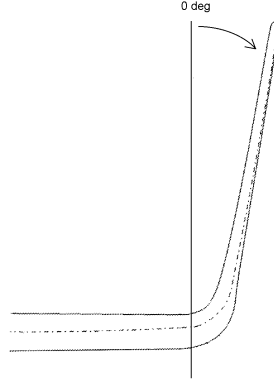


Figure 3.14: Definition of the cant angle.

The centre of gravity was calculated for each of the different spanwise stations, at each station taking into account the respective size of the front and rear spar. The front and rear spar thickness were looped through a discrete set of different thicknesses, resulting in an optimum between the wingbox weight and the amount of twist and deflection in the wingbox.

$$\bar{x} = \frac{\sum x \cdot A}{\sum A}, \quad \bar{y} = \frac{\sum y \cdot A}{\sum A} \quad (3.7)$$

Assuming the lift to act at 0.25% chord, additional torsion created by the offset from the centre of gravity was also taken into account for each section. The optimum between weight and performance can only be determined once both the weight and the performance are known. The performance will be discussed further on in this section, while the weight will be elaborated on below. The wingbox weight is calculated using the relationship seen in Equation (3.8). This equation assumes a constant wingbox cross-sectional size for the length of each span section, and thus its accuracy increases with decreasing span section lengths. The total wingbox weight will then be the sum of the individual spanwise sections.

$$\text{wingbox weight} = \left(\sum \text{stringer area}_{cs} + \sum \text{skin area}_{cs} + \sum \text{spar area}_{cs} \right) \cdot y\text{-section length} \cdot \text{material density} \quad (3.8)$$

In order to allow for convenient and time-effective evaluation of the structure, a structural idealisation was performed. The idealisation assumes all the skin area to be lumped into booms. These booms, conveniently located at each stringer location, obtain a reference area which is proportional to the stringer area together with the sum of the area surrounding the boom. Equation (3.9) shows the expression for determining the boom areas. The expression contains the term σ_2/σ_1 and takes into account the different load cases that can be applied to the wingbox.

$$B_r = \frac{t_D b}{6} \cdot \left(2 + \frac{\sigma_1}{\sigma_2} \right) \quad (3.9)$$

Once the internal forces on the wing were established and a structural idealisation has been performed, the next step is the calculation of the stresses under which the structure operates. The normal stress due to bending is estimated using Equation (3.10), assuming only one direction of loading. In order to properly evaluate this expression, the moment of inertia is first required. The moment of inertia of the cross-section was calculated using Equation (3.11), taking into account both the stringer area and geometry, as well as the spar height h and base b .

$$\sigma = \frac{M_x y}{I_{xx}} \quad (3.10)$$

$$I_{xx_{wb}} = \left(I_{xx_{st}} + A_{st} \cdot d_{st}^2 \right) + \left(\frac{1}{12} b h^3 \right)_{\text{front spar}} + \left(\frac{1}{12} b h^3 \right)_{\text{rear spar}} \quad (3.11)$$

¹⁷URL <https://www.google.com/patents/US20130092797> Cited on 03-07-2017

Once the normal stresses on each segment had been established, two of the failure modes could be checked for. The structure would be subjected to both tension and compression due to the wing bending moment. The compliance with the tensional strain was evaluated by simply comparing the normal stress to the maximal tensional yield strength of the material. The compressive force, however, needed to be evaluated in a more elaborate manner.

The compressive force will be fully taken up by the stringers, which in this case will be assumed to have a more efficient T-shape, which is depicted in Figure 3.15¹⁸. The T-shaped stringers are assumed to have a constant thickness for both the flange and the web, with two unique values for the width and height.

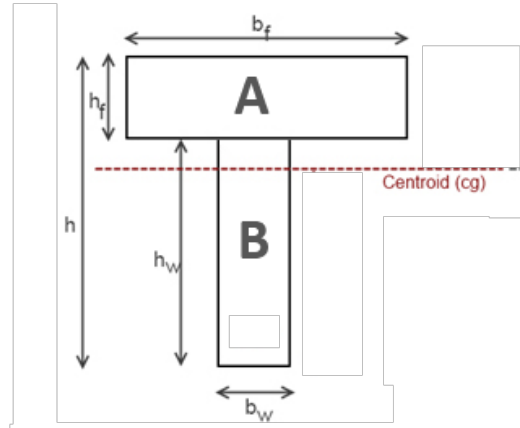


Figure 3.15: Stringer geometry in the T-shaped configuration.

After calculation of the moment of inertia of this stringer, the buckling force was determined with the help of the Euler buckling theorem. Taking into account only the first buckling mode of the beam and a simply supported setup, the expression simplifies to Equation (3.13). By dividing the buckling force by the stinger area the critical buckling stress can be found, which allows for easy comparison with the applied normal stress.

$$I_{xx,st} = \left(\frac{1}{12} b_f \cdot h_f^3 \right)_A + \left(\frac{1}{12} b_w h_w^3 \right)_B + \left[A_A \cdot \left(\frac{1}{2} h_f - \bar{y}_{st} \right)^2 \right] + \left[A_B \cdot \left(h_f + \frac{1}{2} h_w - \bar{y}_{st} \right)^2 \right] \quad (3.12)$$

$$P_{cr} = \frac{\pi^2 E I_{xx,st}}{l^2} \quad (3.13)$$

The direct evaluation of shear stresses was slightly more complex: it follows a two-step approach. The first straightforward check was seeing if the shear force divided by the cross-sectional area (leading to a shear stress) is not higher than the yield shear stress of the material used in the wingbox. The second calculation includes the evaluation of shear flows around the outer perimeter of the wingbox. The shear flow was calculated using the structural idealisation method. The method includes first making a so called 'cut' in the outer perimeter of the wingbox, at which the stress will then be zero. Starting from the cut section and working around the surface, section by section the shear flows are calculated using Equation (3.14). This equation simplifies significantly after the realisation that there is an axis of symmetry (I_{xy} becomes zero), an uni-directional loading and the fact that all the skin area was lumped into the booms. The resulting Equation (3.15) is used to express the shear flows around the wingbox.

$$q_b = - \left(\frac{S_x I_{xx} - S_y I_{xy}}{I_{xx} I_{yy} - I_{xy}^2} \right) \left(\int_0^s t_D x ds + \sum_{r=1}^n B_r B_r x_r \right) - \left(\frac{S_y I_{yy} - S_x I_{xy}}{I_{xx} I_{yy} - I_{xy}^2} \right) \left(\int_0^s t_D y ds + \sum_{r=1}^n B_r y_r \right) \quad (3.14)$$

$$q_b = - \frac{S_y}{I_{xx}} \sum_{r=1}^n B_r y_r \quad (3.15)$$

After evaluating the shear flows over the entire surface, what was left was an open-ended section without shear and a structure which is not properly balanced. In order to ensure moment equilibrium is still maintained, a constant shear flow $q_{s,0}$ is added to the structure. Equation (3.16) symbolises this relationship and is used to determine the constant shear flow, which is then superimposed onto every 'open section' shear flow q_b , to arrive at the shear flow in each segment.

$$\sum T = \int_0^s q_b ds + 2Aq_{s,0} \quad (3.16)$$

¹⁸URL <https://www.fhwa.dot.gov/hf1/partnerships/uhpc/hif13032/chap02.cfm> [cited 22 June 2017].

Equation (3.16) has the added benefit that if the section were to be subjected to a torque (T), this can simply be added in the calculation by setting the sum of moments equal to the applied torque, instead of zero for a section under pure shear.

Once the shear flows are known, the intra-stringer shear failure mode can be evaluated using the shear buckling expressions developed by Timoshenko. Timoshenko's method is a numerical approximation and therefore relies on the amount of nodes taken into account for accuracy. Taking a significant large number of equations, such that the error is lower than 9% [35] but computations can still be performed in a timely manner, the calculation process can be initiated. In order to evaluate Equation (3.17), one first needs to evaluate some constant factors. These factors, the flexural rigidity, slenderness of the plate, and shear correction factor, given in Equation (3.17), all depend on the shape and material chosen for the cross-section and are thus changing throughout the span of the wingbox. However, due to the slender nature of the plate sections between stringers, critical shear values for the wingbox were found to be a factor of 10+ larger than the applied stresses.

$$\left\{ \begin{array}{l} D = \frac{Et^3}{12(1-\nu^2)} \\ \beta = \frac{a}{b} \\ k = 5.35 + 4\frac{b^2}{a} \\ \tau_{cr} = k\frac{\pi^2 D}{b^2 h} \end{array} \right. \quad \begin{array}{l} (3.17a) \\ (3.17b) \\ (3.17c) \\ (3.17d) \end{array}$$

Next to the actual failure of the wingbox, the structure needs to remain rigid enough to stay within set deformation limits. This is especially important in a structure such as a wing, where an extra 5° in angle of attack could mean the difference between achieving the maximum angle of attack or stalling the aircraft. Two types of deformation were considered, firstly the bending of the wing due to the applied bending moment and secondly the twisting of the wing due to torsion. The bending deflection is obtained by assuming the beam to deform elastically over the entire length. Once the geometrical properties of the beam are known and the applied bending load per spanwise section of the beam had been calculated, the beam deflection can be obtained through integration as seen in Equation (3.18). The constants of integration are solved by starting at the root where the beam is assumed to be clamped and thus has zero deflection and angle. For each following beam, the constants are obtained by taking the respective deflection and angle of the previous beam section.

$$\left\{ \begin{array}{l} \frac{d^2 y}{dx^2} = \frac{M(x)}{EI_{xx}} \\ \frac{dy}{dx} = \int_0^x M(x) dx + C_1 \\ y = \int_0^x \left[\int_0^x M(x) dx + C_1 \right] dx + C_2 \end{array} \right. \quad \begin{array}{l} (3.18a) \\ (3.18b) \\ (3.18c) \end{array}$$

The final consideration in the structural design of the wingbox is the torsion of the wing. As mentioned before, excessive twist on a wing section can have detrimental effects on the lift producing capabilities of a wing. This cannot only lower the efficiency, but also be potentially dangerous to the operation of the aircraft. The twist of the beam is dependant on the shear flows going through the section, as well as the enclosed area, shear modulus and the thickness of each segment of the outer edge. It is calculated according to Equation (3.19). One should notice that once the twist has been established, it follows a linear relationship with the length of the beam.

$$\frac{d\theta}{dz} = \frac{1}{2A_R G} \oint_R \frac{q}{t} ds \quad (3.19)$$

For further elaboration on the inner workings and verification of the structural model, the reader is referred to Section 4.4.

Winglet Morphing

In the following paragraphs the process of obtaining the final concept of winglet morphing is described in a chronological order. The intermediate decisions taken and additional research needed to take these decisions are all presented. The plots and numerical values substantiating all decisions taken can be found in the paragraph 'Results'. First, why a morphing winglet? Winglet morphing could benefit the overall performance of the wing for two different considerations: an aerodynamic point of view and a structural point of view. From the aerodynamic analysis it could be concluded that winglet morphing and full integration into the current wing (taking into account the need of actuators), will not benefit the performance of the wing.

Winglet Morphing Structural Considerations

By analysing the loads on the structure, it could be seen that winglet morphing from a structural point of view could potentially benefit the overall performance of the wing. Through analysis it was found that the main cause of failure of the structure of the wing is the bending moment imposed on the wing by aerodynamic loads. The wingbox, which is the main supporting structure of the wing, is designed for the worst-case load scenario. This results in a wingbox which is structurally overdesigned for many load cases, such as normal cruise conditions. Winglet cant morphing provides a solution for decreasing the bending moment in critical situations while optimising the wing for less critical load cases. When winglet morphing is used purely for bending moment relief, two cant settings are relevant: a cant angle of 90° and a cant angle of 0° . During the load cases which are not critical for the bending moment, the winglet will have a cant angle of 90° and functions as an extension of the wing to improve aerodynamic performance. During the critical load cases the winglet will morph to a cant angle of 0° to decrease the bending moment on the wing. This principle allows to use the winglet as an extension of the wing when possible, with even a higher winglet span than the current A330 winglet. In Figure 3.16a it is illustrated how the principle works. The moment arms of the main wing and the wingtip in different configurations are indicated with A, B and C. It can be seen that C is significantly smaller than B. Figure 3.16b shows a graphical result of the effect on the root bending moment for a 0° cant angle and a 90° cant angle.

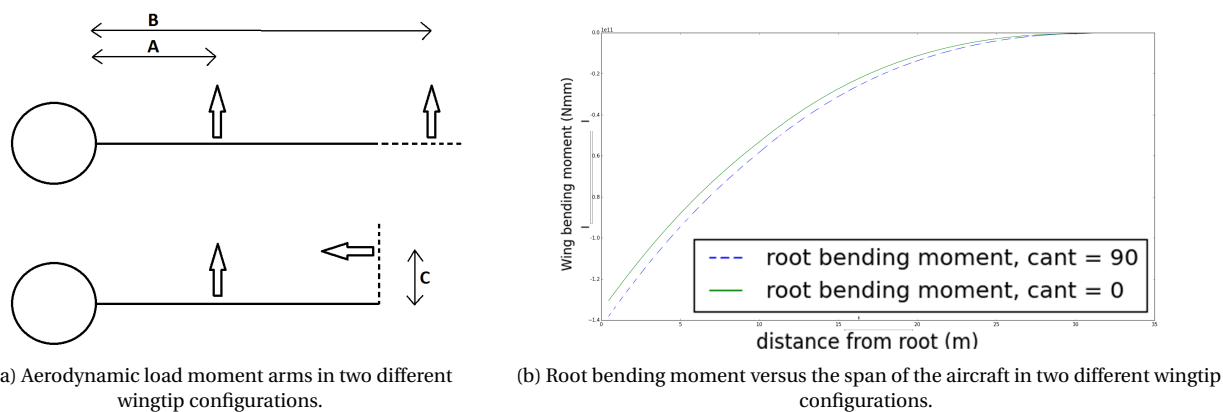


Figure 3.16: Hinge and break-pin connection between one spar of the main wing (left) and one spar of the extended wingtip (right) in different configurations.

With a cant angle of 90° the lift force acting on the winglet acts perpendicular to the main wing: in this situation, the moment arm of the winglet lift force equals the total length of the main wing and a part of the winglet length. With a cant angle of 0° the lift force acting on the winglet acts parallel to the main wing, in this situation the moment arm is significantly smaller. To support this theory, numerical values for different load cases and winglet configurations will be presented in Section 3.3.2.

Actuator System

For the winglet to be able to change its cant angle, an actuator system has to be included in the design. Due to the design choice that the winglet will be hinged around the wingtip, an actuator system has to be chosen which will be able to provide a moment around the hinge point in order to move the winglet. The moment caused by the lift force on the winglet is roughly 67,000 Nm in normal conditions, based on the assumption that all lift from the winglet is generated at a half-span location. This moment will have to be counteracted when the winglet must stay in place by either the actuator or a locking mechanism, and a larger moment has to be generated in order to extend the winglet. Retracting the winglet, i.e. decreasing the cant angle, will require the system to decrease its counteracting moment, so that the aerodynamic forces will perform the work. Since an extended winglet provides higher wing loading compared to a retracted winglet, time is not a critical factor in the extension of the winglet. This is unlike, for example, the aileron system, which has to be actuated almost continuously in order to ensure safe flight. Therefore, extending in 60 seconds would be acceptable for the winglets. This results in a power consumption of roughly 1700 W, based on the work done while rotating the winglet 90° around the hinge in this time span. Three main actuator systems are discussed: hydraulic, electric and pneumatic. The benefits and drawbacks of these types of systems are described below, as well as whether they are able to provide enough torque:

- **Hydraulic.** Using an incompressible liquid, a pump on the one side of the system can move a piston by using high pressure. High torques can be created by hydraulic systems. Just like almost all airliners, the A330 already has a hydraulic system on board. It must however be assessed whether this system can support the extra power needed by the winglet. A major drawback is the fact that a plumbing system will have to be installed inside the wing, in order to deliver the moment at the wingtip. Another drawback is the fact that hydraulic systems may

leak fluid, which may be harmful to other systems and lead to efficiency loss. With the Eaton's Model PV3-300-13F hydraulic pump on board of the A330 which is able to provide 3,000 psi¹⁹, the system would be able to power an actuator possible of delivering over 67,000 Nm torque, which are available on the market. An actuator of this size weighs around 700kg²⁰.

- **Pneumatic.** Due to the high torque required, a pneumatic system can be discarded immediately. Because to the compressibility of air, a lot of efficiency is lost compared to an hydraulic system. Also, the pneumatic system which is available on the A330 would not be able to provide enough pressure, and therefore a new system would have to be designed, unlike for the hydraulic system, which is already present.
- **Electric.** Unlike for the hydraulic and the pneumatic systems, no plumbing has to be installed in order to facilitate an actuator at the wingtip, only a power cable. This will save a considerable amount of weight. A downside to electric motors is that they operate at a high rotational speed, providing relatively low torque. Therefore a gearbox will have to be installed in the wingtip as well, in order to convert the low torque, high rpm output of the electrical motor to a high torque, low rpm shaft which is connected to the winglet. Incorporating a gearbox on each wingtip will lead to a considerable weight increase. A 2,000 W, 2,500 rpm, 7.7 Nm electrical motor would be able to power the morphing winglet under nominal conditions, while only weighing around 10 kg²¹. It should however be noted that this motor is not suitable for in-flight conditions. This motor would require a gearbox with a gear ratio of around 1:10,000 to provide the necessary power and rpm conversion.

A major constraint is the limited size of the space in which the actuator can be built. The wingtip with a chord of 2.5 m and a t/c of 10%, and therefore a maximum height of 25 cm, poses a dimensional constraint for the system. It is questionable whether either a hydraulic or an electrical actuator with gearbox will be able to be integrated in this part of the wing.

The electrical system will require a gearbox which will add a significant amount of extra weight. However, the hydraulic actuator will also bring a weight penalty, even when not taking the extra required plumbing into account. It is not certain if the current hydraulic system will be able to support another subsystem without requiring too large modifications, while the electrical system will be capable of delivering 2 kW of power. Therefore an electrical actuating system will be most suitable for a morphing winglet. It is estimated that the system, mainly comprising an electrical motor, wiring, gearbox and actuating system, will weigh around 250 kg per winglet.

Morphing Mechanism

From the last paragraph it can be concluded that the actuator system is still a major problem that arises with winglet cant morphing. The force needed to cant the winglet down would require a large, heavy and power consuming actuator. The force needed from the actuator can potentially be decreased by the use of a trim tab on the winglet and other passive systems such as a spring. The spring would be in rest when the winglet is at a 90° cant and in tension at a 0° cant, to aid the canting down of the winglet while experiencing aerodynamic loads. However, at this stage it cannot be said if such an actuation system is feasible or not, additional research and force calculations are needed in order to make sure this concept works.

Discarding the idea of active cant morphing for now, another solution was found for an optimal winglet with a morphing mechanism which is kept as simple as possible. The optimised winglet will function purely as an extension of the current wing. The winglet will have a span greater than the current A330 winglet and will have a cant angle of 90° during flight, such that it maximally extends the wing. The connection of the winglet to the main wing will include a hinge and a break-pin system. The pin locks the winglet in place during flight and has a certain preset strength. The pin to hold the winglet in place is designed such that it breaks under a critical load: this critical load equals the maximum allowable load for the wing. Above this load, the wing would fail due to a excessive wing bending moment. When the pin breaks, the winglet morphs up to a cant angle of 0° due to the aerodynamic loads acting on the winglet, this relieves the wing of the excessive bending moment and allows the wingbox to be sized for a lower load. In the event of a pin break the canting up of the winglet would cause a great impact on the hinge connection between the main wing and the extended wingtip. In order to damp this impact sufficiently, a spring or multiple springs could be added at the hinge. In addition to the spring damping, also natural damping occurs since the rotational movement of the winglet creates naturally an aerodynamic damping load in the opposite direction of the rotational movement. The configuration of the break-pin concept can be found in Section 3.3.4. All results regarding the wing structure considerations can be found in the paragraph 'Results' below.

Pin and Wingbox Sizing

Before sizing the wingbox, it needs to be decided under which loads the pins will break. Since it is not desired to have the pins break unnecessarily, these loads have to be chosen carefully. It is decided that for the most critical load cases, which can be found in Figure 3.1, the pins break. This is decided since these cases will not be likely to occur and would

¹⁹URL http://www.eaton.com/ecm/groups/public/@pub/@eaton/@aero/documents/content/ct_195634.pdf [cited 23 June 2017].

²⁰URL <http://ph.parker.com/us/en/hydraulic-rotary-actuator-htr-series-medium-duty> [cited 23 June 2017].

²¹URL <http://www.directindustry.com/prod/adtech-shenzhen-technology-co-ltd/product-114531-1646215.html> [cited 23 June 2017].

require a much stronger and thus heavier wingbox than for most other load cases. Knowing these load cases, the pins can be sized.

In order to size the wingbox, the load cases have to be specified with the corresponding winglet configuration. From earlier analysis it was found that after the two worst cases for which the pin will break, the most critical case is the low-altitude, high-temperature take-off: in this case, the winglet will be kept extended. Below, the cases are mentioned which were analysed to find what case to size the wingbox for.

- Maximum flight velocity at moderate altitude with a gust, with a 0° cant angle winglet.
- Low-altitude, high-temperature take-off, with a 90° cant angle winglet.

It was found that the sizing case is the maximum flight velocity at moderate altitude with a gust and a 0° cant angle winglet. In other words, the highest bending moments occur in this situation, even if the winglet has a 0° cant angle. Before analysing this situation, first another step was taken to confirm if indeed the canting up of the extended wingtip is needed. Dive speed at moderate altitude with a gust with the winglet at 90° cant angle is the starting point, at which the wingbox is put through the structural analysis software to check if canting by the break-pin is needed. The failure modes were analysed and stringer sizes were set to the value at which the buckling and tear-out constraints were just met at the most critical location, thus leading to a minimal weight design. This is done to analyse the additional weight needed for the wingbox in this case. It was found that the additional weight needed for reinforcement, if no break-pin system was implemented, was extremely high, such that no benefits could be obtained for the overall performance of the aircraft. The numerical values and plots are presented in the paragraph 'Results' below. After this analysis, it became evident that the break-pin system was needed to obtain a performance improvement from the retrofit extended wingtip.

Aeroelasticity Analysis

Aeroelasticity deals with an elastic structure in an airflow with sufficient interaction between the two. Two types of aeroelasticity are discussed: first, the phenomenon of divergence is discussed related to the wing with the retrofit winglet and secondly, the occurrence of flutter in the wing is discussed.

Divergence is a static instability where the aeroelastic twist and displacement go to infinity in a non-oscillatory fashion. The lift on the wing generates a torsional moment. This torsional moment creates a rotation which increases the effective angle of attack. Due to the increased angle of attack the lift is increased, subsequently increasing the bending moment. The Airbus A330 has a quarter-chord backward sweep of 30°. With a backward swept wing, bending of the wing causes a decrease of the effective angle of attack. This geometrical characteristic causes divergence not to be an issue. Considering this, it can be concluded that retrofitting the current A330 wing with a winglet will not affect the divergence characteristics.

Another form of aeroelastic instability is the phenomenon of flutter. Flutter is a dynamic instability where the aeroelastic rotation and displacement goes to infinity in an oscillatory fashion. To be precise, flutter itself is not an instability, it is neutrally stable. There is a certain speed at which flutter occurs and only when exceeding this speed, the flutter becomes unstable and oscillations go to infinity. The speed at which flutter in a wing occurs is dependent on the altitude of the aircraft and the eigenfrequency of the wing. The higher the eigenfrequency of the wing, the higher the speed at which flutter occurs. The eigenfrequency of the wing is amongst others dependent on the stiffness and inertia of the wing. Adding weight to the tip of the wing will decrease the overall stiffness of the wing, which will decrease the flutter speed. However, due to the increased root bending moment the wingbox will have to be reinforced, which will counteract the previously mentioned effect.

Results

The following section presents the results from the structural sizing process. The results will be presented and a brief discussion of each result is given.

As discussed in Section 3.1, the first step was the identification of the most critical loading scenarios. Figure 3.17 shows the spanwise distribution of the bending moment for four specific cases: the original winglet under dive speed with a gust, the extended winglet both before and after shearing of the pin under the same load and the extended wingtip under the highest non-dive speed load, the high-temperature, low-altitude 2.5g load. The diagrams shown in Figure 3.18 show how the wingbox designs, both current design and proposed retrofit, deal with the buckling compliance. For both designs, one can see that even under the ultimate loads, there is a margin such that the buckling is not the leading sizing constraint. The critical design constraint for the wingbox design turned out to be the tear-out of the skin near the root of the wingbox, as can be observed in the left hand corner of the diagrams in Figure 3.19. Both for the current wingbox design as well as the extended wingtip design, the sizing was performed through this constraint. Shear out did not approach the material limit in any design. A factor difference existed between the allowable values and the actual values. Two large spikes can be observed in the data in Figure 3.20, these coincide with the ending of the stringers in the span wise direction of the wingbox. The extended wingtip design has a slightly higher deflection, as well as twist, although all within set limits on the allowable twist and deflection, of which a graphic representation can be seen in figure Figure 3.21.

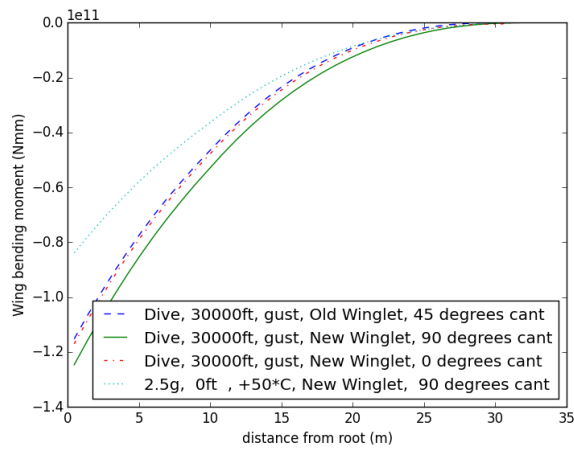
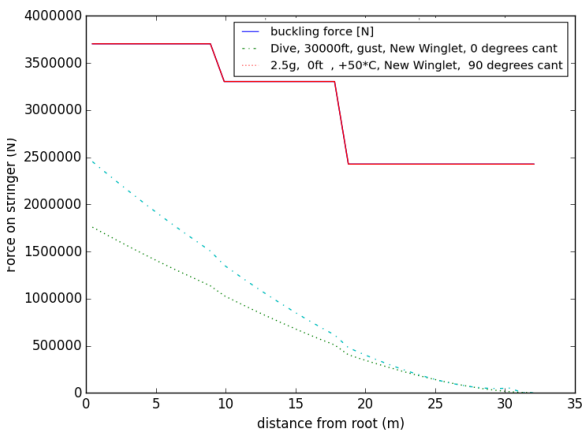
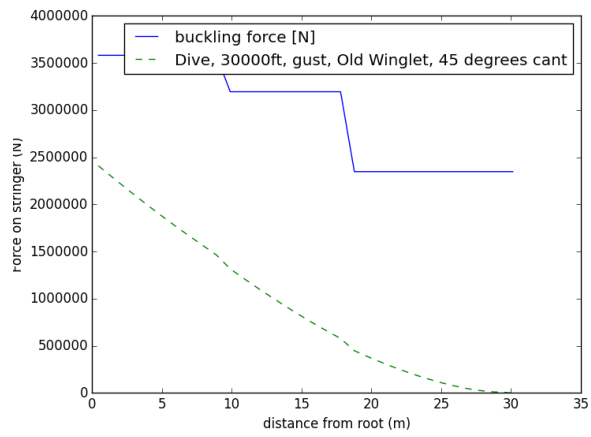


Figure 3.17: Different configurations and their respective wing bending moments as a function of the aircraft span.

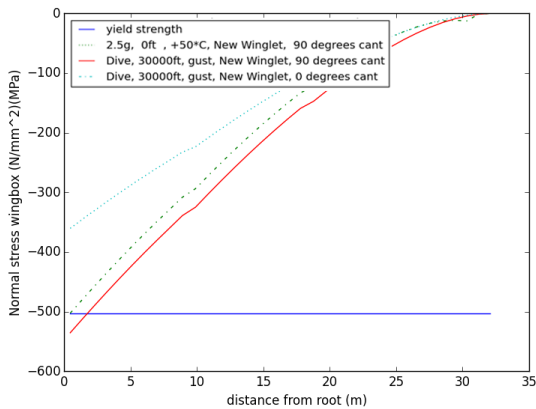


(a) Stringer buckling force constraint and the force applied to the respective configurations.

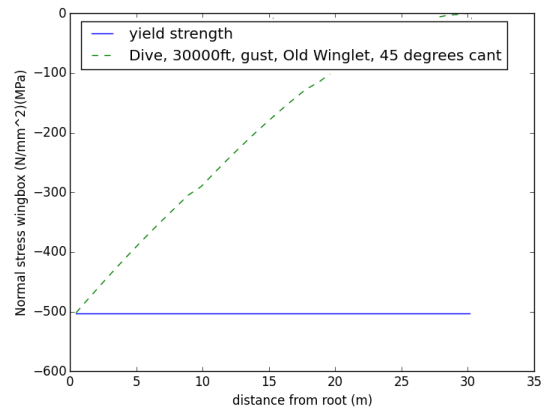


(b) Stringer buckling force constraint and the force applied to the strength of the old wingbox.

Figure 3.18: Buckling force constraints for the extended wingtip and the original winglet.



(a) Tensional yield failure check of the extended wingtip design.



(b) Tensional yield failure check of the current winglet design.

Figure 3.19: Wingbox yield stress comparison.

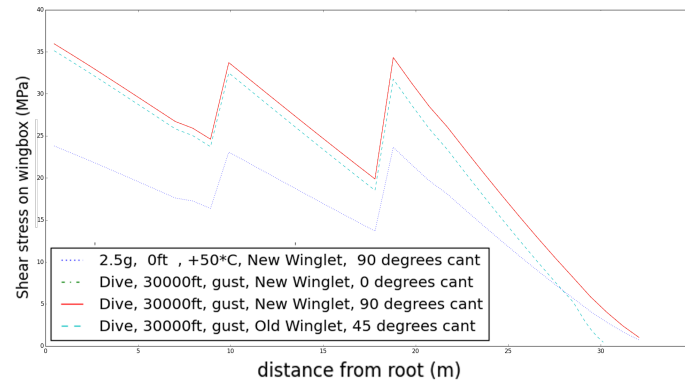
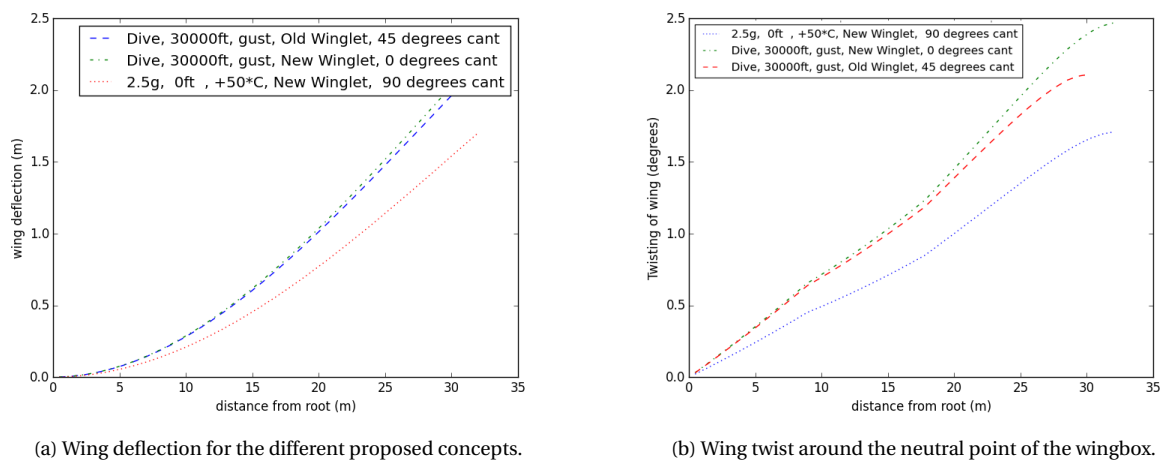


Figure 3.20: Comparison of shear stresses between the proposed and current winglet design.



(a) Wing deflection for the different proposed concepts.

(b) Wing twist around the neutral point of the wingbox.

Figure 3.21: Deflection of the wingbox.

Table 3.1: Overview of the winglet design cases.

Case	Dive, 30,000ft, gust Old Winglet 45° cant	Dive, 30,000ft, gust New winglet 90° cant	Dive, 30,000ft, gust New winglet 0° cant	2.5g, 0ft, +50°C New winglet 90° cant
Wingbox weight [kg] (increase from baseline)	13,513 0.00%	14,722 8.94%	14,016 3.72%	14,016 3.72%
Maximum deflection [m] (increase from baseline)	1.98 0.00%	- -	2.07 4.83%	1.34 -32.10%
Maximum twist [°] (increase from baseline)	2.09 0.00%	- -	2.43 16.54%	1.77 -15.43%

3.3.3. Materials

The current Airbus A330 wing, including its current winglets, mostly consists of aluminium alloys. The use of composite materials in the aerospace industry is growing and winglets made of composite material already exist^{22,23}. For example, the Boeing retrofit blended winglet partly consists of carbon-fibre composite material²⁴. It is decided that the morphing winglet will be partly made of carbon-fibre composite material, similar to the Boeing retrofit winglets. Composites have, for specific components of the structure, favourable characteristics, such as having a high strength while being light-weight. The material choice of the morphing winglets is based on the Boeing blended winglets. The material choices for different components of the winglet will be elaborated upon below.

²²URL <https://catapult.org.uk/success-stories/speeding-production-winglets> [cited 21 June 2017].

²³URL <http://www.totalmateria.com/page.aspx?ID=CheckArticle&site=ktn&NM=227> [cited 21 June 2017].

²⁴URL <http://www.aviationpartnersboeing.com/products.php> [cited 21 June 2017].

- **Leading edge and wingtip:** The leading edge and the wingtip of the winglet are made of aluminium. The main reason for not using carbon-fibre composite material here is that at leading edges the highest risk occurs for a bird strike. Aluminium is able to absorb impacts and will most likely deform while still retaining most of its strength in occurrence of a bird strike, whereas a composite material will most likely delaminate, losing most of its strength. In addition to this, at the leading edge heating occurs during the anti-icing process. Carbon-fibre composites do not perform as good as aluminium at high temperatures, they lose strength and aluminium conducts heat better than composite material²⁵.
- **Trailing edge:** The trailing edge is also made of aluminium. The reason for not choosing a composite is purely in consideration of the manufacturing process. Certain geometric constraints are imposed on composite components due to manufacturing difficulties, such as fibre wrinkling. The trailing edge requires a geometrical shape with a sharp edge, this is not realisable with the current composite material manufacture methods.
- **Upper and lower skin:** The upper and lower skin of the winglet are made of composite material. Composite is suited for these winglet components, since the risk for impact on these components is not very high, no exceptionally high temperatures occur in these areas and the geometry of the skin plates is suitable for the manufacturing process of carbon-fibre composite material.
- **Spars and ribs:** The spars and ribs of the winglet are a laminate, made of carbon-fibre composite. Similar to the upper and lower skin, the spars and ribs do not experience impacts (bird strikes) or high temperatures, so it is possible to use composite material here.
- For further strengthening of the winglet, a honeycomb core is selected. This is suitable for the winglet since it has a high strength-to-weight ratio and it is suitable for composite construction²⁶.

3.3.4. Integration and Configuration

Below the configuration of the extended wingtip is described and a preliminary configuration of the hinge between the main wing and the extended wingtip is presented. In Table 3.2 a full overview of the important wingtip extension parameters can be seen.

Table 3.2: Overview of the key wingtip extension parameters.

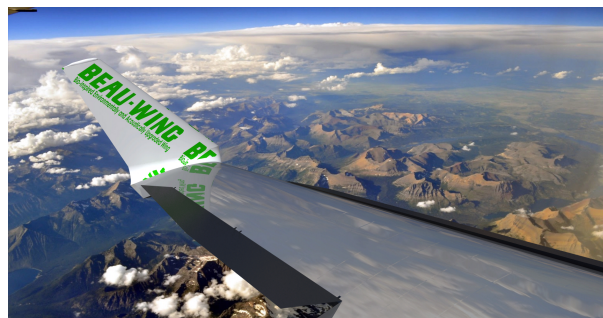
Parameter	Value	Unit	Parameter	Value	Unit
Span	65	m	Max. deflection	2.07	m
Winglet span	3.5	m	Deflection increase	4.83	%
Winglet sweep	30	°	Max. twist	2.44	°
New wing area	367.6	m ²	Twist increase	16.54	%
Wing area increase	1.83	%	Weight	14,016	kg
Aspect ratio wing	10.73	-	Weight increase	3.72	%
Taper ratio	0.4	-	Minimum cant angle	0	°
			Maximum cant angle	90	°

Extended Wingtip

The extended wingtip configuration is based on the Boeing retrofit blended winglet. The extended wingtip will have three spars at the root running till one third of the span of the extended wingtip. At one third of the wingtip span the middle spar ends and a rib is located, the two outer spars run from this location until the tip of the winglet. In Figure 3.22a the retrofitted wing with a flat extended wingtip can be seen. Figure 3.22b shows the retrofitted wing with an extended wingtip after a pin break.



(a) The Airbus A330 wing with a flat extended wingtip.



(b) The Airbus A330 wing with an extended wingtip after a pin break.

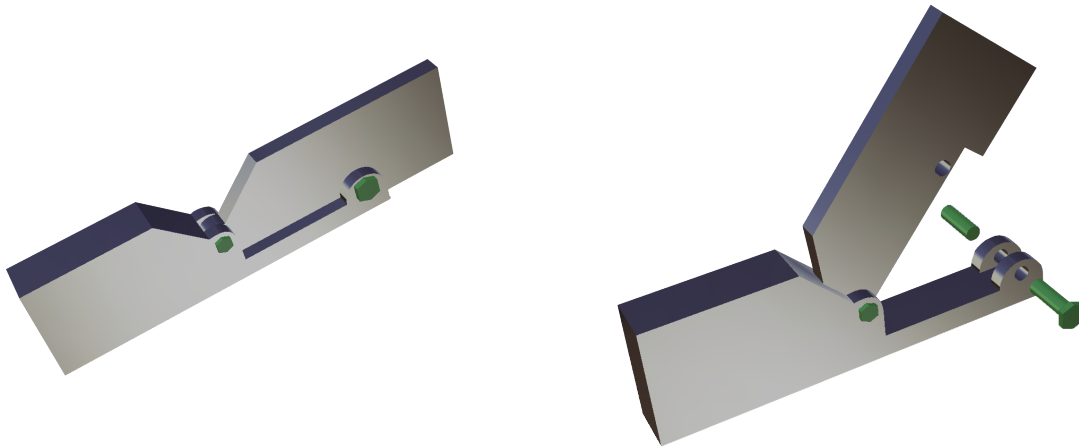
Figure 3.22: Airbus A330 wing with different extended wingtip configurations.

²⁵URL <http://www.ingenia.org.uk/Ingenia/Articles/505> [cited 21 June 2017].

²⁶URL <http://www.corecomposites.com/products/honeycomb/nomex-honeycomb.html> [cited 21 June 2017].

Break-Pin and Hinge System

The spars of the main wing will have to be altered to accommodate the new hinge system. To illustrate these alterations and the break-pin principle a preliminary configuration of the morphing mechanism with break-pin can be seen in Figure 3.23. Figure 3.23a presents a preliminary design of the connection between one spar of the main wing with one spar of the winglet in a flat position with an intact break-pin and Figure 3.23b presents the connection after a pin break. It should be noted that this configuration is purely to illustrate the concept and to introduce possibilities such as the use of a spring in the break-pin concept. No structural calculations have been performed for the dimensions used in the figure or the locations of components. In between the wing and the extended winglet a flexible skin is needed to avoid damage to the main wing, in case the pin breaks: this concept is described in Section 3.4.3.



(a) Hinge and break-pin connection with intact break-pin.

(b) Hinge and break-pin connection after pin break.

Figure 3.23: Hinge and break-pin connection between one spar of the main wing (left) and one spar of the extended wingtip (right) in different configurations.

Lights

Since position lights on both wingtips are mandatory²⁷, they cannot be omitted in the design of the retrofitted winglet. The current winglet has a light positioned on the main wing, as shown in Figure 3.24²⁸. The lights of the new system will, just like the old design, be incorporated in the main wing. This is due to the fact that, for the case when the break-pin of the wingtip would fail due to loading, damage would be done to the lights if they were to be integrated in the winglet. When replacing the break-pin after this scenario the aircraft should be flying as soon as possible again due to costs, and when a light system inside the winglet also would have to be replaced, including possibly damaged wiring around the hinge point, this would add extra costs.



Figure 3.24: The winglet of an A330, with the lighting system clearly visible.

3.3.5. Cost

The cost calculations for the retrofit morphing winglets are based on the Boeing-737 retrofit winglets. The cost of a retrofit winglet on the Airbus A330 can be divided into certain cost aspects:

- development cost,

²⁷URL https://www.ecfr.gov/cgi-bin/text-idx?node=14:1.0.1.3.10#se14.1.23_11385 [cited 20 June 2017].

²⁸URL <https://www.flickr.com/photos/a380spotter/5643729098> [cited 20 June 2017]

- extended wingtip cost,
- retrofit process cost and
- downtime cost.

Development Cost

The extended wingtip concept which has been selected as retrofit for the current A330 wingtip needs quite some research and testing before it is ready to be used in flight. A preliminary estimation is performed for the developments cost of the extended wingtip with break-pin. The development process can be roughly described by the following steps:

- create a detailed structural model in which all critical stresses can be identified and accurately located along the span of the wing,
- perform an accurate analysis of all stresses in the entire wing when the current winglet is retrofitted by a extended wingtip and size the hinge and break-pin system based on this analysis,
- perform bending tests (can be performed on the ground) in order to verify the sizing of the break-pin system and the wingbox reinforcements,
- perform flight tests to come to final conclusions and alterations.

Most likely there will be certification involved when bringing this concept on the market, which means that the concept needs to be properly tested. As the extended wingtip main structure and materials are based on the Boeing 737 retrofit blended winglet and the break-pin system is a passive and simple system, which already consists for other aerospace applications, it is not expected that the development of this concept will take a lot of time. It is expected that the development of this concept will take approximately a year and two engineering consultants will be constantly involved. It is estimated that two engineering consultants will cost \$82,641 for half a year²⁹. Most testing can be performed on the ground, since all sizing involves testing the structure for bending loads. Test set-ups in aircraft halls exist for these types of tests. It is expected that the multiple bending tests required, including all people involved, will cost in the order of \$10,000,000. Since it is difficult to accurately estimate the development cost, as a safety factor, 30% was added on top of the initial estimation. The initial total development cost amounts to \$10,165,282, with the extra 30% added, the final total development cost is approximately \$13,215,000.

Extended Wingtip Cost

The list price of a 767-300ER/F Blended Winglets System amounts to \$2,400,000³⁰. The list price includes the winglets, the modification kit and all other necessary materials and parts. This retrofit winglet has a span of 3.4 meters, whereas the A330 retrofit extended wingtip will have a span of 3.5 meters. It is assumed that the cost for both winglets will be comparable, the different size of the winglets will not make a significant difference in the price of the winglet. Thus, it is concluded that the winglet cost of the retrofit winglet (without actuator) will amount to approximately \$24,000,000. From private communication³¹ it is learned that old parts, if still performing sufficiently or repairable, can be sold quite easily. The returns from the old (current) winglet can be subtracted from the morphing winglet cost. The old winglet will be a second-hand winglet. It is assumed, based on the Boeing retrofit winglet list prices, that the list price of the current winglet (new) is \$700,000 (the current A330 winglet is quite small). Since it is second-hand, a factor of 0.6 will be used. The total return is estimated to be $0.6 \cdot 700,000$, which amounts to \$420,000. The total winglet cost will then amount to: $\$2,400,000 - \$420,000$, which equals \$1,980,000.

Retrofit Process Cost

The costs for installing the extended wingtips on the A330 includes taking off the old winglet and installing the new extended wingtip, plus the hinge and break-pin system. The retrofit process cost will be estimated by calculating the man hours needed and the salary per man hour. The 767-300ER/F Blended Winglets System of Boeing takes 6,000 man hours to install, which results in a time span of two weeks³². The retrofit winglet installing of Boeing includes taking off old parts (part of the wingtip). Since the morphing winglet requires a hinge and break-pin system including a flexible skin, the installation time is estimated to be 150% more man hours than for the Boeing 767-300ER/F retrofit. This amounts to 9,000 man hours. The salary of aircraft retrofit installing engineer is estimated to be around \$25/hr³³. In total, the retrofit installing cost were $\$9,000 \cdot \25 , which amounted to \$225,000.

Downtime Cost

The 767-300ER/F Blended Winglets System of Boeing takes two weeks to install. The retrofit for the A330 will be an extended wingtip with break-pin system, so the installing time is estimated to be 150% longer than for Boeing's

²⁹URL http://www.payscale.com/research/US/Job=Engineering_Consultant/Salary [cited 27 June 2017].

³⁰URL http://www.aviationpartnersboeing.com/products_list_prices.php [cited 20 June 2017].

³¹Private communication, Hans Poelgeest [19 June 2017 14:00].

³²URL http://www.aviationpartnersboeing.com/services_retrofit.php [cited 20 June 2017].

³³URL: <http://www1.salary.com/Aircraft-Mechanic-Jet-hourly-wages.html> [cited 29 June 2018]

retrofit, approximately 21 days. From private communication³⁴ it was learned that per year the leasing of an Airbus A330 costs around \$ 2,000,000. This means that for 1 day of leasing the ownership cost amounts to \$ 2,740. In addition to this, in the time that the aircraft is on the ground, it could also have flown and earned money. This adds even more to the downtime cost and finally the required space in the hangar will also add to the downtime costs. From these substantial costs it can be concluded that the most efficient solution would be to install the winglets during standard checks. For the downtime cost calculation it will be assumed that the retrofit process will partly take place during a C-check, which happens every 2 years and takes 6 days time, or a D-check, which happens every 6 years and takes around 5 weeks. It will be assumed that for retrofitting the extended wingtips during the C-check an additional 15 days of downtime are needed and that for retrofitting the extended wingtips during the D-check an additional 7 days are needed. The revenue of the Airbus A330 is estimated based on revenue information of the Boeing 737-800, since detailed revenue information of the Airbus A330-200 is not available. The Boeing 737-800 has a 186 seat capacity³⁵, whereas the Airbus A330-200 flown by KLM has a 243 seat capacity³⁶. The difference of the seat capacity will be taken into account. The revenues differ per time of the year, it will be assumed that the retrofit process (thus also the C- and/or D-check) will take place in low season. The average monthly revenue of the Boeing 737-800 can be seen in Figure 3.25.

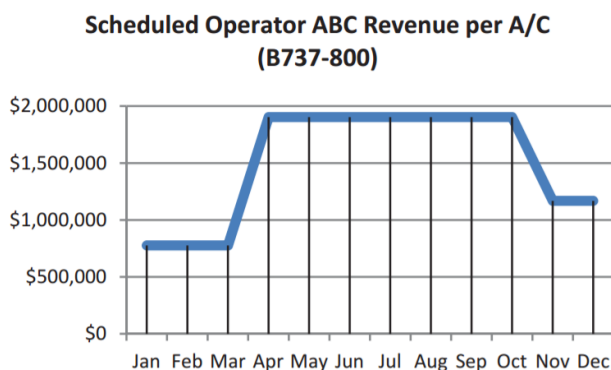


Figure 3.25: An estimation of the average monthly revenue per aircraft of the Boeing 737-800 operated by operator 'ABC' [36].

From Figure 3.25 it can be seen that in low season the monthly average revenue of the Boeing 737-800 equals \$780,000, this equals to approximately \$26,000 a day. When taking the different number of seats into account, it is estimated that the revenue per A330 per day equals \$33,970. When assuming a 5% profit margin this leads to a profit per A330 per day of \$1,698.5. The hangar cost per 12 hours is estimated to be \$1,414, this is based on the hangar costs of Chubu Centrair International Airport Nagoya for Boeing Business Jets, since limited information is available for hangar costs³⁷. The total downtime costs are calculated below.

- Retrofitting during the C-check, in low season, assuming an additional fifteen days of downtime: $\$1,698.5 \cdot 15 + \$1,414 \cdot 30 + \$2,740 \cdot 15 = \$108,997.5$.
- Retrofitting during the D-check, in low season, assuming an additional seven days of downtime: $\$1,698.5 \cdot 7 + \$1,414 \cdot 14 + \$2,740 \cdot 7 = \$50,866$.

3.4. FishBAC

The development of the FishBAC concept started with a brainstorm on implementation. The concept that was initially considered was the integrated morphing trailing edge (Figure 3.26a). Here, the FishBAC is retrofitted behind the rear spar and the transition from wing to FishBAC is completely smooth. This concept would eliminate the gap between the wing and the flap through which air usually flows upwards to re-energise the flow: therefore, it was feared that this concept would not be able to produce the same amount of lift as the current A330 design. The second concept thus introduced an integrated morphing trailing edge combined with trailing edge blowing, shown in Figure 3.26b. This concept would require the installation of a pump.

An existing fear was the fact that the deflection of the FishBAC might be limited in some way. If this would be the case, the FishBAC might not be able to produce the desired amount of lift. Therefore, a concept was introduced in which the flap would be able to both hinge and morph, seen in Figure 3.26c. The last concept is shown in Figure 3.26d: a morphing FishBAC flap that can be extended rearwards. Another challenge for the FishBAC was the fact that it should

³⁴Private communication, Marco Oomen [19 June 2017 14:00].

³⁵URL https://www.klm.com/travel/nl_nl/prepare_for_travel/on_board/seating_plans/737-800.htm [cited 21 June 2017].

³⁶URL https://www.klm.com/travel/nl_nl/prepare_for_travel/on_board/seating_plans/a330-200.htm [cited 21 June 2017].

³⁷URL http://www.centrair.jp/en/business/business_jet/charge [cited 21 June 2017].

replace a single slotted Fowler flap. This meant that, even if the deflection of the FishBAC did not turn out to be limiting, the area increase of the Fowler mechanism would have to be compensated for. The link/track mechanism of the Fowler flap could be used, and the entire rotary mechanism could still be removed.

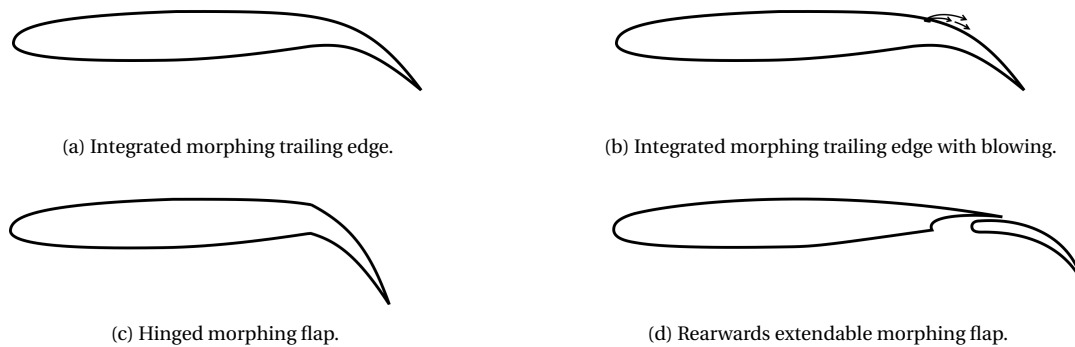


Figure 3.26: Multiple concepts for implementation of the FishBAC.

As a starting point for the aerodynamic and structural design the integrated FishBAC was considered. Reason for this was that it is the simplest concept, for which no additional mechanisms are required. A 2D CFD analysis will show whether this concept is capable of producing the same amount of lift as the single slotted Fowler flap that the A330 currently uses. If it turns out that the concept is not capable of doing this, the other concepts will be considered.

3.4.1. Aerodynamics

As the desired output of applying FishBAC is an increase in performance, the aerodynamics aspect must be carefully assessed. Therefore an investigation was executed regarding the performance of the FishBAC with respect to the old control surfaces. First the impact of the FishBAC flaps will be assessed, after which the effect of the flap fairing removal will be discussed.

Javafoil 2D analysis

A 2D aerofoil analysis has been performed using Javafoil. This program uses a second order panel method to calculate the inviscid airflow around aerofoils, followed by a viscous boundary layer calculation to calculate profile drag and transition and separation locations. For moderate Reynolds numbers, a compressibility correction is implemented such that results for velocities lower than $M = 0.5$ are accurate. This makes it suitable for approach speed simulations. The reason this software was chosen over other 2D software was that Javafoil has the ability to model multiple element aerofoils and is free to use, while other software like Xfoil and MSES do not meet these criteria.

The purpose of the simulation was to check if the new morphed flap can have the same performance as the current Fowler flap, meaning the $C_{l_{max}}$ should not be compromised. The method used was to first analyse the current flap performance and compare it with the morphed flap. All the 2D analyses were performed at the mean aerodynamic chord (MAC). The current flap has a chordwise length of $0.26\bar{c}$, which at the MAC means a chord of 1.88 m. The aerofoil chosen for the analysis was taken from a paper from Airbus which researched the A340 aerofoil, and since the A340 and the A330 wing are essentially the same this was deemed sufficient [37]. The flap dimensions were taken from an A330 wing planform drawing [23] and the deflected position from a structural cut-out drawing [23]. These were imported as a multi-element aerofoil into Javafoil and analysed at the following conditions (approach conditions):

- $\rho = 1.225 \text{ kg/m}^3$.
- $a = 340.29 \text{ m/s}$.
- $\nu = 1.43226 \cdot 10^{-5} \text{ m}^2/\text{s}$.
- $M = 0.21$. Approach speed as per A330 manual.
- $\text{MAC} = 7.26 \text{ m}$ at 11.2 m from centerline³⁸.
- $Re = \frac{v \cdot \text{MAC}}{\nu} = 36,222,901$.

No slats were included in the simulation, since Javafoil would not allow small elements in the first half of the chord. This will lead to results which are off from reality: the $C_{l_{max}}$ will be lower and the α_{stall} will be very low. The latter is due to the fact that only changing a flap angle without pitching down effectively increases the angle of attack at which the aerofoil is flying. This would be compensated by the use of a leading edge slat. However, since it is a means of comparing the two flap performances, the difference in the curves is all that matters. This means that leaving out the slat should not compromise the accuracy of the test.

³⁸URL <http://www2.anac.gov.br/certificacao/Produtos/Espec/EA-9806-09i.pdf> [cited 16 June 2017].

As said before, the morphing flap should have the same performance as the current flap. First, the current flap was analysed in the aforementioned conditions. The backward translation of the Fowler flap was also included by increasing the total chord length of the aerofoil with flap with respect to the morphed one. Next, the clean A340 aerofoil was morphed with a constant curvature, increasing deflection angles until the $C_{l_{max}}$ was matched. This deflection angle δ is defined as shown in Figure 3.27. Javafoil offers different models for calculating stall and transition effects. In this simulation the Eppler stall model [38] and the Granville transition model [39] are used, as recommended in the Javafoil user manual for high Reynolds numbers. After iterating the deflection a couple of times, the final deflection angle necessary was found, which turned out to be 28° . The resulting performance is shown in Figure 3.28 and Figure 3.29.

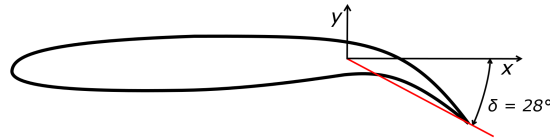


Figure 3.27: Flap deflection angle δ of the FishBAC.

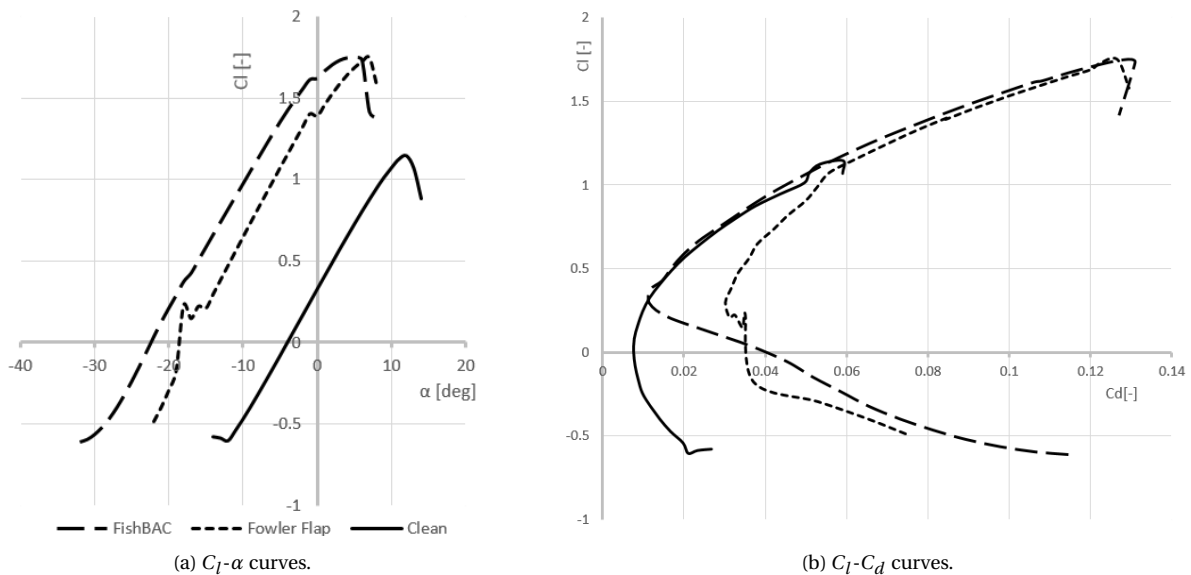


Figure 3.28: Javafoil aerofoil characteristic curves of the different flap configurations. Clean configuration added for comparison purposes. $Re = 36,222,901$.

In the $C_l - \alpha$ curve in Figure 3.28a some interesting things can be seen. First of all, it was concluded that there is a deflection possible in which the $C_{l_{max}}$ is the same as the original one. The α_{stall} is, as expected, very low. The FishBAC has a slightly lower α at all C_l values. However, the $C_l - C_d$ curve looks even more promising. The FishBAC curve lies to the left of the Fowler flap curve at all times, with a substantial difference in the lower C_l regimes. This means that the drag of the morphed flap is lower than the Fowler flap, with a maximum of $0.02 C_d$ improvement at a C_l of 0.3 . Although an aircraft would rarely fly at such C_l when flaps are deployed, it also has less drag at the higher C_l values. Javafoil also showed that transition of the upper edge occurs at the leading edge and separation at $0.96\bar{c}$, so the curvature of the flap is sufficient to let the flow stay attached.

In Figure 3.29, the C_p distributions and streamlines are shown for the final designs. Note that this does not model flow transition and separation, while the polars of Figure 3.28 do include the locations of those events and add a drag penalty accordingly. It can be seen that the pressure at the flap of the FishBAC is much lower than the Fowler flap. This compensates for the fact that the flow over the Fowler flap stays attached longer.

The most important conclusion that can be drawn from these results is that the simple integrated FishBAC concept is able to match the current Fowler flap performance, which means no extra complicated subsystems will have to be added. Therefore, in the rest of this chapter, only this concept will be further analysed.

Flap Fairings

The current A330 flap system has another big disadvantage compared to the FishBAC concept. This is the fact that the flap is actuated from an external actuation system, located outside the wing structure. This means that so-called canoe fairings are needed to cover the flap actuating system. These are seen on every modern airliner nowadays as

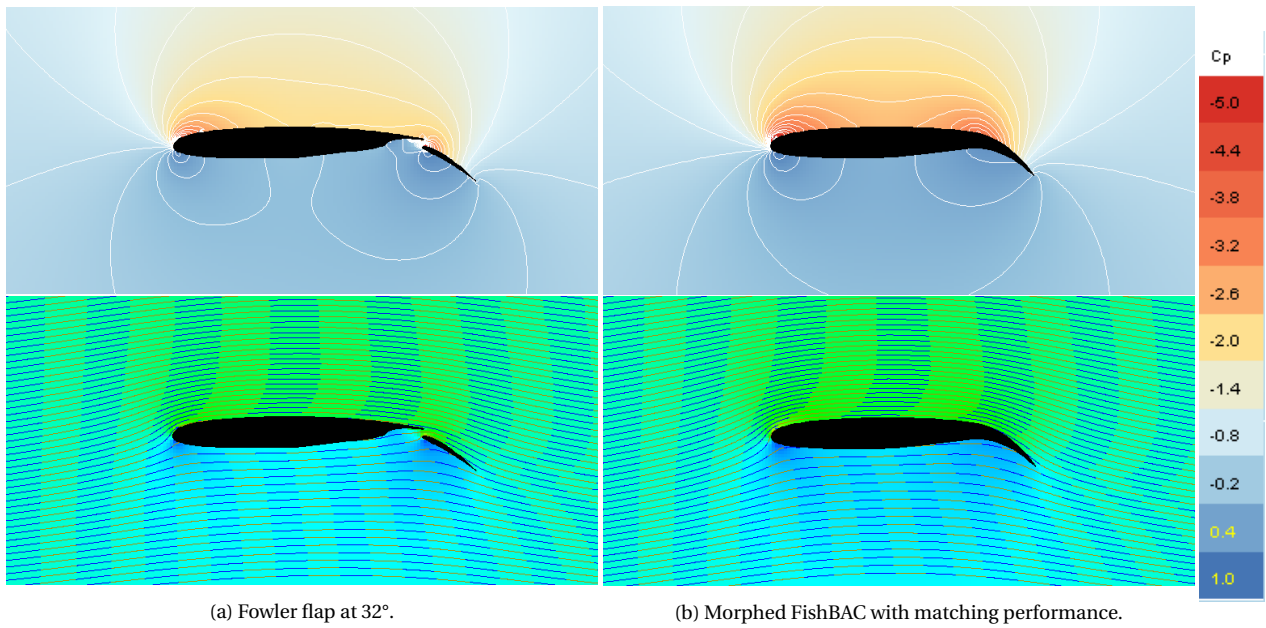


Figure 3.29: Javafoil C_p distributions (top) and streamlines (bottom) around the different flap configurations. Legend for the C_p distributions is displayed on the right hand side. The white lines represent constant C_p lines. $\alpha = 0$, $Re = 36,222,901$.

Pods underneath the wing, shown in Figure 3.30. They add a lot of parasite drag but do not contribute to anything. They also cannot function as anti-shock bodies, since these would have to be on the top side of the wing as this is where shocks occur. With the FishBAC system, the flap fairings would not be needed anymore, meaning they can be removed. A quick calculation on how much fuel can be saved by removing these is given below.



Figure 3.30: A330 flap fairings.

The cruise flight is the longest and most fuel consuming part of the flight, hence the benefits will only be calculated for the cruise phase. First the drag of each fairing were calculated. These cruise conditions were used:

- $\rho_{cruise} = 0.348 \text{ kg/m}^3$, according to the international standard atmosphere (ISA) at flight level 37.
- $C_{D_{fairing}} = 0.05$ [40].
- $S_{fairing} = 0.3$ Front view assumed to be a square of 0.6×0.5 m.
- $v_{cruise} = M \cdot a = 0.82 \cdot 295.070 = 242 \text{ m/s}$.

The drag then could be calculated according to Equation (3.20).

$$D_{fairing} = \frac{\rho_{cruise}}{2} \cdot C_{D_{fairing}} \cdot S_{fairing} \cdot v_{cruise}^2 = \frac{0.348}{2} \cdot 0.05 \cdot 0.3 \cdot 242^2 = 152.85 \text{ N} \quad (3.20)$$

For the 8 flap fairings the A330 has, this equals to a total drag reduction of 1,222.8 N. In approach ($\rho = 1.225 \text{ kg/m}^3$ and $v = 71 \text{ m/s}$) this is $47 \cdot 8 = 376 \text{ N}$. Here, the wing-flap fairing interference drag reduction is neglected. This procedure should be very easy to conduct, since the fairings are just bolted onto the skin. The downside of this procedure is that the Ram Air Turbine (RAT) is located in one of these fairings on an A330. It will have to be moved to the wing fairing, which should be a minor operation. There is enough space there and next generation Airbus aircraft like the A350 already have their RAT in the wing fairing. For further research, a more detailed design of this RAT has to be made.

Lift Distributions

Before the structural design can be started, it is necessary to know the lift force on the flap. The lift distribution was assumed to be triangular spanwise (see Figure 3.31). After this, a linear equation $L = ax + b$ was set up for the lift line with boundary conditions according to Equation (3.21).

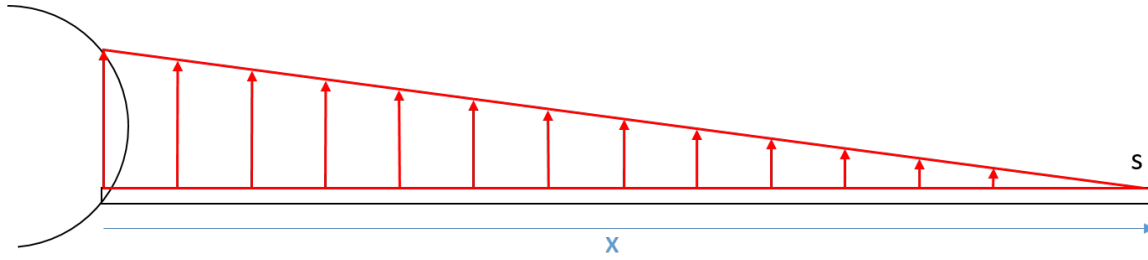


Figure 3.31: Free body diagram of the assumed span-wise lift distribution.

$$L = W = \int_0^s (ax + b) dx \quad (3.21) \quad x = s \text{ then } L = 0 \quad (3.22)$$

The values were calculated according to Equation (3.23) and Equation (3.24).

$$a = \frac{-2W}{s^2} = \frac{-2(2.33 \cdot 10^3 \cdot 9.81)}{27.33^2} = -61.20 \quad (3.23) \quad b = -a \cdot s = 61.20 \cdot 27.33 = 1,673 \quad (3.24)$$

Next, this spanwise distribution was used to calculate the load on both the inboard and outboard flap. A maximum load factor of 2.5 was included to find the ultimate load. When looking at the chordwise pressure distribution of the extended flap in Figure 3.32, it was concluded that roughly a fourth of the total lift is carried by the flap. For the inboard flap the lift thus equals:

$$L_{inboard} = \frac{1}{4} \cdot n_{max} \int_0^{6.821} (-61.20x + 1,673) dx = \frac{1}{4} \cdot 2.5 \cdot 9,986 = 6,241 \text{ N} \quad (3.25)$$

The final step in calculating the flap load was, similarly to the span-wise distribution, assuming a triangular lift distribution on the flap as is shown in Figure 3.33. The chord of the flap at the MAC is $0.26\bar{c} = 1.87 \text{ m}$ as taken from an A330 planform drawing [23]. Equation (3.23) and Equation (3.24) were applied again only now $W = L_{inboard}$ and $s = \bar{c}_{flap} = 1.87 \text{ m}$. This procedure was repeated for the outboard flap ($6.821 < s < 9.869$) and the final results are shown in Equation (3.26) and Equation (3.27).

$$L_{y_{inboard}} = -3,569.6x + 6,675.16 \text{ [N]} \quad (3.26)$$

$$L_{outboard} = 2,213.4 \text{ N} \quad L_{y_{outboard}} = -1,265.9x + 2,367.3 \text{ [N]} \quad (3.27)$$

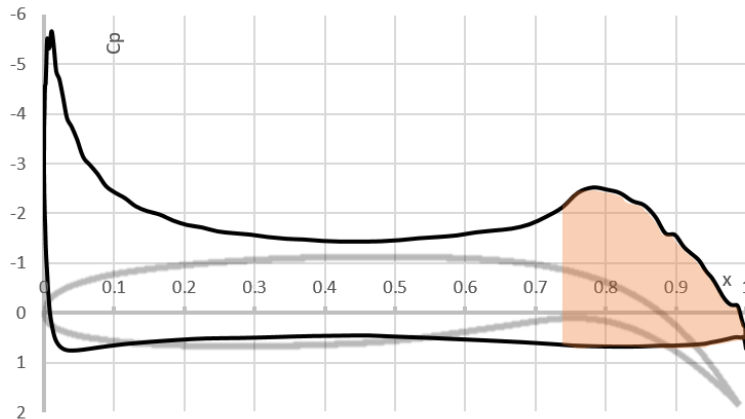


Figure 3.32: C_p distribution of the FishBAC flap in extendend condition during approach. The shaded area is the lift that the flap takes. Generated in Javafoil ($\alpha = 0$).

3.4.2. Structures

Besides the aerodynamic component of the FishBAC retrofit, it was also essential to assess the structures aspect. This meant anything related to the loads on, as well as in, the structure should be analysed, such that appropriate materials can be chosen. First the assumptions will be established, after which the design process will be elaborated. This design process consists of calculating the loads and stresses present in the centre beam, the stringers, the tip, the tendon and the skin.

Assumptions

Structural design is a complex procedure that requires a lot of time and effort. In order to construct a preliminary structural design, assumptions needed to be made. Below the assumptions for this design process are stated, along with their expected impact.

- FB-1** The deflection of the FishBAC can be modelled with simple beam theory. Beam theory only holds for small deflections, but the FishBAC experiences a very large deflection. This means the shortening of the FishBAC as it morphs is not taken into account in this analysis. While the results of this analysis are therefore not entirely accurate, beam theory is still used to obtain a design relatively quickly.
- FB-2** The skin material is assumed to have a Poisson's ratio of 0. In reality, when a material is stretched in one direction, its dimensions in the other directions decrease. Due to the relatively low strains (<5%), it can be assumed that the skin does not lose width or thickness when stretched.
- FB-3** The lift distribution on the flap is considered to be triangular. In reality, the lift distribution is very complex and it depends on a lot of parameters. Typically, the lift decreases towards the leading edge, which is why this distribution is chosen.
- FB-4** The assumed load case is approach with maximum load factor. This means the flaps are fully extended and the load factor on the aircraft is high (2.5). In reality, the aircraft is not likely to ever experience these loads, so this means the FishBAC will be overdesigned.
- FB-5** The drag on the flap is assumed to be negligible. In reality, the flap does experience a drag force, but it's considered negligible compared to the force in the tendons.
- FB-6** The mass of the FishBAC is assumed to be negligible. The mass of the FishBAC is very low compared to the lift it experiences. This means the FishBAC is slightly overdesigned due to this, since its weight will pull the flap in the downward direction and contribute to the desired deflection.

The structural design was a challenge in the design of the FishBAC flap, as it requires a cross-section that can withstand large loads and still bend significantly. There were a large amount of design parameters that were all linked. To find an optimal design, iteration is definitely a necessity. As a first step, a free body diagram of the retracted FishBAC flap is presented in Figure 3.33. Note that the height of the FishBAC flap at the root has been exaggerated for the purpose of clarity.

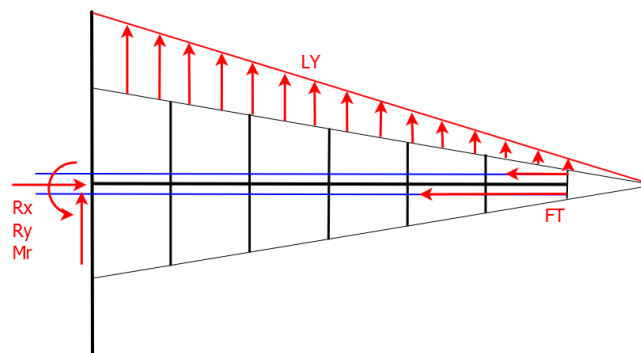


Figure 3.33: Free body diagram of the FishBAC flap in retracted state.

Figure 3.33 shows the FishBAC design with a centre beam in the middle, with vertical stringers that support the skin of the FishBAC flap. The tip of the flap was a hollow triangle. The vertical stringers extend throughout the entire span of the flap, but throughout the span there were a discrete number of centre beams. L_Y represents the lift distribution. F_T represents the force applied by the actuation system to morph the flap. The tendons are always under tension to withstand lift loads, but the actuation system will increase the tension in the lower tendon, which will morph the flap. R_x and R_y represent the reaction forces in the x and y direction respectively. Finally, M_r represents the reaction moment. Equation (3.28) presents an equation for the lift distribution.

$$L(x) = 7469 - 3956 \cdot x \quad (3.28)$$

Centre Beam Design

The first step of design was designing the centre beam. This structure will carry most of the loads, while it must also provide the required deflection. The design process was an iterative one, so all steps used will be described below. A

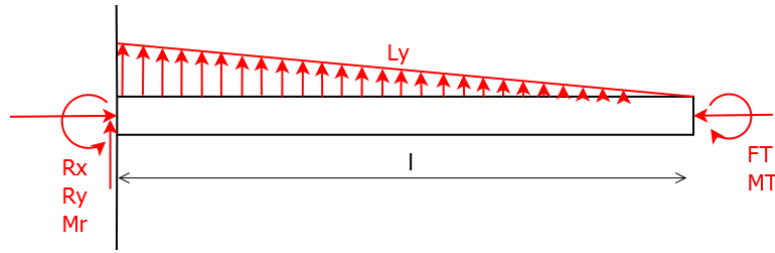


Figure 3.34: Simplified loading of the centre beam.

simplified load case of the one shown in Figure 3.33 is presented in Figure 3.34, where the beam in the figure is the centre beam. The cross-section of this beam was assumed to be a simple rectangle, which means its moment of inertia and cross-sectional area can be represented according to Equation (3.30) and Equation (3.29). The forces in the two tendons create a moment M_T about the beam that is used to deflect the tip downwards, and a compressive force F_T .

$$A_{cb} = b_{cb} h_{cb} \quad (3.29)$$

$$I_{xx,cb} = \frac{1}{12} b_{cb} h_{cb}^3 \quad (3.30)$$

The loading case from Figure 3.34 could be used to find the required force and moment to achieve a certain deflection of the beam. If the deflection δ is known, beam solutions could be added and the force and moment required to achieve the deflection of the tip of the beam can be calculated according to Equation (3.31)³⁹.

$$\begin{cases} M_T = \delta \cdot \frac{2E_{cb}I_{xx,cb}}{l^2} + \frac{L_Y l^2}{4} & (3.31a) \\ F_T = \frac{M_T}{d_y} & (3.31b) \end{cases}$$

In Equation (3.31), E_{cb} represents the Young's modulus of the centre beam, l represents the length of the beam and d_y represents the distance between the centre beam and the tendons. The reaction forces were calculated from force equilibrium, according to Equation (3.32), and used as an input for the internal moments. The equations for this can be found in Equation (3.33).

$$\begin{cases} R_x = F_T & (3.32a) \\ R_y = \frac{l}{2} \cdot L_0 & (3.32b) \\ M_r = -\left(\frac{L_0 \cdot l^2}{6} + M_T\right) & (3.32c) \end{cases}$$

$$\begin{cases} M = M_r - R_y \cdot x - \frac{L_0}{2} \cdot x^2 + \frac{5L_0}{6l} \cdot x^3 & (3.33a) \\ N = R_x & (3.33b) \\ S = R_y - x \cdot \frac{L_0}{2l} + L_0 \cdot x & (3.33c) \end{cases}$$

When the internal forces and moments were known, the stresses in the centre beam could be calculated. In Equation (3.34) the normal stress in the beam for a given design was calculated at the point furthest away from the neutral line ($h_{cb}/2$) and in Equation (3.35) the shear stress was calculated. Finally, the maximum stress in the cross section was calculated in Equation (3.36) using Mohr's circle. If the design did not yield under the given loads with a safety factor of $sf = 1.5$, so $\sigma_{max} \cdot sf < \sigma_y$, it continued on to the next stage of the design: buckling.

$$\sigma_z = -\frac{M \cdot \frac{h_{cb}}{2}}{I_{xx,cb}} - \frac{F_T}{h_{cb} b_{cb}} \quad (3.34)$$

$$\tau = \frac{S}{A} \quad (3.35)$$

$$\sigma_{max} = \frac{1}{2} \sigma_z + \sqrt{\left(\frac{1}{2} \sigma_z\right)^2 + \tau^2} \quad (3.36)$$

To be able to design the centre beam for buckling, it was assumed to be a simply supported beam under compression by a force F_T . The critical buckling load of the design was calculated according to Equation (3.37) and was compared

³⁹URL <https://www.grantadesign.com/resources/shapes/solutions/elastic.htm> [cited 13 June 2017].

to the applied load F_T with a safety factor of 1.5 ($P_{cr} > F_T \cdot sf$). If the beam fails, a stringer was added to reduce length L and increase the critical buckling load P_{cr} . When the design had a certain amount of stringers under which it would not buckle, its weight was estimated by assuming a stringer thickness and calculating the weight of the centre beam and stringers combined. The lightest design was chosen and continues on to the stringer design.

$$P_{cr} = \frac{\pi^2 E_{cb} I_{xx,cb}}{L^2} \quad (3.37)$$

Stringer Design

To calculate stringer dimensions, first a free body diagram (FBD) needed to be drawn of both the system as a whole and an individual stringer. The FBD of the actuated FishBAC flap is shown in Figure 3.35a and the FBD of an individual stringer is presented in Figure 3.35b.

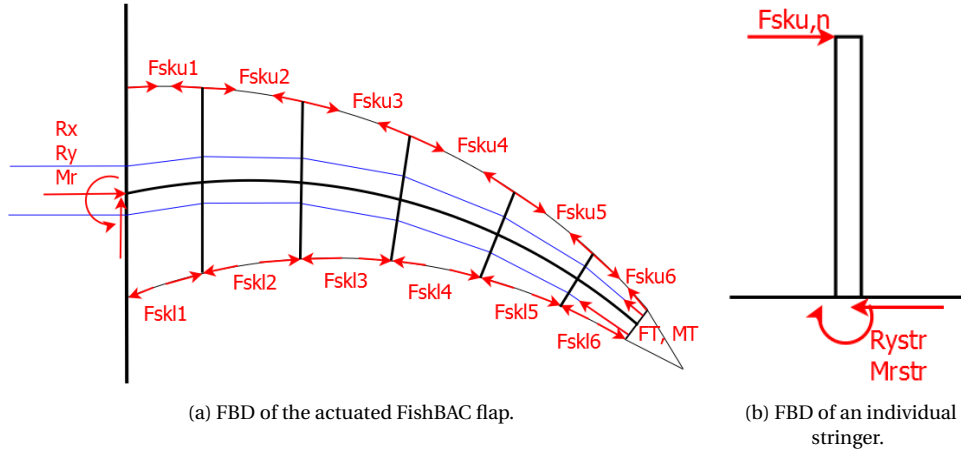


Figure 3.35: FBD's of the actuated FishBAC flap.

F_{sku} represents the force on the stringer caused by the stretching of the upper skin, and F_{skl} represents the force on the stringer caused by compression of the lower skin. Note that the skin is divided into different sections by the stringers, so there are 6 skin panels and 5 stringers at this point. Since one skin needs to be stretched more than another, there will be a resultant force on the stringer. The magnitude of this force was calculated by first finding the deflection of the skin using Equation (3.38), which is standard beam theory.

$$w = \frac{1}{EI_{xx}} \int_0^x M dx = \frac{1}{E_{cb} I_{xx,cb}} \int_0^x M_r - \frac{1}{2} \cdot L_y \cdot x^2 - R_y \cdot x dx \quad (3.38)$$

To find the stretch of a panel of skin, the deflections caused by both stringers were calculated and added, using simple geometry according to Equation (3.39). The height of each stringer was calculated in compliance with the triangular geometry of the FishBAC. Note that n represents the stringer number. Once the elongation of the skin was known, the strain could be calculated using Equation (3.40), and finally the stress in the skin according to Equation (3.41). It was checked if the skin did not yield under the given load with a safety factor of $sf = 1.5$ ($\sigma_{sk,n} \cdot 1.5 < \sigma_{y,sk}$). If the skin yielded, a material with different properties was chosen.

$$dl_{sk,n} = \cos\left(\frac{w_{n-1}}{2}\right) \cdot \frac{h_{st,n-1}}{2} - \cos\left(\frac{w_n}{2}\right) \cdot \frac{h_{st,n}}{2} \quad (3.39)$$

$$\epsilon_n = \frac{dl_{sk,n}}{l_{sk,n}} \quad (3.40)$$

$$\sigma_{sk,n} = E_{sk} \cdot \epsilon_n \quad (3.41)$$

Next, the lower skin panels were checked for buckling, as these skin panels would be under compression once the FishBAC is extended. For this, Equation (3.42) [41].

$$P_{cr,sk} = \frac{k\pi^2 D}{b^2} \quad (3.42a)$$

$$k = \left(\frac{mb}{a} + \frac{a}{mb}\right)^2 \quad (3.42b)$$

$$D = \frac{Et^3}{12(1-\nu^2)} \quad (3.42c)$$

In this equation, D stands for the flexural rigidity of the skin, a is the length of the skin between two stringers and b is the length of the skin panel in spanwise direction. m is a factor which depends on the fraction $\frac{a}{b}$: if this fraction is

smaller than $\sqrt{2}$, m is equal to 1. This is the case for the strips of skin between the stringers: in spanwise direction, they run along the entire length of the flaps, while a is in the order of centimetres. $P_{crit,sk}$ was then compared to the force in the skin, which is found by multiplying the previously found stress with the cross-sectional area of the skin. If the skin buckled, another material needed to be considered. Eventually it turned out the skin could not be designed out of a single polymer without buckling. To solve this problem, aluminium strips were added to the skin as a reinforcement. Once the stress in each panel was known, the forces on the stringers were calculated according to Equation (3.43).

$$F_{sk,n} = \sigma_{sk,n} \cdot A_{sk} - \sigma_{sk,n-1} \cdot A_{sk} \quad (3.43)$$

The maximum internal moment of the stringer is located at the root, while the internal shear is constant throughout the stringer. This meant the highest stress were experienced at the root of the stringer. The shear stress and normal stress at the root are represented by Equation (3.44). The maximum stress in the cross-section was then calculated using the Mohr circle from Equation (3.36). Note that a flat plate is assumed as the cross-section for the stringers, with dimensions h_{str} , which depends on the amount of stringers and the stringer number, and t_{str} . The width of the stringers depended on the amount of centre beams chosen for the design. Again, $\sigma_{max,str}$ was compared to $\sigma_{y,str}$ of the material chosen for the stringers ($\sigma_{max,str} \cdot sf < \sigma_{y,str}$). If the design failed, a larger thickness was chosen.

$$\left\{ \begin{array}{l} \sigma_{str,n} = -F_{sk,n} \cdot \frac{h_{str,n} \cdot \frac{t_{str,n}}{2}}{I_{xx}} \\ \tau_{str,n} = \frac{F_{sk,n}}{A_{str}} \end{array} \right. \quad (3.44a)$$

$$\tau_{str,n} = \frac{F_{sk,n}}{A_{str}} \quad (3.44b)$$

Using the aforementioned method, each stringer could be given an individual thickness, such that the lowest weight possible was achieved.

Tip Design

The triangular tip of the FishBAC is subjected to a large loading, since both tendons, as well as the centre beam, are connected to it. This loading manifests itself primarily as shear and torque, as shown in the FBDs in Figure 3.36. The chosen load case was a deflected FishBAC and the tip has a height h_{tip} .

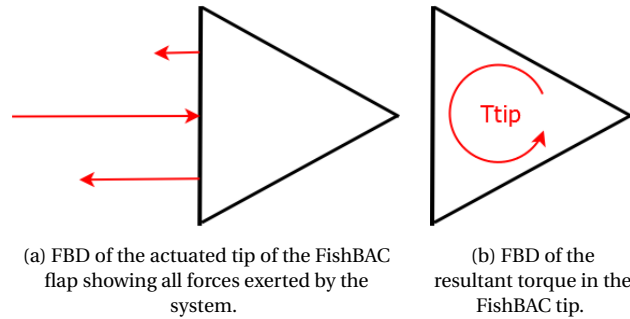


Figure 3.36: FBD's of the tip of the actuated FishBAC flap.

The two rightmost elements of the triangle were sized based on the internal torque. First the shear stress caused by the torque was calculated, and using the maximum shear stress of the material the thickness of these plates was found, in accordance with Equation (3.45) and Equation (3.46).

$$q = \frac{T_C \cdot dy}{2A_{encl,tip}} \quad (3.45)$$

$$t_{tip} = \frac{q}{\tau_{max}} \quad (3.46)$$

The leftmost vertical plate is also loaded under shear. Since all forces cancel out, there is no resultant shear in the cross-section, but there is an internal shear that is specifically large between the centre beam and the lower tendon, namely equal to F_T if the beam is fully actuated. The thickness of this section can be calculated using internal shear, according to Equation (3.47). While the expected thickness of this section was higher than that of the other sections, in any regard, the largest thickness would be used.

$$t_{tip,v} = \frac{F_T}{\tau_{max} \cdot h_{tip}} \quad (3.47)$$

Tendon Design

The design of the tendon was based on the force F_T . It is assumed that the tendons have perfectly circular cross-sections and are loaded in pure tension. When this is assumed, their radius was easily computed using Equation (3.48).

$$r_T = \sqrt{\frac{F_T \cdot s f}{\pi \sigma_{y,T}}} \quad (3.48)$$

3.4.3. Materials

As explained in Section 3.4.2, material selection was an integral part of the FishBAC design. Therefore the essential characteristics of the individual components had to be assessed and a suitable material was selected. This process will be elaborated below and the final configuration will be presented.

Inner structure

Materials pose a large challenge in the design of morphing structures. A structure provides a load-carrying framework, but in case of a morphing FishBAC it should also allow for large deflections. This means one requires a material that has a low Young's modulus but a high yield stress. Several materials were investigated and eventually it was decided that heating a reinforced polymer would provide both structural integrity and flexibility.

Within the aerospace industry there are several thermoplastics that could provide the resin of the composite: PEEK (polyetheretherketone), PEKK (polyetherketoneketone), PEI (polyetherimide) and PPS (polyphenylenesulphide)⁴⁰. When combined with carbon fibre (CF), these resins form a composite with excellent stress properties and stiffness. For a morphing design, however, a flexible structure is required as well. Therefore the composite can be heated to the glass transition temperature of the resin, and morphed with relatively little force while maintaining a lot of its strength⁴¹. Table 3.3 presents some characteristics of these thermoplastics reinforced with 30% carbon fibre^{42,43,44,45,46}. It compares the material glass transition temperature T_g , density ρ , tensile modulus E and tensile strength σ_F .

Table 3.3: Properties of (30%) carbon fibre reinforced thermoplasts.

Material	T_g [°C]	ρ [kg/m ³]	E [GPa]	σ_F [MPa]	Notes
CF/PEEK	143	1,410	7.85	131	
CF/PEKK	159	1,310	1.5/20.1	8.9/357	90°/0° fibre orientation
CF/PEI	215	1,390	21	207	
CF/PPS	90	1,450	34	178	

Out of these options, CF/PPS was chosen due to its low glass transition temperature and high tensile yield strength. While the tensile modulus seems too high for a morphing structure, it can be heated to its glass transition temperature in 30 seconds which will reduce this modulus drastically³⁶. From here it can be morphed up or down using the FishBAC structure. PPS is a semi-crystalline thermoplast. This means its molecular chains are partially aligned. These chains form ordered regions called lamellae, and larger spheroidal spherulites. The result of this process is an increase in strength and stiffness both below and above T_g . Below T_g , a semi-crystalline polymer is more brittle than an amorphous one. Above T_g , a semi-crystalline thermoplastic will be less viscous and allow for more controlled morphing and better load resistance [42].

While copper wires heat the CF/PPS to its glass transition temperature, the FishBAC actuation system is deployed. Table 3.4 displays the properties of CF/PPS both at room temperature and at T_g . If the CF/PPS is heated up too much, it will delaminate, and hence the temperature needs to be carefully controlled to stay near the transition point (90-110 °). Once the required deflection is obtained, the heating is switched off and the CF/PPS will cool down in 30 seconds³⁶, and it will regain its initial properties.

Materials for aircraft applications cannot be chosen without considering their fatigue behaviour. Flaps are deployed at least twice per flight, sometimes more, so for flaps fatigue can definitely not be neglected. CF/PPS is known for excellent fatigue properties, with very limited permanent deformation, most of which occurs early in life. Even after a test of 1,500,000 load cycles at 85% of the failure stress, a CF/PPS sample showed very little permanent deformation [43]. Less information is known about thermal fatigue since it is a very new research area in composite sciences. Since the composite is not heated close to its melting temperature, thermal fatigue is not expected to be as large of an issue in this case.

⁴⁰URL <http://www.compositesworld.com/articles/composites-101-fibers-and-resins> [cited 16 June 2017].

⁴¹Private communication, Dr. Irene Fernandez Villegas [16 June 2017 11:00].

⁴²URL <http://www.plasticomp.com/complet-1cf30-pps> [cited 16 June 2017].

⁴³URL <http://www.cnplastics.com/pdf/Carbon%20Filled%20PEEK%20Extruded.pdf> [cited 16 June 2017].

⁴⁴URL <http://www.plasticomp.com/complet-1cf30-pei> [cited 16 June 2017].

⁴⁵URL https://www.cytec.com/sites/default/files/datasheets/PEKK_032012-02.pdf [cited 16 June 2017].

⁴⁶URL http://www.boedeker.com/peek_p.htm [cited 16 June 2017].

Table 3.4: Properties of CF/PPS.

Property	Value	Unit
ρ	1,450	kg/m ³
T_g	90	°C
σ_F	187	MPa
σ_F at 107° C	77	MPa
E	34	GPa
E at 107° C	14	GPa

Skin

Since the skin was designed under the assumption that it does not carry any loads except during its stretching, it was most useful to find a material that is specifically very ductile so it will not yield under the strain, in accordance with Equation (3.40) and Equation (3.41). Since the skin comes into contact with the air during flight, it will experience very low temperatures. This means it will need to operate at temperatures as low as -50 °C. To meet these requirements, polyether-ester block copolymer (TEEE/COPE) with 10% glass fibre was chosen. It has an operating temperature range of -70 to 100 °C, excellent fatigue behaviour and does not yield under the stresses of stretching it⁴⁷. Table 3.5 shows the most important properties of the polyether-ester block copolymer⁴⁸.

Table 3.5: Properties of polyether-ester block copolymer with 10% glass fibre.

Property	Value	Unit
ρ	1,260	kg/m ³
σ_y	32	MPa
E	1.1	GPa

Tendon

The tendon is part of the actuation system that will morph the flap. This means it will carry a large tension load. To keep the diameter of this tendon as low as possible, a tendon with a very high maximum tensile stress was chosen: Dyneema. Dyneema is a lightweight high-strength oriented-strand gel spun through a spinneret. While its yield strength is comparable to that of a steel cable, its density is much lower, resulting in a much lighter cable. Table 3.6 shows the most relevant properties of Dyneema⁴⁹.

Table 3.6: Properties of Dyneema.

Property	Value	Unit
ρ	0.96	kg/m ³
σ_y	3,090	MPa
E	172	GPa

3.4.4. Integration and Configuration

With the exact design known, the last step was to integrate the FishBAC system. This process will be elaborated below, as the actuation mechanism will be investigated and the final configuration will be visualised.

Actuation Mechanism

Once the entire FishBAC mechanism was sized, the next step was to size the actuation mechanism. For a desired deformation of the FishBAC a specific torque had to be achieved by the actuator. In order to be able to use the current hydraulic system for the FishBAC actuation, this torque should be producible by a rotary actuator operating within the power budget of the hydraulic pump, which for the A330 was found to be equal to 3,000 psi [44].

The starting point for the actuator calculations is the downward deflection angle of the flap, as previously defined in Figure 3.27. A certain actuator rotation is required to achieve this deflection. Naturally, if the diameter of the actuated

⁴⁷URL <http://web.rtpcompany.com/info/data/1500/RTP1501-55D.htm> [cited 16 June 2017].

⁴⁸URL <http://web.rtpcompany.com/info/data/1500/RTP1501-55D.htm> [cited 16 June 2017].

⁴⁹URL <https://www.matbase.com/material-categories/natural-and-synthetic-polymers/polymer-fibers/synthetic-fibers/material-properties-of-Dyneema.html> [cited 21 June 2017].

pulley guiding the tendon is equal to the distance between the tendons, those two angles are equal. However, if this is not the case, a correction factor is needed which results in Equation (3.49)

$$\theta_{act} = \theta_{flap} \cdot \frac{d_T}{D_{pull}} \quad (3.49)$$

Here, d_T is the distance between the tendons and D_{pull} is the diameter of the pulley. Multiple rotary actuators were evaluated using the Helac product catalog⁵⁰ and the Parker company website⁵¹. Many actuators are able to achieve a maximum rotation of either 90°, 180° or 360°. Setting the rotation angle of the actuator to this maximum value, the required diameter of the pulley can be found. For a maximum angle of 90°, this resulted in Equation (3.50).

$$D_{pull} = \frac{\theta_{flap}}{\theta_{act}} \cdot d_t = \frac{28}{90} \cdot 0.01 = 0.0031 \text{ m} \quad (3.50)$$

Obviously, a pulley diameter of 3.1 mm was not feasible. This does however prove that a maximum rotation of 90° is more than sufficient, and that the pulley (and thus actuator) could be downsized as far as possible. However, the minimum pulley diameter will be said to be equal to the diameter of the tendon. The main thing that should be accounted for when sizing the actuator is the drive torque, which is equal to the force in the tendon times the diameter of the driving pulley (and thus, as stated before, the diameter of the tendon). With a force F_T of 294,926 N and a tendon diameter of 16.6 mm, the required actuator torque is thus 4,896 Nm, or 43,331 in-lbs. The Parker medium duty HTR series offers rotary actuators with an output torque ranging between 300 in-lbs and 600,000 in-lbs, at respective weights between 11 and 1,560 lbs. Assuming a linear relationship between output torque and weight, an actuator with an output torque of 43,331 in-lbs will weigh approximately 123 lbs, or 55.7 kg. This specific actuator is a rack and pinion type with two racks, where linear motion of the racks is translated into rotational motion of the pinion. It is expected that an actuator specifically tailored for this application will weigh considerably less than this off-the-shelf product.

Final configuration

Table 3.7 displays the final design parameters for the FishBAC flaps. Both the outboard and the inboard flap will be replaced by a FishBAC. Figure 3.37 shows the configuration for the inboard flap, with 5 stringers and 4 centre beams. For illustration, Figure 3.37a shows the outer skin of the inboard FishBAC flap. The striped sections represent sections made from Aluminium 6061. Figure 3.37b shows the internal structure of the inboard FishBAC.

Table 3.7: Design parameters for the FishBAC flaps.

	nr	Inboard flap	Outboard flap	Unit		nr	Inboard flap	Outboard flap	Unit
w_{fb}		6.82	11.25	m	t_{str}	1	0.006	0.006	m
c_{fb}		1.8876	1.8876	m		2	0.003	0.003	m
r		0.35	0.35	m		3	0.005	0.006	m
n_{cb}		2	7	-		4	0.003	0.004	m
b_{cb}		0.061	0.06	m		5	0.003	0.003	m
h_{cb}		0.029	0.026	m	t_{sk}		0.005	0.005	m
sp_{cb}		2.773	1.4065	m	r_T		0.0055	0.0047	m
n_{str}		5	5	-	W_{tendon}		1.91	4.85	kg
sp_{str}		0.2563	0.2563	m	W_{skin}		106.47	210.55	kg
h_{str}	1	0.065	0.065	m	$W_{CF/PPS}$		242.33	386.78	kg
	2	0.055	0.055	m	W_{Al}		66.3	109.37	kg
	3	0.044	0.044	m	W_{tot}		417.01	711.55	kg
	4	0.032	0.032	m					
	5	0.024	0.024	m					

Total weight

Combined, the total FishBAC flap system was found to weigh 1,578 kg per wing. The old flaps plus actuator system weighed roughly 1,350 kg based on empirical relationships. So a weight increase of roughly 228 kg is the result of retrofitting FishBAC flaps.

However the weight of the flap track fairing needs to be deducted from this number. These are assumed to be a box with sides of $0.5 \times 3.6 \times 0.4 \text{ m}^3$ with one side missing, the one which is attached to the wing itself. They are made of

⁵⁰URL https://www.helac.com/uploads/file/actuators/product-brochures/Helac_Actuator_Product_Catalog_011917.pdf [cited 19 June 2017].

⁵¹URL <http://ph.parker.com/ca/en/hydraulic-rotary-actuators> [cited 20 June 2017].

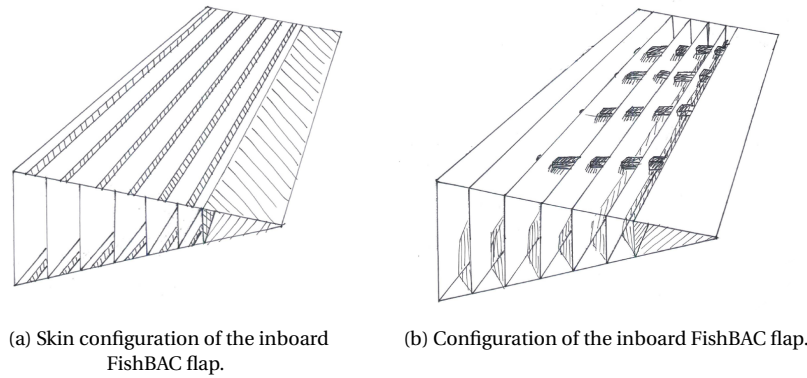


Figure 3.37: FBD's of the tip of the actuated FishBAC flap.

a 1 mm aluminium skin with a density of $2,702 \text{ kg/m}^3$ [40]. In total, eight of them will be removed. The final weight then is given as in Equation (3.51).

$$W_{fairings} = 8 \cdot (2 \cdot 0.5 \cdot 3.6 + 0.4 \cdot 3.6 + 2 \cdot 0.5 \cdot 0.4) \cdot 0.001 \cdot 2,702 = 117.6 \text{ kg} \quad (3.51)$$

This means that the total weight increase of the FishBAC is 100 kg, rounded off.

3.4.5. Cost

To make an estimation of the total FishBAC retrofit cost, a similar approach was adhered to as used for the winglets. The total cost were subdivided into four categories: development, product, process and downtime cost.

Development Cost

A lot of development is still required before the FishBAC retrofit will be able to enter the market. Currently, the FishBAC mechanism has been tested on a very small scale in low-speed wind tunnel tests. No analysis has been done on the mechanism as an integrated part of the wing, or at conditions that are representative for the actual flight conditions. The design will still have to pass the following steps during its development phase:

- compute a detailed numerical model of the FishBAC integrated into the wing,
- perform a detailed 3D CFD analysis of the model to check if the FishBAC can generate sufficient lift,
- perform a detailed 3D finite elements method (FEM) analysis of the design to check if additional structural sizing is required,
- construct a scale model of the FishBAC integrated into a wing,
- perform structural tests, such as bending tests to evaluate the stiffness of the centre beam,
- test the model in a wind tunnel to validate the CFD results,
- get the design certified and
- perform flight tests over a period of two years.

It was assumed that all development up to and including wind tunnel tests will be done by five engineering consultants over a period of four years. Following the estimation that these consultants cost approximately \$82,641 for half a year, this results in a cost of \$3.3M. Usage of a high speed wind tunnel will cost approximately \$500k for 1,000 hours⁵². Additional structural tests were estimated to cost a total of \$10M (similar to the structural tests of the winglet). Finally, \$5M was allotted to certification of the product, as this will be an extensive process, since it includes test flights on the A330-200. In total, the development costs were calculated to be \$18.8M. Since cost estimates are difficult to compute at such an early stage of the development, the development costs will have a safety factor of 1.3, which comes down to \$24.44M.

Product Cost

The product cost primarily depend on material costs. It was found that CF/PPS prepregs can be bought at approximately $50\text{--}100 \text{ €/m}^2$ ($56\text{--}112 \text{ $/m}^2$, US dollars) per ply prepreg of 1m^2 ⁵³. Assuming a ply thickness of 1mm, the composite costs $\$38.62\text{--}\77.24 per kg. Aluminium is known to cost $\$2.26$ per kg⁵⁴. Finally, the skin was approximated to cost the same as the CF/PPS, since they are both high performance engineering polymers. Table 3.8 shows the costs of each component of the FishBAC for both flaps on both wings. In conclusion, the total material costs would be in the range of $\$86\text{k--}\134k . In addition to this, the actuators would cost $\$5\text{k}$, which amounted to a total of $\$90\text{k}$ for both wings. The assembly of the FishBAC flaps was expected to take up to 20,000 man hours, at a salary of $\$25$

⁵²URL <https://www.aa.washington.edu/AERL/KWT/rateguide> [cited 26 June 2017].

⁵³Private communication, Dr. Irene Fernandez Villegas [16 June 2017 11:00].

⁵⁴URL: <https://www.metalprices.com/metal/aluminum/aluminum-6061-extrusion-billet-price> [cited 27 June 2017]

per hour, this comes down to \$500k. In total the production costs of the FishBAC flaps, for both wings and both flaps, came down to \$0.776 – 0.824M. A safety factor of 1.3 is added to account for future changes. This meant the total cost of the FishBAC came down to \$1 – 1.1M.

Table 3.8: Material costs for the FishBAC.

Component	Price [\$/kg]	Weight [kg]	Cost [\$]
CF/PPS	38.6	1,258.2	48,592.5
	77.2	1,258.2	97,184.9
Aluminium 6061	2.3	351.3	794.0
Skin	57.9	663.1	36,675.5
Total			86,062.0 - 134,654.4

Retrofit Process Cost

To these material costs, a labour cost for assembly is added. It is expected that FishBAC flaps take a total of 13,500 man hours to produce and integrate, 1.5 times as long as the winglets. At \$25 per man hour, the production and integration costs will be \$337.5k for the entire system on both wings.

Downtime Cost

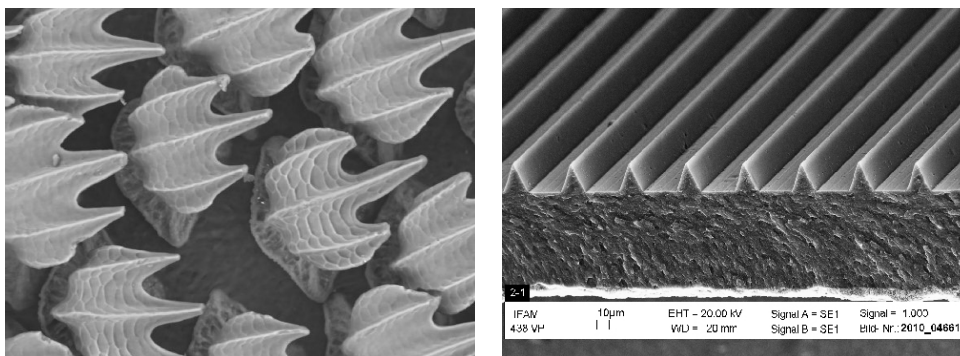
The downtime of the flaps was assumed to be 1.5 times that of the winglets, roughly 30 days. There were basically three scenarios of the FishBAC retrofit. It could be retrofitted simultaneously with the winglet during either a C- or a D-check, or separately during either check. The costs are elaborated below.

- Retrofitting during the C-check: in low season, assuming an additional 24 days of downtime, but assuming winglets are also retrofitted so neglecting 15 days: $\$1,698 \cdot 9 + \$1,414 \cdot 18 + \$2,740 \cdot 9 = \$65,398$.
- Retrofitting during the C-check: in low season, assuming an additional 24 days of downtime: $\$1,698 \cdot 24 + \$1,414 \cdot 48 + \$2,740 \cdot 24 = \$174,396$.
- Retrofitting during the D-check, in low season, assuming an additional 16 days of downtime, but simultaneously with the winglet so neglecting 6 days: $\$1,698 \cdot 10 + \$1,414 \cdot 20 + \$2,740 \cdot 10 = \$72,665$.
- Retrofitting during the D-check, in low season, assuming an additional 16 days of downtime: $\$1,698 \cdot 16 + \$1,414 \cdot 32 + \$2,740 \cdot 16 = \$116,264$.

Now all the costs are known. Depending on when the retrofit will be performed, the costs will vary.

3.5. Sharkskin

Nature is an inspiration for many engineering applications. Natural selection has, over millions of years, optimised organisms in certain fields. The shark is a particularly interesting animal for the aerospace industry, since the texture of its skin makes it more aerodynamically efficient than smooth skin does [45]. Figure 3.38a shows a close-up of the structure of the skin of a shark, and Figure 3.38b shows the coating that was created to mimic the effect.



(a) Microscopic structure of a shark's skin.

(b) Engineered shark skin.

Figure 3.38: Sharkskin structure.

3.5.1. Aerodynamics

Sharkskin works by reducing skin friction drag in the turbulent regime. Friction drag is caused by the interactions of molecules in fluid. At the surface of an object, the velocity of a fluid is zero. Moving away from the surface, each fluid layer has a higher velocity, until the mean flow velocity is reached. When the flow becomes turbulent, it introduces

randomness, cross-flow and non-parallel relative velocities, introducing a large amount of drag. Transition to turbulent flow occurs near a Reynolds number of $Re = 500,000$ over a flat plate. The Reynolds number is a function of fluid density ρ , velocity V , length L and dynamic viscosity μ according to Equation (3.52) [46].

$$Re = \frac{\rho V D}{\mu} \quad (3.52)$$

While fully developed turbulence exhibits complete randomness in its velocity distribution, near the surface the so-called viscous sublayer displays organisation. Stream-wise vortices dominate this viscous sublayer and are the cause of much of the chaos in the outer layers of the turbulent boundary layer, as illustrated in Figure 3.39. Streamwise vortices translate and rotate along the surface in the cross-flow direction. As they interact with the surface and with other neighbouring vortices, they emit new vortices into the boundary layer. These vortices tangle with other vortices and result in transient velocity vectors in the cross-stream direction that can become as large as those in the average flow direction, resulting in additional fluid drag. Reducing the bursting behaviour of the vortices in the viscous sublayer will generate a considerable reduction in global drag [46].

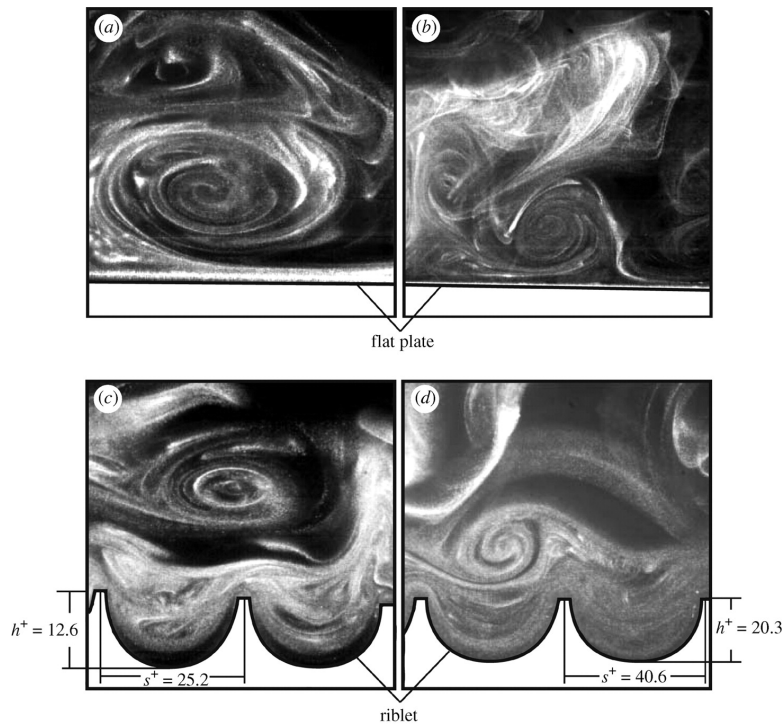


Figure 3.39: Visualisation of streamwise vortex propagation. Note that the flow would propagate into the plane of the page.

(a) represents the drag-decreasing case on a flat plate, (b) represents the drag-increasing case on a flat plate, (c) represents the drag-decreasing case on a riblet surface and (d) represents the drag-increasing case on a riblet surface [46].

As Figure 3.39 illustrates, riblets interact differently with vortices than a flat plate. The precise mechanism that causes the riblets to reduce the cross-stream translation of the stream-wise vortices in the viscous sublayer is not entirely understood yet. Part of it is caused by the decrease in wetted surface area. As vortices form above the riblet surface, they remain above these riblets and only rarely interact with the tips, while the valleys of the riblets only rarely experience high velocity vortices. This means only the tips of the riblets experience high-shear stresses, and the cross-stream velocities in the valleys of the riblets are much lower than those above a flat plate. This means that a large amount of the aforementioned bursting behaviour of the vortices in the viscous sublayer is inhibited, hence reducing skin friction drag [46].

Configuration

There are multiple possible configurations for a sharkskin, displayed in Figure 3.40. Multiple studies have focused on finding an optimal riblet configuration for maximum drag reduction.

Out of the shown options, blade riblets are known to have the highest drag reduction. However, this drag reduction is mostly achieved with very thin riblets. While very efficient, such a structure will be subject to intensive wear of the inherently weak structure these dimensions create. Scalloped riblets are the most widely applied version to date. Their geometry compromises a little on performance, but it is much more durable and thus a more realistic option for

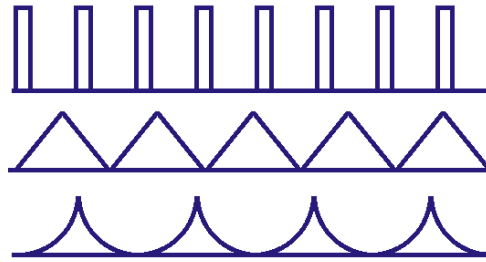


Figure 3.40: Possible sharkskin configurations. From top to bottom: blade riblets, scalloped riblets and sawtooth riblets.

widespread application. Finally, sawtooth riblets achieve the worst drag reduction of the set. They are, however, the most durable. Table 3.9 summarises the possible riblet geometries and their properties [47].

Table 3.9: Summary of riblet geometries and their properties [47].

Riblet shape	Maximum drag reduction	Durability
Blade	9.9%	Rapid wear due to small thickness
Scalloped	6.5%	Acceptable durability
Sawtooth	5%	Most durable option

To choose an optimum riblet geometry, one must balance performance and durability. Although it might sound attractive to choose the large drag reduction that blade riblets offer, this additional effect will not last for long. This is why scalloped riblets were chosen for the sharkskin design. It should be noted that scalloped riblets are the current standard, and are being manufactured by many companies such as Fraunhofer⁵⁵. Ultimately, these films have also been used in long-term flight tests by Boeing and Airbus [48].

Now that the general geometry has been chosen, more precise dimensions of the riblets can be found. Before a preliminary geometry analysis can be started, some of the drag reduction equations need to be elaborated slightly. A sharkskin reduces the shear stress on the surface of an object. Drag reduction is seen as the ratio of the shear stress on a sharkskin surface, $\Delta\tau_{sh}$, over the shear stress on a flat plate, τ_{fl} . It is presented as a function of the Reynolds number. Figure 3.41a shows the drag reduction for different scalloped riblet configurations. It becomes clear that a smaller angle of the scallops generates a better distribution. Note that in this case, the Reynolds number is defined as $S^+ \cdot 10,000$. It is immediately apparent that the Reynolds numbers here are very low. This is due to the fact that these experiments were conducted in oil instead of air or water. Using oil allowed the team to increase the riblet size and reduce the Reynolds number while still obtaining appropriate results. Their results have also been validated to be close to actual wind tunnel tests at Reynolds numbers of 400,000 [48]. This validation will be elaborated upon in Section 4.4.4.

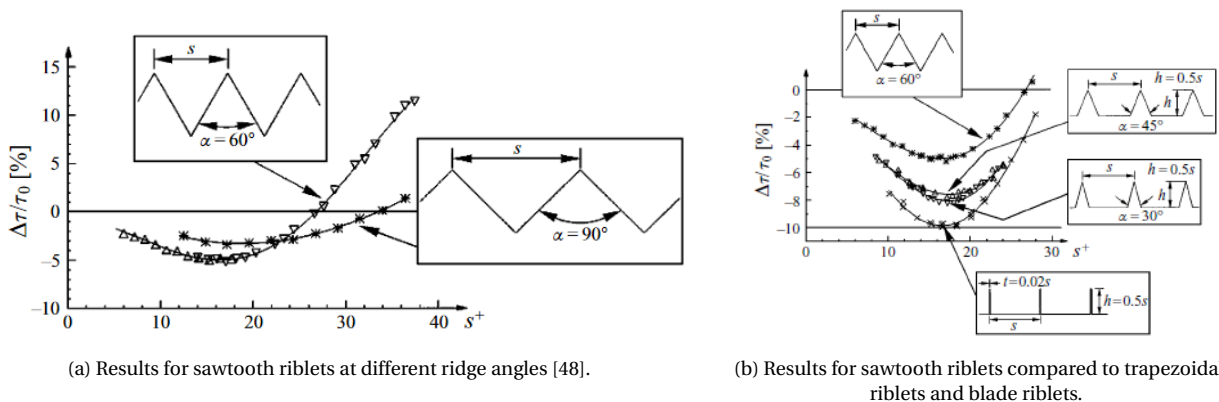


Figure 3.41: Drag improvements of different sharkskin geometries.

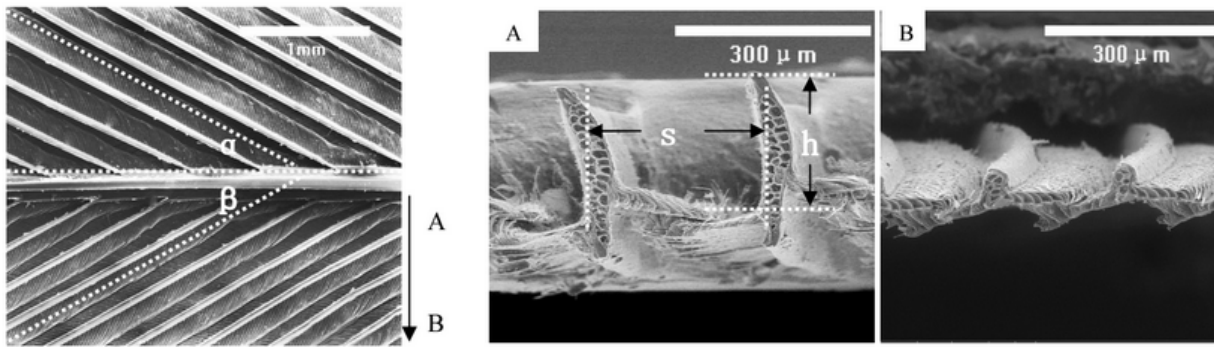
Figure 3.41a shows that a narrower triangle (smaller α) yields a better drag reduction. In further research, no further optimisation was conducted with this sharkskin configuration, but it was concluded that a 60° ridge angle is superior

⁵⁵URL http://www.ifam.fraunhofer.de/content/dam/ifam/en/documents/Adhesive_Bonding_Surfaces/Paint_Lacquer_Technology/low-drag_surface_riblet_coating_fraunhofer_ifam.pdf [cited 12 May 2017].

to a 90° ridge angle [48]. An additional consideration is adding spacing between the riblets, which has been shown to provide a better performance (8.2% as opposed to 6.5%), as illustrated in Figure 3.41b. While further optimisation of the riblet dimensions would generate a more optimised result, doing research on this is outside of the scope of the DSE. Therefore, this will be a recommendation for further research. For a more elaborate plan for the validation of the sharkskin, the reader is referred to Section 4.4.4.

Herringbone Riblets

Sharkskin is a relatively developed concept. This means that there have actually been a lot of tests, including flight tests, that have produced the expected results. One of these tests test was a scaled wind tunnel test of an Airbus A320 on which a V-groove sharkskin was applied, yielding an 8% net drag reduction in cruise [49]. Most relevantly, both Airbus and Boeing have tested aircraft covered with sharkskin for 70% and have measured fuel reductions of 3% [48], confirming earlier research. These sharkskin types were regular riblets with no yaw angle. However, in 2014, there was a new development in functional coatings: bird-feather herringbone riblets. The concept of the herringbone riblet is based on the feathers of birds, which, much like the skins of sharks, have also evolved to be aerodynamically efficient. Figure 3.42a shows a close-up of such a feather, and Figure 3.42b shows the cross-section of a feather at two locations in the feather.



(a) Structure of a feather. (b) Cross-section of a feather close to the root and further away from the root.

Figure 3.42: Biologically inspiring structure of a bird's feather.

The bird-feather herringbone at two yaw angles and regular sharkskin are displayed in Figure 3.43. The CFD shows that the turbulence in a herringbone riblet structure is much more concentrated. This results in a drag reduction of 15% for a 30° yaw, almost twice as much as regular sharkskin. If this concept can be realised on a scale as large as sharkskin h

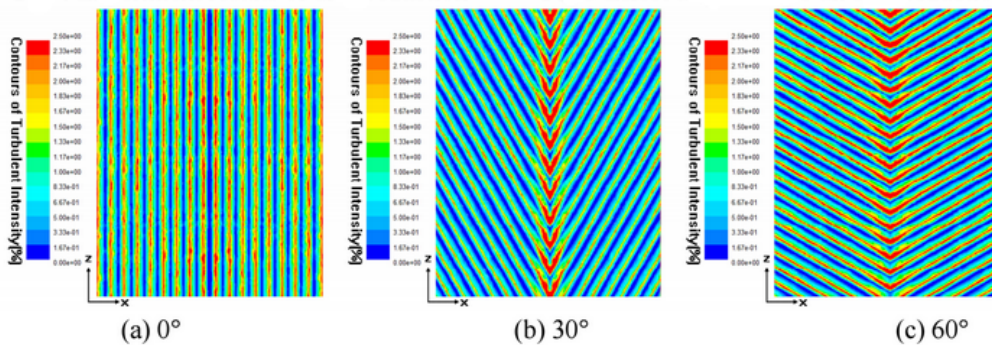


Figure 3.43: CFD analysis of different riblet configurations. (a) Represents a 'traditional' sharkskin, (b) represents a herringbone at 30° yaw and (c) represents a herringbone at 60° [50].

It is important to note that the aforementioned results were obtained in a water tunnel at a Reynolds number of no more than $Re = 400,000$ [50]. In cruise, the A330-200 experiences a Reynolds number of $Re = 125 \cdot 10^6$. This means that the results should not be taken out of context without consideration. While a prediction of viscous drag behaviour is very complex and outside of the scope of the DSE, an approximation based on test data can be made and investigated in the future. Sharkskin loses 20% of its drag reducing effect at transonic Mach numbers [51]. To compensate for this effect, the obtained improvement will be multiplied with a factor of 0.8. An indication of the effect of the herringbone riblets can be calculated in a similar manner as the effect of the sharkskin. If the herringbone riblets yield a 15% drag reduction when compared to a flat surface, and 70% of the aircraft can be covered in riblets, and accounting for a loss in efficiency due to misalignment and fabrication error ($\pm 10\%$), the total improvement can be approximated according to Equation (3.53) [47].

$$\Delta C_D = 0.15 \cdot 0.7 \cdot 0.9 \cdot 0.8 = 7.56\% \tag{3.53}$$

In conclusion, the sharkskin concept will be adapted to a herringbone structure. This means a (much) larger drag improvement can be achieved, at the cost of extra research. Since sharkskin is a more known and commercially accepted concept, this concept will still be referred to as the sharkskin.

3.5.2. Structures

Now that the aerodynamic improvements and general geometry of the sharkskin have been established, the structure will be elaborated upon. Since the effect of sharkskin coating mainly concerns aerodynamics, structures are essentially not considered in design. However, this section will cover a weight estimation of sharkskin. Basically, sharkskin would be a replacement of the top coat, made up out of the same material. Since it replaces the top coat, it will be made out of the same material and it will not add much additional weight to the aircraft. To make an approximation of the added weight of the sharkskin, an approximation of the surface area of the aircraft as a whole was calculated, according to Equation (3.54).

$$A_{surf} = 4 \cdot S + 2 \cdot \pi \cdot R_{fus} \cdot l_{fus} + 2 \cdot S_H + 2 \cdot S_V = 2,633.3 \text{ m}^2 \quad (3.54)$$

It was assumed that the sharkskin texture is added on top of a top coating with a riblet height of 0.3 millimetre [46] and the width at a 60° ridge angle, so the total weight was calculated according to Equation (3.55). Note the factor of 0.7: only 70% of the aircraft can be coated in sharkskin. This is because for example windows, the FishBAC and the landing gear cannot be coated.

$$W = 0.7 \cdot \rho_{tc} \cdot A_{surf} \cdot 0.0003 \cdot 0.00034 \cdot 0.5 = 346 \text{ kg} \quad (3.55)$$

This meant the sharkskin would add an additional 346 kg to the weight of the aircraft, and its reduction in fuel weight would definitely outweigh the added weight.

Another structural consideration was wear of the coating. Microstructures like the sharkskin are very fragile due to their size, and while sharks just heal when their skin is damaged, aircraft cannot. This means that any damage or wear of the sharkskin will result in a compromised performance. Typically, it takes two years until the performance of the sharkskin wears off significantly and the coating on a commercial aircraft needs to be reapplied, for a film application this interval is slightly longer: 4 years⁵⁶.

3.5.3. Materials

Sharkskin is usually made of the material that is used for top coats: epoxy⁵⁷. The epoxy top coat needs to be replaced every two years. This interval can be stretched by using different materials for the top coat. Epoxy can be mixed with other materials to improve durability. Examples are carbon- or glass fibres. At the time of this report, there was no clear research on how these materials are mixed and applied to the sharkskin: therefore, this was a recommendation for further research. For a more elaborate plan of the further research, the reader is directed to Section 4.4. For purpose of this report, pure epoxy was assumed as the sharkskin material, with a density of 1250 kg/m³⁵⁸.

3.5.4. Integration and Configuration

In Section 3.5.1 it was explained that sharkskin is only useful in turbulent flow. Therefore, it would be useful to have some knowledge on where the flow on an aircraft is turbulent, and apply the sharkskin strategically. This would reduce the added weight and cost of the concept without compromising on performance. A full turbulence analysis of the A330-200 was outside of the scope of the DSE and is hence a recommendation for further research. At this point, it is assumed that 70% of the aircraft can be coated in sharkskin, but this number will likely go down.

An additional benefit of applying the sharkskin in optimal positions was the added benefit of not having sharkskin in more fragile places, such as the leading edge. The flow on the leading edge is generally laminar, so applying sharkskin here will not be useful. In the meantime, this part of the wing is subject to bug impacts during take-off and landing, which will damage the sharkskin, meaning any effect it has would be diminished relatively quickly.

Broadly speaking there were two options for the application of sharkskin riblets to an aircraft: a film with the texture imprinted on it can be used, or it can be 3D printed onto the aircraft. A film has the advantage of being generally cheap and the fact that it can be bought off-the-shelf, but it is difficult to apply correctly and requires a lot of labour. 3D printing can be more exact, requires less manpower and is more versatile, since it is not limited by the manufacturer like a film is. Since a herringbone riblet had not yet been developed for aircraft applications, a 3D printer (or applicator) would be the best option. However, since the development of such a printer was still ongoing, the first few years the more conservative film will be used. This is why both methods are considered henceforth. A film could also be manufactured to have the herringbone riblets imprinted.

⁵⁶Private communication, Amber Van Hauwermeiren [19 May 2017 10:00].

⁵⁷Private communication, Amber Van Hauwermeiren [19 May 2017 10:00].

⁵⁸URL http://www.engineeringtoolbox.com/engineering-materials-properties-d_1225.html [cited 26 June 2017].

3.5.5. Cost

Since sharkskin needs to be reapplied every few years, its price depends on the age of the aircraft being retrofitted. While the retrofit costs and downtime costs are therefore dependent on the aircraft, the development costs will be stable.

Machine cost

A Delft-based company by the name of qlayers was at the time developing a machine that will apply sharkskin texture to the aircraft, expecting the purchase price of such a machine to be around \$400k. To increase the speed of the application two machines could be purchased, which meant this cost will be at \$800k.

Development cost

As mentioned throughout the chapter so far, there was still a lot of development of the sharkskin to do, specifically of the herringbone structure that would yield a twice as high drag reduction. It was difficult to make an exact approximation of the costs of such a vast amount of research, but the process could generally be divided into a number of steps, as shown below:

- compute a turbulence model of the A330–200,
- test the herringbone riblets at high Reynolds numbers and riblet optimisation,
- test the herringbone riblets on a scaled aircraft model,
- develop a large-scale application machine,
- get the product certified and
- perform long-period flight tests on a test aircraft.

If the total development time of the herringbone sharkskin would be within 3 years, and the research were done by three postdoc engineers simultaneously, and an engineer cost \$100k per year, the total salary of these engineers amounted to \$900k over these 3 years⁵⁹. Additionally, there were a lot of materials and test facilities involved in this research, that all needed to be paid for. A high speed wind tunnel, at a price of \$500 per hour and an estimated test time of roughly 1,000 hours, would cost \$500k⁶⁰. Finally, there is a lot of certification involved in getting any product on the market. If the herringbone riblets fails, the aircraft as a whole is still operable, so certification should not be as extensive as, for example, a FishBAC or a new winglet. A total of \$5M is allotted to certification.

Finally, a long-period flight test would need to be conducted. During this part of the development, an Airbus A330–200 would need to fly with the herringbone riblets applied to the regions that were computed in the turbulence model for two years (the time the sharkskin would be applied to the aircraft after development). During this period the reduction in fuel use could be measured to validate the performance of the herringbone riblet. This could be applied to any commercially flying Airbus A330–200. If the application costs were on the house and a data-analyst would need to check all the flight data from the test flights (0.1 full time equivalent at a \$100k per year salary, plus some additional costs of a large-scale research), the total costs of this research would come down to \$1M. In conclusion, the entire development process would cost \$7.4M. Since at this point in time it was very hard to estimate the total costs of the sharkskin development and it might take more than three years, a safety factor of 1.3 is applied and the total development cost is concluded to be in the range of \$9.62M.

Retrofit Process Cost

The retrofitting process costs vary for both application processes. Therefore they are both discussed in different paragraphs.

Automatic Application

For the automatic applicator, only the materials and machine maintenance were taken into account. The estimated cost of applying the sharkskin to an aircraft automatically came down to \$100k, which needs to be spent every two years⁶¹. This meant that on a brand new aircraft that will still fly for twenty years, sharkskin would cost \$1.0M.

Film Application

For a manual application with film, the costs were different. First of all, the film could not be removed without damaging the paint layer below. This meant the entire aircraft needed to be painted when the film is replaced. Generally, aircraft are painted every five years, but now it will be painted every two years. A paint job of an A380 takes 6,000 man hours, but the A330–200 is a lot smaller, so only two-third of these hours are considered⁶². This meant a total paint job will be in the range of \$150k, which would be spent every two years. Additionally, the film would likely be more expensive than just raw material for the printer, so the material costs were multiplied by a factor 3, resulting in a \$150k

⁵⁹URL http://www.payscale.com/research/US/Job=Aerospace_Engineer/Salary [cited 27 June 2017].

⁶⁰URL <https://www.aa.washington.edu/AERL/KWT/rateguide> [cited 26 June 2017].

⁶¹Private communication, Amber Van Hauwermeiren [19 May 2017 10:00].

⁶²URL <http://www.dailymail.co.uk/sciencetech/article-3670005/Thirty-four-people-15-days-TON-paint-Amazing-time-lapse-shows-Airbus-A380-plane-getting-makeover.html> [cited 26 June 2017].

cost of just raw materials for each reapplication. Finally, the aircraft is painted over twice as often as it would usually be painted, so the costs of paint are also added to the aircraft. These are estimated to be as high as the cost of the top coat, so \$150k for the entire aircraft, every four years and \$150k every 2 years. This implied that on a brand new aircraft that will still fly for twenty years, sharkskin would cost \$3.75M.

Downtime Cost

To calculate the costs of the downtime of the A330–200 for painting, a similar approach as that of Section 3.3.5 was used. For both application methods, a similar downtime was assumed at this point. It was known that the paint job of an A380 takes roughly fifteen days, and it was estimated that the paint and sharkskin application job of an A330 would take the same amount of time. The application of the film was expected to take five days. These five days were counted every two years, while the other ten days for painting were counted once every four years, so half of it, resulting in an average of ten days of downtime every two years. So during these ten days of downtime, the airline would miss \$73k in revenues. For a brand-new aircraft this would imply a total loss of revenue of \$0.73M in its lifetime.

3.6. Leading Edge Suction

The concept of suction on a wing has been around for a very long time, first proposed by Prandtl in 1914 [52]. The idea behind suction on a wing is that a growing laminar boundary layer will be sucked away before it becomes turbulent. A new boundary layer will start to grow, but the transition point will be delayed. This would greatly reduce the skin friction drag. For a retrofitting purpose, only leading edge (LE) suction was considered [2]. LE suction has been tested very thoroughly. By applying suction on the leading edge, cross-flow disturbance on swept wings can be controlled. This type of laminar flow control has been called Hybrid Laminar Flow Control (HLFC).

During early research on the topic of LE suction, the challenge of applying LE suction was preventing insect contamination and dealing with icing conditions. A possible solution for this was a Krueger flap system. During take-off and landing it deployed a Krueger flap as a high-lift device and as a shield against bugs. For anti-ice, it used a heater system on the nose of the Krueger flap, and a spray nozzle for anti-ice and anti-bug fluid for redundancy [53]. It only used suction on the upper side, because the Krueger flap would not allow it on the underside. Moreover, since the flow velocity is faster on the upper side, it is more effective there. It also used purge air for removal of fluid and debris from the holes. This concept showed most promise out of all HLFC techniques. It was later also tested successfully by Boeing on a 757.

3.6.1. Aerodynamics

The aerodynamic gains of the system were estimated. This was done for four different setups of the HLFC system. The first setup had suction from the root until the engine pylon. For the other three setups, the remaining length of the wing was split into 3 parts. The remaining setups had LE suction from the root to each one of those three lines. The advantage of the first system was that there was less cabling required, the disadvantage being that the HLFC is only applied to a quarter of the wing. The latter concepts had the advantage of more LE suction, but they will require more cabling and more pump power.

Suction System Performance

First, the required parameters for drag calculations had to be specified. These are the wetted area (S_{wet}), Reynolds number and percentage laminar and turbulent flow over the chord. These values can be found in Table 3.10. Here, the laminar-turbulent data for the wing with suction were the lowest values achieved by Boeing during their test [54], at roughly the same locations as the setups. This assumption was deemed valid, due to the fact that it was very difficult to get accurate results for the transition points, as transonic fluid dynamics was still not up to par. For the wing without suction, the laminar-turbulent data came from Javafoil results. Here, the worst-case scenario was taken. This resulted in a laminar region of 4 percent of the chord, and a turbulent region for the remaining 96%. This was used for all setups and all areas of the wing.

Table 3.10: Wing suction parameters.

	S_{wet}	Re	Percentage laminar	Percentage turbulent
Wing section 1	98.28 m ²	505.7 · 10 ⁵	30%	70%
Wing section 2	64.70 m ²	383.2 · 10 ⁵	45%	55%
Wing section 3	58.66 m ²	298.1 · 10 ⁵	48%	52%
Wing section 4	40.63 m ²	193.3 · 10 ⁵	48%	52%

Knowing the percentage laminar and turbulent flow, the Re and the S_{wet} , the drag difference can be calculated using the dimensionless skin friction coefficients for laminar (C_{f_l}) and turbulent (C_{f_t}) flow, using Equation (3.56)⁶³. Here,

⁶³URL https://www.cfd-online.com/Wiki/Skin_friction_coefficient [cited 18 June 2017].

it was assumed that only the upper surface has a change in laminar-turbulent flow. This was a valid assumption to make, due to the fact that there will be no holes on the lower surface.

$$\begin{aligned}
 C_{f_l} &= \frac{1.328}{\sqrt{Re}} \\
 C_{f_t} &= \frac{0.455}{\log(Re)^{2.58}} \\
 F &= C_f \frac{\rho_f v^2}{2} S_{wet}
 \end{aligned}
 \tag{3.56}$$

With the data in Table 3.10 and Equation (3.56), the difference in drag could be calculated. For the first setup, this would only concern the difference in drag of the first section with suction over the first section without suction. For the second setup, it would be this same difference for the first and second section, and so forth. The results of this can be found below in Table 3.11.

Table 3.11: Wing suction parameters.

Drag reduction	
Setup 1	545 N
Setup 2	1148 N
Setup 3	1751 N
Setup 4	2190 N

Krueger Flap Aerodynamic Performance

As the suction system required the leading edge to have a large amount of microscopic holes (with diameters of 40–60 micrometres), in the order of 19 million, it was important that the majority would not be obstructed by potential insect residue [54]. One of the potential solutions was using a Krueger flap that could be deployed during the take-off and landing phases, when the insect density is at its highest [55]. However, as the Krueger flap would replace a currently present slat, it was necessary to assess the effect this replacement had on the aerodynamic performance and the actuation mechanism.

For the potential change in performance, one could look at the test that has been conducted by Boeing, where two slats were replaced with two Krueger flaps on the left wing. The Krueger flap covered a length of 6.7 ft and the test showed that only a slight reduction in lift capability was present, as $C_{L_{max}}$ decreased by 0.05 [54]. For this specific aircraft, the Boeing 757, this corresponded to approximately a 0.67 m/s increase in stall speed. Although the Boeing 757 is smaller than the Airbus A330, these values can be considered valid first estimates. As for the drag increase or reduction, no significant change was present when the Krueger flap was in landing configuration. However, when the aircraft was taking off, the Krueger flap showed a slight increase in drag. The last parameter related to the change in performance is the pitching moment and especially the stability of the aircraft itself. It was concluded that the Krueger flap did not affect the longitudinal characteristics of the aircraft to such an extent that different handling or trimming of the aircraft is required [54].

As this performance assessment was only related to the aerodynamic properties, it is also essential to investigate the noise performance of the Krueger flap and compare it to the noise performance of the slats. It was found that a study was conducted where a Krueger flap and a slat were assessed on their noise capabilities. For a certain configuration, the Krueger flap was found to be slightly louder, however, this says nothing conclusive about the Krueger flap noise in general [56]. The visualisation of the flow of the tested configuration can be found in Figure 3.44.

The upper simulations in Figure 3.44 show the Krueger flap, whereas the bottom figures show the slat streamlines and Mach values for the specific regions of the aerofoil. As can be observed from Figure 3.44a and Figure 3.44b, the gap present in the lower side of the aerofoil causes a slight distortion in the flap, whereas this is not the case for the slat configuration. This means a slight increase in noise will be present for this specific configuration ($\sigma = 30^\circ$, $\alpha = 27^\circ$), in which σ is the deployment angle of the Krueger flap and the slat respectively. The high tunnel installation angle of attack was used to produce local C_p distributions, comparable to a free-air angle of attack of 2.2° . Although a slight noise increase would be present, other studies show that this increase is negligible [58, 59]. Therefore it was assumed that the noise increase will have no significant impact on further calculations and research.

Pump

Another big obstacle that needed to be overcome is the suction mechanism. For this, either an active or a passive system can be used. The active system uses a pump to create the pressure difference needed for suction. This could either be done using a compressor working on bleed air, which was done by the National Aeronautics and Space

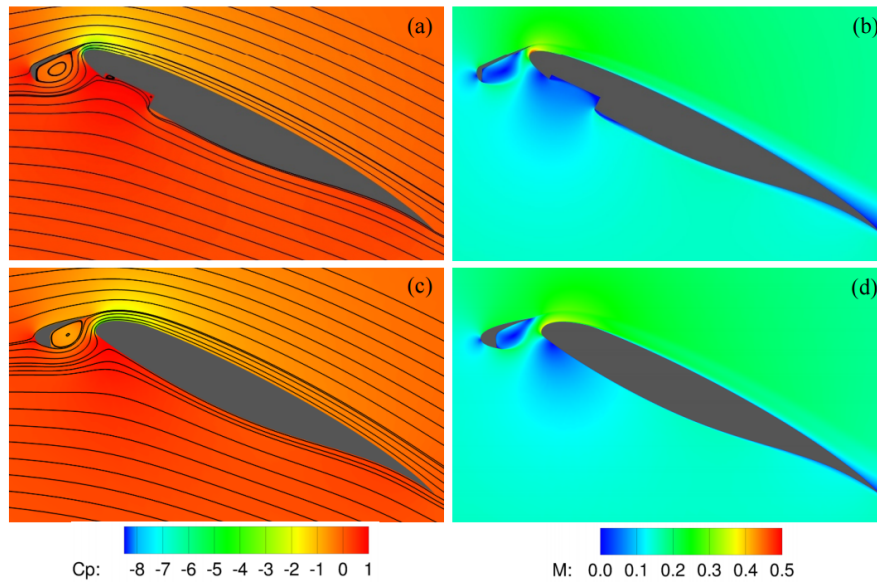


Figure 3.44: Streamlines and contours of pressure coefficient (C_p) and Mach number (M) around two in-tunnel configurations; (a) and (b) for Krueger flap configuration, (c) and (d) for slat configuration [57].

Administration (NASA) for their test model [60] or it could be done using an electric compressor, working on electricity generated by the engine. This no-bleed system was already being used in a similar fashion for cabin pressurisation in the Boeing 787 [61]. The final active system was a system using an external power source, such as a diesel engine, to power the compressor. The passive system on the other hand used pressure differences already available. Since the most outer point of the leading edge is a high pressure stagnation point, this pressure could be enough to have suction for the leading edge to a low pressure area on the fuselage. However, this is only a very small part of the wing, further forward on the wing, the pressure decreases rapidly.

All of these methods had their advantages and disadvantages. The bleed-air system required engine modifications, to take a larger amount of bleed air out of the engine. This would also decrease the efficiency of the engine, as it was already optimised. The electric compressor would have the same effect, as more power needed to be taken off the shaft, but this was more efficient than the bleed air system [62]. The third option, the external engine, would have the side effect that a heavy power source needs to be available. This power source would also require fuel to work. The passive system on the other hand would be limited by the pressure differentials available. Additionally, because it could only be applied on an incremental area on the wing, it could already be neglected.

Due to its increased efficiency, the decision was made to go further with electrical compression. For this, in the relation between electrical engine take-off and fuel consumption was investigated [62]. The empirical relation can be found in Equation (3.57) [62].

$$\begin{aligned}
 k_P &= 0.0057 + 4.60 \cdot 10^{-8} \cdot h - 0.0106 \cdot M - 4.44 \cdot 10^{-13} \cdot h^2 + 1.85 \cdot 10^{-7} \cdot h \cdot M + 0.0049 \cdot M^2 \\
 \dot{m}_F &= k_P \cdot \text{SFC} \cdot P
 \end{aligned}
 \tag{3.57}$$

In Equation (3.57), k_P is the shaft power factor, h the altitude at which the aircraft flies in metres divided by 1 m, M is the Mach number, \dot{m}_F is the fuel mass flow spent on generating the electricity, SFC is the specific fuel consumption and P the required power for the pump. Knowing the added fuel consumption due to the pump, the weight of the complete package and the drag saved, it was calculated if the retrofit will be worth it.

From Equation (3.57), all parameters were known except the required pump power, which was then calculated. The pump would have to create a certain mass flow from the leading edge to the pump. To do this, all the pressure drops on the way had to be overcome: these were pressure drops over the porous skin and pressure drops over the tubing. Knowing this, and knowing the necessary mass flow, an estimate could be made for the required pump power. Hence, the most important parameters to calculate pump power were the pressure drop and the mass flow rate⁶⁴.

In related research, the pressure drop over mass flow rate was calculated for a perforated skin with HLFC [63]. The resulting graph can be found in Figure 3.45. In other research it was found that the required mass flow rate for 5.2 metres of suction was 0.062 kg/s, or 0.012 kg/s · m [54].

⁶⁴Private communication, Dr. Marios Kotsonis [16 June 2017 11:00].

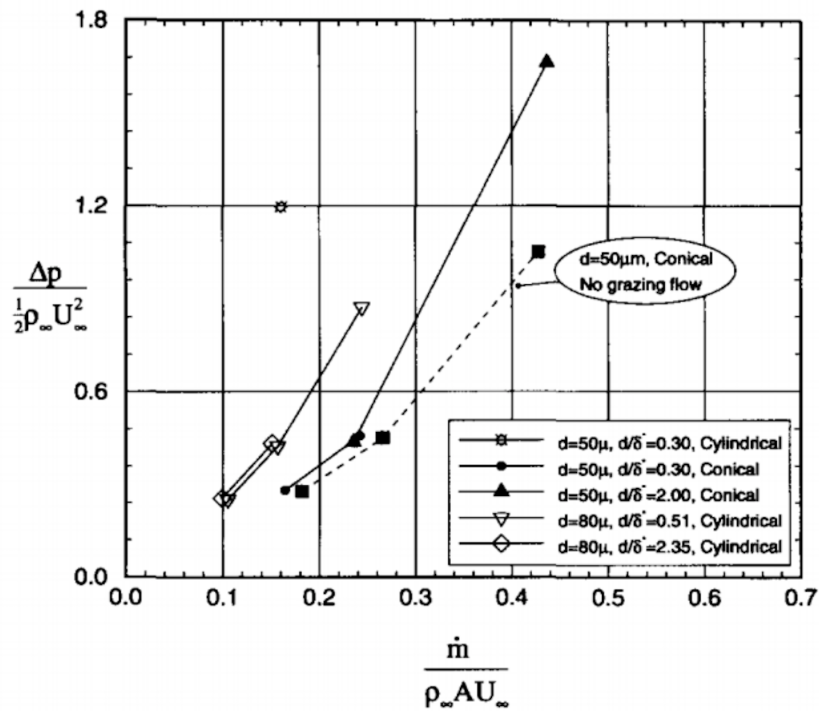


Figure 3.45: Mass flow rate characteristics and static pressure drop of a range of HLFC perforation configurations [63].

With Figure 3.45 and the mass flow, the pressure drop through the perforated skin was calculated. First, it was required to know the specific mass flow. For this, the values used by Boeing were used, as the specific mass flow will be the same. As discussed before, they had a mass flow of 0.062 kg/s for 5.2 metres of HLFC. Over this 5.2 metres, they had 19 million holes with an average diameter of $4.953 \cdot 10^{-5} \text{ m}$ [64], this leads to a total open area of 0.03661 m^2 . This leads to a specific mass flow of 0.2022 . Since the laser in Delft can drill holes with a minimum diameter of 60 micrometers, the cylindrical holes with a diameter of 80 micrometers were used in Figure 3.45. Hence, a specific pressure drop of 0.7 was found, which lead to a pressure drop of $7,137 \text{ Pa}$ over the porous skin.

What was left was to calculate the pressure drop through the tubing from the leading edge to the pump. For this, four different cases were again investigated; these were the same sections as before. For the tubing length, the length from the section to the centre of the fuselage along the leading edge was taken, with a safety factor of 1.1 , to cover for bends in the tubing. The tubing for each section (note: section, not setup) was split into five stages. A total of 32 aluminium tubes were taken at the first stage, with a diameter of 1.72 cm . These 32 tubes would then, after 20 cm , combine into 16 tubes with a diameter of 2.36 cm . These 16 tubes would then, after 20 cm , combine into 8 tubes with a diameter of 3.00 inches. Again, these would combine into 4 tubes with a diameter of 3.63 inches after 20 cm . This stage would again, after 20 cm , combine into 2 tubes with a diameter of 6.68 inches. This last tube, with its larger diameter, would then transport the sucked air to the pump. The changing diameter was chosen to decrease the pressure drop over the total wing. It would also be possible, in a later design phase, to alter the size of each of the tubes, such that at every point on the leading edge a certain optimal pressure could be reached. This was too advanced for this report, and will therefore be done at a later stage. Now, the total pressure drop of the first setup was the pressure drop of the first section, the pressure drop of the second setup was the pressure drop over the first and second section, and so forth. This way, every tube at each stage would have about equal mass flow through them, and it should give a good indication of the pump power needed for the final design, as this was the goal of this section. For the tubing, an outside pressure of $21,663 \text{ Pa}$ was taken, which is the air pressure at the cruise altitude. This was taken because the leading edge will be partly at a stagnation point, and hence this will correspond to the worst case scenario. Using a Pressure Drop Online-Calculator⁶⁵, values of $1,118 \text{ Pa}$ for the first, $2,948 \text{ Pa}$ for the second, $5,491 \text{ Pa}$ for the third and $8,527 \text{ Pa}$ for the fourth setup were found. For the tubing, if only tubes of 1.72 cm were to be used, this would be $5,160 \text{ Pa}$ for the first, $73,920 \text{ Pa}$ for the second, $299,460 \text{ Pa}$ for the third and $840,630 \text{ Pa}$ for the fourth, hence increasing the diameter of the tubes was worth it. By including the pressure drop over the porous skin, this became $8,255 \text{ Pa}$, $10,085 \text{ Pa}$, $12,629 \text{ Pa}$ and $15,665 \text{ Pa}$ respectively.

Knowing the required pressure drop to overcome and the mass flow, the required hydraulic pump power was calculated. For this, Equation (3.58) is used. Here, Q is the volume flow per second, H the hydraulic head in meter and P

⁶⁵URL <http://www.druckverlust.de/Online-Rechner/dp.php> [cited 18 June 2017].

the power in Watt. From [65] it was found that this equals $0.04 \text{ m}^3/\text{s}\cdot\text{m}$.

$$H = \frac{\Delta p}{\rho \cdot g} \quad (3.58)$$

$$P = \rho \cdot Q \cdot g \cdot H$$

By using Equation (3.58), a power required of 2,923 W, 8,332 W, 17,235 W and 30,177 W were found for the respective setups. Note, this value was validated using an online pump power calculator⁶⁶.

Now the code was used to calculate engine off-takes. For this, a 7.5 hour flight profile was chosen, which was the chosen flight mission profile [1]. This led to a fuel consumption of 2.7 litres, 7.7 litres, 15.9 litres and 27.8 litres for the pump, respectively. Since the gearbox and especially the electrical to hydraulic power conversion had a certain efficiency, an efficiency of 0.7 was assumed, this seemed to be in line with the values for medium to small pumps⁶⁷.

Note that the current A330 has an electrical power capacity of roughly 300 kW, which comes from the engine through a gearbox and generator. Here enough capacity should be available for the first and second pump, as they are less than 1% of the total power available, but the last three might require more power than is available. If this were the case, a new gearbox and generator would have to be installed⁶⁸. This would increase the price tremendously, as the gearbox and generator in the current A330 is the same for all engine types the A330 comes with, which are engines from four different manufacturers. Therefore, if a new gearbox and generator would have to be implemented, this would have to go in coordination with these four engine manufacturers, which will cost time and money⁶⁹.

3.6.2. Structures

The structure of LE suction concept consisted of multiple vital components. The most important ones regarding the structural integrity were the LE ribs, the lower and upper skin panel, the Krueger flap with drive mechanism and the front spar. Of these components, only the ribs and the spars were already present in the aircraft, all other components would have to be manufactured and installed.

It was vital for the retrofit that there were no compromises in safety of the aircraft, and that it can still cover the complete flight envelope. These two requirements were vital for the structural synthesis. For the Boeing 757 and the NASA JetStar LE suction test aircraft, they achieved this. Therefore, the risk of it not working was minimal, especially compared to the risk of the pump exceeding hydraulic and weight limitations, or of the aerodynamics not being as predicted. Therefore, a full structural analysis was left out for future research. In this section, some structural pitfalls will be given, and general guidelines on how this future structural investigation will have to be performed.

In Figure 3.46 the cross-section of the HLFC can be found. The outer, perforated skin is attached to the inner, non perforated skin with stringers. These stringers need to be designed in such a manner that the volume between the stringers is about equal, and that the sucked air can be transported along the span from the outer skin to the pump. The outer and inner skin and the stringers are made out of titanium, due to the range of temperatures it will befall over the full flight envelope. These are not only due to skin friction or difference in ambient temperature between take-off and cruise, but also due to heating for de-icing.

Structural pitfalls

First, fatigue could form a problem for the titanium outer skin of the LE. It was not yet completely known if the perforation has any effect on the fatigue life of the aircraft. The JetStar did not find any signs of fatigue during their three-year test phase, though further testing was needed to be sure it will not occur either for over a twenty year life span. They also had a generic bending fatigue test, and concluded that even after 120,000 cycles, the titanium strip did not fail. However, this was done in a lab environment, and not in a use-case scenario [66]. At the TU Delft, the fatigue life of perforated titanium will soon be investigated⁷⁰.

The next pitfall to be discussed are stresses due to temperature expansion. The leading edge is made out of different material than the rest of the wing: titanium and aluminium, respectively. Even within the structure itself, there will be different means of expansion due to temperature difference and the combination of different materials. Therefore, there will be stresses induced due to different amounts of thermal expansion. This will definitely have to be investigated.

The final pitfall was that structural reinforcement might be needed, as the current leading edge is replaced with one with a Krueger flap. This might lead to unwanted forces, which the current structure is not designed for. This structural reinforcement increased the weight, this was taken into account in the weight calculations of this section.

⁶⁶URL http://www.engineeringtoolbox.com/pumps-power-d_505.html [cited 12 June 2017].

⁶⁷URL <http://www.pumpsandsystems.com/topics/pumps/pumps/centrifugal-pump-efficiency-what-efficiency> [cited 13 June 2017].

⁶⁸Private communication, Dr. Arvind Rao [16 June 2017 10:00].

⁶⁹Private communication, Hans Poelgeest [19 June 2017 14:00].

⁷⁰Private communication, Dr. Roger Groves [13 June 2017 15:30].

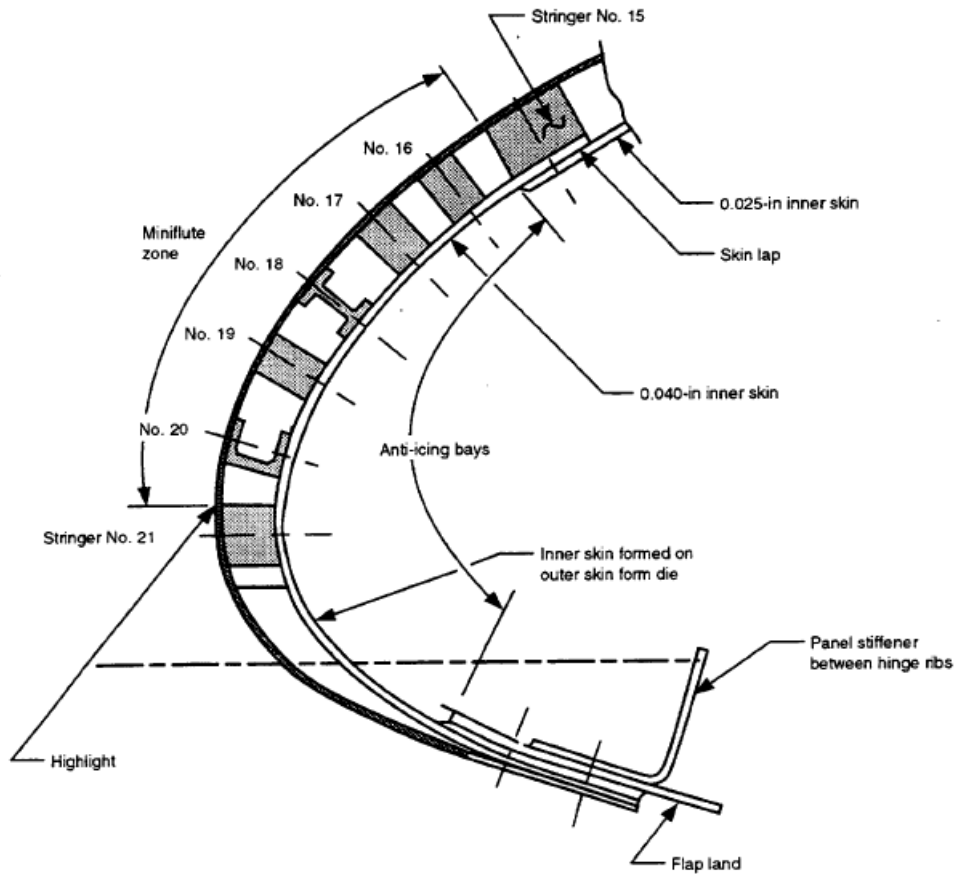


Figure 3.46: Cross section LE Suction [64].

Weight

The weight of the system consisted of multiple parts: the Krueger flap, the tubing, the pump and the skin. These will separately be discussed and a final weight estimate will be given. For the Airbus A330, currently LE slats are being used which do not use slave tracks. In literature the specific weight is given for these types of slats, and also for rigid and variable camber (VC) Krueger flaps [23]. These are 5.8, 25.6, 29.8 kg/m² for the slat, rigid Krueger flap and VC Krueger flap respectively. Knowing the LE high lift device area for the 4 setups, namely 6.4, 13.8, 21.7 and 30.1 m² respectively, the respective weights for the three types of leading edges can be found below in Table 3.12.

Table 3.12: Trailing edge high lift device weights.

	None slave track slats	Rigid Krueger flap	VC Krueger flap
Setup 1 HLD weight	180 kg	164 kg	190 kg
Setup 2 HLD weight	392 kg	355 kg	412 kg
Setup 3 HLD weight	615 kg	556 kg	646 kg
Setup 4 HLD weight	853 kg	772 kg	896.7 kg

As can be seen in Table 3.12, the weight of the flap would either increase or decrease the total weight, depending on if a rigid or a VC Krueger flap was used.

As said before, the tubing would be made out of aluminium. This was chosen due to the fact that pressure drops will be minimised, which is vital for a low pressure system like this [65]. For this, hollow tubes were assumed with a thickness equalling 10% of the tubes, with a max thickness of 0.5 cm. As discussed before, each section consists out of 32 tubes with a diameter of 1.72 cm, 16 tubes with a diameter of 23.6 mm, 8 tubes with a diameter of 29 mm, 4 tubes with a diameter of 36 mm and 2 tubes with a diameter of 66 mm. Their thicknesses will be 1.7 mm, 2.4 mm, 3.0 mm, 3.6 mm and 5.0 mm respectively. All sections will have the same weight for the first 4 levels of tubes, as they are all 20 cm, to have enough time to smoothly go over into the last, thickest tube, to minimise pressure drops.

Using an aluminium density of 2,800 kg/m³⁷¹, weights of 72.4, 297.8, 566.8 and 946.0 kg were found for the tubing of the three concepts. This included a safety factor of 1.1.

⁷¹URL http://www.engineeringtoolbox.com/metal-alloys-densities-d_50.html [cited 20 June 2017].

For the pump sizing, two-stage air compressor pumps of the same wattage were found online⁷². From these, a regression line was made with their power over weight. Equation (3.59) was found, which had a coefficient of determination (R^2) value of 1.00.

$$\text{Mass} = 92.09 \cdot \ln(\text{Power}) - 707.43 \quad (3.59)$$

With Equation (3.59), weights of 27.5, 123.9, 190.9 and 242.5 kg were found for the different respective setups. Then, the weight of the skin was calculated. From the CATIA model, the circumference of the leading edge was found, which is 2.74 m on the root. The circumference of the rest of the wing was scaled to the chord length. This meant that the circumference will equal 0.274 metres per metre chord. Taking the sum of the circumference, the length of the leading edge, the thickness and the density, the weights were found. For the thickness, a combination of the thickness of the skin used by Boeing in their test piece and average thicknesses used for titanium and metal skins were used. Eventually, a thickness of 0.635 cm for both the original aluminium and the retrofitted titanium skin was chosen⁷³ [64]. The thickness of the Boeing test piece leading edge was roughly twice as much, but there seemed to be no structural or other reasons for this, other than simpler titanium production methods. For the non-retrofitted concept, the aluminium of the leading edge was assumed to have a density of 2,800 kg/m³ and for the titanium of the new leading edge, a density of 4,506 kg/m³. Hence the difference in weight would equal the sum of the circumference, the length of the leading edge, the thickness and the difference in density. This led to weights of 363.3, 588.1, 751.4 and 888.9 kg for the setups respectively.

Once the weights were known, they could be summed up. For this, only the rigid Krueger flap were used, as this reached the desired loads, as explained in the section on Krueger flaps. Furthermore, because it weighed less than the variable camber Krueger flap, and finally it will cost less to fabricate, integrate and test. The weight increase can be found in Table 3.13.

Table 3.13: Weight summation.

	Krueger flap	Tubing	Pump	Skin	Total weight increase
Setup 1 HLD weight increase	-16.0 kg	72.4 kg	27.5 kg	363.3 kg	443.2 kg
Setup 2 HLD weight increase	-37.0 kg	297.8 kg	123.9 kg	588.1 kg	972.8 kg
Setup 3 HLD weight increase	-59.0 kg	566.8 kg	190.9 kg	751.4 kg	1,450.1 kg
Setup 4 HLD weight increase	-81.0 kg	946.0 kg	242.5 kg	888.9 kg	1,996.4 kg

3.6.3. Materials

As retrofitting the suction system onto the wing requires partly removal of the leading edge, it was important that the new leading edge was capable of withstanding the loads that would otherwise be present on the old leading edge. Therefore the choice of materials was crucial in order for the system to perform reliably during cruise and other flight phases.

As the new leading edge consisted of several components, each with their own respective function and purpose, different materials were used for each component. One can distinguish three main components, which are the skin, the stringers in between the two skins and the valve and duct system.

Regarding the material choice for the skin, Boeing and NASA opted for titanium in the case of the Boeing 757 and the C-140 JetStar respectively [64, 66]. The reason for titanium instead of aluminium lied in the fact that a stronger material than aluminium was required to withstand the loads and hold the suction system. As the temperatures during different flight phases vary significantly, one must take thermal expansion into account. Therefore all the other components, such as the stringers and fittings, would also be made of titanium. By combining the two titanium sheets and the titanium stringers as well as the titanium fittings, a very stiff assembly is obtained. Since the suction system operated on low pressure and temperature settings, the ducts and valves could be made out of aluminium. These suction settings also allowed the use of rubber sleeves and hose clamps to connect the various components [65]. Only for the ducts that drive the turbocompressor a different material had to be used, as the pressure and temperature were significantly higher in these ducts. In this case a material such stainless steel had to be used in order to withstand these specific conditions.

The integration of the system with respect to the compatibility of the new materials with the old materials was not a problem. The attachments that clamp the titanium edge to the front spar are designed in such a way that they can accommodate the loads that are associated with strain compatibility, differences in Young's moduli and different thermal expansion coefficients [64]. Otherwise thermal expansion problems would occur, as the leading edge was made of titanium and the wing box is made out of aluminium.

⁷²URL <https://www.sumake.com> [cited 21 June 2017].

⁷³URL <http://www.keytometals.com/Article95.htm> [cited 21 June 2017].

3.6.4. Integration and Configuration

As the performance of the suction system had been investigated, it was essential to check whether or not the system would fit in the leading edge of the Airbus A330. The suction system consisted of two major components; the Krueger flap and the pump system with its corresponding ducts and valves. First the integration of the Krueger flap will be discussed, after which the integration of the suction system will be analysed.

Krueger Flap System

The Krueger flaps were designed to operate in conjunction with, and be driven by, the existing slat drive system [64]. This indicates that the implementation of the Krueger flaps is relatively simple, although the scale of the retrofit is still significant. This information was based on the reference aircraft that was used by NASA, and thus the case could be different for the retrofitted A330. As the A330 also used slats and has a similar track and drive system, it could be assumed that the implementation of the Krueger flaps to the A330 was also relatively simple. Since the current slats make use of a track and drive system, changes had to be made in order to implement the bar linkage system that will deploy the Krueger flap [64]. This meant that the current rail system has to be removed and a new system containing a four bar linkage has to be implemented. As the Krueger flap's main purpose was to protect the leading edge from insects, a pivot point at the end of the support structure was also required, in order for the Krueger flap to rotate in such a way that it could protect the leading edge. A fully retracted Krueger flap can be found in Figure 3.47, whereas the anti-bug concept is visualised in Figure 3.48, in which the hinge arm indicates the pivot point.

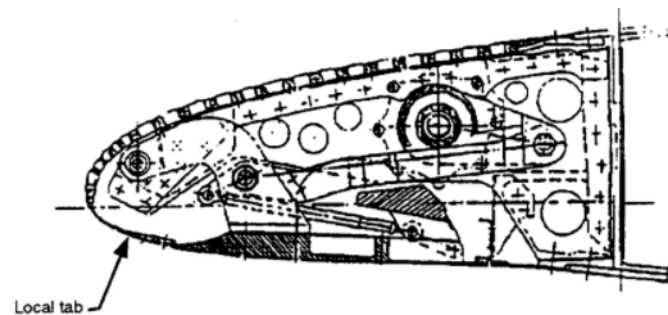


Figure 3.47: Fully retracted Krueger flap [64].

Although the pump could only provide suction for a limited section of the leading edge [65], it was decided to analyse the complete LE section to compare the results. However, as it was expected the suction system will be unfeasible due to the high weight and limited performance improvement, for now only the inboard slat will be replaced, which has a length of approximately 5.1 m [23]. As the inboard slat had a separate and different track and drive system when compared to the outboard slats, retrofitting exclusively the inboard slat could be done irrespective of the outboard slats.

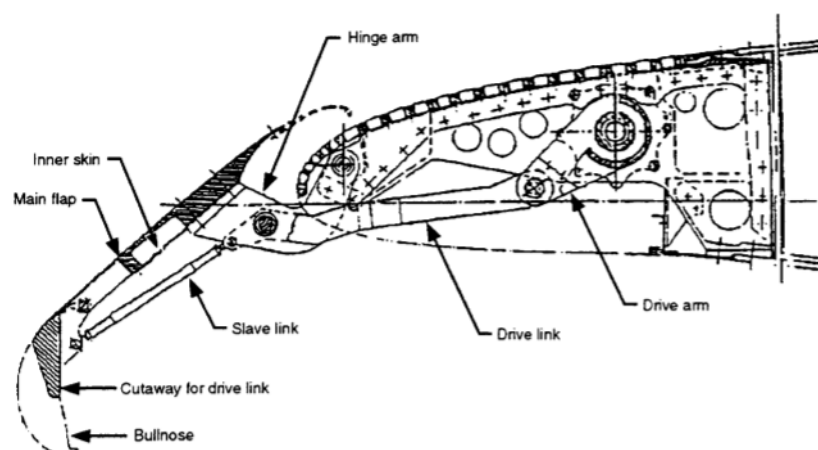


Figure 3.48: Full extension of Krueger flap for LE protection [64].

It was found that the distance from the most forward point of the leading edge to the first spar is approximately 1.25 m, as obtained from the 3D modelling software CATIA and a guideline A330 wing drawing [23]. The length of the Krueger flap itself would be roughly 0.9 m [64], which meant a total chord extension of approximately 51 cm could be achieved when the Krueger flap is fully extended. This chord extension is measured from the forward tip of the bullnose to the forward tip of the leading edge and corresponds to roughly a 5% chord increase.

Pump and Suction System

The other main component that has to be installed is the pump and suction system. This includes a new gearbox, a new generator, an additional pump and all the necessary ducts to suck the air from the leading edge. This integration was quite hard and would take a significant amount of man hours to realise. A cross-section of the new leading edge not including the Krueger flap is visualised in Figure 3.49.

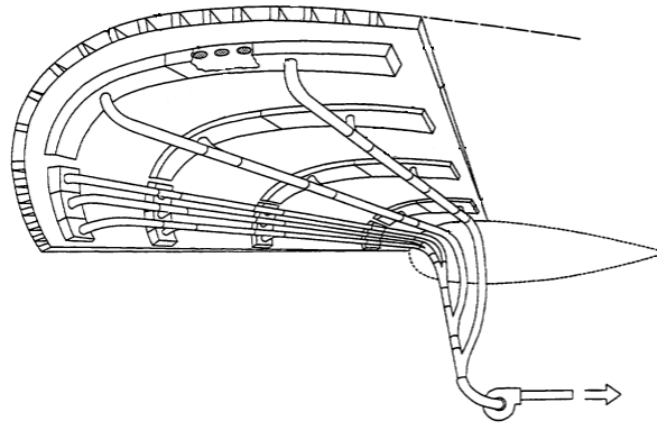


Figure 3.49: Overview of new leading edge (not containing the Krueger flap) [65].

As can be seen in Figure 3.49, a lot of new components would be present in the new leading edge. Holes would have to be drilled in the new and existing ribs in order to allow for the duct placement. The gearbox, generator and pump would have to be placed in either the engine pylon or fuselage. As it was not certain how big these components would be, it was assumed these components will be placed in the fuselage, as the engine pylon has limited space and would require significant reinforcement if a lot of mass were added.

One of the most essential components that had to be attached is the new LE skin assembly. As the current LE skin of the Airbus A330 would be removed and replaced, it was essential that the new leading edge could withstand the same loads as the original leading edge could handle. For this reason, it was chosen to make the new leading edge of titanium instead of the usual aluminium. The way in which the new LE assembly would be attached to the front spar of the wing is visualised in Figure 3.50. Part of the old skin would be reinforced and bolted to the new LE skin assembly in order to create a strong linkage between the two components.

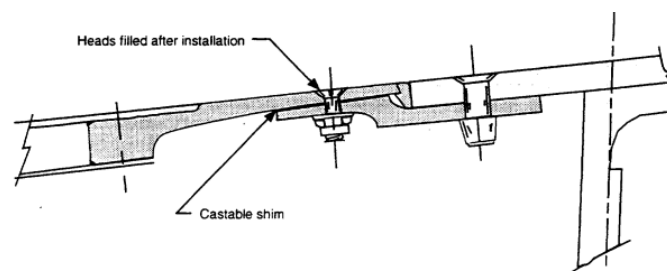


Figure 3.50: Visualisation of new LE skin assembly attachment [64].

Although most of the larger components had been discussed, smaller components of the suction system such as the heat exchanger, the wiring and appropriate sensors would also have to be integrated into the wing and fuselage. Since these units were quite small and easily integrated, they could be placed later in the assembly process. The heat exchanger would most likely be placed in the engine pylon, as this was a section close to the leading edge with enough room available for such a component. As for the sensors and wiring: they would have to be placed in the wing and fuselage, which meant more small holes would have to be drilled in the ribs, if there was no room available.

3.6.5. Cost

The last aspect of the LE suction system that had to be covered is that of the cost. Although the system was relatively mature, there was still a lot of room for improvement regarding weight and performance optimisation. Therefore a significant amount of money might be guided towards the development and research of the suction system. However, as the suction system had already been investigated and the integration has been discussed, only the integration cost will be presented. This meant that this cost estimation would cover all the components, the assembly and integration process as well as the required and man hours. As it was found that setup 4 provided the best results, this design would be used for the cost estimation. Since less man hours, ducts and other components will be necessary for the

other three setups, these options will most likely be cheaper than setup number 4. Therefore, if setup 4 proves to be too expensive, another setup might be optimised as it is cheaper and there is more money left for potential development.

As the suction system consisted of a lot of components, of which most would be specifically made for this retrofit, not many off-the-shelf products would be used. This also means that the cost estimation will be a very rough approximation, as everything will have to be outsourced if the appropriate machines are not available. For this outsourcing, the company providing the cheapest yet most reliable parts would have to be contacted, which was unknown at this point. Therefore the total cost estimation would be mostly based on engineering knowledge and reference or similar projects, if applicable.

Disassembly and Ducts

Starting with the disassembly of the skin, the cost that came with this process would be approximately \$15,000⁷⁴. This could be concluded when the cost of this procedure was assumed to be equivalent to a longer than usual maintenance visit. When the skin had been removed from the leading edge, the actuator mechanism has to be replaced and the appropriate ducts and valves have to be installed.

As for the cost of the ducts, an approximation was made of the total cost, as the material and weight of the components were known. As the required duct shapes could not be bought off-the-shelf, they will have to be manufactured and produced by a third party company. This meant a higher price would have to be paid than just for raw aluminium. At the time of writing raw aluminium was at a price point of \$1,867.00 per ton⁷⁵, which was equal to a price of \$1.87 per kg. With this knowledge, the total value of the raw aluminium required to manufacture the ducts was easily computed, which resulted in a total cost of \$1,769. However, as a significant amount of this aluminium would be waste, as the ducts are hollow, it is likely more aluminium will be necessary. As companies add value to the product by manufacturing and production, a 13% increase in price will be likely⁷⁶. However, as companies would also have to pay their employees and include a profit margin, the final price will most likely be much higher. Therefore it is safe to assume that the final cost for the ducts, valves and connectors lie at about \$5,000. Assuming the required man hours for the integration of the ducts to be 200 hours, these costs would quickly add up to \$5,000, when an hourly wage of \$25 is assumed. This meant that the total cost for exclusively integrating the ducts would be approximately \$10,000.

Gearbox, Generator and Pump

Due to the additional power required to facilitate the pump and suction system, a new gearbox and generator would have to be placed as well as the pump itself. These rather large components would be quite expensive and their integration would require a significant amount of man hours. As the Airbus A330 used an integrated drive generator (IDG) manufactured by UTC Aerospace Systems, this IDG would be used for the cost estimate. However, it might be the case this IDG delivered too much power, which would unnecessarily increase the mass and thus reduce the overall efficiency of the aircraft. The benefit of using a IDG is that it combines the gearbox with an oil-cooled generator, which meant this single unit will essentially consisted of two components that would otherwise take up significantly more space. The price was assumed to be approximately \$1.5M for this combination of gearbox and generator. As for the pump itself, a price of \$500k was assumed, which meant the total price of the additional big components that would have to be placed into the wing and fuselage would be roughly \$2.0M. However, this did not include the required man hours to integrate these components. Therefore an additional the equivalent cost of 150 man hours would be added to the total cost, and this came down to \$2.0M.

Krueger Flap

The last components that had to be taken into account for integrating the suction system are the Krueger flaps, the actuators and the skin assembly. A single moderate-span Krueger flap costs approximately \$0.85M, where the price was independent of the Krueger flap's length. As the Airbus A330 has 7 slats on each wing [23], the total cost of the Krueger flaps was approximately \$11.9M. However, this cost only included the Krueger flaps themselves and not the man hours required to remove the slats, remove the actuators, place the new actuators and attach the Krueger flap. Therefore a slight increase in cost would be present, as it is assumed that this process would take at least another 200 man hours. Including the cost for the actuators and man hours, it could be assumed that the total cost of the Krueger flap implementation will be roughly \$11.9M. This might have been an overestimation, as smaller Krueger flaps will most likely cost less, however this overestimation would counteract any underestimations that might be present in other approximations.

Skin Manufacturing and Assembly

The last component of the suction system that will be discussed is the skin assembly. Since the skin would most likely be made by a third party, the same approximation could be made as was done with the tubing cost estimation. Therefore the cost of raw titanium would be \$3,182, in the case of 888.9 kg titanium required for the skin and stringers, with a price of \$3.58 per kg⁷⁷. However, due to added value by companies, profit margins and the underestimate of

⁷⁴URL <http://www.turkishtechnic.com/Upload/342014105726327.PDF> [cited 25 June 2017].

⁷⁵URL <http://www.lme.com/metals/non-ferrous/aluminium> [cited 25 June 2017].

⁷⁶URL <http://data.worldbank.org/indicator/NV.IND.MANF.ZS?end=2015&locations=NL&start=2005> [cited 25 June 2017].

⁷⁷URL <http://www.infomine.com/investment/metal-prices/ferro-titanium> [cited 25 June 2017].

the required titanium, this total cost would be most likely in the order of \$7,500. The last essential step was to drill the holes into the skin in order to allow the suction system to work. As a reference the Boeing 757 was used to estimate the required holes for suction. This wing had a suction panel of 6.28 m containing roughly 19 million holes. If this hole density were scaled to the Airbus A330, approximately 181 million holes would have to be drilled, if the span extension due to the winglet was taken into account. If the laser was able to drill approximately 10 holes per second⁷⁸, the time required to drill all the required holes would be approximately 208 days of full-time drilling. This duration might even be on the low side, as this approximation did not account for potential outage and assumes full autonomous operation of the laser. To reduce this manufacturing time, multiple lasers might have to be used. Cost-wise, the power required to keep the lasers running will not be the deciding factor, as this amount will be in the order of \$5,000⁷⁹, and thus negligible compared to the other costs. However, most lasers were quite powerful and could operate for 24 hours straight, which meant the time required to drill the holes would be significantly longer than 208 days. This meant the suction system was most likely unfeasible due to the high costs, the sub-par aerodynamic performance increase and the long time required to drill the holes in the skin.

The integration of this skin assembly is taken into account at the Krueger flap cost estimation mentioned before. Therefore the total cost of implementation the LE suction system was found by adding up all the costs of the various assembly processes. The total cost approximation therefore resulted in a value of about \$13.9M.

3.6.6. Conclusion Leading Edge Suction

By using the performance analysis code, as specified in Chapter 4, the optimal design was chosen. This would be a function of the decrease in drag, and increase in weight. For this, the mission profile introduced in the baseline was used [1]. Here, the extra fuel required for the pump was seen as extra take-off weight. The standard aircraft over the mission profile had a required fuel weight of 21,541.54 kg. It was found that all four setups decrease the fuel consumption. The first concept decreased it by 0.4%, or 13.9 kg, whereas the second decreased the fuel consumption by 0.05%, or 20.3 kg, the third by 0.11% or 40.4 kg and the fourth by 0.02% or 7.3 kg. Therefore, it was chosen not to continue with LE suction for the retrofit. Since there still was room for improvement in the future, such as more efficient pumps or better and lighter materials, all the aspects in its design, such as a reliability, availability, maintainability and safety (RAMS) analysis, were still performed.

⁷⁸Private communication, Roger Groves (26 June 2017).

⁷⁹URL: <http://support.epiloglaser.com/article/8205/29954/power-consumption-and-your-laser> [cited 26 June 2017].

Full Aircraft Analysis

4.1. Configuration

The following figures represent the entire retrofit wing. A total of four retrofit concepts were implemented into the Airbus A330 wing. The retrofit components of the wing are shown in Figure 4.1 and Figure 4.2 with a 'BEAU-wing' print. The old winglet is replaced by the new extended wingtip. The flaps are replaced by the FishBAC concept, chevrons are added to the thrust-reverser sleeves and a large part of the entire wing surface is coated with a sharkskin coating. In order to have a clear view of the entire configuration, the sharkskin coating is left out of the image. The ailerons and spoilers were given an arbitrary angle.



Figure 4.1: The Airbus A330 retrofitted wing with a 90° cant extended wingtip.



Figure 4.2: The Airbus A330 retrofitted wing with a 0° cant extended wingtip.

4.2. Retrofit Characteristics

As all concepts have been designed to a detailed extent, they can be applied onto the wing to obtain the final configuration. As it is yet unclear how these concepts interact when they are all present on the same wing, an analysis has to be conducted. Therefore another performance assessment has been conducted, which is presented below. Besides this performance assessment, the aerodynamics and structures aspects are also revisited, which can be found in the following sections.

4.2.1. Aerodynamics

Concerning the aerodynamics of the wing, the fuel savings will be discussed first, as these directly relate to the emission requirements of NO_x and CO₂. Furthermore, the noise reduction and performance will be assessed to check whether or not the estimated performance increase was a correct estimation.

Fuel Savings

One of the main requirements for the aerodynamic performance is requirement **SRW-05**: ‘The fuel consumption of the retrofitted aircraft on a reference mission shall be reduced by at least 7.5% per passenger kilometre compared to the reference aircraft’. In the Baseline report of this project [1] a base performance and reference mission was created. The most relevant parameters are summarised here:

- Operational empty weight (OEW) = 120,200 kg¹.
- Design payload weight = 24,035 kg¹.
- Design fuel weight = 85,765 kg¹.
- Cruise time = 7.5 hours.
- Cruise speed = Mach 0.82.
- Cruise altitude = FL370.
- $C_{L_{cruise}} = 0.585$.
- $S = 363.1 \text{ m}^2$.
- $A = 9.26$.
- $e = 0.68$.
- $C_{D_0} = 0.0326$.

Next the benchmark L/D was calculated, starting with a value for C_D . To calculate the drag coefficient, Equation (4.4) was used. With the above values, the C_D was found to be 0.0499. In cruise conditions this results in a drag of 184,742 N. Combined with the lift of 2,165,819 N, the lift-to-drag ratio for the current A330 in cruise was found to be 11.72.

The next step is to determine the improvements of every concept and combine them. It was assumed that there are little to no interactions between the concepts, since they all operate in a different area of the wing. It can be argued that the sharkskin and the FishBAC interact with each other, but those interactions are assumed to be negligible. This means that the results of the separate concepts can be superimposed onto each other. A summary of the changes of each applied concept is given here:

- Winglets: $A \cdot e$ improvement of 9.19%. Weight increase: 1,500 kg. Surface area increase of 6.6 m².
- FishBAC: Drag reduction of 1,223 N. Weight increase: 100 kg.
- Sharkskin: Drag reduction of 7.56%, which equals 14,000 N. Weight increase: 304 kg.
- Chevrons: No performance change. Weight increase: 63 kg.

These improvements can be subdivided into groups. One with zero-lift drag changes, one with induced drag changes and lastly the weight increases. The new C_{D_0} was calculated by deducting the drag reductions of the FishBAC and the sharkskin from the total drag mentioned before and applying the drag equation. A new $C_{L_{cruise}}$ was calculated by adding the weights to the OEW. With the new aspect ratio and Oswald efficiency factor from the winglets, a new induced drag was calculated. Next, Equation (4.4) was applied again and a new C_D was found. Applying the lift and drag equations once more gives the final drag and lift to be 153,290 N and 1,999,140 N respectively. This results in a new lift-to-drag ratio of 13.04. Now it is possible to say something about the aerodynamic performance improvement according to Equation (4.1):

$$\frac{L/D_{new}}{L/D_{old}} = \frac{12.85}{11.72} = 1.0967 = 9.67\% \text{ improvement} \quad (4.1)$$

In approach things change slightly. The exact same method as described above is applied with minor parameter differences, which include:

- Approach weight = 160,000 kg.

¹URL <https://booksite.elsevier.com/9780340741528/appendices/data-a/table-1/table.htm> [cited 27 June 2016].

- Approach speed = Mach 0.21.
- Approach altitude = 0 m.
- Approach + take-off time = 30 min.
- $C_{L_{approach}} = 1.35$.
- $C_{D_0} = 0.13$.

A note about the C_{D_0} value that is stated above: according to a master thesis research the C_D is roughly 0.17 higher with 30° flaps and gears deployed when compared to cruise conditions [67]. With the C_{D_i} during approach known, it can be determined what the value of C_{D_0} is. Furthermore, the FishBAC now adds another improvement of 0.005 on C_{D_0} from the more efficient flaps as taken from Figure 3.28b. The fairings have less drag improvement in Newton due to the lower speed. The sharkskin is a little more effective on the C_{D_0} than in cruise, since it is more effective at lower speeds. The winglet A_e improvement stays unchanged. All together, this changes the L/D according to Equation (4.2).

$$\frac{L/D_{new}}{L/D_{old}} = \frac{6.68}{6.10} = 1.0947 = 9.47\% \text{ improvement} \quad (4.2)$$

The next step is to calculate the actual fuel consumption decrease with these improvements. During the baseline phase a Python script was written which calculates the fuel consumption of a flight of certain range and certain payload wherein it was possible to include an aerodynamic improvement [1]. First, the fuel consumption in cruise was calculated at FL370, $M = 0.82$, for 7.5 hours. The values for C_{D_0} , weight, A_e and the wing surface area were updated, and a new fuel consumption was calculated. This leads to a total fuel consumption decrease of 10.5% in cruise. All improvements can be seen in Table 4.1, first for each product, secondly for the total retrofit. The different products seem to have a small stacking effect.

Table 4.1: Performance increase in cruise for each product.

Product	Performance increase [%]	Fuel savings [kg]
Sharkskin	7.92	2,808.2
Winglet	1.78	632.9
FishBAC	0.65	228.8
Chevrons	-0.04	-15.5
All	10.51	3,729.2

It is assumed that the part of flight when the aircraft is not in cruise is mostly approach, therefore, this is grouped into one category of 30 minutes. This it calculated at zero altitude and $M = 0.21$. Absolute fuel savings are lower than for cruise, due to the lower time covered in this part of flight. Results can be found in Table 4.2.

Table 4.2: Performance increase in approach for each product.

Product	Performance increase [%]	Fuel savings [kg]
Sharkskin	0.47	13.8
Winglet	7.51	222
FishBAC	4.93	145.7
Chevrons	-0.04	-1.3
All	13.05	386

Adding the results of the previous calculations, a total fuel reduction of 10.7% can be achieved. Fuel reduction per concept, as well as the weight of each concept, is shown in Table 4.3. The total retrofit will meet the fuel consumption reduction requirement. For FishBAC and chevrons it can be argued whether they are worth retrofitting, due to the low fuel savings or even extra fuel usage. However, these concepts play a major role in noise reduction and will therefore not be discarded.

Emission Improvements

Requirements **SRW-04-EMISCO-01** and **SRW-04-EMISCO-02** state that the CO_2 and NO_x emissions of the aircraft shall be reduced by respectively 7.5% and 9% per passenger kilometre. Both CO_2 and NO_x emissions are linearly dependent on thrust setting². Therefore, reducing the thrust setting with 9% will satisfy both requirements. Assuming steady flight, the thrust is equal to the drag of the aircraft. Therefore reducing the drag with 9% is required. This reduction is achieved by the concepts, which provide a total drag reduction in cruise of 11.1%. In approach, the drag reduction is even higher, namely 12.4%. It can be concluded that the requirements for emissions are therefore met.

²URL <https://www.easa.europa.eu/document-library/icao-aircraft-engine-emissions-databank> [cited 27 June 2016].

Table 4.3: Total performance increase for each product.

Product	Performance increase [%]	Fuel savings [kg]
Sharkskin	7.45	2,822
Winglet	2.14	855
FishBAC	0.92	375
Chevrons	-0.04	-16.8
All	10.7	4,115

Noise Improvements

Requirement **SRW-04-EMIS-03** states that the retrofitted aircraft shall achieve at least a 6.5% reduction in the perceived noise emission of flying aircraft. A decrease in noise has multiple advantages, such as lower airport take-off fees, less chance of getting fined by crossing noise limits and increased in-flight comfort for the passengers and crew. For the first of these advantages, Schiphol airport will be taken as example. Here at the moment the A330 falls in category B for noise, which means they get the base charge for take-offs. If the retrofitted aircraft can reach the lowest category, category C, the take-off fee will be 20% lower [68]. This is the only quantifiable cost decrease.

Before a 6.5% reduction can be achieved on the decibel scale, first the current noise levels have to be set. It has been found that the stock A330-200 is 14 dB below the ICAO Chapter 3 and 4 requirements [69]. At Schiphol airport, when an aircraft goes below 18 dB below the chapter 3 and 4 ICAO requirements, it gets a 20% decrease in take-off charges [68]. Hence, a 4 dB decrease in effective perceived noise level in decibels (EPNdB) is needed. The baseline noise, as specified in Chapter 3 and 4 of the ICAO requirements, are 87.5 EPNdB for flyover noise, 96.7 EPNdB for sideline noise and 97.9 EPNdB for approach noise [70].

As the aircraft takes off and climbs towards cruise altitude, the jet engine noise becomes the dominant factor. This is because most of the high frequency noise coming from the airframe is absorbed by the atmosphere, but the low frequency jet engine noise remains³. This jet engine noise was reduced using chevrons for the retrofitted concepts. Because no exact noise reduction predictions are available for the VGC on the A330-223, the ones achieved by the 777-ER test were taken, which used a GE90-115B engine. Here, a reduction in noise of 2dB in low frequency far field noise was found. This engine is roughly 18 percent more powerful than the engine on the A330. However, because the engine used on the A330-223, a PW4168A, is nearly 10 years older, and historically speaking older jet engines tend to be louder, a 2 dB reduction should also be viable for the retrofit. This still has to be verified using flight tests and engine noise scaling methods[15, 16].

A second noise reduction will come from the removal of the anti-shock bodies and the disappearance of the gaps between the flaps and the airframe. This is, again, a noise reduction which is very hard to measure. This noise reduction will come from less turbulent eddies. Just as with the chevrons, it is advised to test this in flight.

Other than noise reduction from chevrons, there will also be a noise reduction due to a lower required thrust setting and lower take-off speed. This should not be underestimated, as airframe noise scales with velocity to the power of 6 and jet exhaust noise with thrust to the power of 8. The thrust now required to take off with the same field length is 6.5% less than the non-retrofitted aircraft.

Due to the previously mentioned noise reduction techniques, it is expected that the 4 dB reduction needed for the A330 to get into a lower noise category will be achieved. This will have to be validated with a flight test, but with the data available, there is enough proof to make this assumption, and take this into account in the return on investment.

4.2.2. Structures

In Chapter 3 extensive structural analyses have been performed. The main contributors to change in structural design are the FishBAC and the extended wingtip. The chevrons and sharkskin do not impose changes in the structure. In Section 3.3.2 an extensive redesign of the wingbox is performed by adding 500 kg of weight in the form of stringers. The FishBAC is designed in such a way that the lifting capacity of the flap remains unchanged. This implies that there are no more loads than the current Fowler flap, so no additional reinforcements are necessary regarding the wingbox. It is assumed that there are no aerodynamic interactions, however, this does not imply that the same can be said about the structure. At this stage of the project it is useful to do a full structural analysis with all the concepts applied with the design loads defined in Section 3.1. This is best done with a FEM analysis, since there are intricate interactions which cannot be modelled by analytic tools. This is outside the scope of this project and is therefore recommended in further research.

³Private communication, Abhishek K. Sahai [22 May 2017 10:00].

4.2.3. Stability and Control

With the alteration in the aircraft weight (distribution) and the aerodynamic improvements stemming from the retrofit solution, it is logical that there will be a shift in aircraft stability and control (margins) to accompany this change. The full analysis of the aircraft falls outside of the time frame of the project up until this phase, however, some valuable first remarks can be stated.

First, the addition of weight to the wingtip and the overall increased surface area of the new wingtip extension will be discussed. The added weight at the outer edge of the wing will increase the overall inertia of the aircraft, making it harder to alter the angular rotation of the aircraft. Next to the weight making it harder to rotate the aircraft, the additional wing surface at the end of the wing will generate an aerodynamic force from the air pushing against the 'plate' to counter any rotation.

The addition of a new flap system will influence the aircraft handling. The speed of deployment, but also the difference in lift distribution over the flap surface will cause the pitching moment of the aircraft to be different than for the unaltered A330 aircraft. Contrary to the wingtip extension case, the removal of flap track fairings from the wing will lower the aircraft inertia and make it easier to change its angular momentum, when considering this alteration alone.

In the case that the suction system would be implemented, it will alter the overall chordwise lift distribution. Similarly to the flap alteration, this will alter the pitching moment generated by the wing. Due to the selective application of the suction concept, some areas closer to the wing will become more efficient in producing lift, whilst more outer edges will remain equal in performance. This shift in relative lifting force between the inner wing surface and the outer wing surface (where the most effective controlling surfaces are located) will require larger deflections of the control surfaces to obtain the same rolling force.

4.2.4. Performance

Take-off performance

With changes in the aspect ratio, Oswald efficiency factor and C_{D_0} , the take-off distance will change as well. In the baseline report a program was developed which calculates the take-off distance given the following parameters [1]:

- Take-off weight = MTOW = 230,000 kg.
- Take-off altitude = 0 m.
- $C_{L_{T/O}} = 2.21$ (assumed unchanged after retrofit).
- Ground friction coefficient = 0.05.
- Screen height = 15 m.
- Aspect ratio = variable.
- Oswald efficiency factor = variable.
- C_{D_0} = variable.

With the values given in Section 4.2.1 the old and new take-off distance can be calculated. Herein the C_{D_0} during take-off is derived as was stated earlier [67]. The take-off distance is the total distance required to get over an obstacle with a height of 15 m at the end of the runway, for which the relevant values are given in Equation (4.3).

$$s_{T/O_{old}} = 2,592 \text{ m} \quad s_{T/O_{new}} = 2,224 \text{ m} \quad (4.3)$$

This indicated an improvement of 368 m can be achieved by the retrofit. This is a significant difference and makes the A330 suitable for significantly more airports: for example the Princess Juliana Intl. airport (Sint Maarten, TNCM), which has a runway length of 2,300 m⁴. Airlines which operate on this airport cannot take off at MTOW and thus can carry less fuel or less payload. With the retrofit, it is possible to fly from this airport at MTOW.

Another way to express the change in take-off performance is to determine which fraction of the full thrust is needed from the engines to match the current take-off field length. With the same program, this was calculated to be a 6.5% thrust reduction. Or in other words, with 93.5% of the total thrust, the field length would stay the same after the retrofit.

Payload-Range

Possibly the most interesting diagram of an airliner to its customers is its payload-range diagram. With the Breguet range equations and the calculated baseline and retrofit parameters, such a diagram can be constructed. To this end, a Python script was developed which gave the range at certain payload and fuel weight, while taking into account the aerodynamic improvement and the added weight of the retrofit. The result can be seen in Figure 4.3.

The fact that there is no clear visible difference between range at maximum fuel and ferry range is quite interesting. This is because the A330-200 tanks are of such capacity that you can fill them completely up until MTOW, without

⁴URL <https://www.airnav.com/airport/TNCM> [cited 26 June 2017].

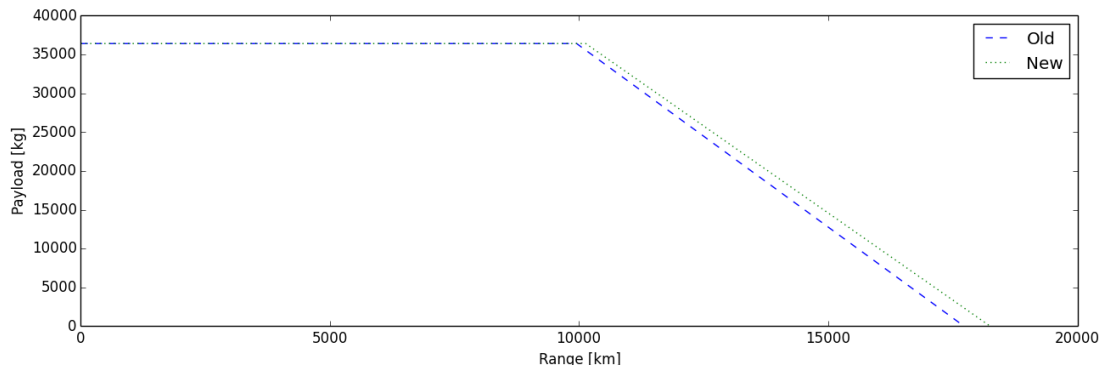


Figure 4.3: Payload-range diagram of the baseline A330 and the new retrofitted A330.

reaching the maximum capacity of the tanks. In other words, the OEW plus the MFW is more than the MTOW. The verification and validation of these results can be found in Section 4.4.6. To conclude, the maximum range at maximum payload increases with 182 km to 8,013 km and that the ferry range increases with 524 km to 18,249 km.

4.3. Communications

One of the essential components of an aircraft is its electrical system, which includes the hardware, software and data handling system. As the retrofits will most likely change these systems, the updated diagrams will be presented in Section 4.3.1 and Section 4.3.2.

4.3.1. Hardware, Software and Electrical Block Diagrams

Table 4.4 shows the interaction between the different hardware and software systems on board of the aircraft. The electrical block diagram, as shown in Figure 4.4, shows the component interactions all drawing power from the main power source(s) of the aircraft. Since this projects concern the retrofitting of an aircraft, only the affected aircraft electrical components are shown. Therefore, this diagram should not be seen as a representation of the complete aircraft.

Table 4.4: Hardware and software interaction diagram.

1. Propulsion system	Fuel burn Total fuel used Engine setting	Fuel burn Total fuel used Engine setting								
Engine setting	2. Pilot		Signal on/off			Signal on/off		Signal desired flap position		
Engine setting	Feedback	3. Autopilot	Signal on/off			Signal on/off		Signal desired flap position		
			4. Actuator LE suction	Suction power setting						
		Suction power		5. Compressor system						
	Signal pin deployment	Signal pin deployment			6. Wingtip extension					
					7. Chevron heating element	Temperature setting				
	Chevron position	Chevron position				8. SMA strip on chevron				
							9. Central flap processing unit	Torque command		
								10. Actuator FishBAC	Contract/extend	
							FishBAC deflection			11. Fish bone structure

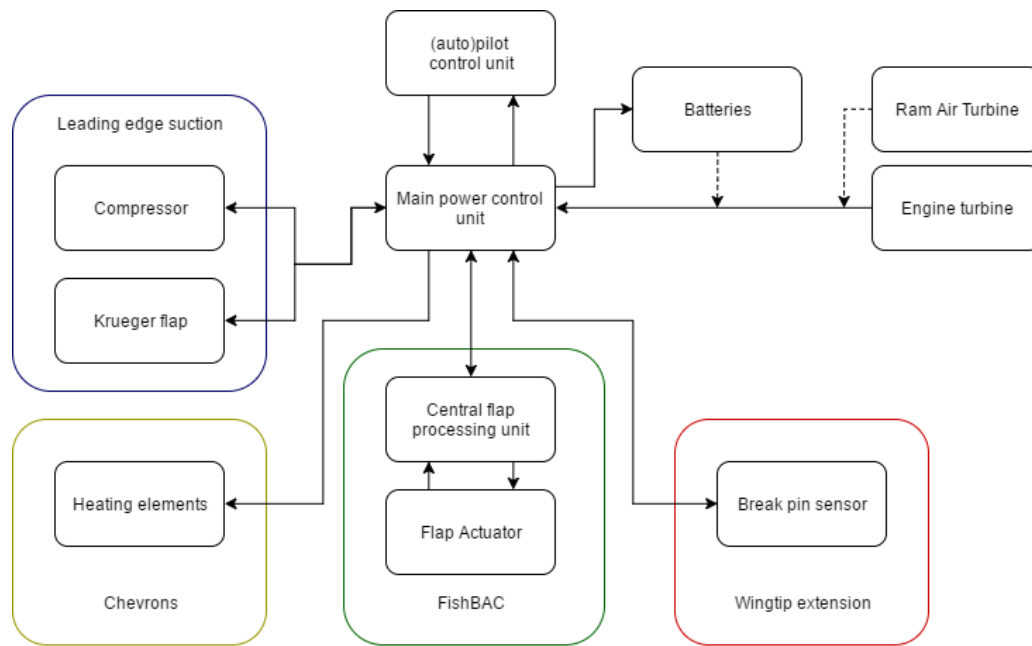


Figure 4.4: Electrical block diagram.

4.3.2. Data Handling and Communication Flow Diagram

In order to store and send valuable results, certain electrical components are necessary that deal with these actions, such as data storage units and data acquisition units. These components will be briefly discussed, after which the relation of the system with the environment will be elaborated upon. As this is more a spacecraft concern and it is quite hard to investigate for aircraft, the case of a test flight will be taken as guideline. This analysis will be discussed after the data handling system has been explained.

Data Handling

An essential component in either an aircraft or spacecraft is the data handling system, which includes the processors and data storage units. These components can save valuable data or, in the case of a spacecraft, store valuable data that can be sent later. The components that do so are the data storage units (or memory), the on-board computer that processes the information and any data acquisition systems, which send outputs to the memory. These components can be found in Figure 4.5, where the specific signals are indicated above the inputs and outputs. This figure also shows the relationship of the system with the ground system. This relationship will be discussed hereafter, as it is part of the communication flow diagram. Due to convenience, it was decided to combine the data handling block diagram and communication flow diagram.

Communication Flow Diagram

A communication flow diagram has already been presented in the midterm report [2], however, as more information is known regarding the layout and relationship between the essential components, an upgraded version can be constructed. This upgraded version of the communication flow diagram can be found in Figure 4.5 and, as mentioned before, also includes the data handling aspects. The pilot can be considered as a starting point in this diagram, however as many relationships are present and most blocks rely on input or feedback signals, there is no real concrete beginning and ending.

Although a communication flow diagram is more likely to be found in spacecraft-related subjects, such a diagram can also be useful for aircraft-related projects. As the communication flow diagram illustrates the flow of data through the system and shows the relationships with the environment, the diagram focuses on test flights and the connection with the ground station. As most concepts that will be applied to the Airbus A330 do not require specific sensors, they are not visualised in the diagram. Examples of such concepts are sharkskin and winglets, which do not make use of actuators and thus only require general sensors. Moreover, this research concerns specific retrofit concepts, it was decided to focus on sensors and components that will be added due to these procedures. Therefore all sensors and strain gauges that would have been present in the aircraft, irrespective of the retrofits, have been disregarded in the communication flow diagram.

4.4. Verification and Validation

In order to check whether or not the obtained values and results are correct and reliable, a verification and validation process has to be conducted. This section will present the verification and validation process for each concept, if applicable.

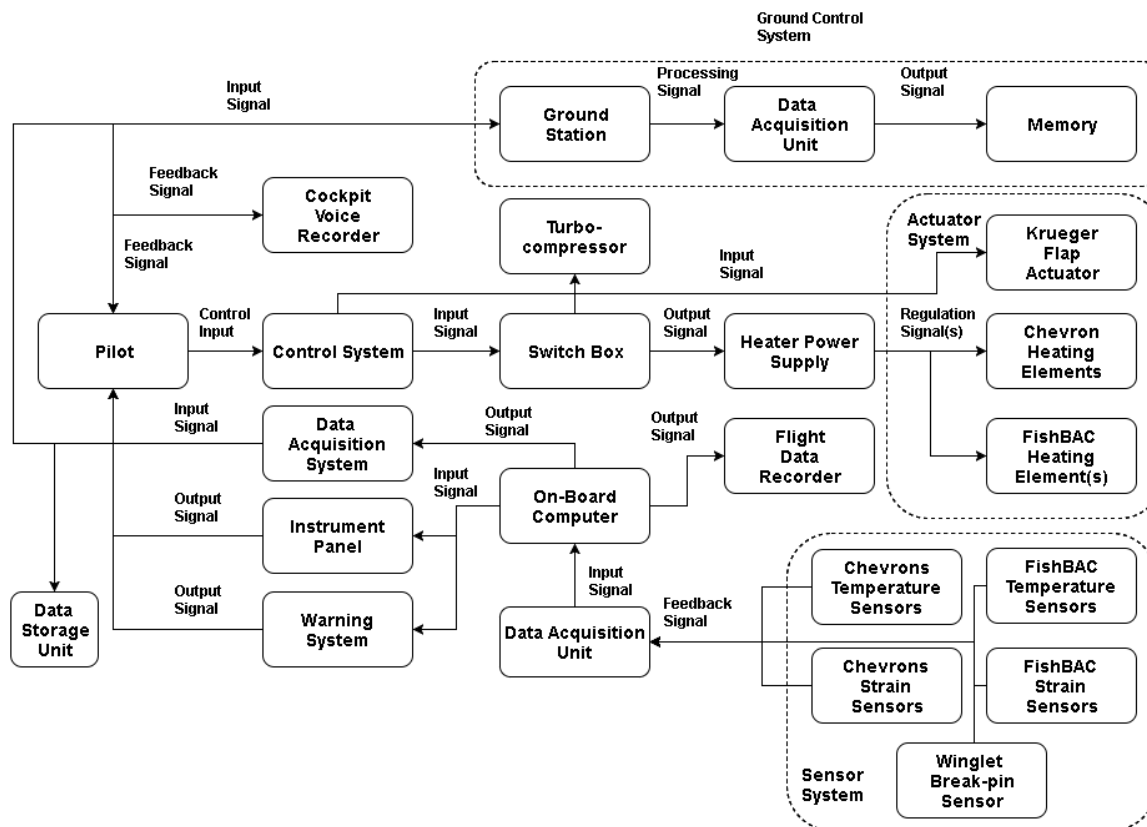


Figure 4.5: Communication flow diagram including data handling components.

4.4.1. Chevrons

Although no models and calculations were used to obtain performance values of the chevrons, verification and validation still have to be conducted in order to check whether or not the obtained values are correct and reliable. Initially, it was decided to verify and validate the noise requirements with the FLIGHT program⁵. However, it was found that this program does not achieve the proper resolution to obtain reliable results when small changes are made to the wing layout. Therefore, research papers were investigated in order to obtain an estimate for the achievable noise reduction due to chevrons. One research paper in particular proved to be very useful: the decibel reduction by applying chevrons was obtained from test flights with the Boeing 777-300ER and GE-115B engines [13]. It is assumed that these values do not have to be verified or validated, as they are obtained from test flight data by a respected company, peer-reviewed and published in a well-respected journal. However, it is essential to check whether or not these results will be achieved when the chevrons are applied to the Airbus A330, as it is a different aircraft with different engines.

As noise calculations are complex, first the assumption was made that the chevrons retrofit on the Airbus A330 would achieve the same reduction in noise emission. However, this assumption has to be verified and validated and thus professors and people involved with the Boeing 777 chevron project were contacted if this assumption was correct^{6,7}. The advice was given to scale the noise of the GE-115B engine such that the noise reduction of the engine of the Airbus A330 (a PW4168a) can be obtained. Papers were investigated that presented empirical relationships and scaling laws for jet noise in subsonic and supersonic flows [15, 16]. Since these scaling laws were quite elaborate and required specific parameters of which the values were unknown, it was decided that this method is outside the scope of this research. Therefore the assumption of equivalent noise reduction will remain, backed up by the knowledge of Mr. Sahai and Mr. Mabe.

4.4.2. Winglets

As the design of winglets required the use of elaborate models and modelling, verification and validation is an essential step in providing reliable results. First the VLM program Tornado is verified and validated, after which other essential software is verified and validated.

Software Specification: Tornado

In order to analyse the aerodynamic performance of an Airbus A330 wing retrofitted with various winglets, a VLM has been used. The VLM program is called Tornado and the code has been developed by Tomas Melin as a part of his

⁵Private communication, Antonio Filippone [19 May 2017].

⁶Private communication, Abhishek K. Sahai [13 June 2017].

⁷Private communication, Jim Mabe [1 June 2017].

Master Thesis at the Royal Institute of Technology in Sweden [71]. Tornado calculates the aerodynamic forces on an aircraft using a method that is fast enough for real time application. In order to understand what the program does and how to use it, various variables are explained below. All these variables have to be specified before running the program. All information was obtained by testing the program and using information from the Tornado user manual [72].

- **State variables.** The state at which the aircraft is flying needs to be specified before running the program. The state variables are altitude in meters, speed in the form of Mach number and angle of attack in degrees.
- **Computing variables.** Various computing options need to be chosen. It needs to be specified if the Prandtl-Glauert correction will be applied and the lattice method needs to be chosen. The mesh type has to be selected, as well as the number of chord-wise panels, the number of span-wise panels and the number of flap-chord panels. Dependent on the type of result that is wanted, a sweep parameter has to be indicated. In this case, the sweep parameter means the parameter that is the variable during the result plot (the x-axis variable). During the winglet design, the sweep parameter was chosen to be the angle of attack. The range of angles of attack and the steps taken in between need to be indicated.
- **Input parameters.** The geometry of the wing is the main input of the program. This includes the number of wings (for example the main wing, rudder and vertical stabiliser) and the number of partitions (parts of the wing to give it the right shape). Per partition the quarter chord sweep, the root and tip twist, the dihedral, root and chord aerofoil, the root chord length and the taper need to be indicated.
- **Output parameters.** Using the angle of attack as sweep parameter, the following output parameters were selected: lift coefficient, drag coefficient and wing loading, shear- and moment values for different locations at the wing. Using these, plots were generated to interpret the data.

Software Testing: Tornado

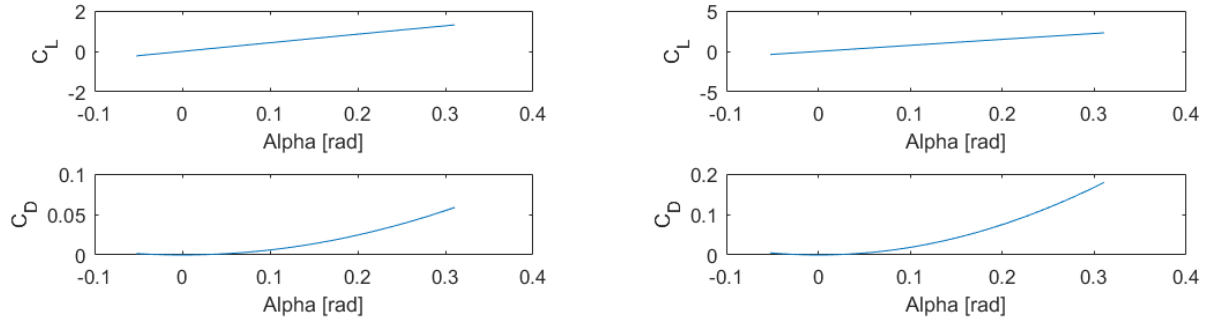
To have an idea of the correctness of the program and to see what influence different inputs and settings have, different inputs were tried and the results were compared to each other. All tests were immediately documented and the related diagrams were saved per test to draw conclusions from. Below, the most important tests and conclusions will be described and, when relevant, the corresponding results plots are shown. For each test, one input variable was changed and all other parameters were kept constant. The following tests were done before using the program for the winglet design process:

- The influence of different dihedral angles of the winglet partition on the wing (in this case, the dihedral is the same as the winglet cant angle) was first analysed. All state variables, computation variables and output variables were kept constant. The geometry of the Airbus A330 wing was implemented and the cant angle of the winglet was varied, the results with a cant angle of 90°, 60° and 30° were compared. Reliable results were obtained from the program as far as is known by common knowledge. Higher cant angles (this means a flatter winglet) give higher lift coefficients, the drag coefficient exponentially increases over angles of attack and is higher for higher angles of attack.
- The influence of variations in mesh plot were analysed by keeping all input, state, computation and output parameters the same, except for the type of mesh plot. There are six mesh types available in Tornado which are applicable to a wing. From comparisons of the results, it could be seen that the mesh type does not influence the results by much, only small variations were observed. From this, it was decided that the mesh type as is used in a tutorial available on the website of Tornado⁸ is sufficient to use, this is the linear mesh type.
- The effect of the Prandtl-Glauert correction was tested by comparing results with and without the correction at a Mach of 0.82. From literature, it is known that the Prandtl-Glauert correction is most applicable for $0.3 < M < 0.7$ [73]. However, since the aircraft cruise speed is at a higher Mach number than 0.7, it was considered more relevant to test the influence at this Mach number. There was a significant change in results and although a Mach of 0.82 is actually out of the scope of this correction, it was decided to always use the correction above a Mach of 0.3 since it will most likely give more reliable results (even for Mach 0.82) than without using this. From Figures 4.6a and 4.6b it can be seen that, with the Prandtl-Glauert correction, the calculated lift coefficient for the entire wing is significantly higher than without the correction. The induced drag changes accordingly, this is as expected: the lift coefficient should rise when subjected to a Prandtl-Glauert correction. The results can be found in Section 4.4.2.
- To analyse the influence of the mesh size of the four partitions of the wing on the results, the mesh size was varied while keeping all other variables the same. Calculation times increase exponentially with decreasing mesh size. Due to limited computing power available, a trade-off had to be made between accuracy and the time it would take to complete a certain number of iterations. To determine an optimal mesh size, the mesh size was varied from 2×2 to 21×21 . The upper bound was set at 21×21 , because this took roughly 20 minutes and further iterations were deemed too time-consuming. In Figure 4.7 it can be seen that the solution quickly converges. In other tests, it was concluded that increasing the resolution of only the winglet partition did not

⁸URL <http://tornado.redhammer.se> [cited 15 June 2017].

greatly increase the accuracy of the total solution. This did, however, increase computing time. Therefore, it has been decided to vary the amount of panels per partition, so that each panel covers roughly the same area. Keeping in mind the time to compute a solution, it was decided to cover roughly 1 m^2 per panel. The solution of this mesh resolution is shown as the red dot in Figure 4.7, and it can be seen that this solution is close to the converged values.

- There are two options available for the lattice method, it is indicated in the program that option 1 is the standard for Tornado. The results deviated slightly, however, the second option takes more than five times longer for calculations. Option one was chosen to be always used.



(a) Lift and drag coefficient versus angle of attack without the Prandtl-Glauert correction.

(b) Lift and drag coefficient versus angle of attack with the Prandtl-Glauert correction.

Figure 4.6: Lift and drag coefficient versus angle of attack from Tornado.

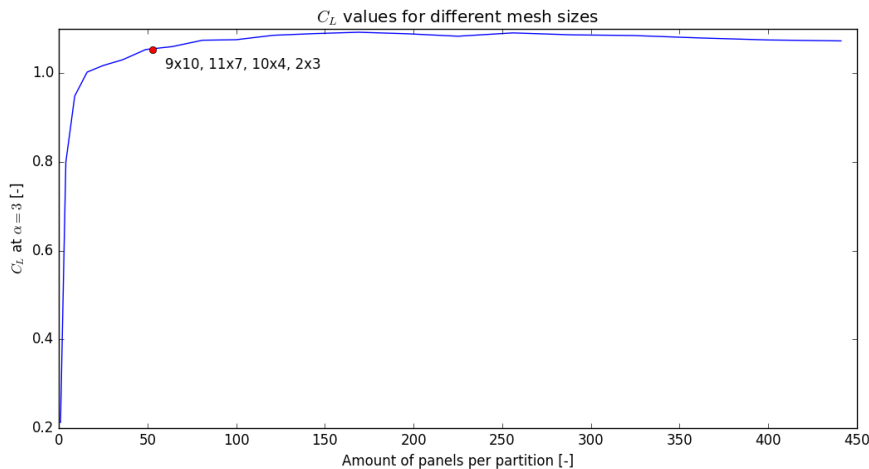


Figure 4.7: Convergence of the solution for smaller mesh sizes.

Furthermore, a choice of aerofoil had to be made. After verifying that it was impossible to implement an own aerofoil (in further research this might be possible), the aerofoils in Tornado were analysed with help of the online program Airfoil Tools⁹. With the knowledge that the Airbus A330 wing aerofoil is a supercritical aerofoil with a certain approximately known thickness and camber, an aerofoil from Tornado was selected which was most comparable to the A330 aerofoil. This aerofoil in Tornado is called SC20610.

Software Validation

Resources were not available to compare outcomes of the simulation from Tornado with experimental outcomes. Validation was done by comparing outcomes of the simulations with theory and basic knowledge. The following irregularities in the results were found and investigated:

- All design parameters of the winglet were varied, to see if they had logical outcomes in the simulations. The cant-, twist-, sweep-, taper- and toe angle were varied. The first four showed a logical outcome, while difficulties arose for a change in toe angle. It could be seen in the geometry plot that a non-zero toe angle showed some discontinuities in the mesh. Although it was first accepted, the actual results of the simulations showed large

⁹URL <http://airfoiltools.com> [cited 15 June 2017].

variations in lift and drag. Toe angle was therefore deemed unfit to be taken into account in Tornado, and was therefore set to 0° .

- The plots of C_L showed linear behaviour, which can be seen in Figure 4.8. This is of course not in line with reality, where the wing would have stalled between 15° and 20° . From this, it can be concluded that Tornado is not capable of simulating flow separation and therefore stall behaviour cannot be modelled. This has implications for the design, since the new winglet cannot be designed for $C_{L_{max}}$.
- Due to the fact that the values of the drag coefficients were low enough to lead to L/D values which exceeded those of glider aircraft, the drag coefficient from Tornado was investigated. It was concluded that Tornado only calculated the induced drag C_{D_i} , which is based on the lift coefficient, the aspect ratio and the Oswald efficiency factor, shown in Equation (4.4). Therefore, it should be noted that Tornado is only capable of calculating induced drag, and factors as zero-lift drag C_{D_0} cannot be simulated. The design can therefore only be optimised for maximal lift over induced drag. This means that the product of the aspect ratio and the Oswald efficiency factor will be maximised.

$$C_D = C_{D_0} + C_{D_i} = C_{D_0} + \frac{C_L^2}{\pi A e} \quad (4.4)$$

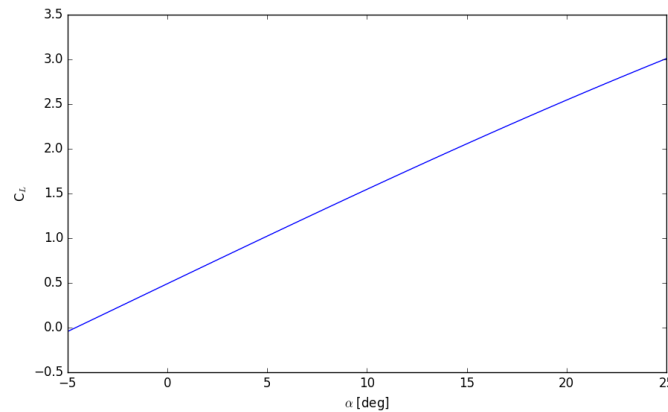


Figure 4.8: C_L - α curve for the A330 wing and winglet.

Structures Model Verification & Validation

After having established a plan of action for the structures model, it was time to start having the model take shape. The model is built up of modules, each with its own goal. The individual modules are integrated into the overall program in order to generate the full model. The modules are further broken up into units which all perform one calculation. After verifying and validating all the input values, code verification was started. Starting from the ground up, each individual unit was first checked for accuracy and consistency. Then all units were integrated into the module to create for example a method for the determination of the shear stress between the stringers. The same was done for the modules which after integration form the complete structural model. The complete model was subsequently checked for accuracy and consistency too. Once the model code had been evaluated and debugged, the next step in the verification and validation section was the evaluation of the model for its consistency with reality. This step could not be performed for all calculations, however, was performed on all relevant units and modules and, most essentially, the final model.

Input Value Verification & Validation

The first verification step was the consistency check for all units (are the units implemented in the correct magnitudes?), as well as the validation of any outcome data. It was chosen to write the program using the units N and mm as the main units. Each calculation uses one of these two units, or a derivative thereof. An example of this is the maximal shear stress which is given in N/mm^2 , which is conveniently also MPa. Tests were conducted to verify the wing loading and the maximum root bending moment. The aircraft in consideration, the Airbus A330-200, weighs a maximum of 230 tonnes at maximum take-off weight. Comparing the values of lift with the maximal weight of the aircraft ($230,000 \cdot 9.81 \text{ N}$) times the ultimate load factor of 2.5, a good indication was obtained of the order of wing load that should be expected. The same was done for the root bending load, taking the loading and placing it as a single vector at 40% span to simulate a typical airliner wing loading.

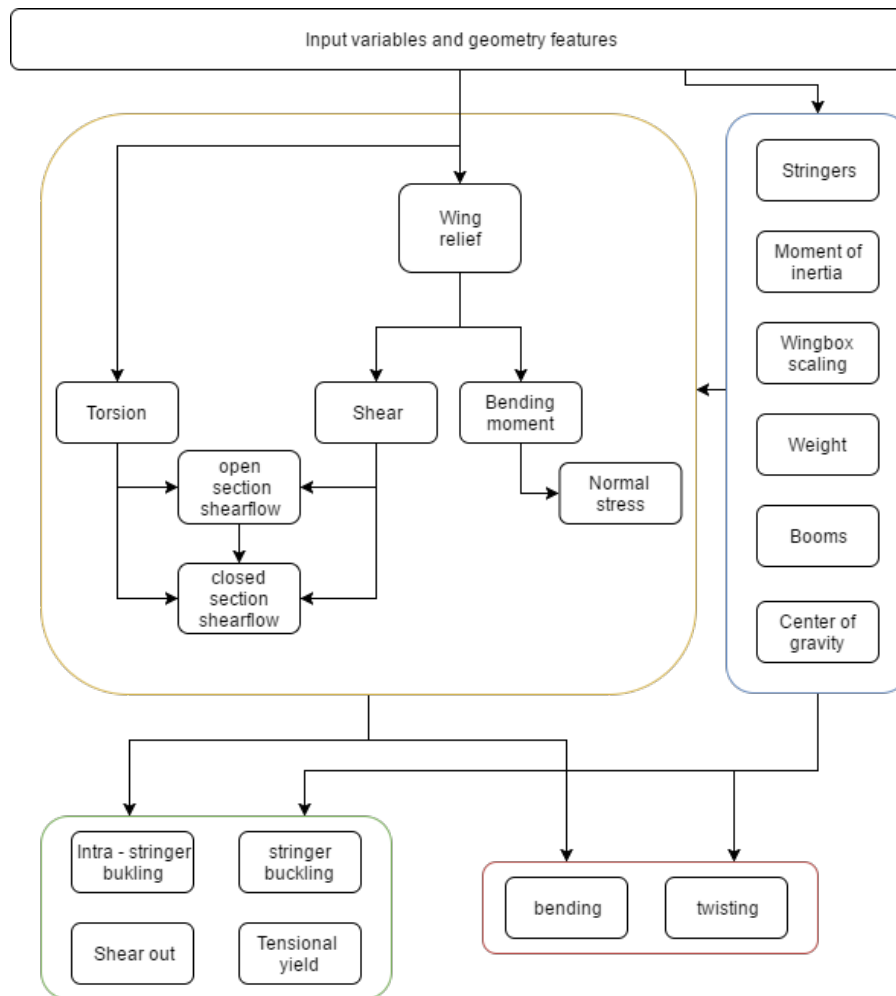


Figure 4.9: Structures program plan.

Unit verification

In the section below, an elaboration is given on the unit verification process throughout the entire model. For easy reading, the process has been broken up into the modules to which the units belong.

Below, a couple of geometry units are considered.

- **Centre of gravity.** A couple of symmetrical cross-sections with known/obvious locations of the centre of gravity were tested in the program, to see if the centre of gravity was placed in the correct (known) location of the cross-section. Numerous other cross-sectional shapes were then tested, the centre of gravity shifted more forward and more aft, these results were checked by hand.
- **Weight.** The weight of the wingbox is calculated by multiplying the cross-sectional area with the length of the spanwise section and then multiplying this with the density of the material. Tests were conducted by changing the span, as well as the variables defining the cross-sectional area and it was checked if the weight would increase or decrease with the correct amount.
- **Moment of inertia.** The moment of inertia calculation was verified by a calculation by hand for two different geometries, both symmetrical and asymmetrical [41].
- **Booms.** Examples concerning structural idealisation were found in literature and compared to the structural idealisation applied to the wingbox from the A330 structural model [41]. The models showed no deviation for the given case. Two other worked-out solutions from literature were further compared, in order to arrive at the verification conclusion.
- **Wingbox scaling.** The wingbox does not follow a fixed shape throughout the entire span of the wing, this is scaled with the respective chord size. The wingbox is defined as having a preset height and length as a function of the chord at said location. The wingbox size is checked at locations throughout the wingbox to check if it adheres to the set-out sizing, following a linear decrease from root to tip.
- **Stringers.** The current A330 has stringers ending at three locations throughout the wing. To approach the stringer area as much as possible and not add unnecessary weight, the stringers are ended here in the model as well. The model takes this into account by decreasing the stringer area by one-thirds and two-thirds at the two respective stringer end points.

After the geometrical definitions, to the stress-related calculations were considered. The stress calculations were integral to the determination of the wingbox not failing under the most extreme loads, and formed the basis for the design process.

- **Wing bending relief.** Next to the applied lifting load, the wing structure is subjected to the effects of gravity. The gravity force counteracts the lifting force generated by the wing and lowers the overall loading on the wing during cruise operations. The loading was verified visually by plotting the wing loading over the wing which is subjected to no lifting force and checking the magnitude and location of each force.
- **Bending moment.** The bending moment in the wing follows from the location at which the lift is generated. Checks were done by loading the wing with known distributed and point loads and then comparing the results of the closed-form expressions for the moment with values generated by the model.
- **Normal stress.** The normal stress was verified by taking values of M , y and I_{xx} for which the stress outcome is known from literature and comparing this with the values from the software.
- **Torsion.** The loading from a location other than the centre of gravity, leads to a torsional force in the wing. The torsional force is first obtained by assuming the lifting force to have a fixed distance from the centre of wing box. This is tested and compared with known solutions.
- **Shear.** The shear force per section is taken by summing up both the lifting force over the past wing section(s) and subtracting the relief from the structure and accessories. The values were compared for multiple load cases, comparing every time at certain locations along the span if the shear loading matched the pre-verified solution.
- **Sectional Shear flow.** The shear flow is obtained by taking the moment of the shear flow around the wingbox surface and should therefore, by definition, equal the set moment value. Checks are done by taking the moment around different points in the wingbox and ensuring that all moments are balanced with the subject torsion.

Following the force module units, the verification process moves on to the failure mode analysis.

- **Stringer buckling.** For the stringer buckling, the shear stress was simply multiplied with the stringer area, followed by a comparison with the yield stress to evaluate if buckling will occur. A simplified case was applied and the outcome compared.
- **Tensional yield.** Tensional yield only comprised of a comparison of values of stress and yield stress of the material.
- **Shear out.** Analogous to tensional yield, the shear out only comprised of a comparison of stress values.
- **Intra-stringer buckling.** The intra-stringer skin buckling follows from a method set out by Timoshenko [35] and this was also the source of verification material. The plate in consideration had a very slender shape, for which the theory is weaker compared to more square shaped cases. Therefore the verification material was limited to verification of input parameters and output values of the sub-factors, yet no actual comparison of a full solution of a slender plate could be done. The verification therefore evolved around dummy cases of square plates.

Finally, the deformation units will be verified.

- **Bending.** The bending calculations were verified by using known fixed solution cases of the Euler beam theory. The beam was subjected to a simulated point load case, as well as a distributed load case. The deflection along the beam was compared between the known solution of the Euler beam deflection and the simulated cases (Figures 4.10a and 4.10b). Two things were found from the verification. Firstly, it was discovered that a deviation existed between the two solutions, due to the discretisation in the structures model. This deviation, however, decreased when the span station size was also decreased. The second lesson from the verification was the realisation that due the fact that the Euler beam theory does not assume linear bending, the superimposed case delivers a smaller deviation than the case which assumes the beam to be one continuous section.
- **Twist.** The twist unit verification was slightly more straightforward. A simplified load case was applied to a simplified beam segment. This beam was then compared with a known solution, from which it was observed that the errors in this section tended towards zero, if not for a floating point error.

Modules

After checking each individual unit, the next phase was the module testing in order to ensure proper integration of the individual units. During this phase of the integration, the main focus was on the interaction between individual units, as the unit verification had previously occurred.

- **Geometry module.** The geometry module checking evolved around the correct exchange of information and aligning the correct y -station (spanwise location) with the matching geometrical features. The checks were predominantly performed with dummy cases and print statements throughout the code. By varying one aspect at a time and checking if the changes are as planned, the code was finally brought into full working order.

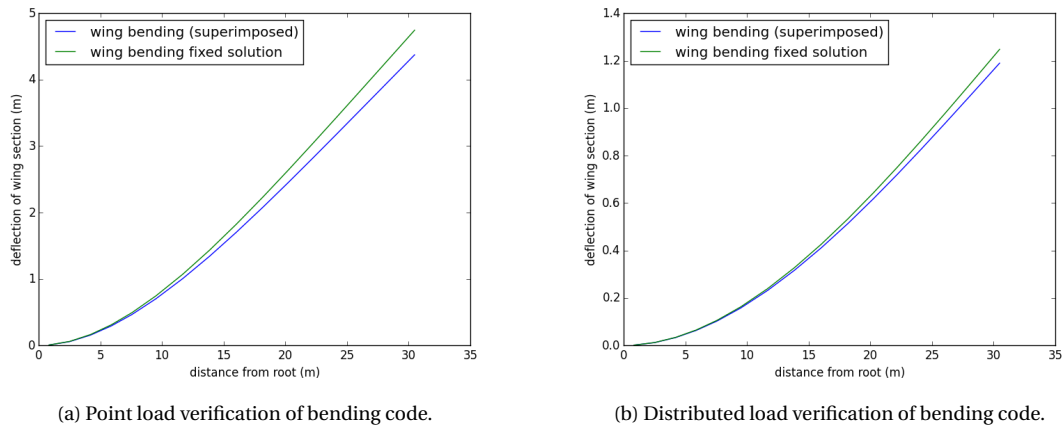


Figure 4.10: Load verification of code.

- **Force module.** The force module has two main interactions, the first is the interaction between the moment and normal force units. Tests were conducted by reverse engineering the moment from the normal force and checking if this aligned with the supposed applied moment force.
- **Shear and torsion module.** The interactions of the shear and torsional force are tested first individually and then in parallel. When applying a pure torque load, the total moment of the shear flows should be equal to that moment and the vertical and horizontal forces equal to zero. For the shear force, this should be exactly opposite: no torsional moment, and the shear flows evaluated over all the surfaces should add up to the applied shear. For the final combined case it was checked if horizontal shear would add up to zero, since there is no applied horizontal force, the vertical shear was evaluated to be equal to the applied shear and finally the generated torque was evaluated to be equal to the applied torque. This was then checked for alignment with the loads of the correct y -station to be given the green light after all the checks panned out.
- **Failure mode.** The failure mode checking consisted of end-of-the-line checks and only needed correct input values, combined with the already checked unit segments, in order to properly function. The alignment tests were conducted with dummy value strings.
- **Deformation** The main check for the deformation module was the integration of the applied forces and the correct syncing of the applied forces, y -station length and the updating geometrical modules. Checks were performed, each step along the way adding one more variable and analysing the outcome to check if the output was logical. For instance, after the integration of variable stringer area into the module, checking if the wing would have a larger deflection.

Structures Model Validation

A pitfall which has brought down many (engineering) projects in the past is the unknown unknowns. To minimise the odds of this occurrence, a validation process is conducted. Validation of the structures model is largely based on the effective validation of the sub-unit calculation methods. Once validated, the units together represent a certain level of accurate representation of the physical phenomenon. Almost equally valuable, the methods give a good overview of where the representation lacks in accuracy. Knowing what the model can and cannot represent is a powerful tool and in this fashion, one can steer clear from trying to extract data from places where the model is deficient.

The calculation methods are sourced from different pieces of literature, while others are fundamental to classical engineering. The main inspiration for the stress methods was the work from T.H.G. Megson, 'Aircraft Structures for Engineering Students' [41]. Deflection and twist came from the well-known Euler beam theory and have been discussed in the previous section. What is left is the intra-stringer buckling, which stems from the work of the late Stepan Prokopovych Timoshenko, whose work is still an inspiration for many engineers. [35].

4.4.3. FishBAC

Within the design of the FishBAC flaps, two pieces of software were used: Javafoil and a code that calculates the baseline structural design of the FishBAC.

Structural Design Code Verification

Figure 4.11 shows the flow diagram for the Python code that was used to design the FishBAC. Essentially, the software establishes a design and calculates if it fails under the applied loads. If the design fails, a new design is chosen until one is reached that passes all the load criteria. All the designs are added to an array and their weights are computed. Between the design of each major component (centre beam, stringers and final design) a lightest design is chosen. Additionally, a few constraints are placed on dimensions for the purpose of fitting in the flap. For example, the height of the centre beam with the two tendons cannot be higher than the height of the tip.

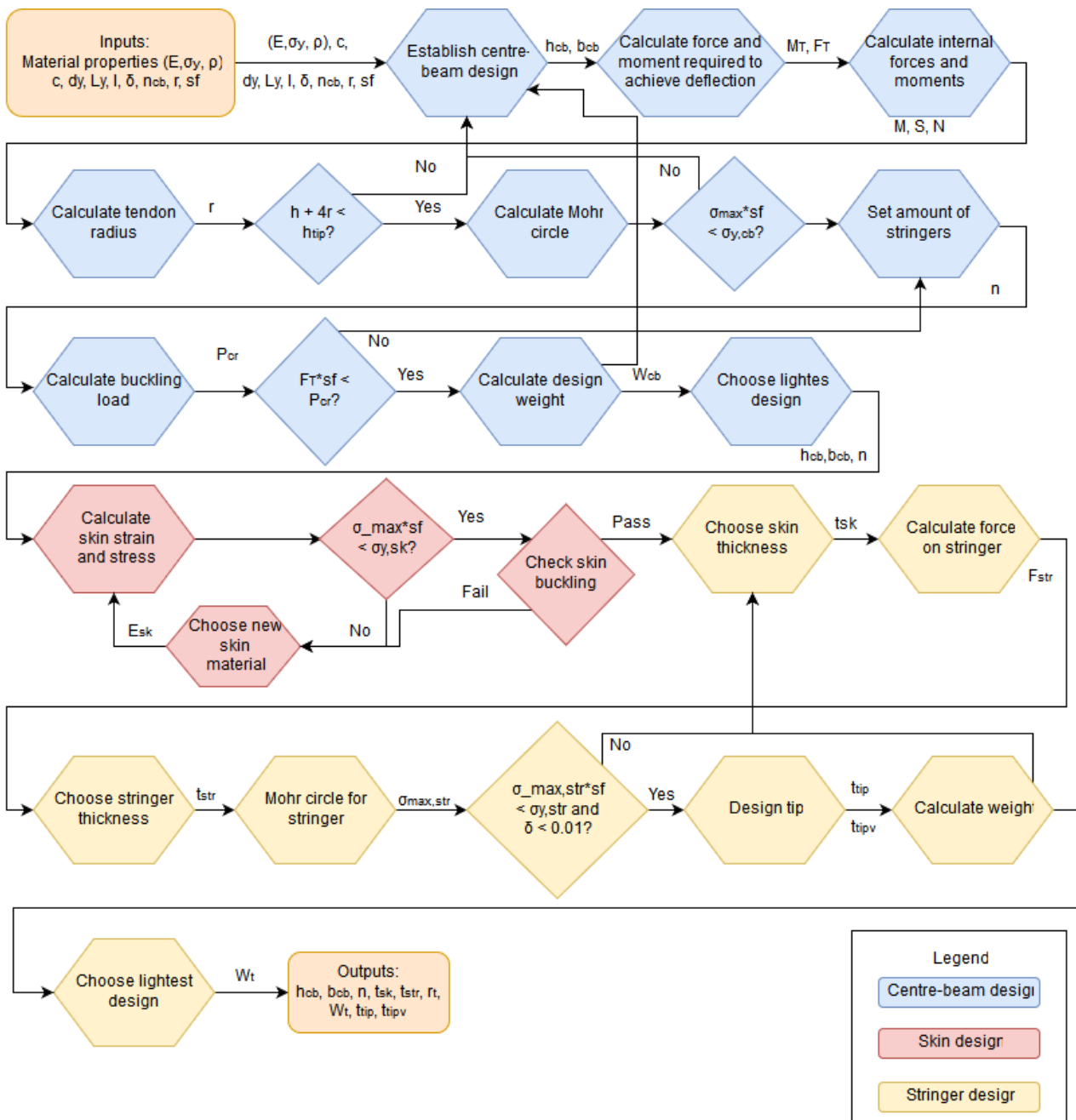


Figure 4.11: Flow diagram of the FishBAC design process.

Verification of this code consisted of unit tests, module tests and finally a full design test.

Unit verification

Unit verification is split up in the modules each unit belongs to. The first module to be considered is the centre beam design.

- **Moment of inertia.** The moment of inertia was computed by hand and by the software and compared to find any differences.
- **Required moment.** This function was tested with dummy values and compared to a calculation by hand. Then, the entire calculation was conducted in the opposite direction to ensure the method used was sound.
- **Internal forces and moments.** In a similar manner as the required moment, the internal forces were computed by both the code and by hand for dummy values. The load and moment diagrams were also checked and compared to expectations. Finally the function was checked by changing input values and checking if the internal forces and moments change appropriately.
- **Size check.** To check if the design fits in the top of the FishBAC, the height of the centre beam is added to four times the radius of the tendon. If the result does not fit in the tip, a 'fail' is printed, along with the missing space. In the end, the final design is also checked.

- **Mohr circle (maximum stress).** Maximum stresses were computed by hand and code with dummy values and then compared. Then these values were changed, to see if the maximum stress changed accordingly.
- **Yield criteria.** The difference between the maximum stress and the yield stress were printed, along with a 'fail' if the structure failed under the loads. The logs were checked to see if any negative result also got a failing result, and then if any negative result ended up in the final design array.
- **Buckling load.** The buckling load was compared to calculations by hand with dummy values. Then these values were changed to see if the buckling load changed accordingly.
- **Buckling criteria.** The difference between the compression and the critical buckling load were printed, along with a 'fail' if the structure failed under the loads. The logs were checked to see if any negative result also got a failing result, and then if any negative result ended up in the final design array.
- **Total weight.** Total weight of the centre beam design was also computed by hand and compared to the resulting configuration. A check was made to ensure an appropriate weight penalty was given to a design with more stringers.

The second module is the skin design, of which verification method is elaborated on below.

- **Skin strain and stress.** The skin strain and stress were compared to calculations by hand with dummy values. Then these values were changed to see if the skin strain and stress changed accordingly.
- **Skin yielding criteria.** The difference between the stress on the skin and the yield stress were printed, along with a 'fail' if the structure failed under the loads. The logs were checked to see if any negative result also got a failing result, and then if any negative result ended up in the final design array.
- **Skin buckling criteria.** The skin buckling criteria is verified by calculating the difference between the normal stress due to compression of the skin and the yield stress of the skin material. If the result passes a 'pass' is printed, along with the difference to ensure no negative values pass through this filter.

The final module is that of the stringer design. This module also includes the design of the tip of the FishBAC.

- **Skin strain and stress.** The skin strain and stress were compared to calculations by hand with dummy values. Then these values were changed, to see if the skin strain and stress changed accordingly.
- **Skin yielding criteria.** The difference between the stress on the skin and the yield stress were printed, along with a 'fail' if the structure failed under the loads. The logs were checked to see if any negative result also got a failing result, and then if any negative result ended up in the final design array.
- **Stringer internal loads.** The internal loads of the stringers were compared to calculations by hand with dummy values. The load and moment diagrams were also checked and compared to expectations. Then these values were changed, to see if the internal loads changed accordingly.
- **Stringer Mohr circle for maximum stress.** The maximum stress of the stringers was compared to calculations by hand with dummy values. Then these values were changed, to see if the maximum stress changed accordingly.
- **Stringer yield criteria.** The difference between the stress on the stringer and the yield stress were printed, along with a 'fail' if the structure failed under the loads. The logs were checked to see if any negative result also got a failing result, and then if any negative result ended up in the final design array.
- **Skin buckling criteria.** The difference between the compression and the critical buckling load were printed, along with a 'fail' if the structure failed under the loads. The logs were checked to see if any negative result also got a failing result, and then if any negative result ended up in the final design array.

Modules

To test the different modules, each result was checked by hand. This meant that if a final result of a certain cross-section of the centre beam was found, this cross-section had the calculated load applied to it, and then the following was checked:

- centre beam and tendon height not too large,
- deflection under applied loads,
- maximum internal stress,
- critical buckling load and
- weight with stringer penalty.

To test the skin module, a similar approach was taken, but this time the following was checked:

- skin strain,
- skin stress,
- maximum stress in the skin and
- skin (shear) buckling stress.

To test the stringer module, the same approach was used, but this time the following was checked:

- force on each stringer,
- maximum stress in each stringer and
- maximum stress in the tip.

Finally, to verify the weight calculation, a weight estimation was conducted by hand, by knowing the dimensions and densities of each component of the FishBAC.

Structural Design Code Validation

A full validation of the structural design is outside of the scope of the DSE, since it would involve building the FishBAC flap and testing it. However, a plan can be conducted to validate the model. The validation procedure of the FishBAC structure is elaborated on below. To minimise the costs of the testing, first a prototype of a single centre beam of the outboard flap is tested, then the entire inboard flap and then the entire outboard flap. The following steps will be required in the validation procedure:

- construction of a prototype of one centre-beam according to the known geometry of the outboard FishBAC flap, using the same production method as described in Section 5.3,
- applying the calculated moment and see what happens (does the structure last under the applied loads and does it achieve the required deflection?),
- applying additional forces to simulate lift and drag on the section,
- (thermal-) fatigue testing of the single centre beam,
- construction of a prototype for the inboard flap of the A330–200,
- testing if the configuration will fail under the applied forces,
- testing if the configuration reaches the required deflection,
- (heat-) fatigue testing of the entire system,
- constructing of a prototype for the outboard flap of the A330–200,
- testing if the configuration will fail under the applied forces,
- testing if the configuration reaches the required deflection,
- (heat-) fatigue testing of the entire system.

Javafoil

Javafoil was used extensively for the aerodynamic calculations on the FishBAC. This program is a very well verified and validated program. The results of certain aerofoils were compared to the results of other numerical models and of real wind tunnel test results. The conclusion is that Javafoil tends to overestimate $C_{L_{max}}$, but will do this for all the aerofoils. Therefore, for comparison purposes it is still useful. It also tends to overestimate the C_D at lower C_L values, but the same point can be made here¹⁰. This was corrected for in the validation of the data acquired. It was taken into account that the C_d and C_l of the real aircraft would be a little lower than the Javafoil results. That turned out to be the case when compared to an A340 $C_l - C_d$ plot given in [74]. Therefore, the results of Javafoil were deemed to be validated.

4.4.4. Sharkskin

While there was no software involved in the design of the sharkskin in this report, there is a lot of future research involved in the subject. Therefore, the basics of the sharkskin have already been validated by extensive research by both Airbus and Boeing. The herringbone riblets, however, are relatively new and their expected drag reduction needs to be validated [48]. The herringbone structure was tested alongside a regular sharkskin, both numerically and in an experimental test. In both cases the results of the regular sharkskin confirmed expectations, which is how the herringbone was verified and validated in this research [50]. This is why the results of this research were deemed to be reliable, while a conservative estimate was made.

Since actual turbulence calculations are very complex and have not yet been solved so far, a reliable model that explains how sharkskin reduces skin friction drag is yet to be introduced. While there are models that are used to simulate turbulent flow behaviour on the sharkskin, they can only provide an approximation of the benefits under certain boundary conditions and approximations. The actual values of the drag reduction caused by sharkskin can only be found by testing.

4.4.5. Leading Edge Suction

In this section, LE suction will be verified and validated. This will be done for the aerodynamic equations, the Krueger flap performance, the pump engine off-take, the pump required power and the production methods for the porous skin.

¹⁰URL <http://www.mh-aerotoools.de/airfoils/javafoil.htm> [cited 15 June 2017].

Aerodynamic Equations

To calculate the drag reduction by the use of HLFC, Prandtl-Schlichtings skin friction equation was used. This is an equation derived in 1932 which has been referenced in many papers. The equation has also been validated [75]. The outcomes of the equations validated themselves, since the drag reduction was the difference between the skin friction drag between the wing with and without LE suction. Since these are all positive, which means a drag reduction is achieved, and because they scale upwards with increasing wing sections, the results make sense.

Krueger Flap Performance

For the Krueger Flap Performance, a combination of research papers were used [54, 58, 59]. The change in performance of a Krueger flap over a LE slat has already been determined in literature [54]. The conclusion of this report was copied for the case of the retrofitted A330, without going to deep into the numbers. Therefore, this is assumed to be correct. The validity of this report is strengthened by the fact that Boeing and NASA stressed that no compromises were made on the flight envelope and safety of the aircraft when a Krueger flap was used.

The noise data is also already validated by multiple sources [57–59].

Pump Performance

For the pump performance, both the engine off-takes and the required pump power will be validated.

The pump engine off-take was validated using literature [62]. An article has been consulted that has been widely used and referenced in the sector, and was advised by Professor Roelof Vos of the TU Delft. This equation was also already verified and validated in the article, and hence will be assumed to be accurate.

For the required pump power, first a unit test will be performed of Equation (4.5) and Equation (4.6).

$$\begin{aligned}
 H &= \frac{\Delta p}{\rho \cdot g} \\
 [H] &= \frac{\text{N} \cdot \text{m}^{-2}}{\text{kg} \cdot \text{m}^{-3} \cdot \text{m} \cdot \text{s}^{-2}} \\
 [H] &= \frac{\text{N}}{\text{kg} \cdot \text{s}^{-2}} \\
 [H] &= \text{m}
 \end{aligned}
 \tag{4.5}$$

From Equation (4.6), it is found that head has the unit meter. This can now be imported into Equation (4.6) to verify the units of power required.

$$\begin{aligned}
 P &= \rho \cdot Q \cdot g \cdot H \\
 [P] &= \text{kg} \cdot \text{m}^{-3} \cdot \text{m}^3 \cdot \text{s}^{-1} \cdot \text{m} \cdot \text{s}^{-2} \cdot \text{m} \\
 [P] &= \text{N} \cdot \text{s}^{-1} \cdot \text{m} \\
 [P] &= \text{W}
 \end{aligned}
 \tag{4.6}$$

From Equation (4.6) it is found that the power required has a unit of watts, which is exactly what was required. For validation of the results, and to see if the equation was applied correctly, they were validated using an online pump power calculator¹¹.

Porous Skin Production

The time required to drill all the holes in the LE appears to be extremely exaggerated, at a minimum of 208 days. Therefore, Dr. Roger Groves, who works on production of this drilling, was contacted to validate this. He confirmed the values, and it was learned that possibly multiple lasers could be used side-by-side¹².

4.4.6. Full Aircraft Analysis

For the full aircraft analysis a Python script was written to calculate, for example, the payload-range diagram. The program was verified by doing unit tests, for instance by changing the fuel weight and checking if the range decreased, which was the case. The longest flight flown with an A330–200 today is a ferry flight from Toulouse Blagnac to Melbourne (TLS–MEL) which is roughly 17,000 km¹³. The maximum calculated ferry range is 17,725 km. The longest non-stop passenger flight is from Rome Fiumicino to Buenos Aires (FCO–EZE) with a distance of 11,194 km¹⁴, which is nicely in between the maximum range at maximum payload and the ferry range. Taking the previously mentioned comments into account, it was concluded that the developed program is validated and verified.

¹¹URL http://www.engineeringtoolbox.com/pumps-power-d_505.html [cited 12 June 2017].

¹²Private communication, Dr. Roger Groves [26 June 2017].

¹³URL <http://www.airliners.net/forum/viewtopic.php?t=352007> [cited 27 June 2017].

¹⁴URL <http://www.routesonline.com/news/38/airlineroute/270863> [cited 27 June 2017].

4.5. Reliability, Availability, Maintainability and Safety

This section addresses the reliability, availability, maintainability and safety (RAMS) of the five concepts that were developed. An initial RAMS assessment was performed in the midterm report [2]. Since the preliminary design phase only started after the midterm report, a lot of updates have been made since with regard to this initial assessment. In this section, an updated version of the RAMS assessment of each concept is presented.

4.5.1. Chevrons

Reliability

Chevrons score high on reliability. An important factor attributing to this is the fact that the chevrons and the trust reverser sleeve will be a single integral part. This way, no single weaknesses will exist near potential connection points. In addition, this design does not comprise of a lot of moving parts. Both the NiTiNol plates and the composite substrate have excellent fatigue properties; the fibreglass composite has less favourable, although acceptable, characteristics, but it will be easily accessible for maintenance. In addition, the fact that the fibreglass cover is allowed to move in-plane relative to the carbon substrates reduces strain, and thus limits fatigue. Finally, no extensive modifications are made to the wing: only a small amount of weight will be added close to the centre of gravity, which means stability of the airplane will be virtually unchanged.

Maintainability

Due to their location at the edge of the thrust-reverser sleeve, it is very easy to access the chevrons for maintenance. The components that will be most prone to failure are the NiTiNol plates and the wiring system. If one of these components fails, the fibreglass cover can easily be detached and the components within the chevrons can be replaced. However, the wiring system running from the chevrons through the engine nacelle towards the wing will be more difficult to access: in case of a malfunction in this area, the thrust-reverser sleeve will have to be removed. Probability of occurrence for this event is low, because the wires are completely shielded by the fibreglass cover and do not move during flight. Should the fibreglass cover be damaged, the entire thrust-reverser sleeve would have to be replaced. It is, however, very unlikely that this will happen, as it would require serious impact.

Availability

The good fatigue properties and high accessibility of the chevrons result in a high availability. Spare sleeves with chevrons can be kept by the operator, minimising downtime in case the sleeves must be replaced. This maintenance action takes approximately 2.5 hours¹⁵. The NiTiNol strips will be even easier to replace. The most extensive maintenance action will be a replacement of the internal wiring within the sleeve, but this will rarely occur. The chevrons can be visually inspected during the daily inspection, but internal defects cannot be spotted this way. Therefore, the chevrons will also be inspected thoroughly during the aircraft C- and D-checks.

Safety

Failure of the chevrons will not affect safety in any way, as they only work towards noise reduction during take-off and landing. The only result of chevron failure is that they will no longer disturb the engine exhaust flow, which even decreases drag. Since the chevrons are located behind the engine, there is no danger of loose parts being sucked into the engine and damaging it. Instead, they will be blown rear- and downwards by the engine exhaust flow, not posing any danger to the aircraft.

4.5.2. Winglets

Reliability

The break-pin winglet design is quite an innovative concept. However, the usage of break pins on aircraft is not entirely new: they are already being used to control the direction of an engine, should it ever happen to come loose. This way, collision with the wing is prevented. The fact that this technology has already been implemented on aircraft increases its reliability. Moreover, its moving mechanism is simple: the pin is a static component, the only moving parts are the dampers. Impacting the reliability of the concept is the snap load margin: while lift loss due to premature pin failure should be prevented, an overdesigned pin can lead to very dangerous situations, ultimately even resulting in the entire wing shearing off. The desired fracture load should thus be evaluated very carefully. To increase reliability of the concept, redundancy can easily be incorporated. Instead of a single pin, multiple pins can be included in the design, all designated to fail at the same load. This way, premature failure of a single pin will not immediately lead to snapping of the winglet.

Maintainability

The maintainability of this concept is very high. Since the pin is a static component, it will just have to be checked at regular intervals. This can easily be done at every aircraft check, as within an instant it can be determined if the pin

¹⁵Private communication, Hans Poelgeest [19 June 2017 14:00].

still functions. To this end, it should be ensured that the pin is readily accessible. Spare pins can easily be stored at the maintenance hangar as replacement components, such that maintenance can immediately be performed if required. The damping system of the winglet should be easily accessible as well. If necessary, manholes can be constructed that guarantee this ease of access.

Availability

In line with maintainability, availability for the break-pin winglet design is very high. As stated before, ease of access shall be ensured in the detailed design of the concept. As long as it is ensured that spare pins are always in stock at the maintenance hangar, downtime for maintenance on the break-pin will never be more than a couple of hours. Should maintenance on the damping system be required, the aircraft will be out of service a bit longer: it is expected that this will last about a day.

Safety

Improper functioning of the design may have catastrophic consequences, depending on the type of failures. The concept may fail due to either under- or over-designing. In the first case the pin will break prematurely. This will lead to lift loss due to the sudden surface area loss of the winglets, and great discomfort for the passengers. However, the plane should still be able to fly normally, although it will be required to do a forced landing at the first possible opportunity. An airstrip of sufficient length should be available: due to the decreased surface area, the approach speed of the airplane will be higher. The second failure type is a lot more severe: in this case the break pin does not fail when the wing is under critical loading. This may lead to the entire wing shearing off, as it will not be able to sufficiently alleviate the loading. Obviously, consequences of this type of failure will be catastrophic, meaning it must be prevented at all costs.

4.5.3. FishBAC

Reliability

A very important reliability aspect for the FishBAC is redundancy. Since the trailing edge control surfaces play a vital role in getting an aircraft safely on the ground, sufficient redundancy had to be assured. The fact that multiple fishbones are used to morph a single flap ensures some redundancy in itself. The fishbones have been sized to an extent that they can carry 1.5 times the expected maximum loads on the wing. Therefore, if one fishbone fails, the others can still deflect the trailing edge while withstanding the aerodynamic loads on it. This would, however, lead to a different deflected shape than desired. Fortunately, the type of actuator considered is a rack and pinion actuator with two racks driving the pinion. This implies that the actuators offer redundancy within themselves: if one rack fails, the other one will still be able to actuate the pinion.

The retrofitted FishBAC mechanism will be powered by the same hydraulic system that is currently used to power the rotary actuators of the Fowler flaps. This is favourable in terms of reliability, as it reduces the extent of the retrofitting operation. Some valves and tubes must be installed, but this will not affect the reliability of the hydraulic system. The material that was chosen for the centre beam and stringers is already being used on actual aircraft¹⁶. The usage of materials that have been proven in flight is a much more reliable approach than using novel materials.

Maintainability

Ease of accessibility is an important parameter in terms of maintainability. When a component within the subsystem fails, it should be easily reachable for maintenance. This reduces downtime and maintenance effort. In case of the FishBAC, the centre beam and the stringers are both made of thermoplastic composite and will be welded together. The skin, however, will be glued to the stringers. Although it requires a significant amount of effort, adhesive bonds can be broken using heat or the appropriate chemicals, but the heat required for this will exceed the maximum allowable temperature for both the stringers and the skin. Therefore, in case a defect occurs, the respective section will have to be removed and replaced by cutting the flap at spanwise locations just before and after the defect. It was identified early on that this approach would be detrimental in terms of sustainability: therefore, a safe-life approach was adhered to during the design phase.

Availability

Due to the safe-life design of the FishBAC, its availability will be very high. The inside of the FishBAC mechanism can be inspected during the aircraft D-checks, when the aircraft has been disassembled. This way, the backside of the FishBAC can be accessed. Since no specific additional actions are required for this, it will not increase the duration of the check.

¹⁶Private communication, Dr. Irene Fernandez Villegas [16 June 2017 11:00].

Safety

During the design of the FishBAC, a primary goal was to ensure that the design would be at least as safe as the current flap design. Safety is a vital aspect for trailing edge control surfaces, as it will be almost impossible to safely land an aircraft once they fail. This risk will always be present to some extent, however, the implementation of redundancy, the safe-life design philosophy and the excellent fatigue properties of the materials have reduced the probability of occurrence for this risk to a minimum.

The materials chosen for the FishBAC themselves do not cause any safety issues, as none of them are toxic or in other ways hazardous. Welding of composites should not lead to any safety hazards either: welding is achieved by melting the thermoplastic resin of the composite. Some chemical substance will be present in the composite, as this has been used to improve handling of the fibers during construction. Some of this substance might be released during welding, but this should not pose any problems¹⁷.

4.5.4. Sharkskin

Reliability

Sharkskin has a high reliability. This has to do with the fact that there are no moving parts. Once the coating has been applied, it will stay in place. The coating will be subject to wear, which will gradually decrease its effectiveness. However, the wear behaviour of the material is known and can thus be accounted for in maintenance intervals. Therefore, this does not decrease the reliability of the sharkskin.

Maintainability

For maintenance of the sharkskin there are two options: manual film application or automated application. In both cases the current top coating will have to be removed first: when this is done manually, it will be unavoidable that the underlying paint layer has to be removed as well. Machined removal can be done very precisely, so in this case it can be ensured that the underlying paint layer is not affected¹⁸. Regardless of which maintenance option is chosen, the coating will be easily accessible.

Availability

For a continuous high-end performance, the sharkskin coating will have to be reapplied every four years (film) or two years (automated). According to Boeing, most airlines have their topcoat replaced every four years, usually during a scheduled C- or D-check¹⁹. This means that the amount of times the aircraft will be out of service due to coating maintenance will double with the introduction of automated applied sharkskin. In case of manual application, the maintenance interval will not change with respect to the current coating. However, trained professionals will be required and the aircraft will be out of service significantly longer per maintenance session than for automated application. If reinforcing material can be added to the automated silicone coating, its maintenance interval can be increased, thus increasing availability.

Safety

The usage of sharkskin coating will not lead to any safety hazards in-flight. There is no danger of sudden failure: even in case of a bird strike or other impact, only a small portion of coating will be affected. There will thus be no sudden large decrease in efficiency. In case of manual application of the sharkskin coating some safety hazards may arise for the personnel: inhalation of residue from the removed coating should be prevented.

4.5.5. Leading Edge Suction

Reliability

The suction system is a very complicated system with many different components, such as ducts, valves and tubes. At each connection, there is a certain risk of leakage. To some extent, leakage will be unavoidable, but regular maintenance will be required to keep this an absolute minimum. The leading edge holes provide some reliability issues as well: the tiny holes can get clogged very easily by bugs, dust and ice particles in clouds. The Krueger flap prevents bug impact on the leading edge during take-off and landing, however, it is not capable of shielding the leading edge from tiny dust particles. Moreover, the Krueger flap will not be extended anymore once the aircraft traverses clouds, which means it cannot shield the mechanism from ice particles. The Krueger flap itself is quite reliable: it is already commonly used on aircraft and thus falls in the category of proven technology.

Maintainability

As stated before, the suction system consists of many different parts. Most of these parts are hidden within the wing leading edge and the fuselage, which means they will be difficult to access for maintenance. Fortunately enough, the leading edge is bolted to the rest of the wing, which means it can be detached. Once this is done, the entire inside of

¹⁷Private communication, Dr. Irene Fernandez Villegas [16 June 2017 11:00].

¹⁸Private communication, Amber Van Hauwermeiren [19 May 2017 10:00].

¹⁹URL http://www.boeing.com/commercial/aeromagazine/aero_05/textonly/fo01txt.html [cited 23 June 2017].

the leading edge can easily be reached. However, removing the leading edge is a time-consuming operation, and apart from the D-checks it is not expected that this can be done within the time budget of the standard aircraft checks. A solution would be to install manholes on the leading edge. The Krueger flap is very easily accessible, which positively influences maintainability.

Availability

If manholes can be installed on the leading edge, the blowing system will have a medium availability. The hydraulic system will have to be checked for leakage quite regularly, but with easy access to the leading edge this will not take a lot of time. However, a lot of spare parts will have to be available at any time for replacement, should it be required.

Safety

Although the plane will still be able to fly if the suction system malfunctions, failure can still lead to severe safety issues. Since airlines will always want to bring as little fuel on board as possible, the fuel amount will be tuned to the expected consumption with a fully functioning suction system. Therefore, in case the system fails and the aircraft becomes less efficient, its range will suddenly decrease. This can be really dangerous if an airplane has to loiter or do a go-around.

4.6. Operations and Logistic Concept Description

In order to obtain a clear overview of the product operation cycle and additional logistical aspects, it is important to look at the associated activities and required resources. First the operational aspects of the aircraft and the maintenance will be discussed, after which the logistical aspects will be elaborated upon.

4.6.1. Operation and Maintenance

As it is important to know whether or not an aircraft is still suitable for operation, regular maintenance checks have to be scheduled. During operation, bird strikes might occur, bugs may stick on the wing and since the aircraft is already experiencing high aerodynamic loads, it is possible for components to perform sub-optimal or get damaged during flight. Quick inspections are performed at the gate every 24 to 48 hours, whereas slightly more elaborate inspections are performed weekly [76]. For the retrofit, here a quick inspection of the sharkskin could easily be done. As this is replaced regularly, it should also be checked on a regular basis. Other than that, a visual inspection and a fluid level check are performed during daily maintenance, whereas during the weekly checks the engines are inspected and a light overall check is performed²⁰. The state of the chevrons can also be inspected here, to see if there are no signs of fatigue for the fibreglass cover. The larger maintenance inspections are shown in Figure 4.12. In this figure, the operational duration is expressed in months or flight hours (FH), whereas the maintenance duration is expressed in MH. One may notice no B-checks are present: the reason for this is that current airlines discard B-checks, as they are often associated with older aircraft types [76].

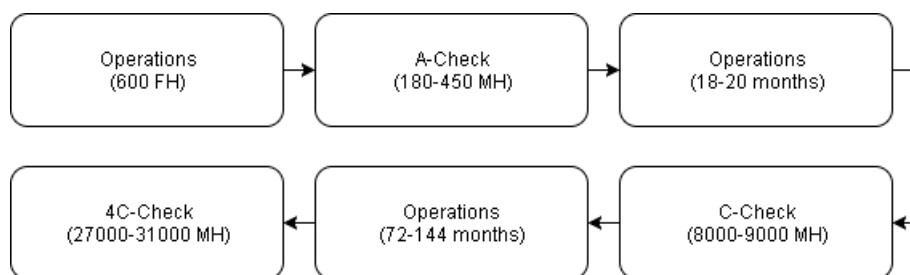


Figure 4.12: Simplified maintenance flow diagram showing larger maintenance procedures.

In between longer periods of operation, smaller maintenance checks will still be performed (e.g. several C-checks will be performed before a 4C-check will be performed). As 4C-checks (also known as D-checks) can be categorised as heavy checks that are performed every 12 years for the A330²¹, it would be beneficial if the concept has a lifetime of this specific duration or significantly longer. This would indicate that the concept can be replaced and, as the aircraft will be stripped down during this check, no unscheduled maintenance would be necessary [77].

4.6.2. Logistics

Logistics is an important factor in the aviation industry, as the planning as well as the availability and distribution of resources can reduce or increase the cost significantly. During maintenance it is important that all necessary tools and materials are present and available for use. This means that if a component or coating has to be replaced, there should

²⁰URL http://www.aircraftmonitor.com/uploads/1/5/9/9/15993320/basics_of_aircraft_maintenance_programs_for_financiers__v1.pdf [cited 17 May 2017].

²¹Private communication, Hans Poelgeest [19 June 2017 14:00].

always be available spare parts present. In case of a coating, the necessary materials can be stored relatively easily near suitable airport hangars. For this, as discussed before, an automated process will be used. As the retrofit becomes successful, more and more of these automatic applicators will be available at airports. For the first few years, though, this will not be the case. Therefore, to be sure the sharkskin can be successful, automatic applicators will have to be stationed at the largest airports through which most of the retrofitted A330s come. If larger retrofit components need replacement, storage of spare parts can be an issue. For smaller retrofits this replacement process can be conducted overnight at the gate, but larger retrofit maintenance requires appropriate equipment and thus a hangar might be necessary. It is possible, if no thrust-reverser sleeves with chevrons are available, to replace this temporarily with the regular thrust-reverser sleeve, which are more readily available. It is also possible for the aircraft to fly without the sharkskin, but this will increase fuel consumption and will have to be taken into account while planning the flight. Parameters that are important for efficient maintenance can be found in Figure 4.13.

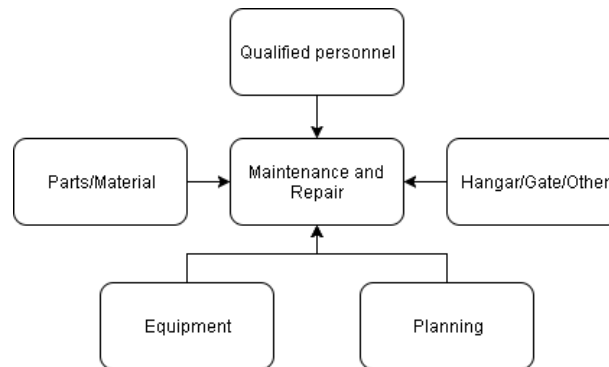


Figure 4.13: Parameters that influence maintenance process.

Another important factor related to logistics is that of the distribution of ground support and personnel. During maintenance and repair as well as during operation, it is important that the resources are properly allocated. This means that spare parts and other essential equipment should always be easily accessible and nearby the corresponding airport or hangar, in order to allow for a smooth maintenance process. The logistics regarding the personnel is also important in order to obtain efficient and quick maintenance. If a concept requires extensive maintenance and inspections, more man hours are required, which in turn will lead to higher costs [77]. Overall, the logistics are especially important for airlines, as proper planning will avoid any unnecessary increases in cost.

4.7. Sensitivity Analysis

This section discusses the sensitivity of the design of each product, for a major change in parameters. First the effect of changing the mission duration will be discussed. Next, for each product, possible changes in its parameters will be discussed. These parameters may include, but are not limited to, weight, aerodynamic performance and noise performance of the product. The effects of these possible changes on the overall performance of the aircraft are covered, and the feasibility will be assessed. Finally, there will be a discussion per concept whether it is still feasible if the type of aircraft on which it should be retrofitted will be changed.

4.7.1. Effects of Mission

Changing the mission duration or the amount of payload on board has its consequences for the amount and percentage of fuel saved per trip. The decrease in drag coefficient due to the products will be the same, but since the amount of fuel on board can vary, this has consequences for the fuel savings.

The two main parameters of a mission were varied: cruise time and payload weight. The influence of both is shown in Figure 4.14. Firstly, it can be concluded from Figure 4.14a that the cruise time and therefore the range has an effect on fuel savings. However, the minimum percentage fuel reduction is always above 10.2, which means that requirement **SRW-05** will always be met. It would however be optimal to not cruise between 2 and 5 hours, since improvements here are smaller than for shorter or longer cruise times. Secondly, by looking at Figure 4.14b, there is a clear trend between payload weight and fuel savings. More on-board payload weight will make the retrofit more efficient compared to a standard A330 with the same payload. However, these differences are in the order of 1% of the total improvement.

4.7.2. Chevrons

Possible Changes in System Parameters

Because the chevrons are a low-weight and relatively low-cost concept, the risks are reasonably low.

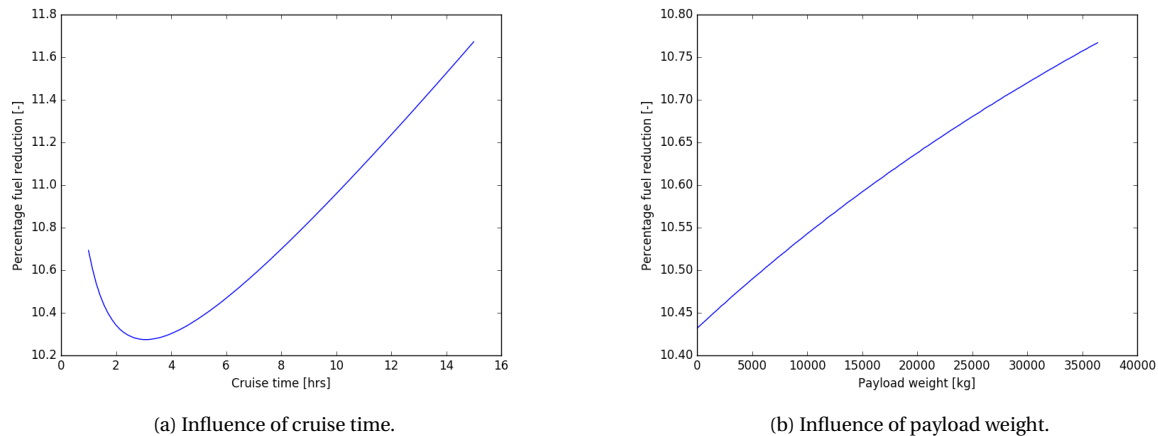


Figure 4.14: Influence of mission parameters on fuel savings.

- **Weight.** The chevrons weight was found to be 63 kg. If this would double to 126 kg, it would still not have detrimental effects, as this is still less than the accounted weight for a single passenger.
- **Noise.** It was expected that a decrease of 2 dB would be achieved for low-frequency exhaust noise. This, together with the lower thrust requirement, would lead to the aircraft being in a lower noise category. This would decrease take-off and landing costs. As a noise decrease is the only purpose of chevrons, chevrons are very sensitive to this. However, since noise is very hard to simulate, the actual noise reduction will have to be derived from test flights. A less drastic measure could also give more insight in the noise decrease, namely scaling the results achieved by others to the engine of the A330-223. Examples of such scaling are available [15, 16], but since this goes too far for this design stage it is listed as a recommendation.

The feasibility of chevrons will be most sensitive to changes in their noise performance. Therefore, scaling of results of other engines should be done, possibly followed by flight tests. If chevrons cannot provide a major noise decrease, the aircraft may not fall under a lower noise category and the noise requirement will not be fulfilled.

Possibility of Retrofitting Other Aircraft

As mentioned earlier, applying chevrons is a relatively simple procedure. The only prerequisite is that the aircraft has to contain thrust-reverser sleeves that can easily be replaced. As most commercial aircraft have this feature, the market can be stretched from only the Airbus A330 to most likely a significant amount of other aircraft. Although retrofitting is relatively simple, additional research has to be conducted to check whether or not the aircraft will achieve the same noise reduction as the Airbus A330. By investigating and creating more accurate noise models, it will be possible to assess the noise performance of different engine nacelles. This indicates that it will definitely be possible to retrofit chevrons to other aircraft, however, more knowledge has to be gained about the noise performance in order to guarantee the customer the same or a better noise reduction will be achieved.

4.7.3. Wingtip extension

Possible Changes in System Parameters

There are several major design parameters of the wingtip extensions, which, if changed, can influence the feasibility of the design. These parameters are listed below:

- **Span.** The current span of the wingtip extension is limited to 3.5 m, so that it makes maximum use of an increased aspect ratio while still remaining in the same aerodrome sizing category, on which landing costs and airport availability are based. Decreasing the span would lead to a loss in efficiency, while increasing the span would lead to an increase in landing rights costs and loss of the right to land on relatively small airports.
- **Weight.** If the wingtip extension or break-pin system were to be heavier than initially designed for, the overall efficiency of the retrofitted aircraft would of course go down. However, this has no major structural implications for the wing, since the extra weight at the wingtip can provide wing bending relief.
- **Aerodynamic performance.** In the case that the aerodynamic improvement is less than predicted in the aerodynamic model, it should be assessed whether the improvement still outweighs the weight added by the break-pin system and the reinforced wingbox. This could be the case due to the fact that Tornado is not able to model C_{D_0} . Wingtip extensions will have to be further analysed in for example a CFD analysis in order to decrease uncertainty about their aerodynamic performance.

Wingtip extensions are most sensitive to aerodynamic performance. Due to deficiencies in Tornado, this cannot be accurately modelled. Due to the fact that the wingtip extension is the second best product in both aerodynamic-

and fuel performance, the possible impact of less aerodynamic performance cannot be nullified. However, the total performance will still meet the requirements, even if wingtip extensions will be left out of the design.

Possibility of Retrofitting Other Aircraft

There is certainly a possibility that the wingtip extensions can provide an increase in efficiency for other types of aircraft. There must, however, be a careful assessment on the current efficiency of that aircraft, especially if it already has other wingtip devices installed that improve the efficiency of those aircraft. However, the first thing to assess would be the current wingspan of the aircraft. If the aircraft were to just fit in its size constraint, adding a wingtip extension would lead to an increase in costs for landing rights, therefore it is questionable and should be researched whether retrofitting in this case will provide a gain for the airliner.

Furthermore, the current wingbox structure of the aircraft will have to be inspected for whether it will be able to handle the increased loading due to the wingtip extension. Especially in the worst loading case, when the break-pin will be designed to fail, the wingbox structure must be able to endure the loading. If the wingbox will fail under those conditions, it must be assessed whether the extra weight of strengthening the current wingbox will outweigh the drag reduction of the wingtip extension.

4.7.4. FishBAC

Possible Changes in System Parameters

To assess if the viability of the FishBAC flap is affected by any of the design parameters, a sensitivity analysis was conducted below. The following parameters may affect the effectiveness of the FishBAC when changed:

- **Weight.** If the weight of the FishBAC changes due to a change in, for example, materials, resulting in it becoming heavier, this will affect the viability of the design. At this point, the FishBAC is only slightly heavier than the original Fowler flap system. If this weight increases, it might outweigh the fuel savings caused by the flap fairings. However, the noise improvement will still be a considerable way for airlines to be able to take off earlier in the morning and later in the evening due to a lower noise category.
- **Durability.** If the FishBAC flaps turn out to have poor fatigue properties due to repeated heating of a composite, this will affect the viability of the concept. Other causes of a shorter lifespan of the FishBAC include skin fatigue, actuator fatigue and the inability to design a safe-life flap. If the FishBAC only lasts for, for example, ten years instead of twenty, it will become a lot more expensive for newer aircraft. Since the purchase of a FishBAC flap system only becomes profitable in terms of fuel savings in ten years, this means each retrofitted aircraft needs a flap replacement at some point in its life, so the costs are doubled. This will render the concept commercially unattractive and hence non-viable.

What can be concluded is that the FishBAC is sensitive to durability issues. If the durability turns out too low, it must be considered whether retrofitting is worth it. The performance requirements can be met without the FishBAC. However, since the FishBAC also influences noise, this does have an effect on the noise requirement. Therefore the durability will have to be assessed, first analytically, but also by fatigue testing later on in the design phase.

Possibility of Retrofitting Other Aircraft

The FishBAC is limited by its dimensions and the specific load cases on the aircraft. If a wing has the same flap dimensions as the A330–200 (but a similar/lower weight), the FishBAC can easily be applied to it. There are some candidates, such as the A330–300 and the A340 family, but these aircraft are heavier than the A330–200 and a wing loading analysis will need to be computed to see if the FishBAC flaps can function under these loads. When another aircraft with different flap dimensions is considered, it will not be transferable to this aircraft.

4.7.5. Sharkskin

Possible Changes in System Parameters

There are a few design parameters that will affect the feasibility of the sharkskin concept when they are changed. These parameters and their effects are listed below.

- **Weight.** While a weight approximation was made in Section 3.5.2, the weight of the sharkskin can still change if, for example, another material is required. However, even if the weight of sharkskin doubles, the reduction in fuel weight it causes will still be larger.
- **TRL.** Due to the fact that sharkskin is still in development, performance on an entire aircraft at cruising speed is not entirely known. A conservative value for drag reduction was taken, but it could turn out even lower. Therefore it could turn out that sharkskin provides less drag reduction than expected. Sharkskin will be profitable even when the total drag reduction is 1%. However, due to the fact that sharkskin accounts for a major percentage of the drag reduction of all the products, this may cause the requirements not to be met if sharkskin were to under perform.

- **Durability.** The durability of sharkskin coating is one of its main drawbacks. At this point a reapplication every two years is worth it. However, if the effects of the sharkskin wear off after only one year, airlines will not be interested any longer.

The fact that the TRL of sharkskin is low, which brings uncertainty to its drag reduction abilities, makes sharkskin and the total retrofit package sensitive to this issue. Since sharkskin is the major contributor in drag reduction and therefore fuel- and emissions reduction, these requirements cannot be met if sharkskin is to under perform greatly.

Possibility of Retrofitting Other Aircraft

The sharkskin is a very flexible concept that is not limited by the dimensions of an aircraft. It can easily be applied to another aircraft once its geometry is known. To get the best results for the least amount of money, a new turbulence model would have to be computed to find an optimum configuration for the sharkskin. If a film is used, it can easily be applied to other aircraft. A robot that applies the sharkskin would need to know the geometry of the new aircraft to apply the riblets, after which it could apply the sharkskin without much extra effort. The costs would increase if the aircraft is larger and more top coat material is required.

4.7.6. Leading Edge Suction

Although suction will not be applied as a retrofit to the Airbus A330, it might still be useful to conduct a sensitivity analysis. If certain parameters are positively affected, possibly the LE suction system will perform significantly better. In this case, it might be worth considering to sell it as a retrofit for airlines. First the results of possible changes in system parameters will be discussed, after which the possibility of retrofitting other aircraft will be explained.

Possible Changes in System Parameters

As the sensitivity analysis will check whether or not the specific concept yields positive results when the essential parameters are slightly changed, it is necessary to carefully select these parameters. In the case of the LE suction system, mass is the first parameter that has to be assessed. As another limiting factor of the suction system is power, this will be assessed secondly. These system parameters will be assessed below:

- **Mass.** Using the same calculation method that was used in Section 3.6.5, halving the mass results in more positive values, although the maximum fuel reduction in this case will only be 0.65% for setup 4. This means massive changes to the mass will not be beneficial for the overall improvement of the system, which means mass is not the limiting factor.
- **Pump power.** Because the equation used to calculate the energy required for the pump is a potential energy equation, the required pump power can only decrease or increase when either the efficiency of the pump or the roughness, diameter or length of the tubing changes. For this report, smooth aluminium tubing was used, with a pipe roughness of 0.03 mm and a pump with an efficiency factor of 0.7. The smoothness and length of the tubing will not change dramatically. What can change, is the efficiency of the pump. For this sensitivity analysis, the case of LE suction throughout the wing will be taken. By assuming an efficiency of 0.35 and one of 1.00, the pump power required becomes 60,354 W and 21,123.9 W. This leads to an expected pump mass of 306.29 kg and 209.6 kg. This is only 60.8 kg heavier and 35.4 kg lighter, leading to a total weight of 2,057.2 kg and 1,961 kg for the complete system. Hence it can be said with certainty that the pump is not very sensitive to changes, as the original pump was only a fraction of the total system weight.

LE suction is not very sensitive to change in its system parameters. This is also due to the fact that it was decided to not implement this system in the retrofit package, due to its low performance.

Possibility of Retrofitting Other Aircraft

As the suction system requires an extensive integration process and heavily relies on the currently present leading edge layout, retrofitting the suction system on other aircraft than the Airbus A330 will require significant modifications. As all components have to be manufactured to match the leading edge layout, a new research has to be conducted for each aircraft to find the optimal duct distribution. Apart from this duct distribution, an investigation must also be started regarding the spar strength and connection points. If the spar is unable to withstand the loads that pass through the leading edge skin assembly, research has to be conducted to check whether or not reinforcement would be able to solve this problem. Finally, the Airbus A330 requires an extra pump and a new gearbox and generator. These will have to be certified and accepted by the engine manufacturer. If other aircraft also require these new components, these will again have to be certified and accepted, as different aircraft will most likely make use of different engines. Therefore, the conclusion can be drawn that the suction system is not ideal as a retrofit. When a completely new aircraft is built, it can be implemented during the manufacturing and assembly process, although only if its performance increases significantly within the near future and better ways are found to drill the holes in the skin panel.

4.8. Compliance Matrix

To check whether or not the requirements have been met, a compliance matrix has been established. This compliance matrix shows all the requirements along with the specific results. A ‘yes’ indicates that requirement has been met by the final design, a ‘no’ indicates this specific requirement is not met. The compliance matrix for the system requirements can be found in Table 4.5. As not only system requirements were set up, but also stakeholder requirements, it is essential to assess those as well. The stakeholder compliance matrix can be found in Table 4.6, which adheres to the same format as mentioned earlier. The driving requirements mentioned in Table 4.5 can also be found in Section 2.1.2, however, for the other requirements the midterm report should be consulted [2].

Table 4.5: Compliance matrix for technical requirements.

Code	System Requirement	Yes/No	Remarks
SRW-01	The system shall be retrofitted to the reference aircraft, the Airbus A330-200 (A330-223).	Yes	
SRW-02	The concepts used in the system shall be pre-existing concepts.	Yes	
SRW-03	The system shall have a pre-determined lifecycle.	Yes	
SRW-04	The retrofitted aircraft shall reduce the impact on the environment when compared to the reference aircraft, in line with the ACARE Flightpath 2050 goals.	Yes	
EMIS-01	The retrofitted aircraft shall achieve at least a 7.5% reduction in CO ₂ emissions per passenger kilometre.	Yes	
EMIS-02	The retrofitted aircraft shall achieve at least a 9.0% reduction in NO _x emissions per passenger kilometre.	Yes	
EMIS-03	The retrofitted aircraft shall achieve at least a 6.5% reduction in the perceived noise emission of flying aircraft.	Yes	
SRW-05	The fuel consumption of the retrofitted aircraft on a reference mission shall be reduced by at least 7.5% per passenger kilometre compared to the reference aircraft.	Yes	
SRW-06	The retrofitted aircraft shall maintain an engineering budget equal to or better than the reference aircraft.	No	The mass budget was violated.
SRW-07	The retrofitted aircraft shall maintain the same reliability standards as the reference aircraft.	No	Maintenance intervals become more frequent.
SRW-08	The retrofitted aircraft shall maintain the same safety standards as the reference aircraft.	No	Further tests are still needed to indicate this.
RED-01	Any altered control surfaces shall be redundant.	Yes	
RED-02	Any added coating does not have to be redundant.	Yes	
SRW-09	Each individual concept shall at least contribute to either a reduction of fuel consumption, a reduction of noise emission, a reduction of CO ₂ emission or a reduction of NO _x emission.	Yes	
SRW-10	At least one of the concepts shall include morphing technology.	Yes	

As can be seen from Table 4.5 and Table 4.6, several requirements are not met. The requirements regarding the reliability and safety cannot be verified and validated at this moment, as this requires more knowledge of the individual components of each concept. As a lot of testing and certification will be necessary, this requirement is said to be not met, until proven otherwise. The same is the case for the requirements related to the controllability and the load cycles. However, in the case of the requirement related to the engineering budget, the same cannot be said. Although the noise significantly decreased, the added mass due to the different concepts and the additional power required for the actuation mechanisms indicate that this requirement will not be met. This result will not change in the future, as a significant amount of mass will have to be added in order to implement all the designs. Therefore, this requirement should have been identified as a killer requirement in the start of the design phase, since it is nearly impossible to make changes to the wing without adding mass for potential actuators.

Table 4.6: Stakeholder compliance matrix.

Code	Stakeholder Requirement	Yes/No	Remarks
SRW-SH-1.1	The lifetime cost of the retrofitted aircraft shall not exceed the lifetime cost of the reference aircraft.	Yes	
Cost-01	The system shall have a total lifetime cost of at most \$8.2M for a 9 year old Airbus A330-223.	Yes	
SRW-SH-1.2	The system shall withstand no less than 40,000 load cycles.	No	Further tests/ re-research will be necessary.
SRW-SH-1.3	The system shall perform no less than 800 hours of service before a maintenance check.	Yes	
SRW-SH-1.4	The system shall be repairable with existing maintenance equipment.	Yes	
SRW-SH-1.5	The system shall be inspected with existing non-destructive testing methods.	Yes	
SRW-SH-2.1	The system shall be made of existing materials.	Yes	
SRW-SH-2.2	The system shall be made with existing production techniques.	Yes	
SRW-SH-2.3	The system shall be produced by using existing technologies.	Yes	
SRW-SH-2.4	The system shall be implemented with existing tools.	Yes	
SRW-SH-3.1	The system shall comply with existing aircraft regulations.	Yes	
SRW-SH-3.2	Any parts removed from the Airbus A330-200 wing shall be disposed of according to the life cycle policy of Airbus' components.	Yes	
SRW-SH-4.1	The retrofitted aircraft shall maintain the same controllability as the reference aircraft, with a maximum allowable margin of 5%.	No	Further testing is needed on this point.

Project Implementation

With the final product designed to a preliminary extent and verification and validation conducted, the design aspects of this project are finished. However, more research and development will be necessary to stay on top of the retrofit market. Therefore a plan will be made regarding the activities in the nearby future, which can be found in Sections 5.1 and 5.2. The production plan describes the assembly and integration process of the individual components onto the aircraft, which can be found in Section 5.3. Finally, the cost breakdown and return on investment are documented in Sections 5.4 and 5.5 respectively.

5.1. Project Design and Development Logic

The project design and development logic will elaborate on the next steps in the realisation of the Smart Retrofit Wing as a commercial product. Before any (aerospace) product can be launched, it is subject to a vast amount of optimisation, testing, validation and certification. Due to the different TRLs of the chosen concepts, each concept will take a different amount of time to validate and certify. To start generating profit as soon as possible, all concepts will be developed simultaneously and released individually once they are certified and their production chain is established. Within the next four years, the BEAU-wing catalogue will gradually expand with more and more innovative concepts. From a marketing standpoint, it is also a good idea to establish a good reputation first and release more innovative concepts gradually.

Figure 5.1 shows the general planning of the next phases of the design. While concepts have been developed in some detail, they can be optimised using validation data. After their optimisation, their performance needs to be validated with prototypes. The next step is to set up manufacturing and perform full aircraft tests. When the tests are conducted, the products can be certified and the large-scale production of a component can be started. Since each component is developed individually, the component optimisation and validation are also discussed on an individual basis.

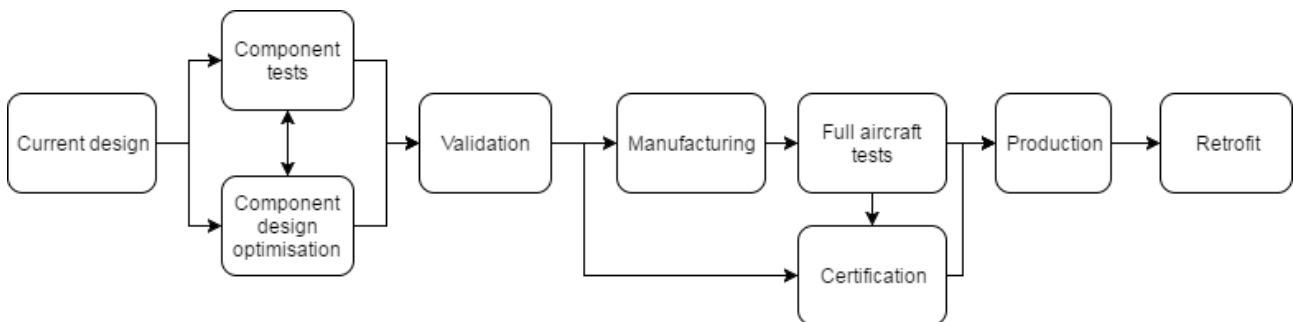


Figure 5.1: General planning of the future development of the Smart Retrofit Wing.

5.1.1. Chevrons

Figure 5.2 shows the optimisation and validation of the chevron concept. Chevrons are the most developed among the concepts, and are expected to have the shortest development time and hence be released first. Since the concept is fully developed they will only be tested a few times. A flight test will confirm the noise reductions chevrons cause.



Figure 5.2: Further development of the chevrons.

5.1.2. Winglets

The retrofit concept of the winglets has become an extended wingtip with a break-pin system. In order to successfully design this retrofit wingtip, further research and development needs to be performed for the details of the concept

components. First of all, the hinge between the main wing and the wingtip needs to be designed and structurally analysed in detail, all dimensions should be carefully calculated. In addition to this, passive damping systems could be a solution for the impact of a canting wingtip after a pin-break, this should be analysed and tested. Secondly, the break-pin location and dimensions should be calculated. The dimension of the pin is of crucial importance, such that it has exactly the right breaking point, as is the purpose of this system. The optimisation and validation process is shown in Figure 5.3. To design the break-pin system, a wind tunnel test of the winglet is conducted to optimise it aerodynamically and to find the loads on the winglet during a typical flight. The next step is development of the break-pin system under these loads and an extensive testing of the system to ensure its reliability. Finally, the model is flight tested to validate the reliability and performance of the concept.

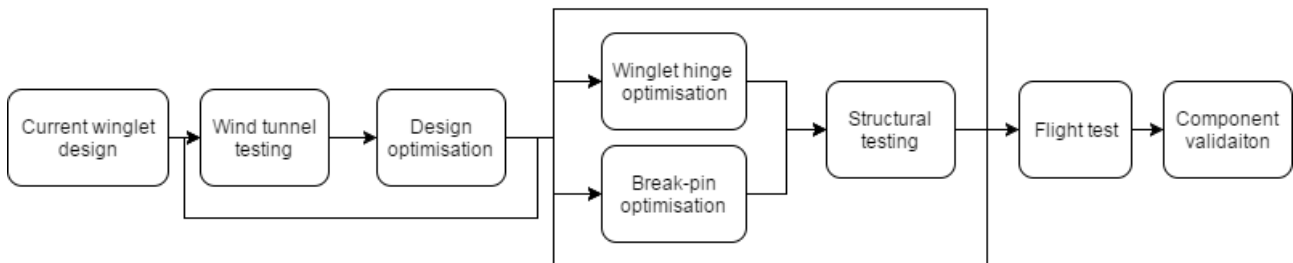


Figure 5.3: Further development of the winglet.

5.1.3. FishBAC

The FishBAC is a concept with a very low TRL. Since a FishBAC will be used on the flaps, and flaps are essential during approach, they need to be very safe. This is why a safe-life philosophy was adhered to during design. To release the FishBAC as a reliable and beneficial replacement of the flaps on an A330, these characteristics need to be validated. Moreover, the structural design of this flap can be optimised further with more appropriate deflection approximations. When a more optimised design is finalised, a prototype can be built and tested. While all materials were chosen for their excellent fatigue properties, thermal fatigue is still a relatively undiscovered area in aerospace structures and materials. The safe-life design of the FishBAC cannot be guaranteed without a test of its (thermal) fatigue properties. In the meantime, a wind tunnel test can confirm the aerodynamic performance of the design. Finally, a flight test is conducted to validate the performance of the FishBAC as a flap replacement. An overview of the total development process is shown in Figure 5.4.

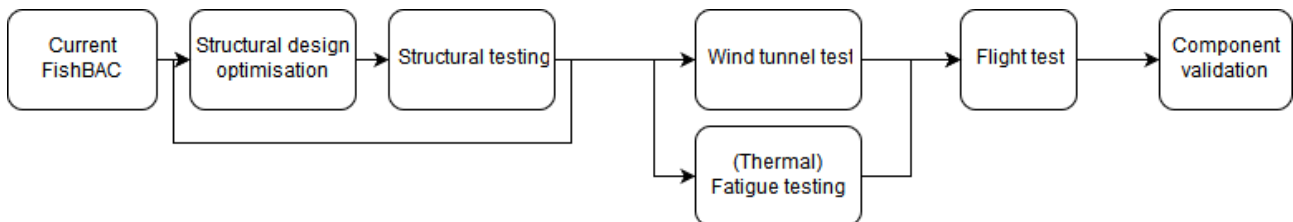


Figure 5.4: Further development of the FishBAC.

5.1.4. Sharkskin

Since the herringbone riblets are a new take on an existing concept, with a very large drag reduction, a vast amount of research and development needs to be conducted. While the general steps of the research were covered in Section 3.5.5, they are repeated and elaborated on below.

- **Compute a turbulence model of the A330.** This is specifically useful to find the regions on the aircraft to which sharkskin can be applied most efficiently and in turn to reduce costs. This would concern a numerical analysis, not a wind tunnel test, and can be conducted alongside riblet optimisation.
- **Test the herringbone riblets at high Reynolds numbers and riblet optimisation.** This would be a next step to the studies done so far on the herringbone riblets [50]. This study was conducted at very low Reynolds numbers, compared to the ones the aircraft will fly in. To validate the performance of the herringbone riblet, a test at higher Reynolds numbers needs to be conducted. Additionally, there has been no research on the optimal geometry or herringbone riblets, hence this needs to be found as well. The following factors can be varied in this process:
 - riblet height,
 - riblet angle,

- riblet spacing,
 - width of the herringbone structure and
 - angle of the herringbone structure.
- **Test the herringbone riblets on a scaled aircraft model.** Before money is invested in a large-scale test of the herringbone riblets, a wind tunnel test on a smaller scale can be conducted. In this test, a model of the A330 is (strategically) coated with sharkskin and put inside a wind tunnel. The Reynolds number the aircraft typically encounters during take-off, cruise and approach are tested in this tunnel. The resulting drag (reduction) will give an indication of the true potential of a sharkskin texture. To ensure reliable results of this test, three versions need to be conducted and compared:
 - bare aircraft model,
 - optimised regular sharkskin and
 - optimised herringbone riblets.
 - **Develop or purchase a large-scale application machine.** While the sharkskin on the models can be applied with a relatively small 3D printer (applicator), actual aircraft need a much larger applicator that can cover the entire aircraft without taking the aircraft apart. This applicator also needs to be either very fast or very cheap, such that multiple applicators can be used at once. A Delft-based company called qlayers is developing such a machine at this point, and they have already started the first test-trials with a small scale model¹. An alternative would be purchasing this machine when it is fully developed, and using films until this time.
 - **Perform long-period flight tests on a test aircraft.** To fully validate the sharkskin as a means of drag reduction, a long-period flight test needs to be conducted. This test will also provide useful insight in the durability of the coating. During this test, a commercially used A330 will be coated with the herringbone riblets and flown for two years straight. During this time, each flight profile and the fuel used during the flight need to be recorded. After two years, an overview can be made of the total reduction in fuel consumption of the aircraft, as well as the durability of the coating.

This process will be adhered to, but to release the sharkskin as soon as possible, first a less optimised version will be released. Since the sharkskin is reapplied every two years with a very versatile application method, the texture can easily be changed. Figure 5.5 shows the development logic for the sharkskin concept, based on Section 4.4.4.

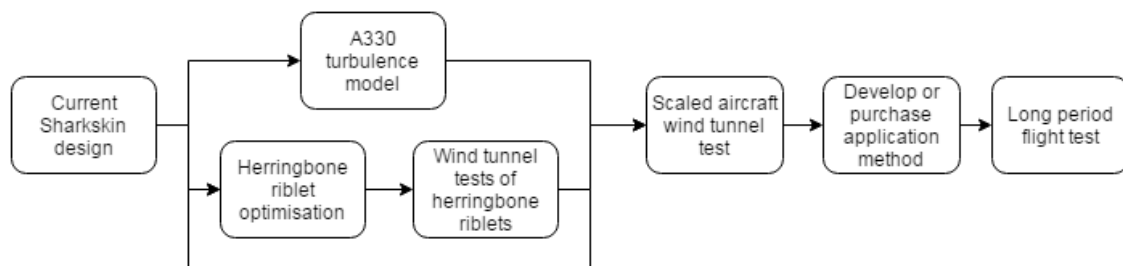


Figure 5.5: Further development of the sharkskin.

5.1.5. Certification

After a full aircraft test of each concept, it can be certified. Aircraft certification can be a long and tedious process. At the base of certification are the test data gathered during all component tests. Eventually, when all concepts are fully developed, their combination can be tested to validate the requirement of 7.5% reduction in fuel consumption and 6.5% in perceived noise of the total retrofit package. Figure 5.6 shows the flight phases covered in such a test mission.

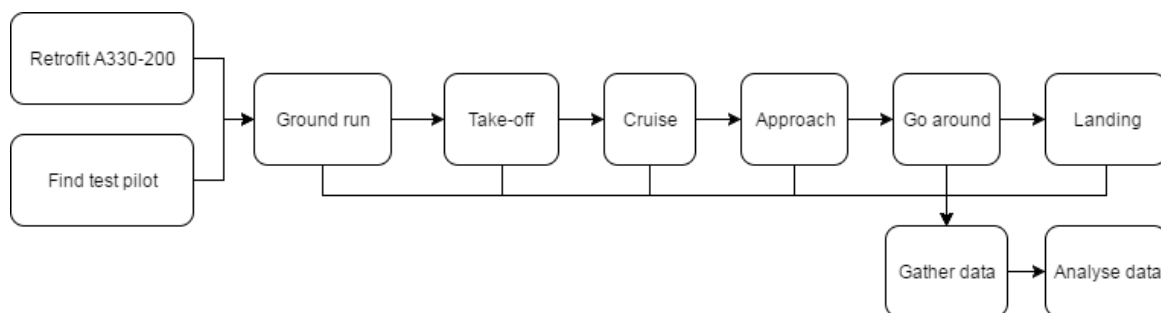


Figure 5.6: Stages in flight tested during a test flight.

¹Private communication, Amber Van Hauwermeiren [19 May 2017 10:00].

5.1.6. Release

The final two steps in the development are production and retrofit or, equivalently, release of the product. Once each component is certified, it can be produced on a larger scale in accordance with the production plan of the concept. For a detailed production plan the reader is referred to Section 5.3.

5.2. Project Gantt Chart

Now that the design development logic is known from Section 5.1, a Gantt chart can be constructed to get an idea of the expected release date of the Smart Retrofit Wing and all the work that needs to be performed during this time. Figure 5.7 shows this Gantt chart, from which it can be concluded that, while the first component of the Smart Retrofit Wing is expected to be released in March 2019, the total combination of concepts will not be released until February 2021. Note that all products are developed simultaneously and the release of one product is not limited by the design stage of the other. In terms of future planning and budgets, this means that some concept development can be funded from the sales of another concept. Another key note here is that sharkskin could be released earlier as a less optimised design, and its sales could fund its own development.

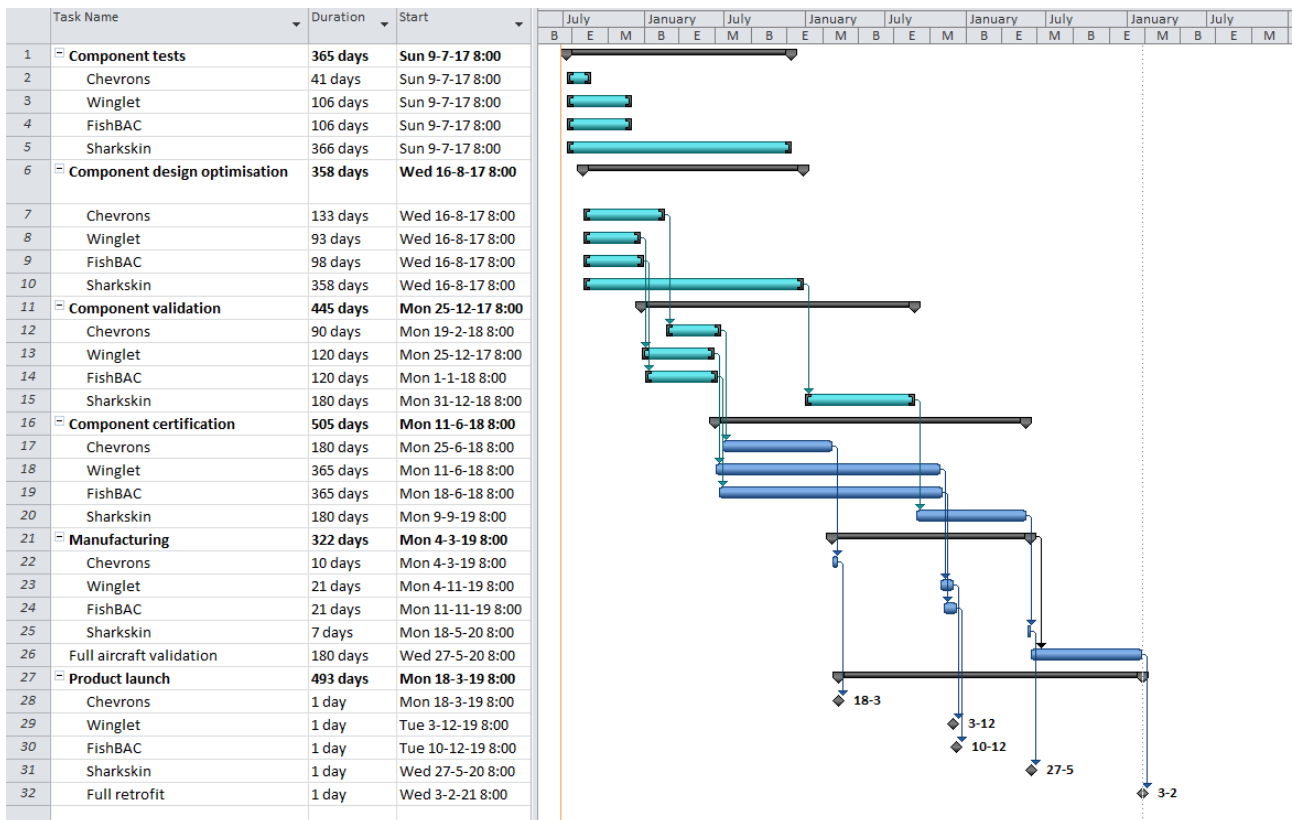


Figure 5.7: General planning of the future development of the Smart Retrofit Wing.

5.3. Production Plan

With the final aircraft and wing configuration known, it is essential to start establishing a production plan and return-on-investment analysis. The production plan for each concept is documented, which covers the assembly and integration process of each individual design. Each production plan will follow roughly the same structure. First the manufacturing process will be illustrated, after which the assembly process will be discussed. Finally, the integration plan will be examined.

5.3.1. Chevrons

As the process of retrofitting the chevrons to the Airbus A330 is not as elaborate as for other concepts (e.g. the LE suction system), the manufacturing, assembly and integration (MAI) plan is relatively simple. In [25] it is mentioned at the end of the article that the main challenge remaining for the use of NiTiNol for aerospace related purposes are the production methods. These were still inefficient and costly. Because this article is over ten years old, the team got in contact with Mr. Mabe, who co-wrote the article, to get an update on the current state of affairs regarding NiTiNol production. It was learned that not only the production was troublesome, but also the supply chain, design allowables and certification². All of these troubles will be discussed here. First, the production methods and the supply chain

²Private communication, Jim Mabe [1 June 2017 10:00].

will be discussed. For a summary of the possible production methods of NiTiInol for shape memory applications, the reader is advised to read Appendix A of the baseline report [1] and the manufacturing and processing review that was found during literature review [78]. In the former, it was concluded that though production is difficult, there are enough promising techniques available.

For the production of the Boeing test models, a vacuum arc melting technique was used which was followed by hot rolling. Then, by use of electrical discharge machining, the plates were made. Finally, threads were cut out for the fasteners. Boeing also performed large-scale testing of a variation on vacuum induction melting, using cold drawn tubes. Both of these are promising and there seemed to be no clear differences in performance³. Because these two production methods are tried and tested, there is enough confidence that test pieces will be able to be made for test flights, and later connections can be made to start a full-scale production program for the NiTiInol plates.

Regarding the supply chain: as it stands, most of the NiTiInol available on the market comes in the form of wires. These NiTiInol wires are used not only for medical purposes, but also for, for example, magic tricks. The memory feature of the alloy (the fact that it can restore its previous state when heated) is a nice party trick. There is, however, no readily available supplier for NiTiInol in the form required for the production methods mentioned before. Therefore a company such as Memry, an SAES company, has to be contacted for production, although they are specialised in NiTiInol for the medical sector⁴.

Component Manufacturing

The chevrons consist of several components that are essential for its design. The four main components are the NiTiInol plates, the carbon composite substrate, the wiring and the thrust-reverser sleeve. The thrust-reverser sleeve will be made of the same material as the original sleeve, which is a fibreglass composite [21]. To increase the structural rigidity of the sleeve, the chevron and thrust-reverser sleeve are made from one sheet, which means area is removed to obtain the triangle-like shape of the chevrons. When the sleeve with chevrons is formed according to the standard procedure, the NiTiInol plates, the carbon composite and the wiring can be added during the assembly process.

Assembly

First of all, the rear has to be removed from the thrust-reverser sleeve. When all components are either manufactured or bought from a third party, the variable geometry actuation system can be assembled. This means that the carbon composite substrate and the NiTiInol plates have to be attached to the chevron by means of attach fasteners. Afterwards, wiring to each NiTiInol actuator has to be established and guided in such a way that the fibreglass covers can be attached on sliding mechanisms to allow for a smooth airflow and protect the fragile components. The thrust-reverser sleeve with all the necessary components can then be attached back onto the nacelle, after which the integration of the wiring has to take place. A visualisation of the assembly process can be found in Figure 5.8.

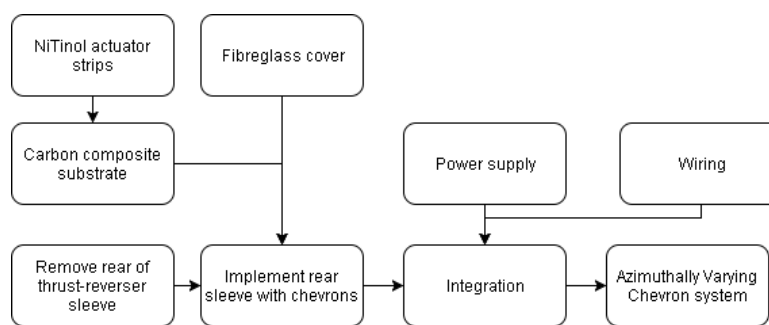


Figure 5.8: Visualisation of the assembly process for AVC.

Integration

The integration of the chevrons is relatively simple, as the only component that is in contact with other sections of the wing is the wiring. After the chevrons and the thrust-reverser sleeve have been re-attached to the nacelle, the wiring has to be guided to the power supply and an additional wire has to be installed that connects the power supply to the cockpit.

5.3.2. Winglets

In this subsection the MAI plan is presented for the morphing winglet. First, a description of the component manufacturing process is presented, then the assembly process is described and finally the integration plan will be elaborated upon.

³Private communication, Jim Mabe [1 June 2017 10:00].

⁴URL <http://memry.com> [cited 12 June 2017].

Component Manufacturing

One of the drawbacks of the use of composite materials in structural components is the manufacturing process. This process is quite expensive and time-consuming. The process has multiple separate steps. The upper and lower skin, made of carbon-fibre composite, are manually laid. The leading edge and trailing edge made of aluminium are produced according to the standard procedure. After producing all the components, they need to be fastened together. Nomex honeycomb consists of phenolic resin-impregnated aramid paper. The honeycomb Nomex paper is dipped in a phenoloc resin to give the Nomex honeycomb high strength. The production is highly automated: presses, dip tanks, ovens and honeycomb saws are used⁵. The Nomex honeycomb can be bought and does not necessarily need to be made in-house.

Assembly

The assembly of the winglet retrofit occurs in two separate work modules, which run simultaneously on different sections of the wing. The first of the two sections concerns the strengthening of the wingbox near the root, in order to cope with the increased loading. The second branch is focused on the installation of the new wingtip extension with break-pin system. Before installing the extended wingtip, the current winglet of the A330 has to be removed. The wing is designed in such a way that the removal of a winglet is not complicated. The winglet is attached with bolts and can be removed without damaging either the main wing or the winglet⁶. Onto the main wing a hinge system needs to be installed, including an extension on the bottom side of the wingbox to hold the break-pin system in place and springs to attenuate the impact of the morphing winglet during breaking of the pin. This system is described in Section 3.3. A graphical representation of the assembly flow can be found in Figure 5.9.

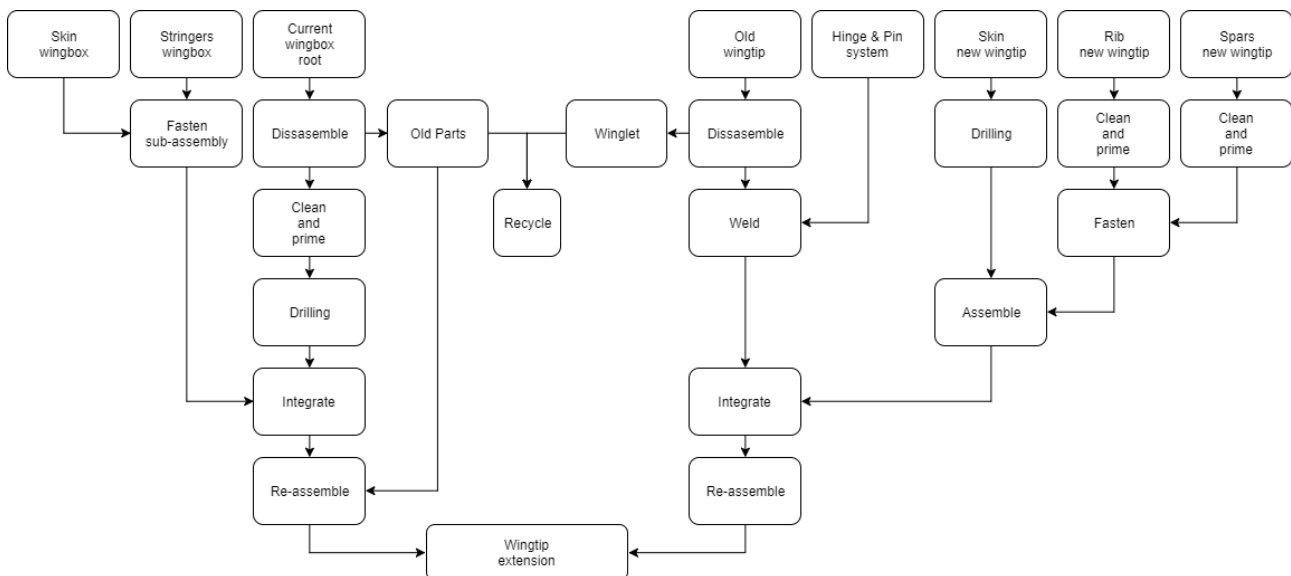


Figure 5.9: Visualisation of the assembly process for the wingtip extension.

Integration

The integration of the new winglet into the current main wing is relatively simple. Since the morphing of the winglet is done entirely passively, no actuation system needs to be installed into the wing. The break-pin system is entirely passive and in occurrence of a flight in which the pin has broken, the pin simply needs to be replaced once the aircraft is on the ground again. Furthermore, since the system is entirely passive, no alterations need to be made to the cockpit systems as the pilot has no interaction with the winglet morphing system.

5.3.3. FishBAC

The FishBAC system consists of several components, each having different interactions with other components. It is important that all of these interactions are appropriately identified and accounted for: this is the main goal of this MAI plan. The following main components of the FishBAC were identified:

- centre beam,
- stringers,
- tendons,
- skin,
- actuation,

⁵URL <https://www.euro-composites.com/en/wabenproduktion> [cited 24 June 2017].

⁶Private communication, Hans Poelgeest [19 June 2017 14:00].

- tip and
- reinforcing skin strips.

In the subsequent sections, manufacturing and assembly of these components will be discussed, followed by the final integration of the FishBAC into the wing.

Component Manufacturing

Both the centre beam and the stringers will be made from CF/PPS, a composite material. This material can either be bought as prepreg or constructed through manual lay-up. Although buying prepregs is the more expensive option, manual lay-up comes with a certain amount of waste and an increase in labour hours. Since 18 FishBAC actuation systems are required for a single retrofit, it is decided that buying prepregs is the more favourable option. CF/PPS prepregs can be bought at approximately 50–100 €/m² (56–112 \$/m², US dollars) per ply prepreg⁷. Holes will be drilled in the stringers to guide the tendons, during which care should be taken to avoid delamination. To this end, the edges of the holes shall be reinforced with metal rings. In addition, small holes must be made near the middle of the stringers through which heating wires can be transferred to the front of the FishBAC.

The tendon will be made from dyneema: lightweight high-strength oriented-strand gel that is spun through a spinneret. The skin material that was chosen is polyether-ester block copolymer with 10% glass fibre. The elastomer skin sheets will be produced by an external party using standard techniques, such as for example rolling⁸. Rotary actuators will be bought from an external party as well: to ensure an optimum weight-to-torque ratio, these actuators will have to be tailored to their required performance. The pulley that will guide the tendon and is driven by the rotary actuator should have an appropriate radius: this should be at least the radius of the tendon. These pulley can be bought as an off-the-shelf product. The last two components will both be made from aluminium: the tip of the FishBAC and the reinforcing skin strips. Both can simply be cut from aluminium sheets, a common procedure in aerospace manufacturing. Holes should be drilled in the vertical tip plate, such that the tendon can be anchored behind it.

Assembly

The centre beam and the stringers will be connected by composite welding, during which the thermoplastic resin of the composite is melted, after which the two components can be joined. The centre beam will also be attached to the aluminium tip: this will be done with a combined adhesive and mechanical bonding to ensure sufficient strength. The stringers will be glued to the skin: composites and plastics lend itself relatively well for this type of joining⁹. Both the tendons and the skin have to be attached to the tip. In the first case the tendon will be anchored behind the tip plate in the same way that cables are fixed on bridges, while the skin will be connected to the tip using an adhesive connection. Finally the reinforcing skin strips should be attached to the rest of the skin: here, an adhesive connection will be used as well. Epoxy- or polyurethane adhesives will ensure excellent high-performance bonding for metals, composites and plastics¹⁰. A summary of the FishBAC assembly process is given in Figure 5.10.

Integration

Once the FishBAC has been fully assembled, the only remaining step is integration into the wing. To this end, the currently used Fowler flap will have to be removed first, including its rotary actuation and link-track mechanism. Once this has been done, the FishBAC can be placed. The rotary actuator will be fixed to the rear spar. The rest of the FishBAC will be connected to the wing by 'extending' some of the ribs within the wingbox rearwards: the first stringer of the FishBAC can be connected to these ribs. On the underside of the wing aluminium skin will cover the area in which the rotary actuator is located: this skin runs until the first stringer of the FishBAC, where the elastomer skin starts. At the upper side no skin is required to cover the area of the actuator: here, the presence of the spoilers is already sufficient.

5.3.4. Sharkskin

For the sharkskin there are two possible assembly methods: manual application using pre-fabricated films or automated application by a 3D-printing robot. Although the robot option is most optimal, due to time constraints in its development the option of applying sharkskin by film is also considered as a temporary method. For this reason, manufacturing and integration will be discussed for both options. Note that assembly will not be considered for the sharkskin, since the concept consists of a single material that is applied directly onto the aircraft.

⁷Private communication, Dr. Irene Fernandez-Villegas [16 June 2017 11:00].

⁸URL https://www.jameswalker.biz/de/pdf_docs/148-elastomer-engineering-guide [cited 26 June 2017].

⁹URL <https://multimedia.3m.com/mws/media/12151150/assembly-solutions.pdf> [cited 26 June 2017].

¹⁰URL http://www.huntsman.com/advanced_materials/Media%20Library/global/files/EUR_Aerospace%20-%20Adhesives_Syntactics_Performance_Araldite.pdf [cited 26 June 2017].

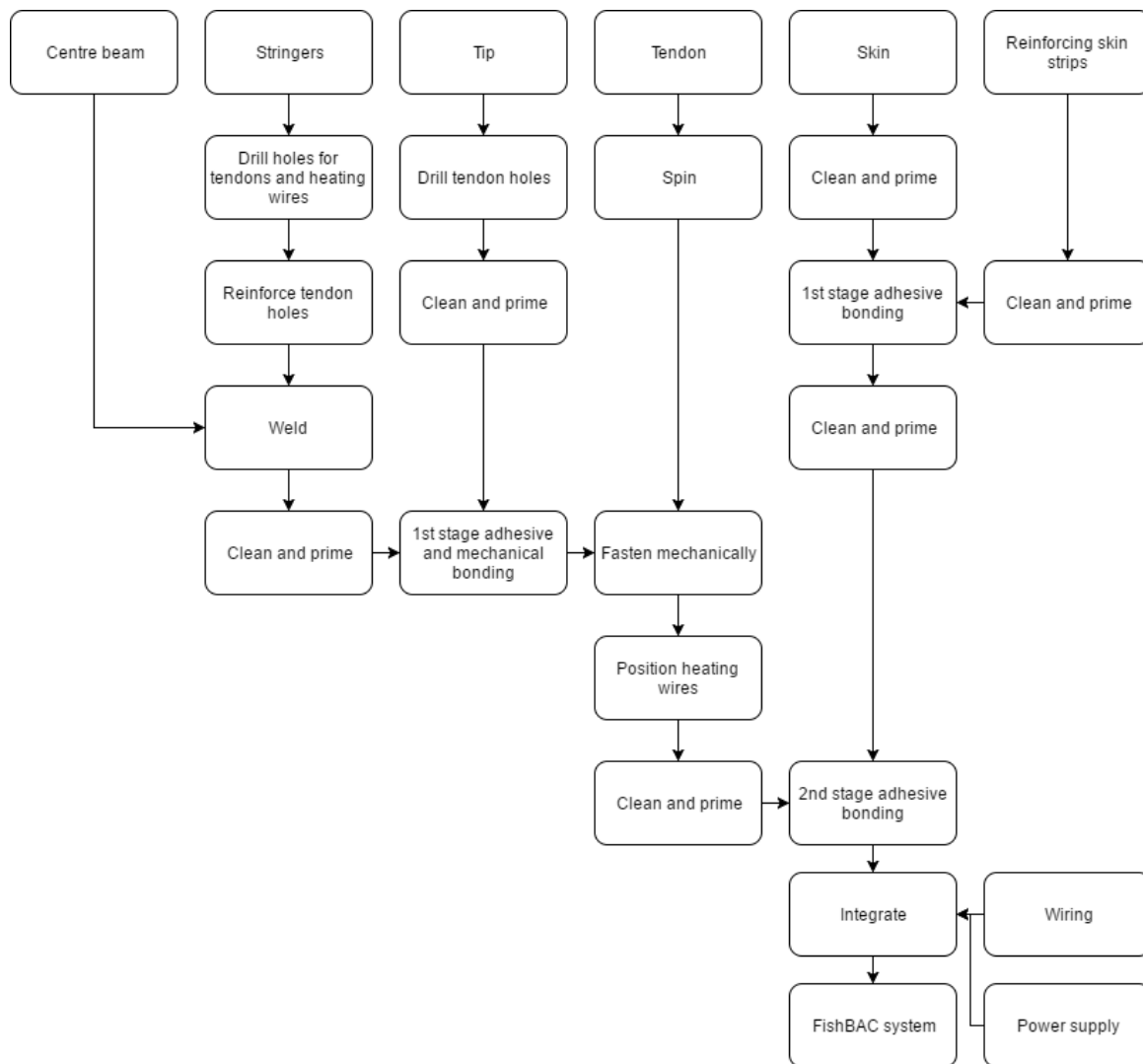


Figure 5.10: Visualisation of the assembly process for the FishBAC.

Component Manufacturing

Film application

The film used for sharkskin application can be bought off-the-shelf. This film does not have the herringbone riblet applied to it, but it is a quick and easy way to get the sharkskin on an aircraft and a possible option for early stages of the retrofit when the automated approach is not finalised yet. The fabrication method of one company that provides sharkskin films (Fraunhofer) is shown in Figure 5.11¹¹. The applicator in Figure 5.11 applies the sharkskin structure to a substrate using a silicone film with a negative sharkskin texture. A feed line adds epoxy to the silicone, after which it is pressed onto the substrate and cured. Within this applicator, an ultra-violet (UV) lamp cures the sharkskin while it is manufactured. By curing the sharkskin under UV light, it becomes UV-stable and improves resistance to erosion, soiling and abrasion. At this point in the development of the application unit, it will roll a square metre per minute¹¹. This is a relatively slow pace, considering the vast amounts of sharkskin required for an aircraft. It implies that the sharkskin will be very expensive to purchase off-the-shelf, since its production time is quite long. Note that, if the silicone film negative is replaced with a different texture, a herringbone riblet can easily be produced with this method.

Automatic application

If an automatic application process is used, the process is very similar to 3D-printing. This implies the machine will need to be extremely precise and it will need to be able to cover large areas within small amounts of time, at very high precision.

¹¹URL http://www.ifam.fraunhofer.de/content/dam/ifam/en/documents/Adhesive_Bonding_Surfaces/Paint_Lacquer_Technology/riblet_en_fraunhofer_ifam.pdf [cited 26 June 2017].

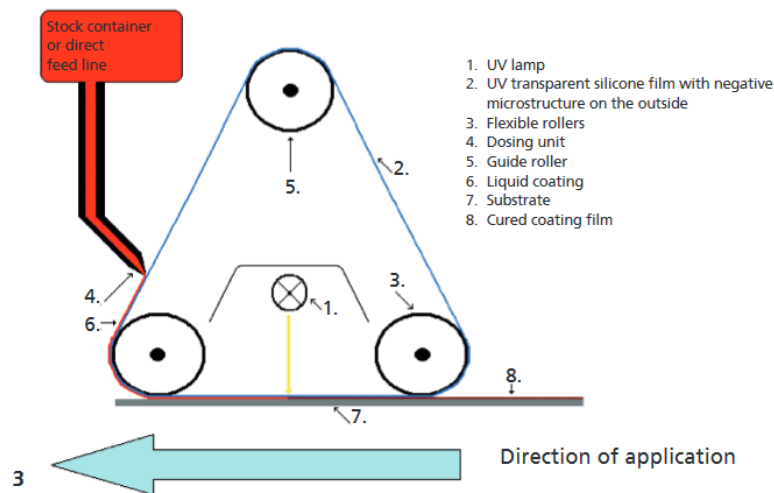


Figure 5.11: Fabrication method of sharkskin film.

Integration

Film application

If the sharkskin is applied to the aircraft as a film, the application will be done manually. Professionals will need to be trained to apply the film in the correct orientation and in the correct way. Additionally, there are always some issues with applying a flat film to a curved surface, which will compromise the performance of the sharkskin and increase the time required for the application process. The possibility of human error also needs to be factored into this process.

Before sharkskin can be applied to the aircraft, the paint layer underneath needs to be prepped. When the sharkskin is applied as a film, it is already (UV-) cured, which means once the sharkskin is on the aircraft, the application process is finished.

Automated application

The automated application process is similar to 3D-printing. The coating is applied while wet but mouldable, and is cured on the aircraft itself. While an automated process implies no human error or man hours are involved in the process, the added curing time means there is still a lot of time involved. It is assumed that sufficient machines are used such that the total, automated application of the sharkskin does not exceed that of manual application with films.

The integration process of the sharkskin provides a good set of characteristics that the machine that applies it should have. To keep prices low, the machine needs to be fast, preferably faster than 1 m² per minute. The actual application piece of the machine needs to be durable, such that it does not need to be replaced during a retrofit. The machine should be precise enough to print a 0.3 mm high structure in the correct orientation in a proper, continuous shape, with a maximum deviation of less than 0.001 mm. The machine should include a UV lamp to cure the sharkskin after it is printed. Finally, the machine would preferably also be able to remove the sharkskin. This implies that when the sharkskin is reapplied while the underlying paint is still in good condition, only the top coat can be removed instead of the entire paint layer. This will reduce the amount of man hours spent on the concept drastically, and might even reduce the costs the airline spends on paint, as the underlying paint layer does not have to be replaced when the top coat is replaced. Ideally, the painting interval of the aircraft will be longer than the current five years, which would be an additional commercial benefit of sharkskin.

5.3.5. Leading Edge Suction

As the suction system has a significant amount of components that must be installed, it is essential to properly plan the assembly and integration process. First the production of the single components will be discussed, after which the assembly process will be elaborated upon. In the last step of the production plan, the integration process of the suction system will be clarified.

Component Manufacturing

The three main components of the LE suction system are the leading edge, the Krueger flap and the pump system, the last two of which are both integrated into the new leading edge. The leading edge consists of an outer skin, stringers and an inner skin. The stringers have to be machined and formed, whereas the skin requires perforation, flattening, preforming and hot sizing [64]. The Krueger flap can be made conform the usual procedure, whereas the rib reinforcements have to be machined from aluminium and titanium. The hinge, drive link and drive arm have to be machined from heat-treated high-strength steel in order to cope with the significant loads. The ducts and valves have to be manufactured specifically for this aircraft, as the inner wing layout will slightly differ from other aircraft. These ducts and

valves can be machined from aluminium, as the pressure and temperature will not be significant enough to have an impact on the material. The pressurisation pump has to be acquired from a third party, as building the pump would be inefficient in terms of cost and benefit. Finally, a new engine strut fairing has to be machined using conventional aeroplane techniques, to locate the anti-ice system and various other components.

Assembly

As it is known what components the suction system consists of, it is possible to create an assembly plan. First of all the skin and stringers have to be attached to form the new leading edge. They will be bonded in a two-stage process using a modified epoxy adhesive, where first the stringers will be bonded to the outer skin and secondly the inner skin will be bonded to the stringers. Proper preparation is necessary, in order to create a clean and smooth bonding with no adhesive voids. After the stringers and skins have been assembled, the additional drilled rib chords can be installed to the suction panel by simple fasteners and by making use of a castable epoxy shim to ensure the closest possible fit [64]. Once the rib chords have been put in, the Krueger flap actuators can be installed into the new leading edge, after which the Krueger flap can be attached.

Integration

Another component that has to be installed is the suction system, which consists of the pump, the heat exchanger, ducts, valves and other subsystem components. The ducts and valves have to be guided through the rib holes to the suction panels on the leading edge. After the turbocompressor, ducts and valves have been installed, the new leading edge can be attached to the wing by again using a castable shim. A release agent was applied to allow future disassembly, whereas lastly close-tolerance high-strength shallow-head bolts were installed to complete the joint [64]. A visualisation of the assembly process can be found in Figure 5.12. As can be seen in this figure, some components of the assembly can be done simultaneously, whereas other components can only be placed after other parts have been assembled. For example, the duct and valves can be placed in the existing leading edge section at the same time that the skin and stringer assembly takes place.

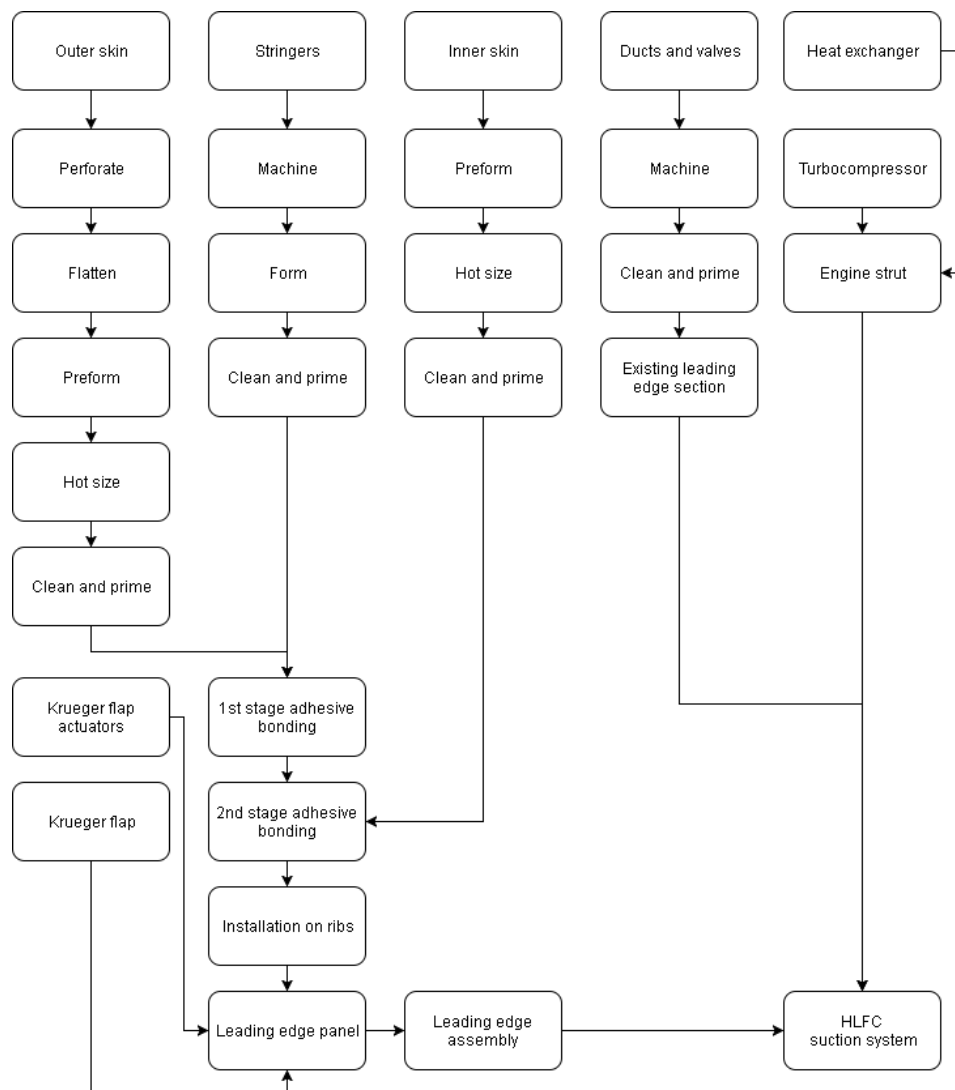


Figure 5.12: Visualisation of the assembly process for the LE suction system.

5.4. Cost Breakdown Structure

In Figure 5.13, the cost breakdown structure (CBS) can be found. The CBS shows all the expected cost elements from this stage of the design to the production. This is split into four components, Manufacturing, Design Continuation, Operations and Logistics and Financing.

First of all, manufacturing consists out of everything related to getting the final product made. This includes supply chain management, which consists of materials for in-house production, and of components produced out of house. Under manufacturing also everything related to the factory itself is listed. This not only includes the acquisition of the factory ground and the factory construction, but it also includes the upkeep of the factory and the acquisition and upkeep of the equipment.

The second subtree is the Design Continuation subtree. This tree consists of all costs which are needed before the concept can be produced. These are costs for optimising the aerodynamic model, possibly by hiring more fluid dynamics engineers or by wind tunnel testing, it includes structural tests, finalisation of the integration, possibly by acquiring or leasing an A330 for close inspection, and it includes certification. Certification on its own consists out of a flight test and certification of the production process for aerospace applications.

The third subtree is the Operations and Logistics subtree. This tree consists of advertisements and salary of the employees. Advertisement is vital for any new company with a new concept in order to succeed. This could include costs such as space on trade exhibitions, or even lobbying.

The final subtree, Financing, is related to all costs relating to financing or bookkeeping. These are interests on possible loans, dividends to possible investors and depreciation of equipment.

5.5. Return on Investment

To sell a product it is very important to have a good business case. In this section, such a case is investigated and the potential profits for both BEAU-wing and the customers are calculated.

5.5.1. Return on Investment BEAU-wing

The initial investment of the company consists of the development and production costs, which have to be earned back by generating revenue from the sold retrofit products. Note that the production costs include the costs of the retrofitting process. The highest costs will most likely be the development costs, which are the hardest to estimate.

With 1,312 A330s in operation today, the market consists of roughly 500 aircraft, as the rest is older than 15 years [1]. From the B737 Blended Winglet retrofit it was found that approximately 50% of all winglet-less 737 were retrofitted¹². If this is assumed to be the same for this particular retrofit, roughly 250 retrofits will be sold. Here it is neglected that this technology might be applicable to other aircraft and even to other fields. With an estimated profit margin of 15% (based on Boeing averages¹³), the total product cost can be broken down. This is shown in Equation (5.1).

$$\text{Product cost} = \left(\text{Production} + \frac{\text{Development}}{\text{No. sold}} \right) \cdot \text{Profit margin} \quad (5.1)$$

In Table 5.1, the estimated costs for each retrofit that will be applied can be found.

Table 5.1: Cost breakdown of the separate retrofit concepts.

	Chevrons	Winglet	FishBAC	Sharkskin	Total
Development costs	\$4,800,000	\$13,215,000	\$24,440,000	\$9,620,000	\$47,275,000
Production costs	\$810,000	\$2,205,000	\$1,437,500	\$1,000,000	\$4,642,500
Product cost	\$953,580	\$2,596,539	\$1,765,549	\$1,194,252	\$5,556,340

Assuming that only full packages will be sold, the break-even point can easily be calculated according to Equation (5.2).

$$\text{Break-even point} = \frac{\text{Development}}{\text{Profit per product}} = \frac{\$47,275,000}{\$5,556,340 - \$4,642,500} = 52 \text{ products} \quad (5.2)$$

This means that after 26 retrofits the development costs will be paid back and from this point on the revenue will be profit for the company (i.e. the return on investment will be positive from this point in time). If all the expected 250 aircraft will be retrofitted, the final return on investment can be calculated, as shown in Equation (5.3).

¹²URL http://www.aviationpartnersboeing.com/about_history.php [cited 27 June 2017].

¹³URL <https://www.stock-analysis-on.net/NYSE/Company/Boeing-Co/Ratios/Profitability#Gross-Profit-Margin> [cited 27 June 2017].

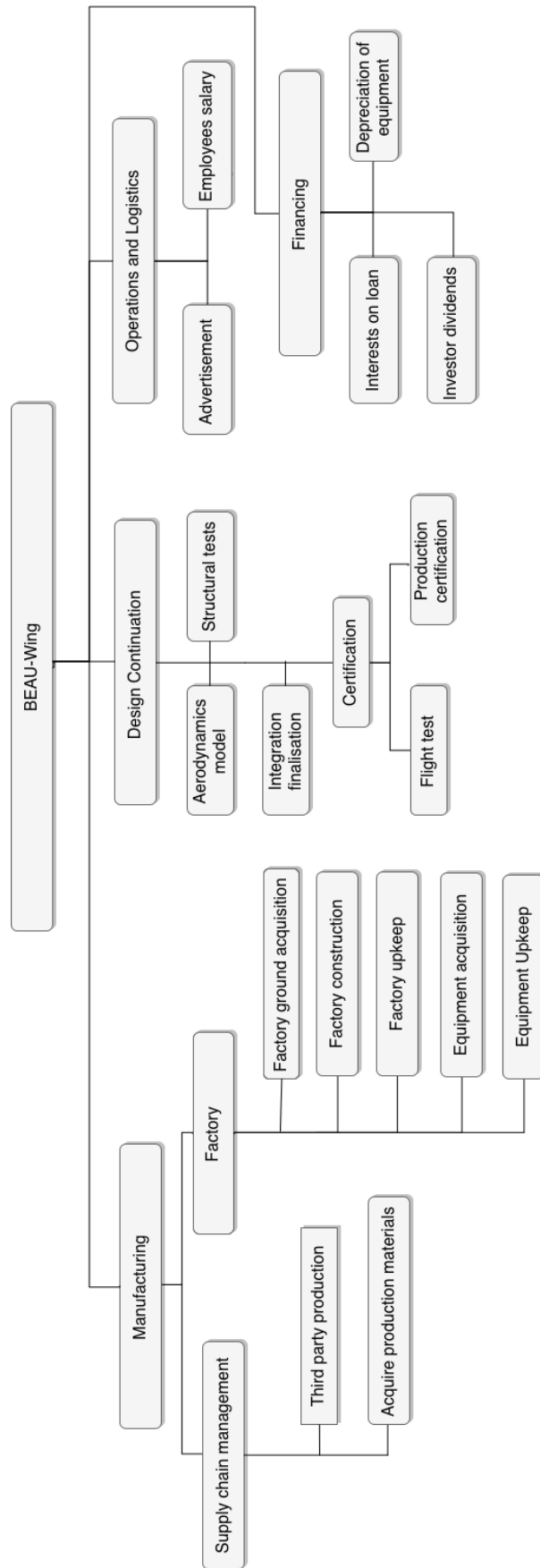


Figure 5.13: Cost Breakdown Structure.

$$\text{Return on investment} = \frac{\text{Income}}{\text{Investment}} = \frac{250 \cdot (\$5,556,340 - \$4,642,500)}{\$47,275,000} = 4.83 \quad (5.3)$$

This result shows that the initial investment will be earned back almost tenfold. Note that this is a very optimistic value, since costs like development costs are usually underestimated and some airlines might not go for the full package, giving BEAU-wing less revenue. Nonetheless, with such a high estimated return of investment, it is safe to say that this product will be profitable for BEAU-wing.

5.5.2. Return on Investment Customer

For a customer the main costs will be the list price and the downtime costs. These costs will be paid back due to the decrease in operational costs. The operational costs that are reduced mainly consist of the fuel reduction and lower noise prices. Again, it is assumed that an airline purchases the complete retrofit package and not just specific components. This means an airline will achieve maximum fuel savings while also falling within a lower noise category, as was concluded in Section 4.2.1.

A total of 4,115 kg fuel is saved every mission, as taken from Section 4.2.1. With the current Jet A-1 fuel price of \$1.354 per litre¹⁴, this fuel reduction comes down to a saving of \$1,810.80 per flight. Regarding the noise level savings, the fact that the aircraft will be in a lower noise class reduces the take-off and landing costs per flight with 20%. As a test case, a daytime landing and nighttime take-off at Schiphol airport will be considered. For a noise category B aircraft (current A330), the costs are \$4.23 and \$6.35 per 1,000 kg for landing and take-off respectively. For a noise category C aircraft (retrofitted A330), these are \$3.38 and \$5.08 [68]. With these costs known, it is possible to calculate the total landing and take-off cost savings per flight. This calculation is shown in Equation (5.4).

$$(\$4.23 - \$3.38) \cdot \frac{\text{MLW}}{1,000} + (\$6.35 - \$5.08) \cdot \frac{\text{MTOW}}{1,000} = \$153 + \$292 = \$445 \quad (5.4)$$

Here, MLW stands for the maximum landing weight and MTOW is the maximum take-off weight. This means that every flight a total of \$2,255.8 will be saved. The additional downtime cost for a full retrofit package, however, will be \$435,400. This value was obtained by assuming that the FishBAC, chevrons and winglets will be installed simultaneously during a C-check in low season. Sharkskin will in this case be applied by machines every two years. As the total product cost is known to be \$5,556,340 for the full package, the break-even point can readily be calculated. The calculation of the break even point for the customer can be found in Equation (5.5).

$$\text{Break-even point} = \frac{\text{Investment}}{\text{Savings per flight}} = \frac{\$5,556,340 + \$435,400}{\$2,255.8} = 2657 \text{ flights} \quad (5.5)$$

It is assumed that the reference mission used to calculate the fuel improvements is flown 2.5 times a day, since per flight the total flight time plus turn around time is 9.5 hours [1]. This means that the time to reach the break-even point equals 1,063 days, which is equivalent to 2 years and 11 months. With an average expected lifetime of 15 years left at the time an A330 is retrofitted [1], the return on investment for the customer can be calculated, as is shown in Equation (5.6).

$$\text{Return on investment} = \frac{\text{Savings}}{\text{Investment}} = \frac{15 \cdot 365 \cdot 2.5 \cdot \$2,255.8}{\$5,556,340 + \$435,400} = 5.15 \quad (5.6)$$

To conclude, in the case that an airline purchases a full package on an aircraft with 15 years of lifetime left, a return of investment of 5.15 will be achieved. This will be different for other packages, however, a return of investment of this magnitude indicates that purchasing the full retrofit package will most certainly be profitable in the long term.

¹⁴URL <http://www.iata.org/publications/economics/fuel-monitor/Pages/price-analysis.aspx> [cited 27 June 2017].

Conclusion

Henry Petroski once said that "*Successful design is not the achievement of perfection, but the minimisation and accommodation of imperfection*". This idea was crucial for this report, as every retrofit comes with its own advantages and disadvantages. It was the task of the design team to overcome these obstacles and fulfil the requirements.

The design of the retrofit was driven by the requirements set in the midterm report [2]. Here, the most important requirements stated that the system should be retrofitted to the Airbus A330 and that it should reduce the fuel consumption of the aircraft by at least 7.5% per passenger kilometre. Two requirements stated that the CO₂ emission should be reduced by 7.5% and NO_x by 9.0%, which are in line with the ACARE goals. In the midterm report, five concepts were chosen in order to meet these requirements.

Knowing the requirements, and hence the task ahead, first an analysis was conducted to check whether or not there is a place in the market for this retrofit. A total of 539 A330 aircraft were found to be in operation, of which 167 are operational in Europe and 185 in the Asia-Pacific region. Other than the A330-200, it was also decided to offer the retrofit to the rest of the A330 family, provided that some changes are made to the design results. This would increase the market to 1,228 aircraft. Finally, it was checked whether other markets could be identified as possible customers. It was found that the market regarding other aircraft besides the A330 might be worth retrofitting for as well. Not all retrofits will fit all aircraft however, as for example the 747 has triple-slotted flaps, which means most likely a FishBAC flap retrofit will be unfeasible. The automotive sector was also investigated, as other vehicles besides aircraft can also benefit from FishBAC technology for active aerodynamics or from the sharkskin coating for its drag decrease.

The first concept to be discussed here are the Variable Geometry Chevrons. With VGCs that azimuthally vary the exhaust noise can be decreased. This works by enhancing the mixing of the hot, turbulent exhaust air with the colder fan air. Because of this mixing, a slight performance penalty will be present; a loss of thrust specific fuel consumption of up to 0.25% [16]. Therefore, the VGCs will only be used during take-off, as in this phase the noise regulations are most strict. The VGCs can be turned off by using a shape memory alloy, namely NiTiInol. By heating NiTiInol, it can change its form. Therefore, it will be produced in such a manner that, when heated, the chevrons bend into the flow, and when it gets cooled down mid-flight, the chevrons bend out of the flow. With this technology, a noise reduction of 2 dB was predicted. This prediction can be improved by scaling the data found in literature to the engine size of the A330, but this was deemed too in-depth for this report. Other than a noise reduction, chevrons also come with a weight penalty of 63 kg and an expected production cost of \$810,000. Structurally, no reinforcements will be needed. Integration will also be straight forward, as the current thrust-reverser sleeve can be replaced by the new one, using the same connection points and mechanisms.

The next concept to be discussed are the winglets. For the winglets, an optimal, static (non-morphing) design was obtained from Tornado, a VLM-based program. The extended winglet spans 3.5 meter beyond the edge of the wing and has a taper ratio of 0.4. The obtained induced drag improvement with the extended wingtip amounts to 8.4%. As mentioned in the first sentence of the conclusion, all good things come at a price. From structural analysis it was found that the winglet span increase of roughly 2 meter per winglet increases the wing bending moment on the wing root by approximately 6-9%. This additional loading adds weight to the structure, as reinforcements will be necessary in order to cope with the higher loads. In order to keep the additional weight and effort of strengthening the wingbox to a minimum, whilst at the same time maximising the performance gains from the retrofit, a 'cant morphing' extended wingtip with break-pin was selected as an optimal solution. The break-pin release system allows the extended wingtip to snap out of the extended position into a lower load position, the 0° cant angle position. The cant morphing design ensures the aircraft takes advantage of the increased efficiency of the extended wingspan design during cruise, whilst not carrying the full penalty of structural strengthening for ultimate loads. These ultimate loads occur so infrequently that the inconvenience of replacing a break pin is more than justified for. After activation of the break pin system and thus putting the wingtip in a 0° cant angle, the root loads are decreased by about 5-7%. The materials selected for the various components of the extended wingtip retrofit are largely based on the Boeing 737 blended winglet retrofit design. In a similar manner, the configuration gained inspiration from the aforementioned retrofit. The total extended wingtip costs, in this context meaning the wingtip component cost, the retrofit process cost and the downtime cost, sum up to approximately \$2.3M. It should be noted that the cost estimation model is based on rough first order estimations and thus only provides an indication of the specific retrofit cost.

The third design is related to the FishBAC concept that will replace the current flaps. Because its main purpose is to efficiently replace the flaps, first a 2D aerofoil analysis was performed to make sure it could reach the same aero-

dynamic performances, i.e. $C_{l_{max}}$ should not be compromised. This was done using Javafoil, a program based on a second-order panel method. By evaluating the integrated morphing trailing edge, a maximum decrease of 0.02 in C_d and an increase of 0.3 in C_l could be found. Another advantage of the FishBAC over the original flap system, is that the flap fairings can be taken off. This alone leads to a drag decrease of roughly 1,220 N in cruise and 376 N in approach. Before this concept could be constructed however, the structures and materials had to be investigated. The FishBAC consists out of three main components: the inner structure, the skin and the tendon. For the inner structure, CP/PPS was chosen as the appropriate material, due to its low glass transition temperature and high tensile yield strength. For the outer skin, polyether-ester block copolymer with 10% glass fibre was chosen. In this case due to its excellent fatigue behaviour and operating temperature range. Finally, for the tendon, Dyneema was chosen. This is a lightweight high-strength oriented-strand gel spun through a spinneret. Overall, a performance increase of 0.92% can be realised, with a product cost of \$427k.

The next concept is a bio-inspired coating, the sharkskin. For the sharkskin, three options for riblet geometries were available: blade, scalloped and sawtooth. These have a respectively decreasing maximum drag reduction, but increasing durability. Because of this trade-off, the scalloped geometry was chosen. This will be used in combination with herringbone riblets, which is based on the feathers of birds. Eventually, the scalloped riblets will be placed in a herringbone V-shape, leading to a total drag decrease of 7.56%. The sharkskin will be made out of epoxy, which needs to be replaced every two years. This interval might be stretched out by mixing the epoxy with other materials, such as carbon- or glass fibres, however not enough research has been conducted to give a proper conclusion. For the application of the epoxy an automatic applicator can be used, which would cost \$100,000 per application.

Finally, the leading edge suction system will be discussed. LE suction works by sucking the air from the top of the leading edge into the airframe, such that this boundary layer can be re-energised and the laminar-turbulent transition point moves backwards. This is done by placing a pump in the undercarriage of the aircraft, which is connected by aluminium tubing to the leading edge. This leading edge is made out of a perforated titanium skin, through which air can be sucked. To find the optimal solution, four different setups were investigated. The first one has LE suction from the root to the engine pylon, the second from the root to half the wing, the third from the root to three-quarter of the wing and the fourth from the root until where the winglet starts. Here, it was found that these concepts lead to a drag reduction of 545 N, 1,148 N, 1,751 N and 2,190 N, respectively. One of the problems with LE suction is that during take-off and approach the holes could get covered by icing and bugs. To solve this problem, the A330 slats would have to be replaced by Krueger flaps, which will be deployed during take-off and approach. It was found that by using a non-morphing Krueger flap, the weight of the leading edge high lift devices could be decreased, with a negligible effect on noise and no compromises regarding lift and flight envelope. Because tubing is required, and because the new leading edge will be made out of titanium instead of aluminium, the overall weight did increase by a significant amount. For the four setups the added weight was found to be 443.2 kg, 972.8 kg, 1,450.1 kg and 1,996.4 kg respectively. Another disadvantage of LE suction is the required pump power, which ranges from 3,000 W to 30,000 W for the setups. Therefore, a new gearbox and generator will have to be installed, increasing the costs. Eventually, for the concepts, it was found that the first setup would decrease the fuel consumption over the reference mission profile by 0.4 kg. Therefore, it was decided to remove LE suction from the retrofit package.

A production cost of \$4,642,500.00 was found for the total package. To have sufficient profit margin, it was decided that the price the customer would have to pay for the complete package will be \$55,556,340. With this price, a break-even point will be reached after selling 52 retrofit packages in order to cover for the development costs of \$47,275,00. As it was estimated that 250 A330s would be retrofitted, 198 aircraft will remain to turn a profit.

Once all the concepts, their price and their consequences are known, the full aircraft analysis can be done. It was found that, by using the FishBAC, new winglets, sharkskin and chevrons, the fuel consumption could be decreased by 4,115 kg. This is for a reference mission, with a cruise time of 7.5 hours at Mach 0.82, as specified in the baseline[1]. This decrease in fuel consumption corresponds to a total fuel reduction of 10.7%.

In the case of the noise requirement, 6.5% on the decibel scale was required. Because this requirement was very hard to formulate quantitatively, the requirement became to get the aircraft 18 dB below the ICAO chapter 3 and 4 requirements, as it gets a 20 percent decrease in take-off charges [68] when it meets this requirement. The current A330 is already 14 dB below the ICAO chapter 3 and 4 requirements, which meant a 4 dB reduction is required. This is expected to be achieved, due to not only the chevrons, but also the other concepts. First of all, there will also be a noise reduction due to a lower required thrust setting and lower take-off speed. This should not be underestimated, as airframe noise scales with velocity to the power of 6 and jet exhaust noise with thrust to the power of 8. The thrust now required, to take off with the same field length, is 6.5% less than the non-retrofitted aircraft. The noise will also decrease due to the fact that the FishBAC covers up gaps that were previously there due to the flaps. Therefore, it is expected that the 4 dB reduction needed for the A330 to get into a lower noise category will be achieved. This will have to be validated with a flight test, but with the data available there is enough proof to make this assumption and carry it over to the return on investment.

For the customer, after purchasing the complete retrofit package for \$5,556,340, it would take 2 years and 11 months to reach break-even. If the airline flies with the retrofit for 15 years, they will have this cost paid back 5.15 times.

To conclude, not all requirements were met. The requirement on noise reduction was not quantifiable and was reworded. The engineering budget of the aircraft increased as mass was added, although the noise was reduced. Other requirements, however, were met with flying colours, such as the fuel consumption and the life time of the retrofit. Therefore, the retrofit is a viable option for any serious airline.

Recommendations

In Chapters 3 and 4, several aspects have already been mentioned that could be improved in further development of the Smart Retrofit Wing. While a detailed design and elaborate testing of the design are an obvious requirement before the Smart Retrofit Wing can be produced, some concepts and design options were discarded during the preliminary design that still have potential. If some conditions change with time these concepts and design options might prove to be very well suited for retrofitting, which means they should not be forgotten. Finally, due to the time constraints of the DSE, not all design models were as detailed as preferred. Before further design is considered, the simplifications in these models should be addressed and recommended improvements should be presented. The most important recommendations for further development of the Smart Retrofit Wing are presented below, organised per concept.

Chevrans

- **Noise reduction mechanism.** The noise reduction mechanism of chevrons is not yet being fully understood. While noise is a complex phenomenon, there are some models that can render an approximation of the expected noise benefits of chevrons.
- **Basic jet engine noise reduction.** There are two methods to assess basic engine noise reduction. Firstly, test values can be scaled to the engines used in the A330-223 [15, 16]. A second option would be a flight test.
- **Geometry optimisation.** When flight tests are conducted, different shapes of chevrons can be considered to find an optimum.
- **Noise testing.** Noise behaviour is dependent on many uncontrollable factors, such as weather conditions, which means any results obtained by future testing need to be normalised.
- **Material selection.** Although the selected materials are appropriate for their purpose, in the future other light-weight alloys might be invented that are also suitable for this specific load case. Therefore, different materials could be used in a future design, such that the additional weight due to the chevrons will be reduced. The carbon-fibre composite could be replaced by a stiffer and lighter material, whereas the glass-fibre should be replaced by an equally flexible yet strong material.
- **Attachment NiTiNol plates.** In the section on chevrons, the attachment of the NiTiNol plates on the chevrons were briefly discussed. Before it can actually go into production, this will have to be validated. Even though the NiTiNol plates can never be sucked into the engine, they can still cause on-ground damage.

Winglets

- **Production process.** The extended wingtip will partially consist of carbon-fibre composites. Since the demand for carbon-fibre composites has been rapidly growing, the improvement of the manufacturing process of composite materials has been of interest. New, more efficient, production methods for the carbon-fibre components of the morphing winglet can potentially be used¹.
- **Flexible skin.** Further research needs to be performed on the flexible skin and on how to implement this skin on the main wing and extended wingtip. The idea is to connect the winglet to the wing with a material similar to the skin of the FishBAC, to cover any disruptions the hinge mechanism introduces to the wing.
- **Aerodynamic analysis.** To obtain more reliable and detailed data on the aerodynamics of the winglet, a CFD analysis could be conducted in addition to the Tornado simulations performed so far.
- **FEM analysis.** For this report, the stresses in the wingbox were modelled with a programme based on a lot of assumptions. Before the design is finalised and tests are conducted that are very expensive, a FEM analysis should be executed to get a better idea of the stress distributions in the wingbox.
- **Material selection.** Further analysis will have to be performed to determine the material choice for the wingtip extension and the break-pin system. For the wingtip extension, it has to be decided whether to go for aluminium, or a composite, which can reduce weight. Effects on the structure of the wing, costs and maintainability will have to be taken into account. The break-pin system will have to be rigid and able to withstand high loads, material choice is very important here. The break-pin itself will have to be made of a strong, but relatively brittle system. If the load case occurs in which the break-pin would break, the break-pin must break, it cannot deform, this can cause the system to jam.

¹URL <https://catapult.org.uk/success-stories/speeding-production-winglets> [cited 25 June 2017].

FishBAC

- **Beam deflection approximation.** Due to time constraints, a preliminary design of the FishBAC has been conducted with beam theory: an approximation of small beam deflections of loaded beams. In reality, the deflection of the beam is very large (1.05 m at a flap length of 1.9 m). This means there are a lot of internal stresses that are not considered in the initial design of the FishBAC. Such a system is outside of the scope of the DSE.
- **FEM analysis.** At this point, it is assumed that the skin does not carry any loads except for the stresses from its own stretching. In reality, the skin will carry loads and it must be designed for these loads. Moreover, the sizing of the stringers is also based on this assumption. Therefore, a FEM analysis of the centre beam, skin and stringers is necessary to obtain a more reliable view of the stress distributions in the structure.
- **Heating system.** The report briefly mentions the use of a heating system to deflect the centre beam, but the detailed design and required amount of heat still need to be calculated.
- **Aerodynamic simulation.** For the design of the FishBAC up to this point, Javafoil has been the basis of all aerodynamic analysis. Before a design is finalised, a more exact flow analysis should be conducted. Suggested software for this is MSES, which also allows for analysis of multiple-part aerofoil sections.
- **Actuator design.** For the weight calculation of the actuator for the FishBAC, an extrapolation was used with different actuators. This indicates that an appropriate actuator still needs to be designed.
- **Material selection.** Although the materials currently used in the FishBAC concept are appropriate for its purpose, other better suitable materials might become available in the near future. These materials might be lighter and have better temperature and strain properties and thus must be considered if they are invented in the near future.
- **Structural effects.** The effect the different aerodynamic loads have on the structural integrity of the full aircraft were not discussed in this report. Hence, before the concept can go to the testing phase, this has to be investigated.

Sharkskin

- **Application method.** Some additional research needs to be conducted on whether an automated application method will be favoured by airlines. It is cheaper and more precise, but it halves the maintenance intervals. The total results on the costs of the retrofit need to be investigated further.

Leading Edge Suction

In Section 3.6 it was decided not to go with LE suction for the final retrofit. This can be attributed to a combination of reasons, such as increased in weight, below-par aerodynamic improvement and the required pump power. Still, recommendations will be given for the next stage of the design process of LE suction, should there be a breakthrough improvement in this area in the future.

- **Tube sizing.** The first recommendation is to, instead of using sets of tubes with equal diameters, have changing diameters depending on the pressure drop required. As the optimal pressure difference at the leading edge is dependent on the optimal mass flow and the pressure drop in the tubing, this pressure behind the porous skin offers a lot of room for improvement.
- **Pump design.** To get a better indication of the size of a pump for suction, more research time needs to be devoted to its design. If a lighter design for the pump can be achieved, it might make suction a viable concept again.
- **Aerodynamic models.** In this report, simple skin friction drag equations for turbulent and laminar flow were used, as transonic simulations are very complex and too in-depth for this report. Before a final marketing campaign can be started, this will have to be improved.
- **Structural models.** In this report, the structural aspect of LE suction was ignored. Therefore, if the concept becomes viable in the future, this has to be investigated.

Other Possible Concepts

During the design phase, some concepts came up that could not be further explored during the DSE for various reasons. They may however be very interesting concepts for future work. These concepts are described below.

Active Cant Morphing Winglet

In the process of designing a retrofit winglet, it was found that with current knowledge and resources, an active cant morphing winglet is not feasible. In Section 3.3.2 different actuator options for active winglet cant morphing were investigated and analysed with respect to a retrofit purpose. No suited actuator was found, however it is not proven that no suited actuator exists. It is recommended that a deeper study on electrical actuators will have to be performed to size the required gearbox and the actuators. While the power requirement can be easily met due to a relatively slow actuating motion, the hinge moment due to the winglets aerodynamic force is in the order of 67 kNm. The system will have to be designed to be able to withstand this moment, and not fail under for example torsional stress. A solution for this can be found in the use of a trip tap on the winglet, to reduce the aerodynamic loads acting on the winglet

causing a large hinge moment which need to be overcome by the actuator. In addition to this, other passive methods such as springs could potentially be used to reduce the required actuator hinge moment. The springs would be in tension once the winglet has a cant angle of 0 degrees and in this setting cause a moment force in the direction of a larger cant angle (canting the winglet down).

Acoustic Liners

A promising concept that was found during the research and investigation of chevrons is that of acoustic liners. Whereas the chevrons only reduce the jet noise, the acoustic liners can help to reduce the fan noise during approach as well as take-off². Acoustic liners can be considered as small holes that are present on the engine inlet, often combined with backing cavities to tune the frequency response, that convert acoustic field related energy to vorticity-bound energy [79].

Although acoustic liners are often already present on the engine inlet, research is still conducted with the purpose of improving the noise performance and reducing potential drag penalties [80, 81]. This means in the future it is also an option to redesign or retrofit acoustic liners if the aircraft does not already possess such a concept [82]. Sections of the inlet containing the small holes are attached to the engine frame with several screws and thus can be easily replaced for a potential retrofit. As the research and development regarding morphing structures progresses, materials might be found with better acoustic properties, which would make retrofitting the inlet viable. Ultimately this could lead to a retrofitted morphing inlet with acoustic liners, however a lot of research and development has to be conducted in order to find adequate materials.

Plasma Actuators

A promising retrofit concept found during early research is the plasma actuator for flow control. A plasma actuator is light-weight, has a low power consumption, does not have any moving parts and has a fast enough response time to be suitable for flow control. However, during research it was found that the successful tests with plasma actuators for flow control are performed mostly at a Reynolds number lower than 10^6 , whilst actual aircraft fly at a Reynolds number (way) higher than 10^6 . State-of-the-art plasma actuators are not powerful enough to be effective at high Reynolds numbers³. As plasma actuators could potentially significantly improve aerodynamic performance, it is recommended that plasma actuators will be further researched in the future and implemented in the BEAU-wing retrofit package when the concept is ready.

²Private communication, Abhishek K. Sahai [13 June 2017 12:00].

³Marios Kotsonis [11 May 2017 14:00].

References

- [1] Arkesteijn, J. P. W., van den Bos, N., Eijkman, M., Faber, N., Meijerman, C. A., Ritzen, L., Vandereydt, B. J. C., and Vervaat, R. M. The Smart Retrofit Wing. Baseline Report, May 2017.
- [2] Arkesteijn, J. P. W., van den Bos, N., Eijkman, M., Faber, N., Meijerman, C. A., Ritzen, L., Vandereydt, B. J. C., and Vervaat, R. M. The Smart Retrofit Wing. Midterm Report, May 2017.
- [3] de Breuker, R. *Project Guide Design Synthesis Exercise “The Smart Retrofit Wing”*. TU Delft, Faculty of Aerospace Engineering, April 2017.
- [4] Gill, E. Verification and Validation for the Attitude and Orbit Control System. AE3211-I Systems Engineering & Aerospace Design, Delft University of Technology, slide 5, March 2017.
- [5] Airbus. *A330 Flight Crew Operating Manual: Flight Preparation 2*, 2003.
- [6] Obert, E. *Aerodynamic Design of Transport Aircraft*. IOS Press BV, 2009.
- [7] Keivanpour, S., Ait Kadi, D., and Mascle, C. End-Of-Life Aircraft Treatment in the Context of Sustainable Development, Lean Management, and Global Business. *International Journal of Sustainable Transportation*, Vol. 11, No. 5, pp. 257–380, 2017.
- [8] European Aviation Safety Agency. *CS–25 Large Aeroplanes*, 19th Edition, 2017.
- [9] Nesbitt, E., Mengle, V., Callender, B., Czech, M., and Thomas, R. Flight Test Results for Uniquely Tailored Propulsion Airframe Aeroacoustic Chevrons: Community Noise. *Proceedings of the 12th AIAA/CEAS Aeroacoustics Conference*, May 2006.
- [10] Mengle, V., Elkoby, R., Brusniak, L., and Thomas, R. Reducing Propulsion Airframe Aeroacoustic Interactions with Uniquely Tailored Chevrons: 1. *Proceedings of the 12th AIAA/CEAS Aeroacoustics Conference*, May 2006.
- [11] Mengle, V., Elkoby, R., Brusniak, L., and Thomas, R. Reducing Propulsion Airframe Aeroacoustic Interactions with Uniquely Tailored Chevrons: 2. *Proceedings of the 12th AIAA/CEAS Aeroacoustics Conference*, May 2006.
- [12] Mengle, V., Elkoby, R., Brusniak, L., and Thomas, R. Reducing Propulsion Airframe Aeroacoustic Interactions with Uniquely Tailored Chevrons: 3. *Proceedings of the 12th AIAA/CEAS Aeroacoustics Conference*, May 2006.
- [13] Mengle, V. G., Ganz, U. W., Nesbitt, E., Bultemeier, E. J., and Thomas, R. H. Flight Test Results for Uniquely Tailored Propulsion Airframe Aeroacoustic Chevrons: Shockcell Noise. *Proceedings of the 12th AIAA/CEAS Aeroacoustics Conference*, May 2006.
- [14] Calkins, F. T., Butler, G. W., and Mabe, J. H. Variable Geometry Chevrons for Jet Noise Reduction. *Proceedings of the 12th AIAA/CEAS Aeroacoustics Conference*, May 2006.
- [15] Kandula, M. and Vu, B. On the Scaling Laws for Jet Noise in Subsonic and Supersonic Flow. *Proceedings of the 9th AIAA/CEAS Aeroacoustics Conference and Exhibit*, May 2003.
- [16] Kandula, M. and Vu, B. Scaling Laws and a Method for Identifying Components of Jet Noise. *AIAA Journal*, Vol. 44, No. 10, pp. 2274–2285, October 2006.
- [17] Elahinia, M. H., Hashemi, M., Tabesh, M., and Bhaduri, S. B. Manufacturing and Processing of NiTi Implants: a Review. *Progress in Material Science*, Vol. 57, No. 5, pp. 911–946, June 2012.
- [18] Stoeckel, D. The Shape Memory Effect - Phenomenon, Alloys and Applications. *Proceedings of the Shape Memory Alloys for Power Systems EPRI*, pages 1–13, 1995.
- [19] Shihl, G. The Effect of the Fiber/Matrix Interface on the Flexural Fatigue Performance of Unidirectional Fiberglass Composites. *Composites Science and Technology*, Vol. 28, No. 2, pp. 137–161, 1987.
- [20] Mabe, J. H., Calkins, F. T., and Butler, G. W. Boeing’s Variable Geometry Chevron, Morphing Aerostructure for Jet Noise Reduction. *Proceedings of the 47th AIAA/ASME/ASCE/AHS/ASC Structures, Structural Dynamics, and Materials Conference*, May 2005.
- [21] Cabell, R. H., Schiller, N. H., Mabe, J. H., Ruggeri, R. T., and Butler, G. W. Feedback Control of a Morphing Chevron for Takeoff and Cruise Noise Reduction. Active 2004, Williamsburg VA, September 2004.
- [22] DellaCorte, C. Nickel-Titanium Alloys: Corrosion “Proof” Alloys for Space Bearing, Components and Mechanism Applications. NASA CP–216272, 2010.
- [23] Rudolph, P. K. C. High-Lift Systems on Commercial Subsonic Airliners. NASA CR–4746, September 1996.
- [24] Nexans. *Aircraft Wires and Cables*, 2nd Edition, 2003.
- [25] Mabe, J. H., Calkins, F. T., and Ruggeria, R. T. Full-Scale Flight Tests of Aircraft Morphing Structures Using SMA Actuators. *Proceedings of SPIE – The International Society for Optical Engineering*, Vol. 6525, 2007.
- [26] Hartl, D. J., Lagoudas, D. C., Calkins, F. T., and Mabe, J. H. Use of a Ni60Ti Shape Memory Alloy for Active Jet Engine Chevron Application: I. Thermomechanical Characterization. *Smart Materials and Structures*, Vol. 19, 2010.
- [27] Elanchezian, C., Ramnath, B. V., and Hemalatha, J. Mechanical Behaviour of Glass and Carbon Fibre Reinforced Composites at Varying Strain Rates and Temperatures. *Procedia Materials Science*, Vol. 6, pp. 1405–1418, 2014.
- [28] Makkar, U., Rana, M., and Singh, A. Analysis of Fatigue Behavior of Glass/Carbon Fiber Epoxy Composite. *International Journal of Research in Engineering and Technology*, Vol. 4, No. 4, pp. 211–216, April 2015.
- [29] Hartl, D. J., Mabe, J. H., Benafan, O., Coda, A., Conduit, B., Padan, R., and Doren, B. V. Standardization of Shape

- Memory Alloy Test Methods Toward Certification of Aerospace Applications. *Smart Materials and Structures*, Vol. 24, No. 8, July 2015.
- [30] ASTM International. Standard Test Method for Transformation Temperature of Nickel–Titanium Alloys by Thermal Analysis. Designation: F2004–05, 2010.
- [31] ASTM International. Standard Terminology for Nickel–Titanium Shape Memory Alloys. Designation: F2005–05, 2015.
- [32] ASTM International. Standard Specification for Wrought Nickel–Titanium Shape Memory Alloys for Medical Devices and Surgical Implants. Designation: F2063–12, 2012.
- [33] ASTM International. Standard Test Method for Determination of Transformation Temperature of Nickel–Titanium Shape Memory Alloys by Bend and Free Recovery. Designation: F2082–03, 2006.
- [34] International Civil Aviation Organization. *ICAO Aerodrome Standards*, 3rd Edition, 1999.
- [35] Timoshenko, S. P. and Gere, J. M. *Theory of Elastic Stability*. Dover Publications, 2nd Edition, May 2012.
- [36] Saltogu, R., Humaira, N., and Inalhan, G. Scheduled Maintenance and Downtime Cost in Aircraft Maintenance Management. *International Journal of Mechanical, Aerospace, Industrial, Mechatronic and Manufacturing Engineering*, Vol. 10, No. 3, pp. 602–607, 2016.
- [37] Reckzeh, D. Aerodynamic Design of Airbus High-Lift Wings in a Multidisciplinary Environment. *Proceedings of the European Congress on Computational Methods in Applied Sciences and Engineering*, July 2004.
- [38] Eppler, R. and Somers, D. M. A Computer Program for the Design and Analysis of Low-Speed Airfoils. NASA TM-80210, December 1980.
- [39] Granville, P. S. The Prediction of Transition from Laminar to Turbulent Flow in Boundary Layers on Bodies of Revolution. Naval Ship Research and Development Center, TN 111, 1974.
- [40] Shoensleben, S. P. Integrated Trailing Edge Flap Track Mechanism for Commercial Aircraft. Master's Thesis, Eidgenossische Technische Hochschule Zurich (ETH), 2005.
- [41] Megson, T. H. G. *Aircraft Structures for Engineering Students*. Butterworth-Heinemann, 6th Edition, November 2016.
- [42] Carraher, Jr., C. E. *Polymer Chemistry*. Marcel Dekker, Inc., 6th Edition, 2005.
- [43] De Baere, I., Van Paepegem, W., Hochard, C., and Degrieck, J. On the Tension-Tension Fatigue Behaviour of a Carbon Reinforced Thermoplastic Part II: Evaluation of a Dumbbell-Shaped Specimen. *Polymer Testing*, Vol. 30, No. 6, pp. 663–672, September 2011.
- [44] Fuel & Motion Control Systems Division. *Manual Engine-Driven Pump on Airbus A330/340*. EATON Aerospace Group, 2012.
- [45] Ball, P. Engineering Shark Skin and Other Solutions. *Nature*, Vol. 400, pp. 507–509, August 1999.
- [46] Lee, S. J. and Lee, S. H. Flow Field Analysis of a Turbulent Boundary Layer over a Riblet Surface. *Experiments in Fluids*, Vol. 30, No. 2, pp. 153–166, February 2001.
- [47] Dean, B. and Bhushan, B. Shark-Skin Surfaces for Fluid-Drag Reduction in Turbulent Flow: a Review. *Philosophical Transactions of the Royal Society A*, Vol. 368, pp. 4775–4806, 2010.
- [48] Bechert, D. W., Bruse, M., Hage, W., and Meyer, R. Biological Surfaces and Their Technological Application – Laboratory and Flight Experiments on Drag Reduction and Separation Control. *Proceedings of the 28th Fluid Dynamics Conference*, 1997.
- [49] Coustols, E. and Schmitt, V. *Synthesis of Experimental Riblet Studies in Transonic Conditions*. Springer Netherlands, 1st Edition, 1990.
- [50] Huawei, C., Rao, F., Zhang, D., and Shang, X. Drag Reduction Study about Bird Feather Herringbone Riblets. *Journal of Bionic Engineering*, Vol. 10, No. 3, pp. 341–349, July 2013.
- [51] Squire, L. C. and Savill, A. M. Drag Measurements on Planar Riblet Surfaces at High Subsonic Speeds. *Applied Scientific Research*, Vol. 46, No. 3, pp. 229–243, July 1989.
- [52] Tollmien, W., Schlichting, H., Görtler, H., and Riegels, F. W. *Ludwig Prandtl Gesammelte Abhandlungen*. Springer-Verlag Berlin Heidelberg GmbH, 1st Edition, 1961. pp. 597–608.
- [53] F. R. Etchberger. LFC Leading Edge Glove Flight – Aircraft Modification Design, Test Article Development, and Systems Integration. NASA CR–172136, November 1983.
- [54] Boeing Commercial Airplane Group. High Reynolds Number Hybrid Laminar Flow Control (HLFC) Flight Experiment: II. Aerodynamic Design. NASA CR–209324, April 1999.
- [55] Maresh, J. L. and Bragg, M. B. The Role of Airfoil Geometry in Minimizing the Effect of Insect Contamination of Laminar Flow Sections. *Proceedings of the AIAA 2nd Applied Aerodynamics Conference*, August 1984.
- [56] Bahr, C. J., Hutcheson, F. V., Thomas, R. H., and Housman, J. A. A Comparison of the Noise Characteristics of a Conventional Slat and Krueger Flap. *Proceedings of the 22nd AIAA/CEAS Aeroacoustics Conference*, June 2016.
- [57] Akaydin, H. D., Housman, J. A., Kiris, C. C., Bahr, C. J., and Hutcheson, F. V. Computational Design of a Krueger Flap Targeting Conventional Slat Aerodynamics. *Proceedings of the 22nd AIAA/CEAS Aeroacoustics Conference*, June 2016.
- [58] Barbarino, M., Dimino, I., Carozza, A., Nae, C., Stoica, C., Pricop, V., Peng, S. H., Eliasson, P., Grundestam, O., and Tysell, L. Airframe Noise Reduction Technologies Applied to High-Lift Devices of Future Green Regional Aircraft. *Proceedings of the 3AF/CEAS Conference “Greener Aviation: Clean Sky Breakthroughs and Worldwide*

- Status*", March 2014.
- [59] Eliasson, P., Grundestam, O., Peng, S. H., Yao, H., Davidson, L., and Eriksson, L. E. Assessment of High-lift Concepts for a Regional Aircraft in the ALONOCO Project. *Proceedings of the 50th AIAA Aerospace Sciences Meeting*, January 2012.
- [60] Douglas Aircraft Company. Laminar Flow Control Leading Edge Glove Flight Test Article Development. NASA CR-172137, November 1984.
- [61] Sinnett, M. 787 No-Bleed Systems: Saving Fuel and Enhancing Operational Efficiencies. *Aeromagazine*, Vol. 4, 2007.
- [62] Scholz, D., Seresinhe, R., Staack, I., and Lawson, C. Fuel Consumption Due to Shaft Power Off-Takes from the Engine. Workshop on Aircraft System Technologies (AST 2013), Hamburg, 2013.
- [63] MacManus, D. G. and Eaton, J. A. Predictions and Observations of the Flow Field Induced by Laminar Flow Control Microperforations. *Experimental Thermal and Fluid Science*, Vol. 13, No. 4, pp. 395–407, 1996.
- [64] Boeing Commercial Airplane Group. High Reynolds Number Hybrid Laminar Flow Control (HLFC) Flight Experiment: III. Leading Edge Design, Fabrication, and Installation. NASA CR-209325, April 1999.
- [65] Boeing Commercial Airplane Group. High Reynolds Number Hybrid Laminar Flow Control (HLFC) Flight Experiment: IV. Suction System Design and Manufacture. NASA CR-209326, April 1999.
- [66] Fisher, D. F. and Fischer, M. C. Development Flight Tests of JetStar LFC Leading-Edge Flight Test Experiment. NASA CP-2487, December 1987.
- [67] March, A. Influence of Low-speed Aerodynamic Performance on Airport Community Noise. Master's Thesis, Massachusetts Institute of Technology, 2008.
- [68] Schiphol Airport. *Charges and Conditions*, April 2017.
- [69] Pfeiffer, U. M. Aircraft Noise Report. Bundesverband der Deutschen Luftverkehrswirtschaft, 2015.
- [70] Airports Council International. *ACI Aircraft Noise Rating Index*, 2010.
- [71] Melin, T. A Vortex Lattice MATLAB Implementation for Linear Aerodynamic Wing Application. Master's Thesis, Royal Institute of Technology (KTH), 2000.
- [72] Melin, T. *User's Guide and Reference Manual for Tornado*. Royal Institute of Technology (KTH), Department of Aeronautics, 2.3th Edition, 2000.
- [73] Schrijer, F. Compressible Aerodynamics. AE2130-III Aerodynamics II Lecture Slides, Delft University of Technology, January 2016.
- [74] Stanewsky, J. E., Fulker, J., and de Matteis, P. *Drag Reduction by Shock and Boundary Layer Control: Results of the Project EUROSHOCK II*. Springer-Verlag Berlin Heidelberg GmbH, 3rd Edition, 1999.
- [75] Monaghan, R. J. A Review and Assessment of Various Formulae for Turbulent Skin Friction in Compressible Flow. ARC CP-142, 1953.
- [76] Unknown Author. Owner's and Operator's Guide: A330-200/-300. *Aircraft Commerce*, Vol. 57, No. 1, pp. 8–39, May 2008.
- [77] Ackert, S. Elements of Aircraft Maintenance Reserve Development. Presented on the IATA Maintenance Cost Conference, October 2010.
- [78] ASTM International. Standard Test Method for Tension Testing of Nickel-Titanium Superelastic Materials. Designation: F2516-14, 2006.
- [79] Zhang, Q. and Bodony, D. J. Numerical Investigation of a Honeycomb Liner Grazed by Laminar and Turbulent Boundary Layers. *Journal of Fluid Mechanics*, Vol. 792, pp. 936–980, 2016.
- [80] Azimi, M., Ommi, F., and Alashti, N. J. Using Acoustic Liner for Fan Noise Reduction in Modern Turbofan Engines. *International Journal of Aeronautical and Space Sciences*, Vol. 15, No. 1, pp. 97–101, 2014.
- [81] Law, T. and Dowling, A. Optimization of Annular and Cylindrical Liners for Mixed Exhaust Aeroengines. *Proceedings of the 13th AIAA/CEAS Aeroacoustics Conference*, 2007.
- [82] Atvars, J. and Mangiarotty, R. A. Parametric Studies of the Acoustic Behavior of Duct-Lining Materials. *The Journal of the Acoustical Society of America*, Vol. 48, pp. 815–825, 1970.

Functional Analysis Diagrams

The functional flow diagram is split up into three figures, Figures A.1 to A.3. The content in Figures A.2 and A.3 is not shown in exactly the right order: this has been done to save space. The functional breakdown structures of both production of the retrofitted component and operation of the aircraft are shown in Figures A.4 and A.5, respectively.

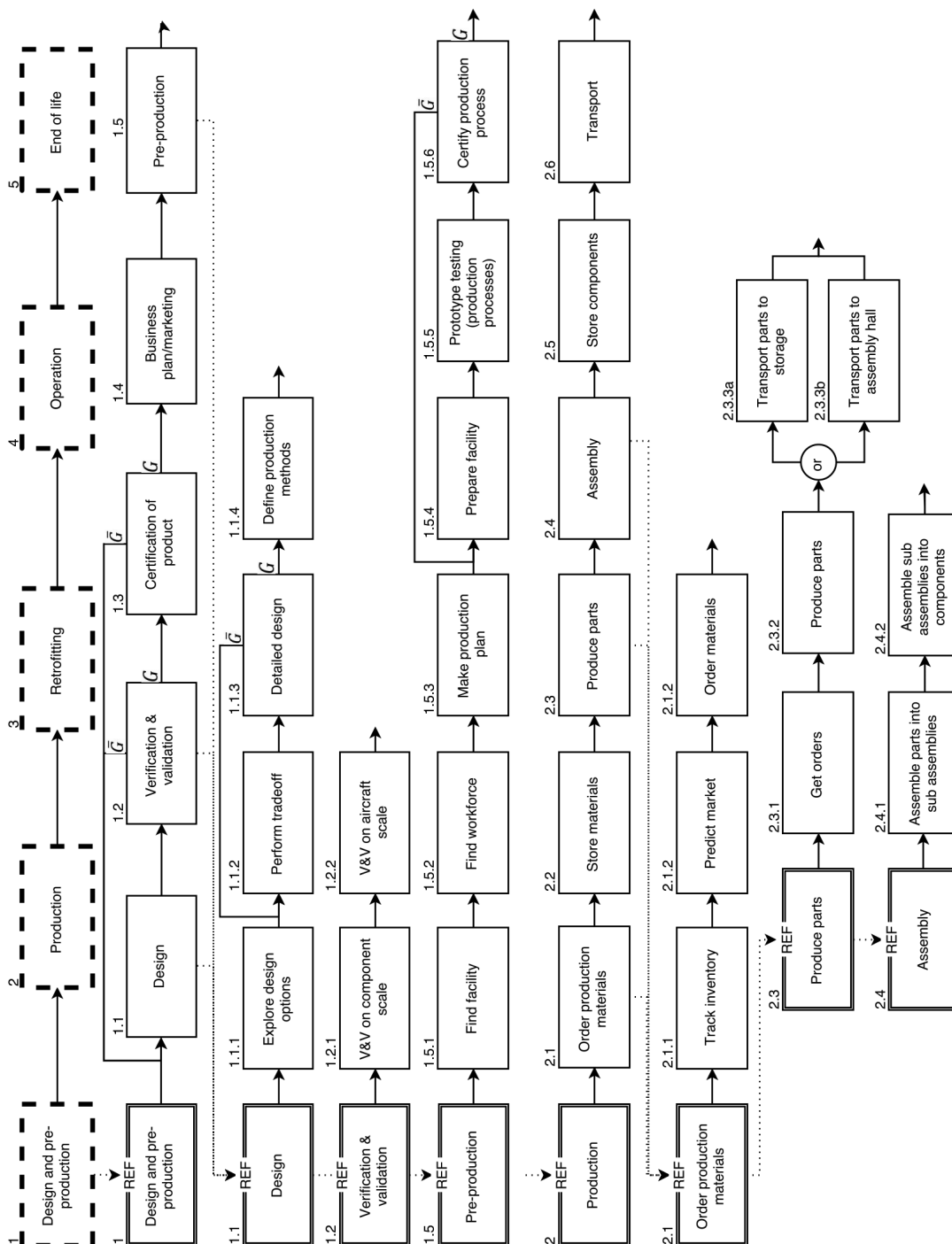


Figure A.1: Functional analysis (part 1/3).

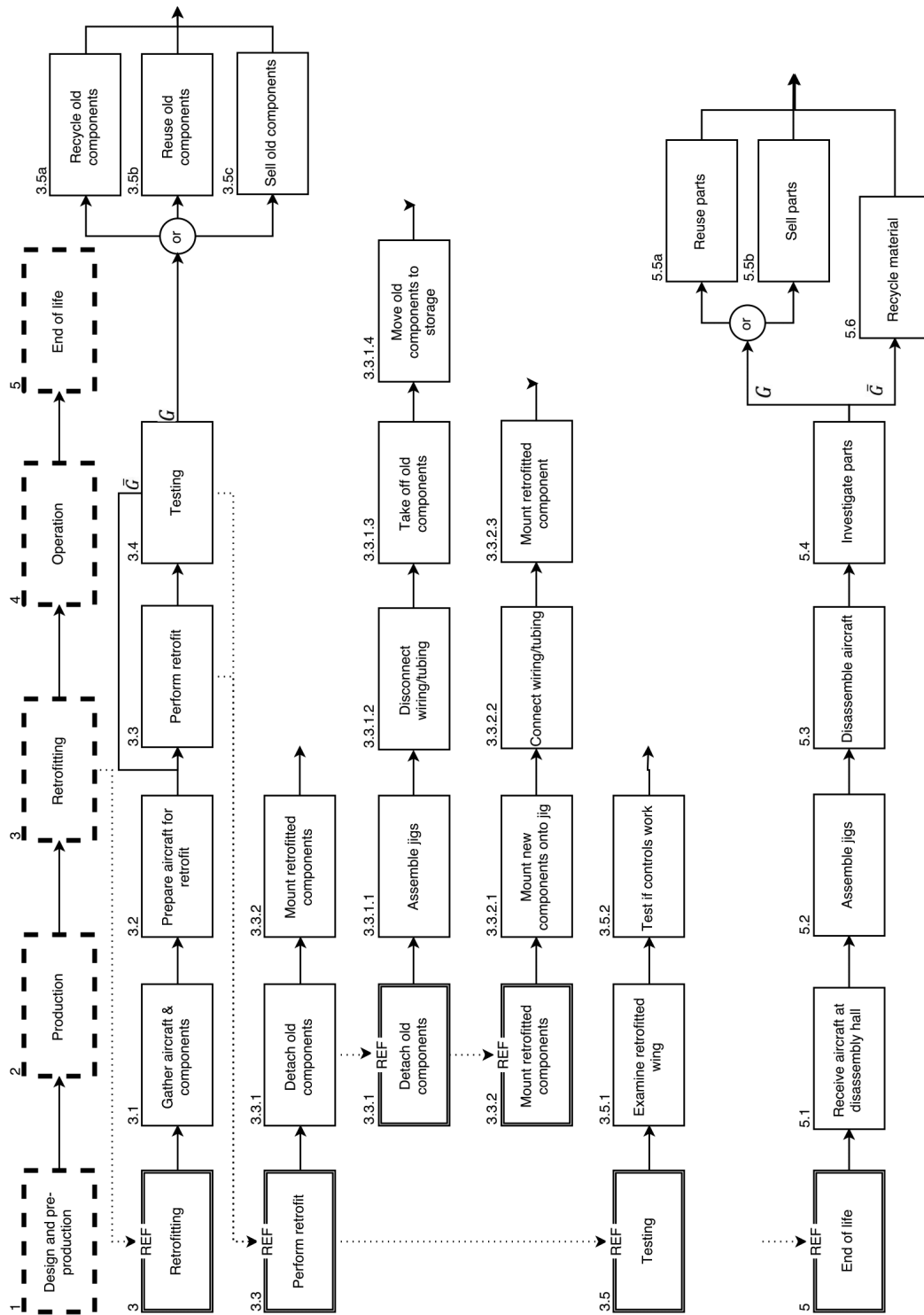


Figure A.2: Functional analysis (part 2/3).

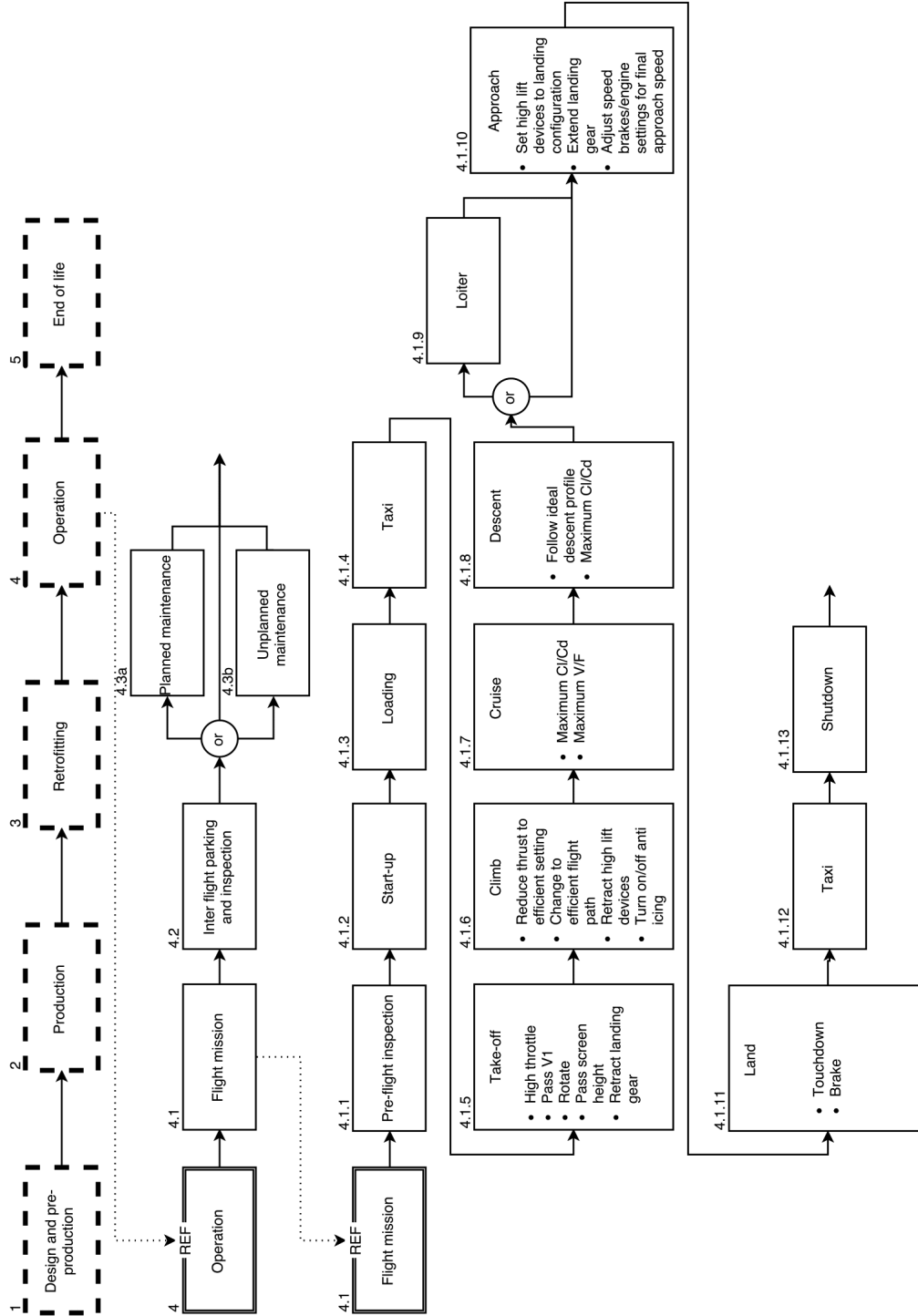


Figure A.3: Functional analysis (part 3/3).

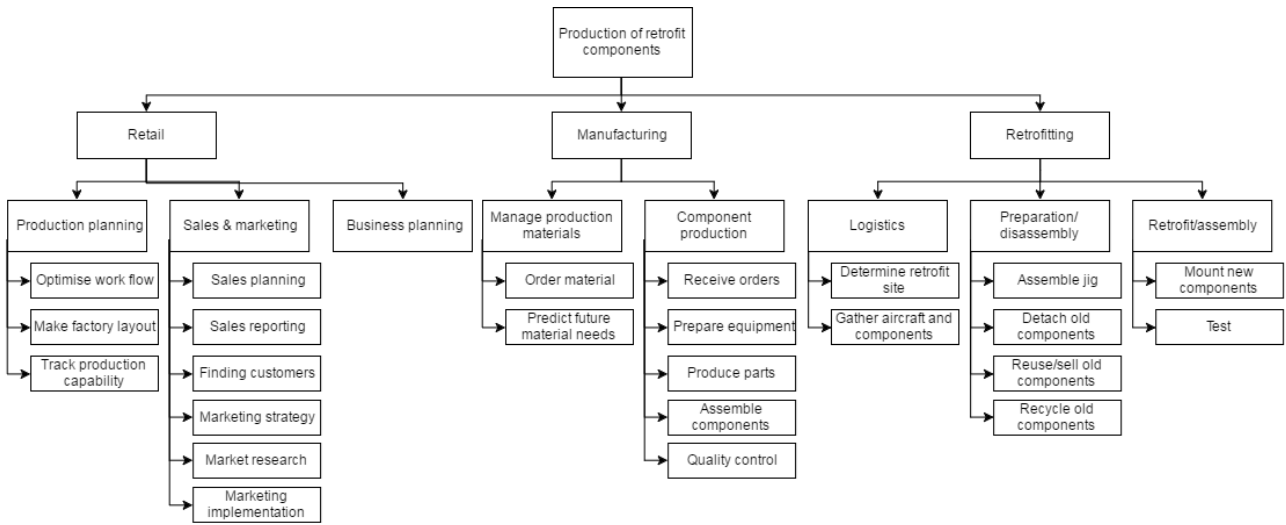


Figure A.4: Functional breakdown structure for production of the retrofit components.

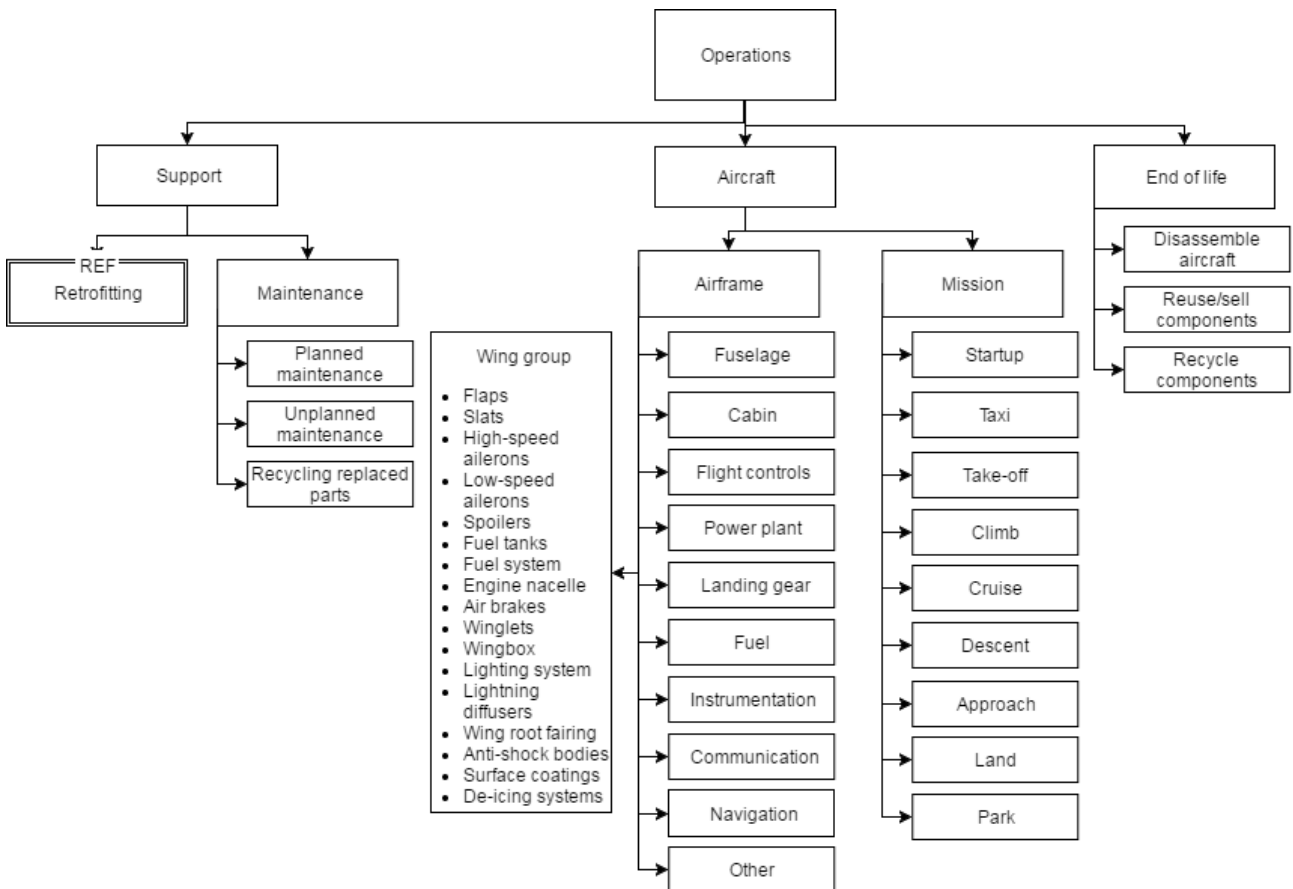


Figure A.5: Functional breakdown structure for operation of the aircraft.

Design Options Trade-Off

The following colour scheme was adhered to for the trade-off tables:

- Green: (6, 7) Concept performs excellent on this criterion.
- Blue: (4, 5) Concept performs good on this criterion.
- Yellow: (2, 3) Concept performs bad on this criterion.
- Red: (1) Concept performs unacceptable on this specific criterion.

Table B.1: Trade summary for wingtip concepts.

	Weight	Performance	Noise	Cost	TRL	Sustainability	Result
SMA winglet	3	7	5	2	5	2	4.50
Constant actuation winglet	3	7	5	3	6	3	4.98
Locking winglet	2	7	5	3	6	3	4.88
Non-moving winglet	4	3	4	4	7	4	4.23

Table B.2: Trade summary for leading edge concepts.

	Weight	Performance	Noise	Cost	TRL	Sustainability	Result
Inboard morphing	5	4	6	4	4	4	4.35
Inboard morphing with blowing	3	4	6	3	4	3	3.85
Outboard morphing with blowing	3	6	7	3	4	3	4.58
Sleeve	3	3	5	5	3	4	3.75
Slat cove filler	3	2	7	6	5	5	4.35
Sucking	3	7	5	2	7	4	5.05
Blowing	4	1	4	2	6	3	2.95
Plasma actuator	3	6	6	3	2	5	4.30
Bug coating	4	5	4	1	6	4	4.05
Sharkskin	3	2	4	6	7	4	4.23

Table B.3: Trade summary for trailing edge concepts.

	Weight	Performance	Noise	Cost	TRL	Sustainability	Result
Morphing, FishBAC	5	7	6	3	4	4	5.05
Sleeve	3	4	5	5	3	5	4.15
Sucking	2	7	5	3	6	3	4.88
Blowing	3	6	5	3	7	3	4.85
Sharkskin	3	3	4	6	7	4	4.53

Table B.4: Trade summary for engine nacelle concepts.

	Weight	Performance	Noise	Cost	TRL	Sustainability	Result
Variable autonomous chevrons	3	2	6	5	7	4	4.28
Variable powered chevrons	3	3	7	4	7	4	4.50
Fixed chevrons	4	1	5	6	7	5	4.25
Inlet morphing	3	4	5	4	3	4	3.85

Table B.5: Trade summary for rest-of-the-wing concepts.

	Weight	Performance	Noise	Cost	TRL	Sustainability	Result
Sucking	1	7	5	1	7	4	4.65
Blowing	1	7	5	1	7	4	4.65
Anti-bug coating	4	5	4	1	6	4	4.05
Sharkskin	4	4	4	5	7	4	4.73

Task Division

Table C.1 and Table C.2 show the work division of this report. For each chapter/section/subsection the person who wrote it is shown. It should be noted that Loes made the CATIA model and that Krista and Nick did the content and spelling check of the report. The models for the wingtip extension were coded by Robin, the structural model for the FishBAC was coded by Linda. Niek did the aerodynamic analysis of the winglet in Tornado and Nick did the aerodynamic analysis of the FishBAC. The concepts were divided amongst different teams. Team winglet comprised of Loes, Niek and Robin, team FishBAC comprised of Krista, Linda and Nick, Bert and Joerie covered both LE suction and chevrons, and sharkskin was entirely designed by Linda.

Table C.1: Task division (part 1/2).

Chapter	Section	Subsection	Person
Preface			Loes
Executive overview			Linda
Introduction			Joerie
Pre-design	Mission statement		Krista
	Functional analysis		Bert
	Market analysis		Bert
	Resource allocation and budget breakdown		Joerie
	Concept trade-off process		Joerie
	Sustainable development strategy		Nick
	Risk analysis		Krista/ Loes
Design	Chevrons	Aerodynamics	Bert
		Structures	Joerie
		Materials	Joerie
		Integration and configuration	Bert
		Cost	Joerie
	Winglets	Aerodynamics	Niek
		Structures	Robin/Loes
		Materials	Loes
		Integration and configuration	Loes
		Cost	Loes
	FishBAC	Aerodynamics	Nick
		Structures	Linda
		Materials	Linda
		Integration and configuration	Krista/Linda
Cost		Linda	
Sharkskin			Linda
Leading edge suction	Aerodynamics		Joerie/Bert
		Structures	Bert
		Materials	Joerie
		Integration and configuration	Joerie
		Cost	Joerie
		Conclusion	Bert
		Leading edge suction	Joerie

Table C.2: Task division (part 2/2).

Chapter	Section	Subsection	Person
Full aircraft analysis	Configuration		Loes
	Retrofit characteristics	Aerodynamics	Bert/Niek/Nick
		Structures	Nick
		Stability and control	Robin
		Performance	Nick
	Communications	H/S, electrical block diagram	Robin
		Data handling and communication flow chart	Joerie
	Verification and validation	Chevrons	Joerie
			Loes (verification Tornado)
		Winglets	Robin (Structures V&V) Niek (validation Tornado)
		FishBAC	Linda
		Sharkskin	Linda
	Leading edge suction	Bert	
RAMS		Krista	
Operations and logistic concept		Bert/Robin	
Sensitivity analysis	Effects of mission	Niek	
	Chevrons	Bert	
	Winglets	Niek	
	FishBAC	Linda	
	Sharkskin	Linda	
	Leading edge suction	Joerie/Bert	
Project implementation	Compliance matrix		Robin
	Project design and development logic		Linda
	Project Gantt chart		Linda
	Production plan	Chevrons	Joerie
		Winglets	Loes/Robin
		FishBAC	Krista
		Sharkskin	Linda
		Leading edge suction	Joerie
Cost breakdown structure		Bert	
Return on investment		Nick	
Conclusion		Bert	
Recommendations		Linda/Bert/Loes	